UNIVERSITY OF OKLAHOMA

GRADUATE COLLEGE

INVESTIGATION OF OILWELL CEMENT MIXING: EXPERIMENTAL STUDIES AND IMPLICATIONS FOR MIXING ENERGY THEORY

A DISSERTATION

SUBMITTED TO THE GRADUATE FACULTY

in partial fulfillment of the requirements for the

Degree of

DOCTOR OF PHILOSOPHY

By

FATEMEH KARBALAEI SALEH
Norman, Oklahoma
2018

INVESTIGATION OF OILWELL CEMENT MIXING: EXPERIMENTAL STUDIES AND IMPLICATIONS FOR MIXING ENERGY THEORY

A DISSERTATION APPROVED FOR THE
MEWBOURNE SCHOOL OF PETROLEUM AND GEOLOGICAL ENGINEERING

BY

_____
Dr. Catalin Teodoriu, Chair

_____
Dr. Carl Sondergeld

_____
Dr. Ramadan Ahmed

_____
Dr. Mashhad Fahes

_____
Dr. Brian P. Grady

I dedicate this Ph.D. dissertation to my supportive husband, Saeed and my lovely daughter, Nahal who are the pride and joy of my life. I love you more than anything and I appreciate all your patience and support during my Ph.D. studies

Acknowledgements

I would like to sincerely thank my academic advisor and committee chair Dr. Catalin Teodoriu for his guidance and mentorship throughout my graduate program. His sound advice, and counsel have been of immense value and benefit throughout this process. He was always open to discussion and very helpful in design and execution of laboratory tests. I would also like to thank Dr. Carl Sondergeld, first for permitting me to conduct NMR measurements in his laboratory, and second for his help and valuable feedback on my NMR results and my dissertation in general. I would like to thank Dr. Ramadan Ahmed for his feedback during the process, and permitting me to attend his lectures in Advance Hydraulic class which helped me to better understand non-Newtonian flow behavior. Special thanks to my other committee members, Dr. Brian Grady and Dr. Mashhad Fahes for kindly accepting to be in this committee and their valuable time in reading my dissertation.

I am also thankful to Mr. Gary Stowe and Mr. Jeff McCaskill for their help in conducting experiments. Completion of this work could not be been possible without their support. I would like to express my gratitude to Dr. Ali Tinni for his valuable input and helping me to understand NMR measurements. Finally, special thanks to Mr. Chinedum Ezeakacha, for his help in conducting cement thickening time tests.

Finally, I owe a special thanks to my family, my mom and dad for supporting me throughout my PhD program, and their encouragement for finishing up this work.

Table of Contents

List of Tables

List of Figures

Abstract

Cement is a key element of wellbore integrity. Mixing condition for cement and how its properties are affected is of great importance but often ignored in the oilwell cement design. Typical cement slurry properties such as basic rheology, thickening time, compressive strength, porosity, permeability and fluid loss can be directly impacted when mixing conditions change. Since the development of slurry properties is irreversible, selecting an appropriate initial mixing condition can be critical for short and long term cement integrity. Generally, cements are designed to perfection in the laboratory but developing similar properties in the field operation is challenging. It is common that the properties of cement slurry obtained from laboratory and field mixing do not correlate very well, which can lead to a variety of cement-job problems.

More than 800 cement specimens were prepared in this study. Using various mixing procedures, we have performed extensive laboratory experiments including UCS (unconfined compressive strength), UPV (ultrasonic pulse velocity), rheology, thickening time and NMR (Nuclear Magnetic Resonance) tests on these specimens. These procedures were differed based on changing shear rate by varying rotational speed of mixing device, changing mixing time and mixing energy. We compared testing results to understand impact of each variable. Finally, empirical models based on power consumption and non-Newtonian flow characteristics of cement slurry are developed to capture the effects of mixing conditions on different cement properties. The new model is tied to a proposed scale up procedure to enable use of laboratory results in the field operations.

Chapter 1: Introduction

1.1 Motivation

Well cementing is an integral operation in the oil and gas industry and it is a key element to ensure wellbore integrity throughout life of the well. Improper cement design can cause well construction risks such as de-bonding and leakage pathways in the near wellbore and through the annulus (Nelson and Gulliot, 2006; Teodoriu et al., 2010). According to data published in 2015 by the Petroleum Services Association of Canada (PSAC), cement cost can account up to 25% of the overall drilling and completion expenditure. Some unsuccessful cement operations can lead to risk of kicks, and blowouts. Deepwater Horizon disastrous tragedy in 2010 is an example where improper cement placement and design was one of the key factors to the well control incident (Graham et al., 2011). According to one of the cement expert testimonies related to this incident (Glen, 2011): "*Cement did not isolate the formations in the Macondo well. For the cement to fail to provide a barrier in the Macondo well, it was either not present across from a producing formation or it was not set and able to act as a barrier to flow, or both. Channeling allowed for a flow path in the annulus for formation fluids. "*

Proper cement design, cement mixing and placement and ensuring cement integrity are critical for safe extraction of oil and gas. In another excerpt from the President Committee's report on Macondo well incident, it stated that (Graham et al., 2011):

"*The decision to proceed to displacement of the drilling mud by sea water was made despite a failure to demonstrate the integrity of the cement job even after multiple negative pressure tests. "*

In a recent ExproSoft report (Exprosoft, 2017) to BSEE (Bureau of Safety and Environmental Enforcement) for update of offshore loss of well control frequency information for 2006-2015, it shows cement problems and poor cement design are key contributors to the loss of well control events (Figure 1.1).

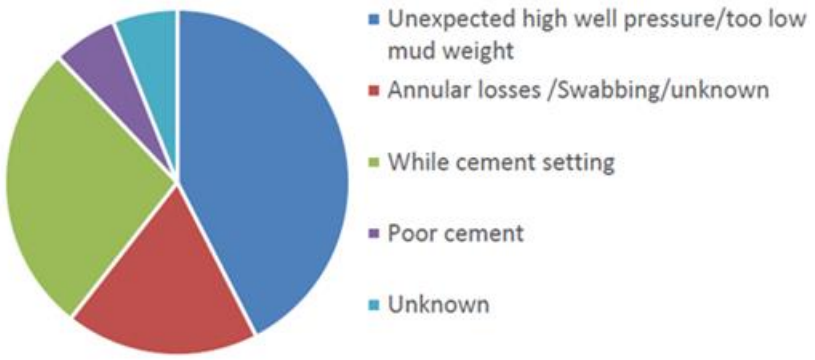

Figure 1.1 Primary contributing factors to loss of well control incidents (LWC) while drilling. Poor cement design and placement are two of the primary contributors to loss of well control events (from Exprosoft, 2017)

The motivation in this work is to understand how different cement properties are impacted by mixing conditions. Similar to construction, in the oil industry, the properties of cement slurry are known to be dependent on the mixing conditions. But little attention has been made in the past to understand how different mixing variables will impact cement properties. In addition, one of the primary goals of this work is to investigate current recommended practices for cement mixing by API (American Petroleum Institute) mixing energy theory.

1.2 Research Hypothesis

Cement mixing process is controlled by utilizing mixing energy, shear rate and mixing equipment. Mixing energy theory states that *slurries of equal mixing energies are*

expected to have matching properties, irrespective of mixing device, shear rate or scale (Orban et al., 1986). The role of shear rate applied by the mixing equipment on cement properties is not very clear. Previous researchers believe the role of shear rate is more significant than the mixing energy (Padgett, 1996**)**. Furthermore, it is not clear how cement properties are impacted by mixing energy, shear rate or mixing time.

1.3 Problem Statement

Cement is one of the primary and possibly the most important downhole barrier against uncontrolled flow of formation fluid. Very limited studies have been conducted to study mixing aspects of cement slurry (Saleh and Teodoriu, 2017). Several open questions exist on whether API recommended mixing energy theory can fulfill its goals (Orban et al., 1986). Additionally, some of these questions are related to the different mixing variables that impact cement properties. Several studies in the literature offer contradictory statements regarding key mixing variables (Orban et al., 1986; Padgett, 1996 and Vidick, 1989). Some studies highlight importance of mixing energy while others focus on optimizing shear rate stating that "*shear rate that a mixing system provides has a greater influence than total mixing energy on cement properties*" (Padgett, 1996). In addition, unlike mixing theories in other industries, API recommended mixing energy theory is exclusive of non-Newtonian flow characteristics. The mixing condition for non-Newtonian substances such as cement can be more complicated, because assuming a constant viscosity is invalid for these substances. The subject of mixing of Newtonian fluids has been studied extensively by many investigators (Foucault et al., 2005; Masiuk and Łącki, 1993; Metzner et al., 1961). In contrast, very little has been accomplished in the case of mixing non-Newtonian fluids. A literature survey of papers related to mixing processes published in other industries such as chemical and civil engineering highlight the

following aspects of mixing process (Metzner et al., 1961, Masiuk and Łącki, 1993, and Masiuk, 2008): i) flow characteristics (Newtonian/non-Newtonian), ii) power consumption, iii) shear rate and mixing time, iv) scale up or similarity criteria, and v) mixing equipment.

There is a need for robust procedures to evaluate cement mixing processes in the laboratory considering non-Newtonian flow characteristics. These procedures need to be scaled up and used in the field operations. There are numerous studies indicating that cement properties in the field do not match laboratory results (Teodoriu et al., 2015; Padgett, 1996 and Sweatman, 2000). Industry procedures for cement operations include verification of the same cement recipe in the laboratory by conducting different cement screening tests (Graham et al., 2011). The laboratory conducts a number of tests to evaluate the slurry's viscosity and flow characteristics, the rate at which it will cure, and its eventual compressive strength. If cement design passes the screening criteria, it can be suitable for application in the field. The impact of change in the scale (laboratory to field) on cement properties is generally overlooked. The process becomes more complex as the operating environment becomes harsher, as in deep, high-pressure, and high-temperature wells.

API mixing energy theory is function of both mixing time and mixing shear rate. In other words, one can achieve a similar mixing energy either by increase in mixing time or shear rate but the properties may be completely different. Cement undergo very active hydration when exposed to mixing water. Longer mixing time cause more uniform distribution of hydrates while higher shear rate in shorter time may not be enough for proper mixing (Takahashi et al., 2011). In addition, cement properties may be impacted

differently by shear rate and mixing time. Since the development of slurry properties is irreversible, selecting an appropriate initial mixing condition (time and shear rate) can be critical for short and long term cement integrity.

1.4 Study Objectives

The impact of mixing for wellbore cement can be very significant and affect its final properties. The primary objective of this study is to understand how mixing condition affect different cement properties. These properties include: i) destructive and non-destructive cement strength (UCS and UPV); ii) rheology; iii) thickening time; and iv) cement porosity.

Specific objectives of this work can be summarized:

- Developing an experimental matrix using factorial design approach,
- Evaluating API recommended mixing energy theory and determining significance and impact of mixing energy, shear rate and mixing time by measuring different cement properties,
- Comparing cement properties from yard mixer with laboratory mixer,
- Investigating power consumption in cement mixing and correlate relevant cement properties such as strength and rheology with mixing power consumption,
- Developing empirical models to optimize cement mixing based on mixing power consumption and cement non-Newtonian characteristics, and
- Proposing a scaling relationship to use experimental results from laboratory to field applications

1.5 Research Methodology

The methodology adopted in this dissertation is classified into four broad categories:

1. **Theoretical study:** Challenges in area of cement mixing and cement properties were investigated by conducting a through literature survey of papers published in the petroleum domain and overall mixing process in other industries. This literature study identified research gaps and the required theoretical foundation for designing experimental tests and formulating predictive models.
2. **Experimental study:** Previous literature shows a gap in experimental work for investigating mixing energy concept in cement operations. Therefore, our goal in this research was to formulate an experimental matrix covering various cement properties such as cement strength, rheology, thickening time, and porosity. More than 800 specimens were prepared for testing.
3. **Statistical analysis:** In order to firmly conclude impact of cement mixing variables, a robust statistical analysis is required. All of the experiments conducted for this research had a minimum of one repeat. UCS and UPV tests were conducted on three samples each so data can be used in the statistical analysis. We have performed ANOVA on all the UCS and UPV tests results.
4. **Empirical Model Development and Scale up Procedure:** Currently, the only model used for cement mixing is the API mixing energy theory. Based on our experimental data, we have developed empirical models for cement mixing power consumptions considering cement's non-Newtonian behavior. In addition, we present a scale up procedure using the developed models in this work.

1.6 Outline of Dissertation

This study is divided into ten chapters. Chapter 1 summarizes the motivation, goals, hypothesis and objectives of this dissertation. Chapter 2 presents literature review of studies related to mixing of cement slurries. This chapter reviews previous studies in field of cement mixing, well integrity and provides a solid background about key cement properties. In this chapter we show that there are contradictory statements throughout the literature on cement mixing phenomenon and impact of mixing energy on cement properties. Chapter 3 describes the fundamentals of design for experiments (DoE) and provides information on statistical analysis of the data. Experiments are backbone of this dissertation in evaluating key cement properties prepared under different mixing conditions. Chapter 4 describes the experimental techniques which include sample preparation, equipment and measurement procedures. Chapter 5 reports results of UCS and UPV testing for cement specimens prepared under different mixing conditions. We will show how significant differences in cement strength are observed when the specimens are prepared at same mixing energy. Further, we discuss impact of mixing time and shear rate on cement strength. Chapter 6 presents results of rheology and thickening time tests. Cement rheology and thickening time are key properties impacting cement pumping from surface to downhole. We will show how these properties are impacted when mixing conditions change. Chapter 7 presents results of NMR testing and porosity measurements to evaluate impact of cement mixing condition on porosity development and pore size distribution. Chapter 8 presents results of cement mixing experiments conducted by using yard type mixer similar to field mixer. In chapter 9, a review of mixing power consumption for Newtonian and non-Newtonian mixtures is

presented. We will show that there is a gap for similar literature in the oilwell cement mixing. Following similar procedures for non-Newtonian mixtures in chemical industry, we developed an empirical model for cement mixing power consumption correlating with cement strength. To our knowledge, this is the first attempt in the oilwell cement literature to evaluate cement mixing by its non-Newtonian flow characteristics. Furthermore, as a pioneer work, a scale up procedure for using results from cement laboratory mixing to field operations is presented. Chapter 10 presents final discussions, conclusions and recommendations from this work.

Chapter 2: Literature Review

2.1. Introduction

The objective of a well cementing operation is to achieve zonal isolation in order to restrict the movement of fluids and gases from one zone to another zone; and to bond and support the well casing at each interval. In recent years, the number of problems with well cement has been reported worldwide. Numerous papers have been written in the literature discussing potential problems and challenges for achieving effective zonal isolation. These include cementing challenges in highly deviated wells, deepwater offshore basins, HPHT wells, annular pressure build up, gas migration, and contamination and cement shrinkage in downhole environments (Sabins, 1990; Ravi et al., 1999; Sweatman, 2000; Stiles and Hollies, 2002; Rusch et al., 2004; Duan and Wojtanowicz, 2005, and Cowan, 2007). Additionally, considering long term integrity aspects, cements and downhole tubulars must be designed to withstand mechanical and chemical degradation because of corrosive downhole situations such as CO_2 and H_2S (Ahmed et al., 2015; Omosebi et al., 2017, and Elgaddafi et al., 2017).

Debonding problems and ineffective zonal isolation and a weak bond between the casing and the cement sheath and the cement sheath and formation may lead to short and long term leakage pathways (Teodoriu et al., 2013). In addition, stress cracking during the life of the well is another concern for wellbore cements (Figure 2.1). Since, several pressure and thermal loads are applied in a typical well, cement needs to withstand all these loads through time. These indicate the importance of an optimum cement design for each downhole application. The design includes rheological properties, thickening time, fluid loss, strength, and other mechanical and chemical properties.

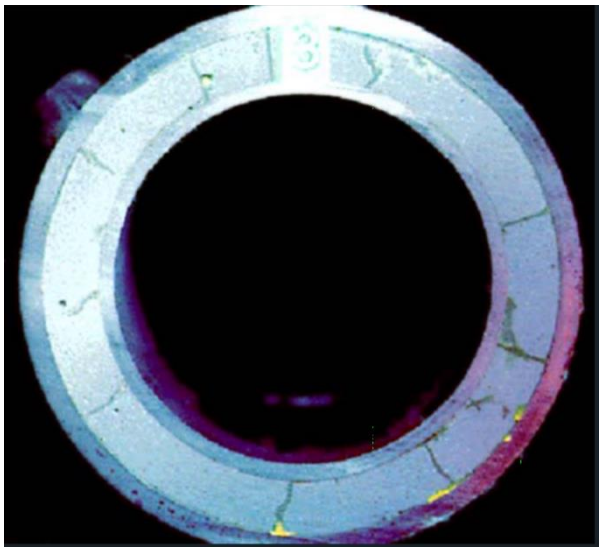

Figure 2.1 Stress cracking in brittle cement (courtesy of Halliburton, 2015)

There are often challenges in obtaining good zonal isolation with cement. In downhole conditions wellbore cement integrity is compromised with time. Other problems include mechanical failure, chemical attack, sustained casing pressure, shrinkage and leakage. Poor cement-formation bond may arise as a result of mud cake which compromises the purpose of well cement integrity. In the downhole environment, cement undergoes reduction in strength (strength retrogression) with time as it is exposed to high temperature and pressure. Such situations usually create a loss of zonal isolation which eventually affects the life span of wellbore (Gibson, 2011). Pressure and thermal dynamic loads occur during well's life are other factors triggering wellbore integrity problems (Teodoriu et al., 2010).

Sustained casing pressure is a critical problem in oilwell cementing. Rocha-Valadez et al., (2014) discussed the issue of sustained casing pressure in their research where data were analyzed and modeled for qualitative analysis of sustained casing

pressure. Sustained casing pressure occurs when pressure regenerates in the well after the pressure has been released. Poor bonding between cement and casing or between cement and formation gives rise to gas leakage which can eventually cause sustained casing pressure. Another issue that should be taken into consideration is the centralization of the casing string. If the string of casing is not centralized in the wellbore, the cement will flow into the areas that provide the lowest resistance. The path the flow takes is typically up the wider sides and this will result in areas that have no cement at all. Taking the path of least resistance is known as channeling. In order to keep this from happening, mechanical centralizers should be used in order to keep issues like this from happening. This was especially important in the Macondo well, where well design called for a specific type and number of centralizers, and in this case, the incorrect centralizer and a lower number of centralizers were used (Graham et al., 2011).

Furthermore, properties of the mixed cement in the field often is not what observed in the laboratory which indicates mixing as another key factor that needs further research and consideration. Although API standards govern the mixing procedures for oilwell cements, it is either difficult to follow specifics in field conditions or sometimes it is great challenge to keep consistent mixing procedures from one laboratory to field because of scale differences.

2.2. Cement and Wellbore Integrity

Wellbore integrity problems and potential leakage pathways can be classified into two categories as shown in the Figure 2.2. The primary risks are more related to poor cement job and the secondary category is more related to the chemical reactions and tensile stresses occurring in the cement (Nygaard et al., 2011; Watson and Bachu, 2009;

Celia et al., 2004). Even after a successful cement sheath is created, the integrity of the well can be compromised by secondary sources such as mechanical (pressure) and thermal loads imposed on the well (Nygaard et al., 2011). Changing fluid density for completion and stimulation can also induce mechanical loads on the inside of the casing, which requires consideration for integrity evaluation. Changes in temperature as a result of injection, or reheating of the wellbore during well shut-ins can impose thermal stresses. Temperature changes in the wellbores have been noted to cause long-term well-integrity problems by creating fractures and fissures in the cement (Milestone and Aldridge 1990; Shen and Pye 1989). Furthermore, corrosion of the casing or chemical reactions of the cement can also create near-wellbore leakage pathways. All of these leakage pathways compromise the wellbore integrity.

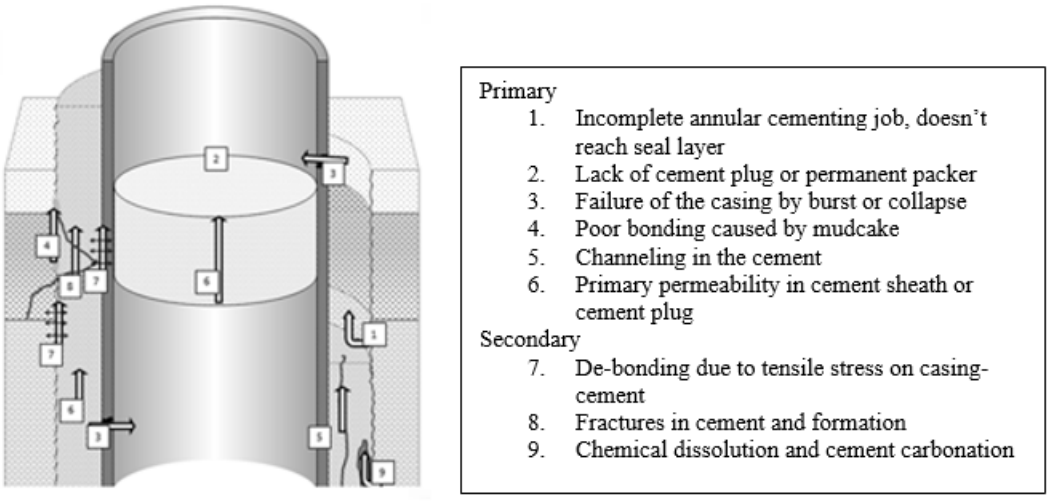

Figure 2.2 Potential leakage paths in well construction (modified after Celia et al., 2004)

The USEPA (US Environmental Protection Agency) and other resources have reported incidents of ground water pollution due to leakages in casing and failures in well construction components (USEPA, 2011). Several other incidents also reported lack of pressure barriers inside the wellbore, where waste water and natural gas spew into the air (USEPA, 2011). Several instances of natural gas migration have been noted. USEPA report on coalbed methane indicated that methane migration in the San Juan Basin was mitigated once abandoned and improperly sealed wells were plugged. The same report found that in some cases in Colorado, poorly constructed, sealed, or cemented wells used for a variety of purposes could provide leakage paths for methane into surface water aquifers.

In order to understand how leakage pathways can be created in a cement column, one needs to consider dynamic conditions in the well. As the well is put into production, the stress in the formation around the well changes, which changes the stress field on the near wellbore (Nygaard et al., 2011). Thermal loads can also increase the risk of debonding and tensile failures in cement. These will open new flow pathways for gas. Another situation where thermal effects can dominate is hydraulic fracturing operations in high temperature environments (HT). Wellbore temperature variations occurring between stimulation and production operations can be extreme, this will impose thermal loads on the wellbore wall. Furthermore, thermal expansion from hydrocarbon production can impose cyclic thermal loads on the near wellbore, this is especially critical in shallower formations (Heathman and Beck, 2006). In addition, one need to consider cement chemical reactions and process of cement hydration. Therefore, in the next section, a review of cement chemistry and hydration is presented.

2.3. Cement Chemistry and Interparticle Reactions

The cementing process begins when the cement slurry is formulated in the laboratory. Portland cement is the most common cement used due to its low cost and widespread availability. The Portland cement slurry begins with the base material, which is typically comprised argillaceous and calcareous rock, such as limestone, shale, or some type of clay. The base rock is heated to temperatures as high as 3000 °F, which allows for the raw material to form into what is called a clinker. The clinker is then ground to the specific size, which is determined by the grade of cement being made. Water is added in order for the cement to become a slurry. The amount of water that is added to the cement varies with the size of the particles. This is a very important relationship to consider because if there is an excessive amount of water mixed with the cement particles, water can be seen on top of the cement and pockets of water can form inside the cement. The different classes of Portland cement can be seen in Table 2.1

Cement solid particles include cement powder and several of other additive such as dispersants, polymers, fluid loss, weight agents and other special purpose additives. Dry cement powder and additives are usually pre-blended and transported to the wellsite where the liquid and solid are mixed (Sweatman, 2015). The Portland cement powder includes several oxides and silicate and aluminum phases as outlined in Table 2.2:

Table 2.1 Portland Cement Classes (Nelson and Gulliot, 2006)

Class	Depth (ft)	Temperature °F	Purpose
A	0-6000	80-170	Used when no special needs are required
B	0-6000	80-170	Used for conditions requiring moderate to high sulfate resistance
C	0-6000	80-170	Used for conditions requiring high early strength
D	6000-10000	170-290	Used where high temperatures and pressure are found
E	10,000-14,000	170-290	Used where high temperatures and pressure are found
F	10000-14000	230-320	Used where extremely high temperatures and pressure are found
G	0-8000		Basic well cement that can be altered for use in wide range of depths and temperatures
H	0-8000		Basic well cement that can be altered for use in wide range of depths and temperatures
J	12,000-16,000	Greater than 230	Used where extremely high temperatures and pressure are found. Can be altered to cover wide range of depths and temperatures

Table 2.2 Typical Mill Run Analysis of Portland cement

Oxide	**Class G wt.%**	**Class H wt.%**
Silicon Dioxide, SiO_2	21.7	21.9
Calcium Oxide CaO	62.9	64.2
Aluminium Oxide Al_2O_3	3.2	4.2
Iron oxide Fe_2O_3	3.7	5
Magnesium Oxide MgO	4.3	1.1
Sulfur Trioxide, SO_3	2.2	2.4
Sodium Oxide		0.09
Potassium Oxide K_2O		0.66
Total alkali as Na_2O	0.54	0.52
Loss on ignition	0.74	1.1
insoluble residue	0.14	0.21
Phase Composition		
C_3S (Tri-Calcium Silicate)	58	52
C_2S (Di-Calcium Silicate)	19	24
C_3A(Tri-Calcium Aluminate)	2	3
C_4AF (Tetra-Calcium Aluminoferrite)	11	15

Note. Adapted from *Petroleum Engineering Handbook Vol 2 Drilling Engineering*, p. 384 by Lake and Mitchel, 2006, Texas: SPE

Cement mixing involves both mechanical and chemical processes. Mechanical process is related to deflocculation. The chemical process is more complicated and occurs shortly after cement powder exposed to liquid. Once cement is exposed to water, hydrates form. The hydration component of silicate phases is calcium hydrosilicate (CSH). This phenomenon can be explained by following chemical reactions of tricalcium silicate (Ca_3SiO_5) or C_3S (Barret et al., 1983):

$$Ca_3SiO_5 + 3H_2O \rightarrow 3Ca^{2+} + 4OH^- + H_2SiO_4^{2-}$$

With more water in the solution, we will have (Gauffinet-Garrault, 2012):

$$C/SCa^{2+} + 2(C/S - 1)OH^- + H_2Sio_4^{2-} \rightarrow CSH$$

The major components of cement crystalline phases are:

- C_3S-Tri-Calcium Silicate
- C_2S-Di-Calcium Silicate
- C_3A-Tri-Calcium Aluminate
- C_4AF-Tetra-Calcium Aluminoferrite

Different than tricalcium silicate, hydration of C3A is fast. This fast reaction dissipates hydroaluminum precipitates (C_3AH_6). This rapid formation of calcium hydroaluminate causes premature stiffening of slurry often described as flash set (Gauffinet-Garrault, 2012). In first few seconds of cement exposure, tricalcium silicates come into contact and form a connected structure. As more CSH precipitates, the structure becomes more reinforced which makes it very difficult to break the gel (Figure 2.3, Nonat and Mutin 1992). The inability to destroy CSH structures once they formed even by mechanical stress applied during mixing. In other words, the process is irreversible. Hydration kinetics are primarily dominated by silicate hydration since it is the primary cement constituent. Several hydration stages are outlined which are illustrated in the Figure 2.4.

These stages include dissolution (stage 1), induction (stage 2), acceleration (stage 3), deceleration (stage 4), and diffusion (stage 5) (Nelson and Guillot, 2006). The initial period of hydration is characterized by dissolution and rapid reactions between C_3S and water that begin immediately upon wetting. After the first stage there is a significant slowdown in the reactions often labeled as dormant or induction time before the rate rapidly increases. Early cement strength is impacted by tricalcium silicate whereas the final strength of cement is impacted by dicalcium silicate (Fink, 2015). Gutteridge and Dalziel (1990) studied hydration behavior of cement for 100 days. Their studies showed logarithmic behavior of hydration reaction plot with time except for C_2S. During the first 40 days, the majority of reactions occur as shown in the Figure 2.5. It can be observed that hydration in the first few days is very active where many of cement phases have steep hydration curves.

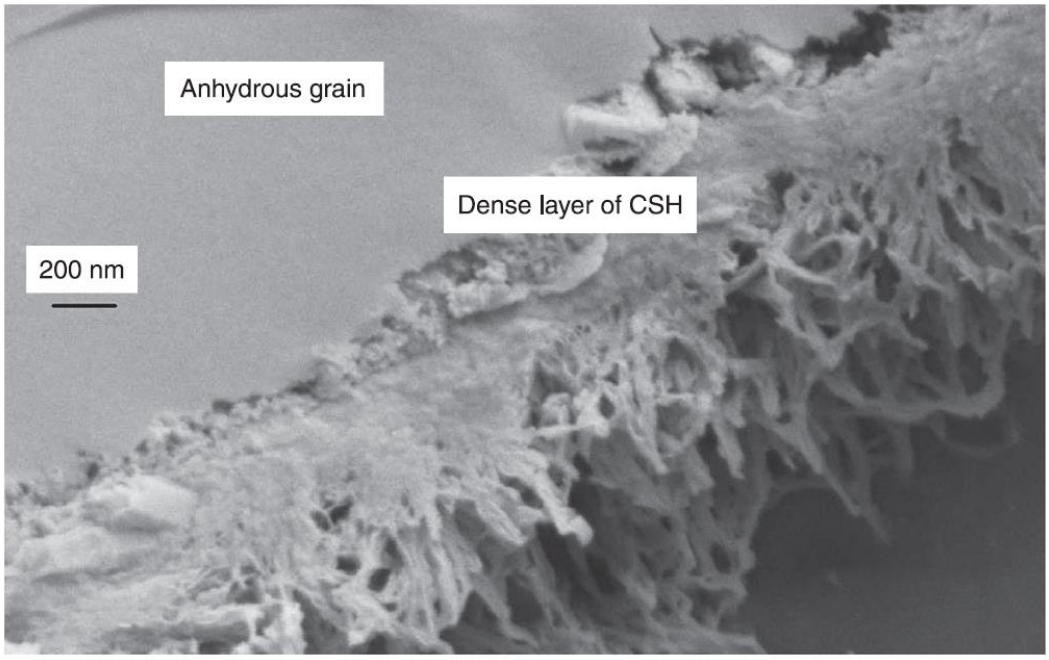

Figure 2.3 SEM image of tricalcium silicate hydrated grain and CSH. SEM image shows a dense layer of CSH around the anhydrous grain. This dense layer corresponds to the hydrate layer formed during the first stage of hydration (from Gauffinet-Garrault, 2012)

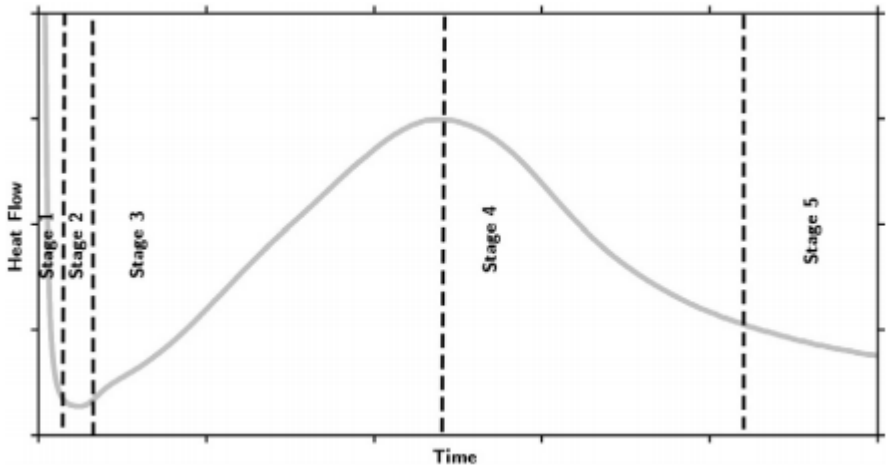

Figure 2.4 Heat flow versus hydration time in cement. Five stages of hydration can be seen. These stages include dissolution (stage 1), induction (stage 2), acceleration (stage 3), deceleration (stage 4), and diffusion (stage 5) (Scrivener and Nonat, (2011))

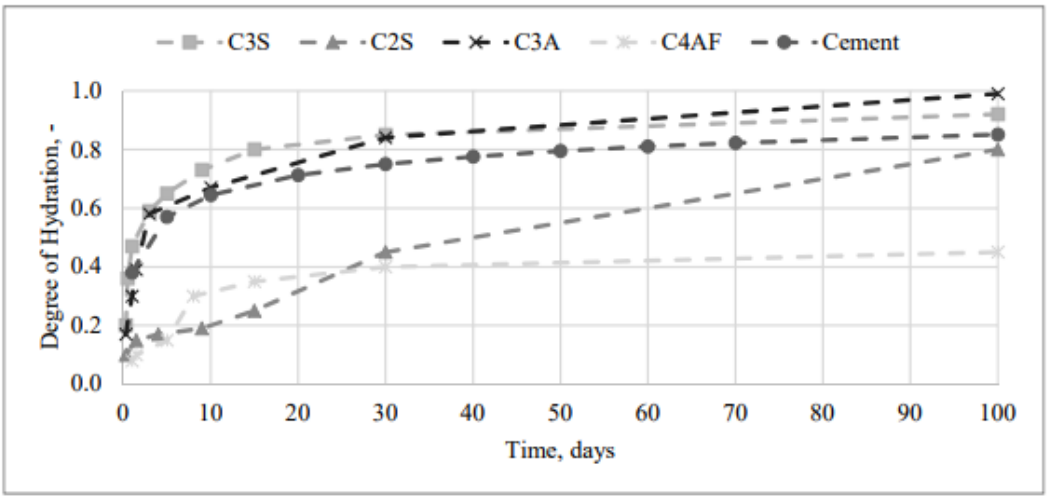

Figure 2.5 Cement hydration with time. The initial period of hydration is characterized by dissolution and rapid reactions between C3S and water that begin immediately upon wetting (Gutteridge and Dalziel (1990))

2.4. Cement Rheological Behavior

In this section we will review some of the important cement properties such as its non-Newtonian rheological behavior. To better understand why cement has non-Newtonian behavior, one must consider the effects that calcium ions have in cement structure. "The predominant attractive forces between the cement particles in the presence of calcium ions create a structured network between the particles which creates a yield stress" (Gauffinet-Garrault, 2012). Unlike Newtonian fluids, in Non-Newtonian fluids, the ratio of shear rate to shear stress is not constant. The apparent viscosity changes with flow and shear rate. Non-Newtonian behavior arises from conditions where there is suspension of asymmetrical elements caused by shape or orientations. In addition, objects that develop mutual interaction changing with flow show this type of behavior as well (Coussot, 2012). One example can be elangated objects where they normally aligned to move in flow direction which on average keep their position with flow direction. In polymer fluids, polymer chains are stretched more along flow direction and as a result the apparent viscosity of the fluid is generally lower. Where apparent viscosity decreases with shear rate, the material will have shear-thinning behavior. In these types of materials, alignments develop rapidly and depend significantly on shear rate. For thixotropic fluids, it takes time for alignment to develop thus the apparent viscosity for a specific shear rate varies in time.

For shear thinning:

$$\frac{d\tau}{d\gamma} \prec 0 \quad \text{.....(2.1)}$$

$$\frac{d\tau}{dt} \neq 0 \quad \text{.....(2.2)}$$

τ is the shear stress and γ is shear rate. Shear-thickening fluids may have opposite behaviour compared to shear-thinning fluids which can be described as:

$$\frac{d\tau}{d\gamma} \succ 0 \quad \text{.....} \quad (2.3)$$

Generally, for shear thickening fluids, the apparent viscosity does not significantly change untill it reaches a critical shear rate value. These materials generally have very complex behavior. Apparent viscosity is defined as:

$$\mu_a = \frac{\tau}{\gamma} \quad \text{.....} \quad (2.4)$$

The equation 2.4 shows that apparent viscosity is a function of shear rate (not constant). The behavior becomes very complex when in fast flow or turbulent conditions.

2.4.1. Yield Stress Fluids

Yield stress fluids include industrial mixtures that behave solid under some conditions and liquids under other circumstances. These materials are solid when stress less than a critical value is applied (Coussot, 2012). As the stress increase above a critical value, they behave as liquids and flow. Some examples for these materials include gels, clay suspension, sledges, creams and cement. Some materials such as cement display a time dependent behavior, for instance they show thixotropic behavior at some time and other behaviors different times. This type of materials behaves solid mostly with elastic or viscoelastic characteristics when stresses are less than the yield value and liquid when yield stresses are exceeding. In existing rheological models, Herschel–Bulkley model is commonly used for these materials (Nelson and Guillot, 2006. This model can represent the material behaviors ranging from very slow flow (low shear rates) to rapid flow.

2.4.2. Cement Rheology

Rheological properties of cement slurries are very complex due to their time dependent Non-Newtonian behavior. Cement slurries are tested using shear stress and shear rate to quantify their flow properties (Nehdi and Rahman 2004). They are tested because composition and wellbore conditions vary, and these parameters are pivotal in determining their flow properties. The testing procedure determines yield stress, viscosity, and how the slurry reacts to shear stress (Shahriar and Nehdi 2012). Yield stress is a property of cement at where shear stresses lower there is no flow and it behave as a solid (Figure 2.6). Since cement is a mixture of solids suspended in water, physically the yield point is equivalent to the slurry's internal friction that must be overcome for it to flow (Shahriar and Nehdi 2012).

2.4.3. Rheological Models

There are four major rheological models that are used in the oil and gas industry; Newtonian, Power Law, Bingham Plastic, and Herschel-Bulkley (Nelson and Guillot, 2006). As stated a Newtonian fluid follows a linear relationship between shear stress and shear rate. The viscosity is the slope of the line passing through the origin. Understanding the rheology of a cement slurry is essential in designing a job for proper placement, mud removal, and determining the pump rate needed to achieve the design requirements (Shahriar and Nehdi 2012). The parameters needed or measured in the design process are pressure and temperature characteristics at wellbore conditions, shear stress and rate flow curve, plastic and apparent viscosities, and the yield point (Shahriar and Nehdi, 2012; Nehdi and Rahman, 2004). Figure 2.6 shows these different flow curves in relation to each other.

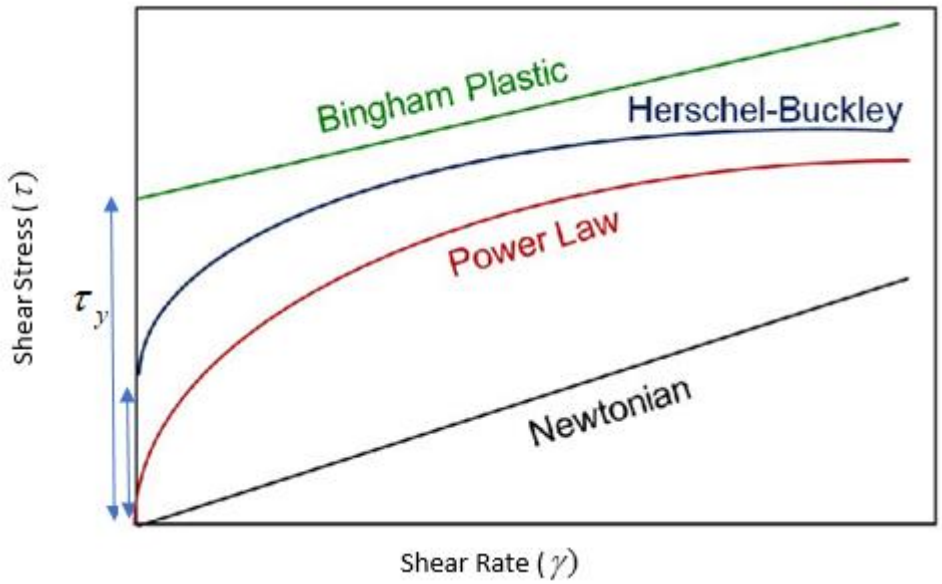

Figure 2.6 Flow curves of interest used in the petroleum industry. Newtonian fluid follows a linear relationship between shear stress and shear rate. The Bingham plastic model does take into account a fluid having a minimum shear stress needed to make it flow, a yield point (τ_y) (Nelson and Guillot, 2006)

The yield point can be seen in Figure 2.6 for both the Bingham Plastic and Herschel-Bulkley models while the Power Law and Newtonian models go through the origin and have no yield point. Table 2.3 shows the flow equations for each model.

Table 2.3 Rheological Model mathematical expressions where is shear stress (Pa), γ˙ is shear rate (1/s), µp = plastic viscosity (cp or Pa s), η = viscosity (cP or Pa s), k = consistency index (lbf.s/ft^2 or Pa. s), n = Power Law Index, τ_y = yield stress (Pa), and c = regression constant; created from (Nelson and Guillot, 2006)

Rheological Model	Equation	Reference
Newtonian	$\tau = \eta\dot{\gamma}$	Newton (1687)
Power Law	$\tau = k\dot{\gamma}^n$	Ostwald (1925) and de Waele (1923)
Bingham Plastic	$\tau = \tau_y + \mu_p\dot{\gamma}\ if\ \tau \geq \tau_y, \dot{\gamma} = 0\ if\ \tau \leq \tau_y$	Bingham (1916)
Herschel-Bulkley	$\tau = \tau_y + k\dot{\gamma}^n$	Herschel and Bulkley (1926)
Modified Bingham Plastic	$\tau = \tau_y + \mu_p\dot{\gamma} + c\dot{\gamma}^2\ if\ \tau \geq \tau_y, \dot{\gamma} = 0\ if\ \tau \leq \tau_y$	Linear fit of Herschel-Bulkley & Bingham Plastic

2.4.3.1 Bingham Plastic Model

The Bingham plastic model does take into account a fluid having a minimum shear stress needed to make it flow, a yield point (τ_y) and a non-zero viscosity at zero shear rate. Furthermore, inspecting the equation in Table 2.3 and the curve Figure 2.6, it can be seen that this model has a linear relationship between the shear stress and shear rate. That means that this model can only give proper results if viscosity of the cement has a linear relationship with shear rate and does not have any curvature to it.

2.4.3.2 Power Law Model

The Power law is a non-Newtonian model as can be seen in Figure 2.6. This model does not have a yield point and therefore does not require a minimum shear stress to be applied for the fluid to flow. The power law model describes a fluid in which shear stress and shear strain form a straight line on a log-log plot. The Power law model is often used to monitor the suspension characteristics and calculate the pressure loss of the fluid in the annulus. The rheological parameter n and K can be calculated using formulas below and readings from a viscometer. θ is the dial reading at specific rpm (N).

$$n = \frac{\log(\frac{\theta_{600}}{\theta_{300}})}{\log(\frac{N_2}{N_1})} \tag{2.5}$$

$$K = 500\frac{\theta_{300}}{(511)^n} \tag{2.6}$$

2.4.3.3 Herschel-Bulkley Model

The Herschel-Bulkley model has a yield point. It also incorporates a non-linear relationship, like the power law, for shear stress and shear rate. One issue is that it is a three-parameter model and these values will have to be extrapolated from experimental

data. For the oil and gas industry, the vast majority of the information on rheological properties from cement is obtained from the coaxial cylinder viscometer measurement which has been shown to be affected by wall slip and inconsistencies in the slurry (Nelson and Guillot, 2006). Further complicating this issue is the standard 6-speed rheometer has rotational velocities that yield inconsistent results. Moreover, the Herschel-Bulkley model combines the features of the Newtonian and Bingham Plastic, and Power Law models (De Larrard et al., 1998). In practice, yield point is equal to the 3 rpm reading. The yield stress, n and K can be calculated using equations listed below.

$$\tau_y = 2\theta_3 - \theta_6 \quad (2.7)$$

$$n = 3.322 \log\left(\frac{\theta_{600} - \tau_y}{\theta_{300} - \tau_y}\right) \quad (2.8)$$

$$K = 500\frac{\theta_{300} - \tau_y}{(500)^n} \quad (2.9)$$

2.5. Cement Mixing Phenomenon

In order to better understand cement mixing phenomenon, we must first understand what a cement slurry is made of and how different dry particles react with water. A cement slurry is made of liquid and solid phases. Depending on applications, liquid phase is made of either fresh water or sea water. This will depend on cement job requirements and applications (onshore or offshore). Before deciding on type of water, required setting time must be established from laboratory testing since brackish water will act more as an accelerator.

In addition to water composition, the ratio of solids to liquid and interparticle reaction have strong impact on rheological properties of cement and its thickening time. The solid volume fraction (SVF) can range from 0.2 to 0.7 (Nelson and Gulliot, 2006). Higher SVF slurries are associated with higher viscosity. The optimum SVF is always a

compromise and depends on several factors such as well depth, required density, well temperature and desired strength and rheological properties. A high viscous cement is not desirable if cementing a depleted section where risk of loss circulation exists. Excessive water in the slurry (low SVF), has a risk of forming high free water, annular gas leakage and low cement strength. Free water is defined as water that is not needed by the cement for reaction. When flow stops, free water separates out to the top of the cement column.

2.5.1 Theory of Mixing Energy for Oilwell Cements

A theory for mixing energy was developed and proposed by Oraban et al. (1986). It was further used and emphasized in others work such as Hibbert et al., 1995, and Vidick et al., 1990. The formula of mixing energy using an API Warring blender is presented as:

$$\frac{E}{M} = \frac{k \times \rho \times \omega^2 \times t}{\rho \times V} = \frac{k \times \omega^2 \times t}{V} \quad \text{.....(2.10)}$$

Based on this equation, mixing energy (E/M) has a direct relationship with shear rate (ω), mixing time (t), and is inversely related to volume (V). k, an empirical constant was experimentally found to be 6.4 10^{-9} N.m/kg.m^{-3}/rpm and ρ is density. Appendix A shows the derivation for API formula based on mechanical power used in the mixing process.

One of the major challenges with the concept of API mixing energy formula is relying on characteristic of Newtonian substances. Cement is a non-Newtonian material which has a non-linear shear stress and shear rate behavior. This non-linear behavior has several implications for the mixing process. In other words, cement rheology can strongly impact its mixing.

The major application of this theory was to produce consistent properties for the slurries prepared in the lab and field. Orban et al., (1986) suggested that the properties of cement slurries such as rheology, fluid loss and strength can change with mixing energy.

They further related mixing to the deflocculation process in which mechanical stresses during the mixing process are found to be critical.

Although, Orban's work was ground breaking in acknowledging the mixing energy concept, others were in disagreement with the concept and application of this theory. For instance, Padgett, (1996) highlighted the importance of shear rate as a phenomenon impacting properties rather than mixing energy (Saleh and Teodoriu, 2017). He showed laboratory experiments and field observations highlighting the effects of shear rate of the mixing system rather than the total energy. He further showed that slurries prepared under high shear rate may have different properties compared to slurries prepared in low shear rate. In addition, his results showed some cement properties such as rheology, free water and thickening time change by mixing energy only for some of the prepared samples. Furthermore, thickening time slightly is affected by the mixing energy (Figure 2.7).

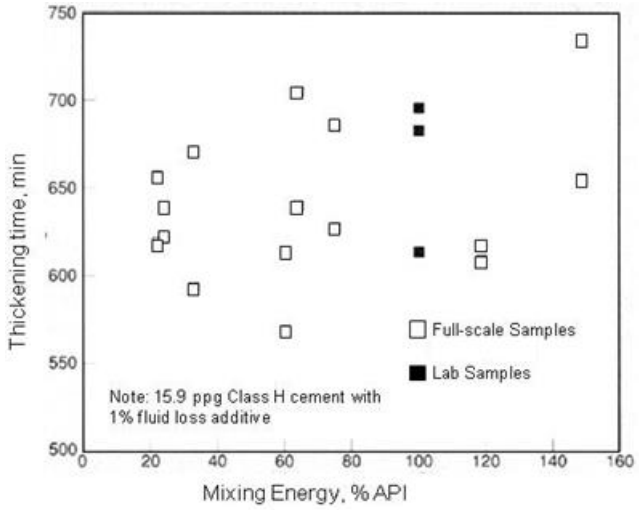

Figure 2.7 Thickening time vs. mixing energy (Padgett, 1996). Thickening time results slightly responsive to mixing energy. No clear correlation was found between mixing energy and slurry properties.

Furthermore, it was observed that the properties changed more significantly when different mixing equipment was used rather than with different mixing energies. This was

more apparent for free water results which was three times higher in the field conditions compared to laboratory tests. Furthermore, it was found that compressive strength did not change with changes in the mixing energy. His work concluded that there was limited application of the mixing energy concept. These results contradicted Orban et al., (1986) work. Padgett explained differences in laboratory and field results due to extremely different shear rates between laboratory and field conditions. The shear rate of centrifugal pumps in the operational condition is generally less than 2,000 Sec^{-1} whereas the laboratory equipment relying on API standards generates more than 30,000 Sec^{-1}. He further recommended a new equation for mixing energy which is directly related to the shear rate:

$$\frac{E}{M} = \mu \times t \times \gamma \quad \text{.....(2.11)}$$

Where μ is the viscosity and γ is the shear rate. The concluding remark from using this new equation according to Padgett, 1996 is "if *the residence time is increased, a low shear device (jet mixer, batch mixer) can exert same amount of mixing energy into a slurry as a high-shear device (laboratory blender). However, because it is shear rate that is more important, the properties will not necessarily be the same*."

Alternatively, another equation is provided for mixing energy by using field scale mixing equipment. The equation is developed based on summing the mechanical work provided by flow through mixing and pumping system (Viddick et al., 1990; and Hibbert et al., 1995)

$$\frac{E}{M} = \sum \frac{P \times t}{\rho \times V} \times 2.35(\frac{kJ}{kg}) \quad \text{.....(2.12)}$$

Where

P is the power in horsepower

t is the residence time of slurry in the mixing device (min)

V is the volume (bbl)

ρ is the density (lb/gal)

2.35 is the conversion factor to kJ/kg

Vidick (1989) highlighted the dual importance of chemical and physical phenomena and deflocculation as crucial steps in the mixing process. In addition, he showed time to be an important factor in slurry yield strength where a longer mixing period increases the yield value. Figure 2.8 shows the dual influence of mixing time and rotational speed (rpm). His results indicated mixing time to be more critical than the shear rate. Figure 2.8 represents consistometer time versus yield value at two different rates of 6000 and 12000 rpm at 15 and 50 seconds. Yield value for both of slurries at 50 seconds time is higher than samples at 15 seconds time regardless of shear rate used.

He further explained his observations due to the growth of hydrates during a longer mixing period. These hydrates will absorb more dispersants over time, therefore increases the yield value. In contrast to Padgett, (1996), Vidick, (1989) showed that thickening time is responsive to mixing energy for measurements conducted at 65 ^{o}C (150 ^{o}F) in an atmospheric consistometer. Although, once deflocculation occurs, there is no further change in thickening time by increase in mixing energy (Figure 2.9). It is worth mentioning that thickening time tests under laboratory conditions were not reported by Padgett, (1996). Therefore, it is difficult to confirm whether both experiments were conducted under similar conditions, acknowledging the fact that temperature has a significant effect on thickening time.

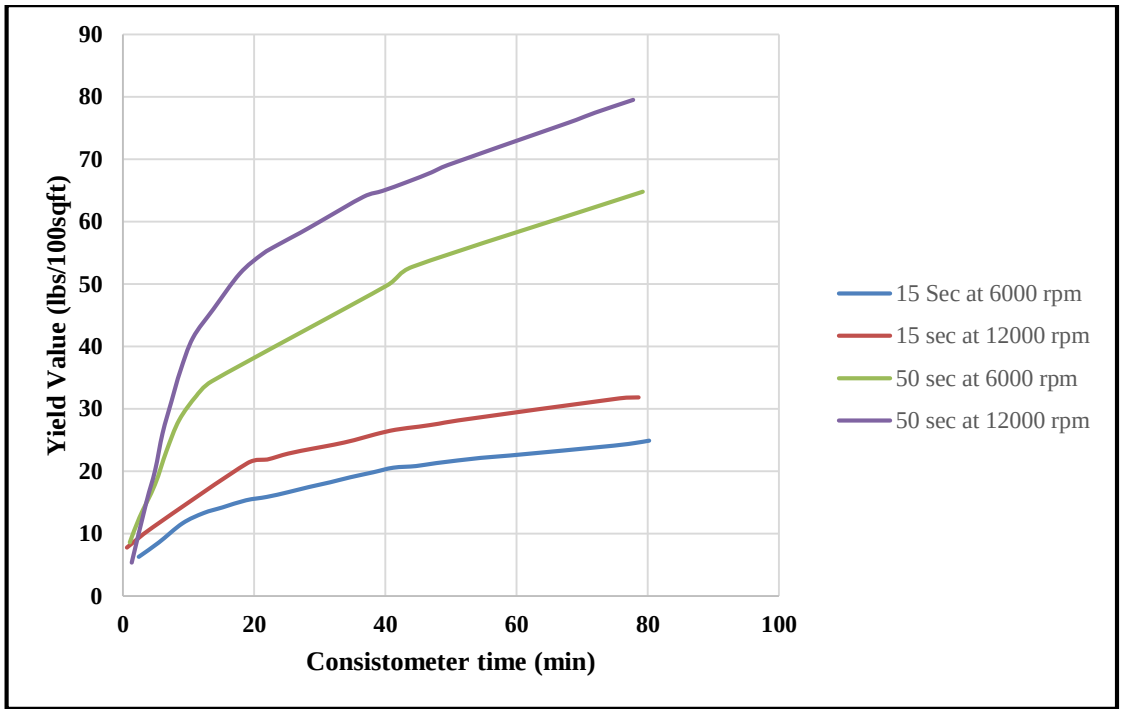

Figure 2.8 Effect of mixing time and rotational speed on yield value. Yield value for both of slurries at 50 seconds time is higher than samples at 15 seconds time regardless of shear rate used (Vidick, 1989)

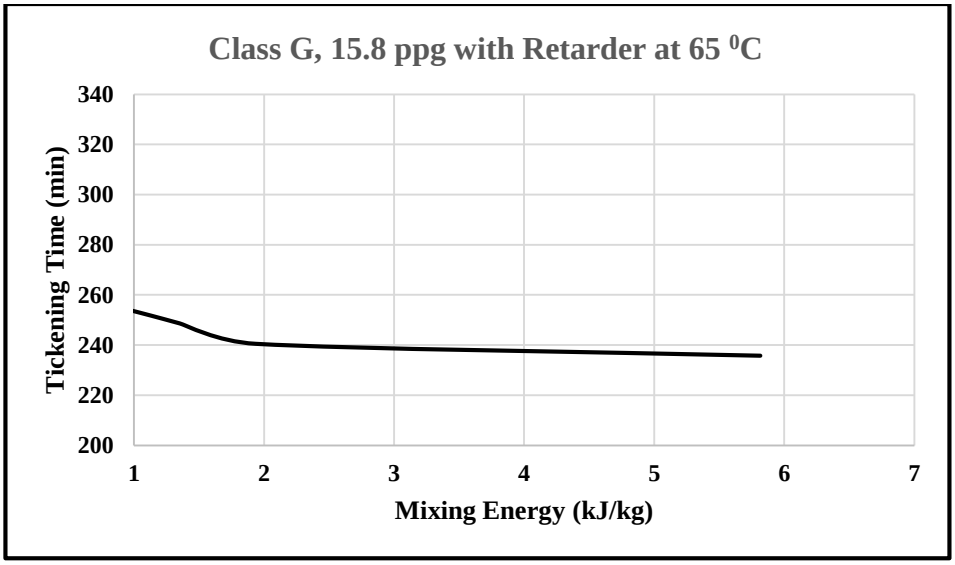

Figure 2.9 Effect of mixing energy on thickening time. Results show that once deflocculation occurs, there is no further change in thickening time by increase in mixing energy (Vidick, 1989)

Heathman et al., (1993) studied the effects of mixing energy on cement slurries using field equipment and coil tubing. They summarized that insufficient mixing energy

imparted to a cement slurry by a mixer at the point of cement-water contact can have definite effects on a cement slurry. His results indicated erratic changes in cement properties due to the lack of adequate cement particle wetting efficiency in the mixing time. As a result, he recommended a minimal energy consumption for wetting cement particles in order to ensure consistent cement properties. In addition, he concluded that there is no significant difference in cement properties from the energy added through batch mixer or pumped through coil tubing. His work further implied that "slurry performance is not affected by batch size, mixing pumps, or pumping through coil tubing".

Vorkin et al., (1993) presented a study on slurry properties of mixtures pumped through coil tubing. This study also included investigations of filter cake generated by squeeze. The study also highlighted the importance of shear energy when plastic viscosity, yield point, filter cake height, fluid loss and slurry consistency had stabilized after reaching a certain level of shear energy. Figure 2.10 shows rheological properties measured for a co-polymer system at 170^{o} F for shear rate at 12000 rpm. This indicates the effect of shear energy on these properties up to 120 seconds, whereas there were no changes in the measured properties afterwards. It should be mentioned that these measurements were conducted for mixture slurries including either latex or co-polymer system and these results may not be accurate for slurries with other additives.

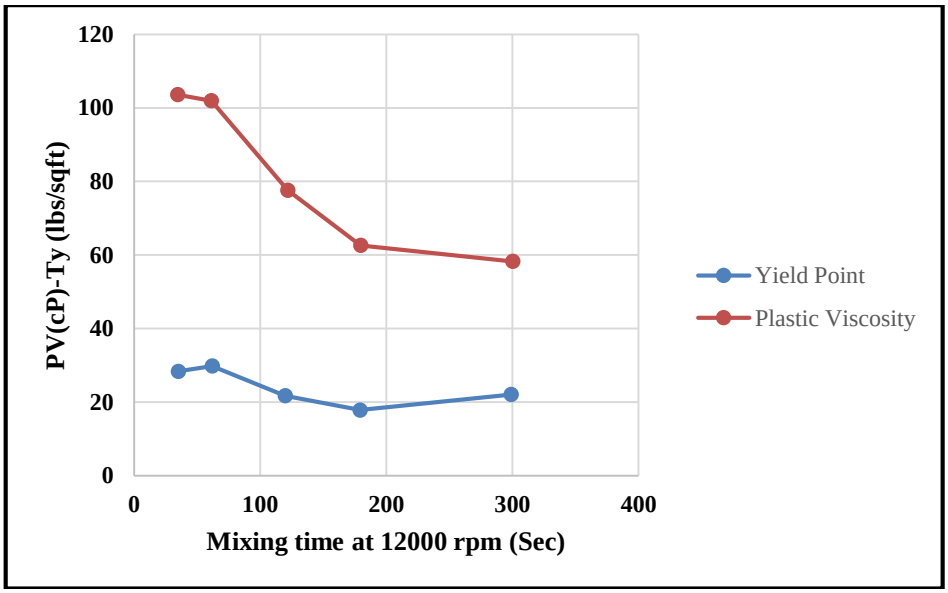

Figure 2.10 Rheology measurements conducted for a co-polymer system at 170ºF. This indicates the effect of shear energy on these properties up to 120 seconds, whereas there were no changes in the measured properties afterwards (Vorkin et al., 1993)

Hibbert et al. (1994) studied the effect of mixing energy during batch mixing of cement slurries. He reported erratic differences between properties under conventional laboratory and operational conditions. The study concluded by that mixing energy was a parameter in cement design, in addition to pressure and temperature. Furthermore, it recommended mixing at API mixing energy level (5.9 E/M) in order to achieve consistent properties. Their results showed that high levels of mixing energy are detrimental to the thickening time (Figure 2.11). It was also noted, that a very short thickening time was reported when the mixing energy exceeded the API recommended level (5.9 KJ/Kg). For the same slurry, the thickening time shortened to less than four hours at a mixing energy of 17.7 kJ/Kg. It must be noted that two slurries (slurry 1 and slurry 2) used in the batch mixing and each had different additives. Slurry 1 had retarder, fluid loss additive and dispersant while slurry 2 had only fluid loss additive and dispersant. This explains shorter thickening time for test results by slurry 2. Except the first point on the graph (Figure

2.11) which mixed in the laboratory, rest of samples were captured through batch mixing in the yard. The slurries were pumped through centrifugal pump and samples captured at different times. Study further implied that since in laboratory condition all the energy is applied to all the volume, it resembles a continuous mix process. Hibbert et al., (1994) also showed importance of mixing time compared to mixing energy. As the mixing time increased during yard mixing tests, less difference between thickening time was observed.

In a recent study, Teodoriu et al., (2015) investigated several aspects of cement mixing specifically differences in cement rheology from laboratory to field mixing. Authors discussed the rheological properties of three cement slurries using three different mixing processes (field, API and a low shear time dependent method (LSTD)) (Figure 2.12). As shown in the Figure 2.12, slurry prepared under the field conditions is thicker than the one prepared using a laboratory API Warring blender. Teodoriu et al., (2015) mentioned that the field slurries will not have the same surface area as the laboratory one. These changes in the surface area explain the difference in rheological properties, thickening time and compressive strength in laboratory mixing. It is believed that smaller particles will create more surface areas, therefore the hydration process will be accelerated which can cause a shorter thickening time.

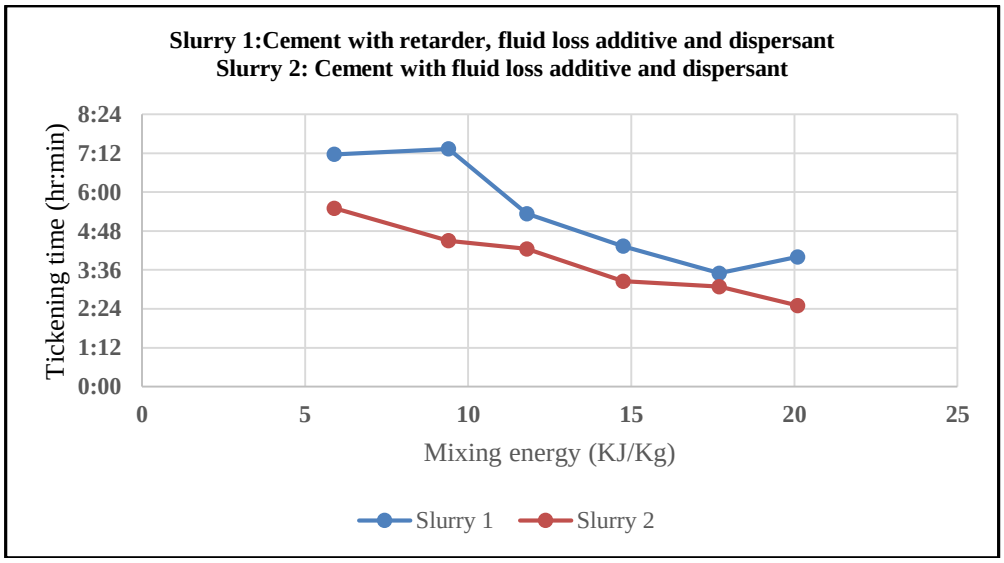

Figure 2.11 Effect of mixing energy on thickening time of different slurries from yard mixing. Results showed that high levels of mixing energy are detrimental to the thickening time (after Hibbert et al., 1994)

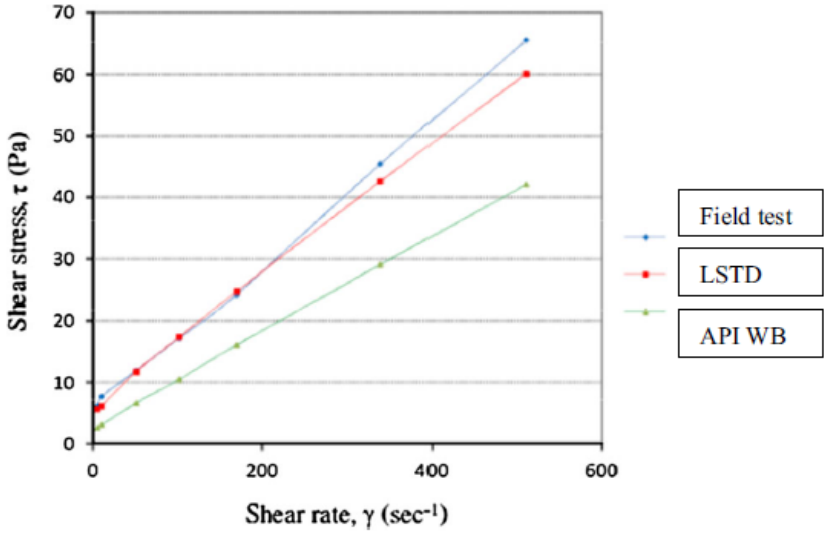

Figure 2.12 Rheological behavior of cement slurries prepared using three different methods. Slurry prepared in the field conditions is thicker than the one prepared by laboratory API Warring blender (Teodoriu et al., 2015)

Although many of the previous authors highlighted the importance of mixing energy on slurry properties, there are still a number of studies that do not fully agree with this concept. A study conducted by Hodne et al., (2000) investigated the effects of time and mixing energy on the rheological behavior of the cement slurries, using three different types of propeller blades and one low shear rate Hobart mixer:

1. Waring Blender propeller blade (WB blade)
2. Hard Metal blender (HM blade)
3. Short-winged propeller blade
4. Hobart mortar mixer (used for measuring mixing energy at lower shear rate)

Experiments were conducted using different slurries of class G and P30 Portland cement. A significant difference in the mixing energy levels was observed, mainly due to the different blade size. Additionally, differences in the mixing energy levels were observed for P-30 and Class G cement. The mixing energy for P30 slurry was greater when using WB and HM blades; however, there was no difference for the shorter winged blade type (Table 2.4).

Table 2.4 Measured mixing energies for class G and P30 Portland cement using three different types of blender (Hodne et al., 2000)

Propeller type cement slurry	Class G (kJ/kg)	P-30 (kJ/kg)
WB-blade	5.6	7.6
HM-blade	3.9	4.6
Short-winged propeller blade	1.8	1.8

The differences in mixing energy for P-30 and class G slurries were explained as due to different particle sizes and surface areas. The P-30 cement has finer particle sizes compared to the class G cement; therefore, it appears natural for the P30 cement to have a larger viscosity compared to class G slurries. This indicates that the concept of mixing energy must be cautiously considered since “to mix a more viscous slurry will require

more energy than mixing a less viscous slurry." Similar observations were made for torque measurements, where the P-30 cement showed higher torque values from the beginning, which indicates a higher input of mixing energy. The value of critical consistency (30 Bc, Bc=Bearden units of consistency) was reached after 285 minutes for the class G cement, and it was above 30 Bc for the P30 slurry from the beginning. The measured gel strength of class G and P-30 is shown in Figure 2.13. The results indicate a higher rate of gel formation for the P-30 slurry compared to class G.

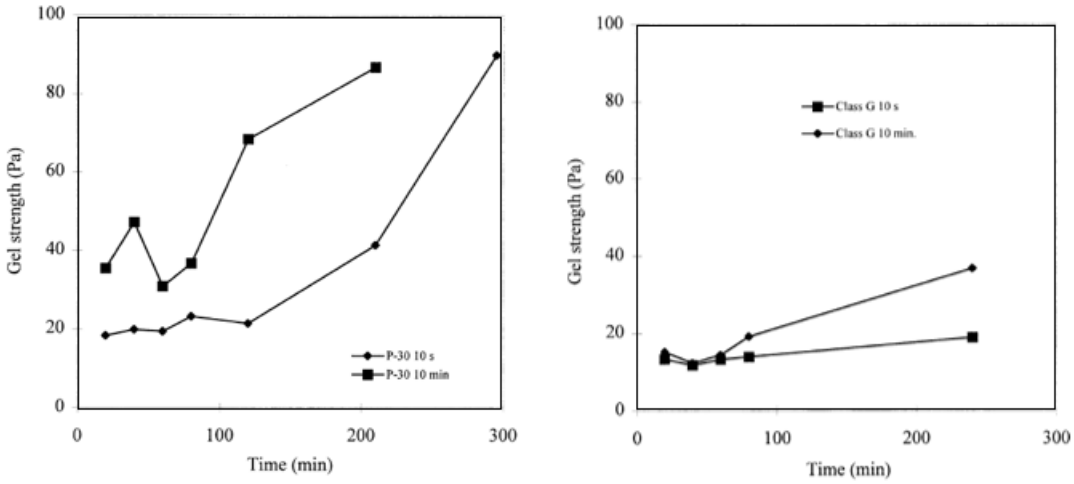

Figure 2.13 Gel strength for class G (right) and P30 Portland cement (left). A higher rate of gel formation for the P-30 slurry was observed compared to class G (Hodne et al., 2000)

The authors concluded that the concept of mixing energy can only be valid for class G cement when slurries are mixed using an original Waring Blender at high speed.

2.6. Cement Deflocculation Process

Cement hydration defines many cement properties such as viscosity, yield strength, thickening time and compressive strength after setting. Various factors affect hydration history including cement type, design, additives, mixing method. The effect of mixing on hydration is not well understood. However, field practice has shown that

mixing energy, duration and efficient deflocculation have an important impact on the whole cementing process (Sweatman, 2000). Failure to wet cement powder will leave a "lumpy" slurry with poor properties. A good mixing system will create a turbulent flow that shears aggregates into smaller particles. Defined by "Kolmogoroff" theory, turbulent flow can be modeled as the "superposition of different size eddies on average flow" (Vidick, 1990). The theory can be used to predict size of eddies from density, viscosity and volume data. In an efficient deflocculation, various size eddies are desirable. Large eddies help in breaking larger particles whereas smaller eddies can help in breaking smaller particles. In equilibrium conditions, the length of small eddies (L) can be given by (Vidick, 1990):

$$L^4 = \frac{\mu^3}{\rho^2 (P/V)} \quad \text{.....(2.13)}$$

μ is the viscosity, P is the power, V is the volume and ρ is the density in the equation above. The equation cannot be used for predicting the amount of time necessary to apply the power to the mixture. Furthermore, Vidick, (1990) presented specific surface area of the silicate and aluminum phase before and after API mixing as described in the Table 2.5:

Table 2.5 Measured surface area of class G Cement (Adopted from Vidick, 1990)

Sample	Total Surface Area (m^2/g)	Silicate Phase %	Aluminum Phase %
Before Mixing	0.8	34	66
After API Mixing	1.3	38	62

Table 2.6 indicates that mixing procedure indeed aggregates the cement but does not breakdown cement particles. It also increases the total surface area but the percentage of silicate and aluminum phases are only slightly changed. Vidick, (1990) further

discussed three distinctive phases of “powder wetting”, “deflocculation”, and “homogenization.” He emphasized that “deflocculation” is the key process for cement mixing as it is for drilling fluids. Experiments conducted with various mixing energy (0.5-9.5 KJ/Kg) showed deflocculation as function of mixing energy; with more mixing energy, deflocculation is increased. Furthermore, viscosity was found as a key indicator for optimum deflocculation and required minimum mixing energy as shown in the Figure 2.14. He explained that there is a direct relationship between the evolution of the mass of slurry on the sieve and plastic viscosity. Experiments indicated the existence of a “break point” in mixing energy where less than critical energy, particles are aggregated together (high viscosity zone). These experiments also implied that further increase in mixing energy will only slightly improve deflocculation. Figure 2.14 illustrates eddy size and sieve percentage versus mixing energy. It can be observed that at mixing energy of above 2.2 KJ/Kg, the eddy sizes and sieve percentage (amount of deflocculation) do not change. This indicates a critical mixing energy threshold in mixing phenomenon of cement slurry.

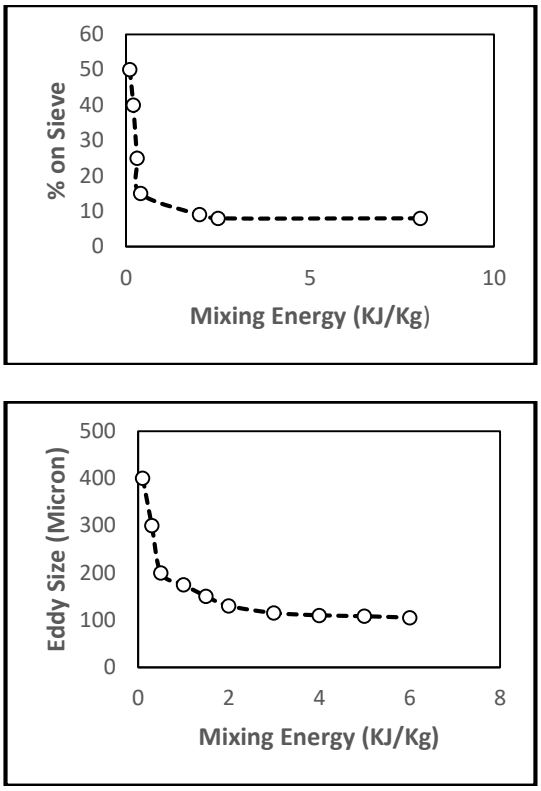

Figure 2.14 Effect of mixing energy on deflocculation (top), Effect of mixing energy on Eddy size (bottom) for class G cement. Increase in mixing energy beyond critical point slightly improved deflocculation (After Vidick et al., 1990).

2.7. Effect of Mixing Water and Water/Cement Ratio on Cement Properties

Mixing conditions including mixing water quality and how it affects slurry properties are of great importance. Cement has a complex non-Newtonian behavior impacted by mixed water characteristics. It is not very surprising to see some key cement properties impacted by the condition of mixed water. In a recent study conducted by Saleh et al., (2018), the effect of mixing water hardness on cement strength, thickening time and rheology was described. Different types of water were produced based on hardness classification, as shown in Table 2.6, and were mixed separately with Class G-Portland cement. Distilled water was used for soft water while all the other water samples were prepared to span the range of the water classifications. The field water was taken from

one of the fields in Western Oklahoma, U.S. and the seawater from Jacksonville's beach in Florida, U.S. The field water obtained was categorized as very hard having a hardness of 300gm/L and 8.61 pH. Seawater was also categorized as very hard having hardness of 9000+ gm/L and 8.73 pH.

Table 2.6 Water hardness concentrations selected based on U.S Guidelines and pH properties (from Saleh et al., 2018)

Type	U.S Department of Interior Guideline	Selected	pH
Soft	Less than 1gm/L	0 gm/L	7
Slightly Hard	17.1 to 60gm/L	32gm/L	8.24
Moderately Hard	60 to 120gm/L	96gm/L	8.54
Hard	120 to 180gm/L	166gm/L	8.32
Very Hard	180 and over gm/L	266gm/L	8.06

The results of thickening time tests summarized in Figure 2.15 show a decline in thickening time as the mixing water hardness increases. The negative correlation presented a constant percentage change, 2.4%, between soft, slightly hard and moderately hard water classifications. In contrast, the percentage change between higher hardness waters, hard and very hard, was smaller with just 0.6% and 1.3% decline, respectively. Results of the UCS tests are reported in Figure 2.16 (results were labeled A to E for different waters). It can be observed that as the cement curing time increases, the cement gains more strength, consistent with studies (Nelson and Guillot, 2006). Results of UCS at one day are very similar for all slurries mixed with different water types except seawater. Furthermore, results show higher UCS for slurry mixed with soft water indicating hardness decreases cement strength. Overall, a mixed effect from water type on cement strength was reported. In one day curing, due to very active hydration of cement, the effect of water hardness is minimal.

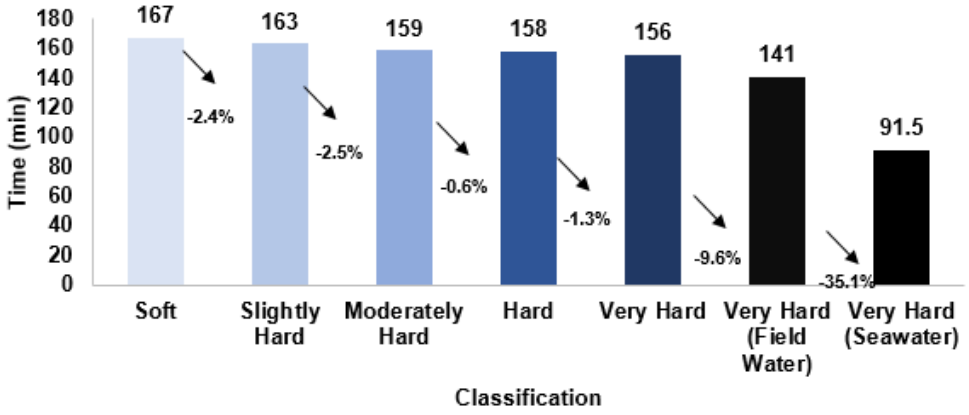

Figure 2.15 Thickening time recorded for API Class G-Portland cement based on different waters selected per hardness classification, plus field water and seawater (from Saleh et al., 2018)

To investigate effect of mixing water temperature, three different API Class G-Portland cement slurries were prepared with water temperatures of 41ºF, 73.4ºF and 105.8ºF to measure the effect of mixing water (soft water sample) temperature on consistency. It can be observed that as the temperature of the water increases, it speeds up the consistency of the slurry, possibly causing it to set faster. The results obtained in Figure 2.17 show how a low mixing-water temperature results in a slower increase in consistency over time in contrast to high mixing water temperatures.

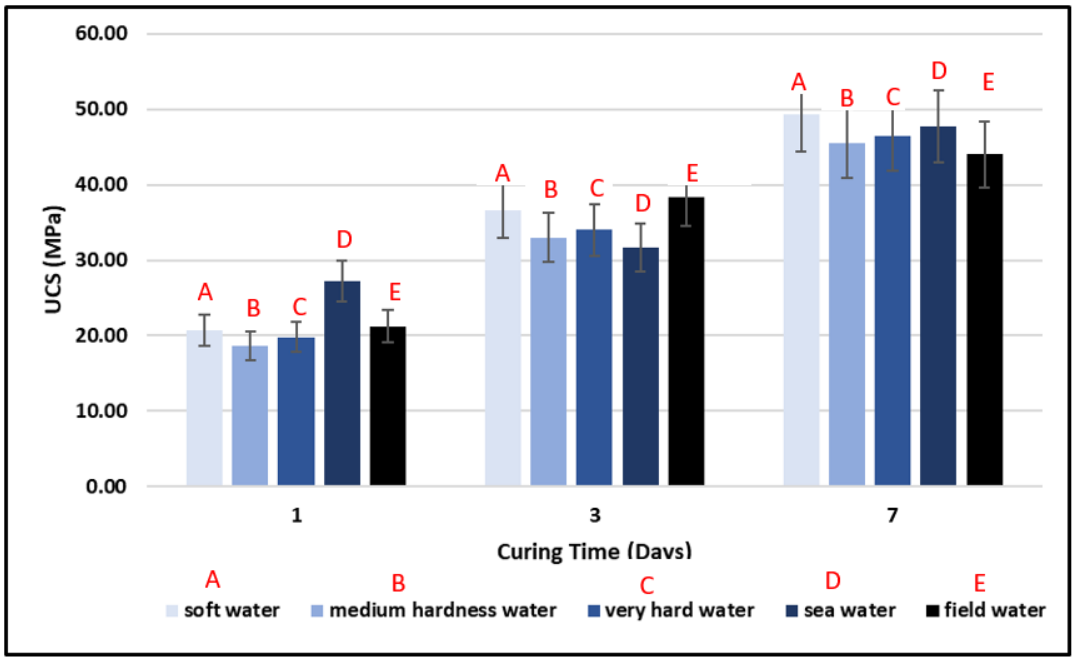

Figure 2.16 UCS of different specimens based on mix water types and curing times. Results show specimen prepared by sea water has higher UCS in 1 day, however, specimen prepared by fresh water show higher strength in 7 days (from Saleh et al., 2018)

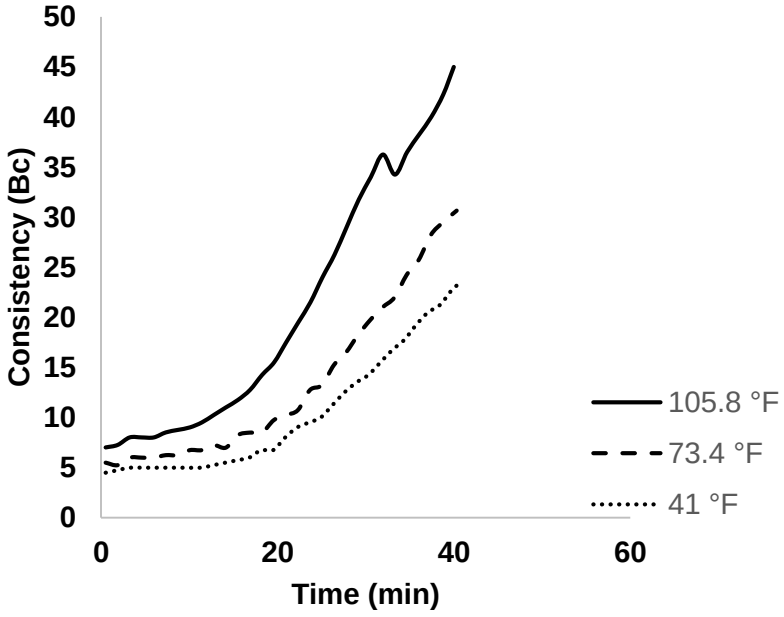

Figure 2.17 Consistency progression for API Class G-Portland cement based on 3 different water temperatures used at mixing (from Saleh et al., 2018)

In addition to mixing water, the effect of mixing time is often neglected in oilwell cement studies. In a study conducted by Takahashi et al., (2011), the effects of mixing time on hydration kinetics of grouting mortars are discussed. The study used X-ray diffraction techniques and Scanning Electron Microscopy to evaluate effect of several mixing parameters on strength, fluidity, hardening characteristics, shrinkage and heat of hydration. The materials consisted of Portland cement, silicious aggregates and superplasticizers. The study also measured early and late stage compressive strength where with longer mixing time, early compressive strength increased; however, no significant difference was observed for compressive strength measured after 28 days. The initial setting time was also increased by increasing the mixing time. SEM and X-ray showed that hydrates are dispersed more uniformly when mixing time is longer. Shorter mixing time caused formation of surface layers with increased water content (Figure 2.18). Top SEM images in Figure 2.18 show upper surface of the sample mixed for 1 min. Bottom SEM show upper surface of the sample mixed for 7 min. We can observe a more uniform distribution of hydrates in samples mixed at 7 min. The authors also discussed mixing time effects through differences caused in the hydration process (Figure 2.19). When mixing time increased, the start of precipitation (beginning of accelerated period) advanced. This is shown as increase in the peak of heat evolution. Authors explained that change in hydration process caused early strength development because of more silicates precipitation.

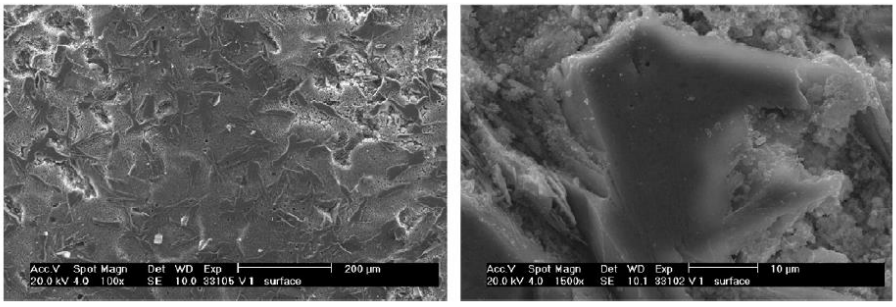

SEM images of an upper surface of the sample mixed for 1 min.

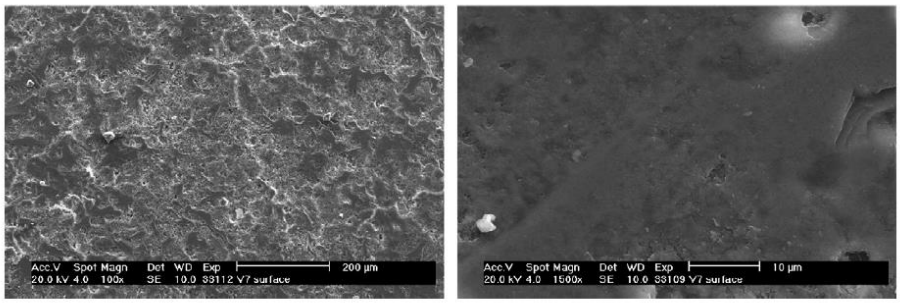

SEM images of an upper surface of the sample mixed for 7 min.

Figure 2.18 Effect of mixing time on formation of hydrates for Portland cement concrete (from Takahashi et al., 2011). At longer mixing time, a uniform distribution of hydrates was observed

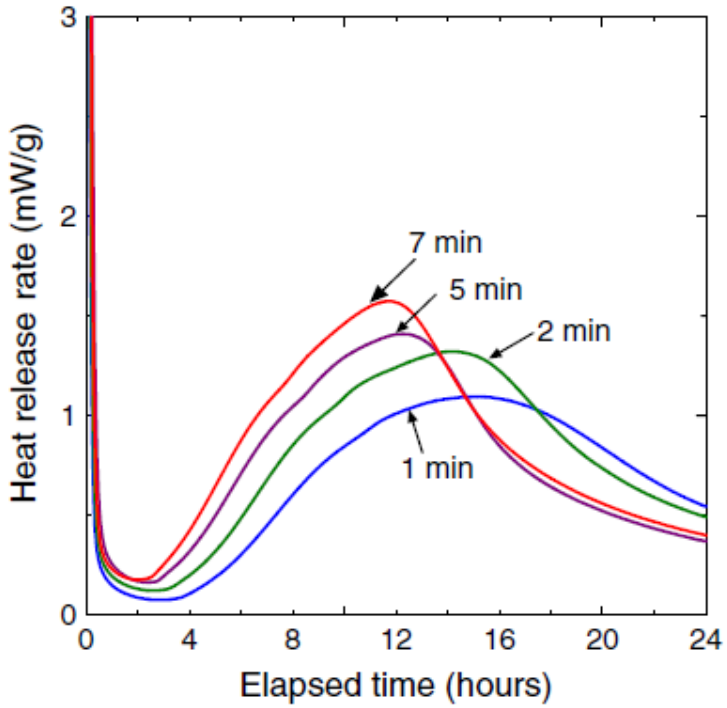

Figure 2.19 Effect of mixing time on hydration process (from Takahashi et al., 2011). When mixing time increased, the start of precipitation (beginning of accelerated period) was advanced. This is shown as increase in the peak of heat evolution.

Han and Ferron, (2015) investigated the effect of mixing method on microstructure and rheology of cement paste. Although, the study investigates ASTM mixing standards, it has some similarities to API recommendation for oilwell cement applications. ASTM C1738 uses a high shear mixer for sample preparation whereas ASTM C305 uses a planetary mixer for more homogenized cement samples. The study revealed significant difference not only in rheological properties but also kinetics and microstructure using different mixing methods. Figure 2.20 shows the two mixers, Chandler high shear mixer blade and set up for ASTM C1738, Hobart mixer paddle and set up for ASTM C305. The ASTM C138 is based on mixing cement at 4000 rpm for 60 seconds then mixing at 12000 rpm for 30 seconds, resting for 150 seconds and a final mixing at 12000 rpm for 30 seconds. Whereas ASTM C305 is based on initial mixing at 140 rpm for 30 secs, resting for 15 seconds and a final mixing at 285 rpm for 60 seconds. The study showed higher viscosity and yield stress values for the slurries prepared according to high mixing ASTM protocol using the Chandler high shear mixing blade. Similar observations were made for the yield stress. These results further demonstrate the effect of mixing procedure and shear rate on slurry properties. The study reported the increase in the plastic viscosity and yield stress using a high shear mixer. The measurements conducted in a calorimeter showed the effect of mixing methods on rate of hydration. It was found that the samples prepared in a high shear mixer displayed accelerated hydration kinetics compared to those prepared in the lower shear mixer.

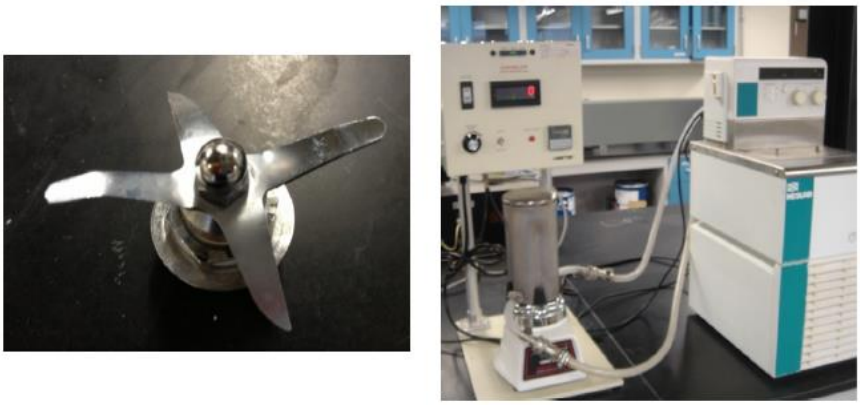

(a) Chandler high shear mixer blade and setup (for ASTM C1738)

(b) Hobart mixer paddle and setup (for ASTM C305)

Figure 2.20 Different mixers used for experiments (from Han and Ferron, 2015). Two different ASTM mixing protocols one using high shear mixer (top) and one low shear mixer (bottom) were used in this study.

2.8. Cement Mixing Condition in Laboratory and Field

A major difference between mixing in laboratory and field conditions is scale. Many of the published data on cement properties are based on preparation in laboratory conditions. Additionally, the majority of literature papers focus on laboratory and surface mixing procedures due to access to cement samples for testing in different mixing conditions (Teodoriu et al., 2015; Nelson and Guillot, 2006; Hibbert et al., 1995 and Vidick et al., 1990). Testing samples while inside wellbore will be very challenging or

even impossible due to closed loop pumping cycle and time sensitivity (setting time) of slurry.

As mentioned earlier, cement slurry is made of solid and liquid phases. The solid phase includes cement powder and many other additives for improving cement slurry performance. The mixing procedures of cement in the laboratory and the field are very different; furthermore, in the laboratory, mixers with different shear rates are used. The recommended API mixer in the laboratory is "Waring Blender." This is a high shear mixer suitable for shearing very small quantities (600 cc) of cement. These mixers are employed for a very short period of time. In laboratory mixing all the shear is applied continuously to the slurry therefore it is defined as direct mixing method (Hibbert et al., 1995). In field mixing, batch mixers are employed which have cycles of low and high shear with different residence times. In addition, a centrifugal pump is used which apply a high shear rate (2000 s^{-1}) over a short period of time (Teodoriu, 2015). The main difference in laboratory and field mixing equipment is their shear rates. Table 2.7 summarizes approximate shear rates in different units:

Table 2.7 Approximate shear rates for different units

Unit	Approximate Shear Rates (S^{-1})
Laboratory Blenders	Max 30,000- Average 3000
Centrifugal Pump	Less than 2000- Average 500
Recirculation lines	1500

As shown in the Table 2.8, a very high shear rate is caused by laboratory blenders. API laboratory mixing of the slurry (API 10B-2) has described mixing procedure as follow:

1. 4000 rpm for 15 seconds (dry cement added to the fluid)

2. 12000 rpm for 35 seconds

API mixing procedure on small laboratory scale sample (600 cc) will provide 5.9 KJ/Kg mixing energy. In the field, the mixing energy might be different depending on scale of the job and mixing equipment. In addition, cement particles may be different or smaller in laboratory mixers due to their small size (one quart) and shorter distance between blender and cement particles (Teodoriu et al., 2015). This will create varriable cement properties compared to what is measured in the laboratory. Table 2.8 describes the characteristics of API Waring blender, low shear mixer, and batch mixer. The characteristics described are shear, loading period, mixing duration, mixing volume, blade type and cement particles movement:

Table 2.8 Comparison of different mixing systems (Adopted after Teodoriu et al., 2015)

Mixing Characteristics	API Waring Blender	Low shear mixer	Batch Mixer
Shear	High shear	Low shear	Low shear (alternating)
Loading Period	Very short (s)	Quite long (min)	Long (min)
Mixing Duration	Very short (s)	Long (min)	Long (min)
Mixing Volume	Small (600 ml)	Small (600 ml)	Large and varying (bbl)
Blade Type	Sharp blades	Propeller blades (Similar to paddles)	Paddles (Centrifugal pumps)
Cement Particles Movement	Short distance	Short distance	Long distance

2.9.1 Mixing Energy Nodes in Cement Field Operations

To better understand cement mixing condition in a well, several energy nodes can be considered. These nodes are related to different segments in cement pumping cycle from surface down into the wellbore. Surface mixing system is illustrated in the Figures 2.2. Generally, there are four major sections in the surface system which include mixing

inside batch tank, into a centrifugal pump, into a triplex pump and through a manifold and inside the wellhead. At the surface, dry powdered cement is mixed with water and other dry additives. Cement dry components are generally blended at a bulk plant before transferred to the wellsite. There are generally two types of mixing, either batch or continuous mixing. If all the ingredients are mixed in a large tank before pumping, it is called batch mixing. Continuous mixing means to mix as it is pumped. Depending on job requirement and well location (onshore and offshore), one of these mixing processes is selected. Usually, for small cement volumes such as liner operation batch mixing is preferred (Sweatman, 2015). In recent years, a more advanced Recirculating Cement Mixer (RCM) system is employed at well sites; this has several advantages over the conventional cement mixer (Figure 2.23). These include more accuracy over cement properties, increased mixing energy and better control over shear rate (Sweatman, 2015). The RCM uses of an axial flow mixer which creates more mixing energy than an old style jet mixer. Other essential equipment used at surface are pumping units. Typically, two high pressure triplex pumps are used. Centrifugal pumps are employed for low pressure mixing of slurry. Many cementing operations require less than 5000 psi pressure but some jobs can be very demanding (deep water offshore) requiring up to 20,000 psi pressure. There are several factors such as cement volume, well depth, anticipated pressure and temperature which will dictate number of cementing pumps.

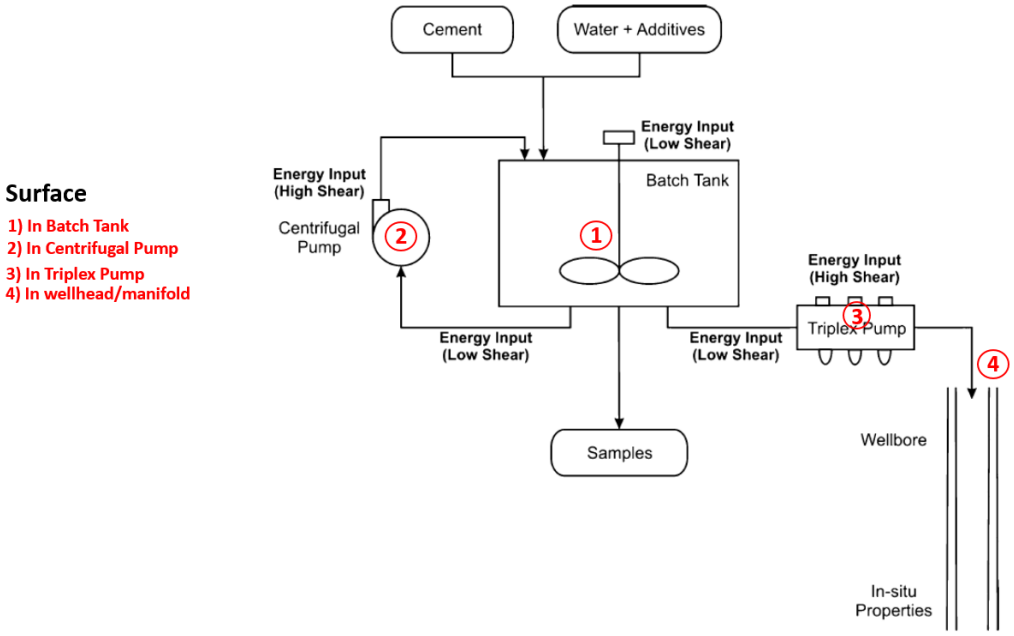

Figure 2.21 Energy Nodes in Surface Mixing. There are four major sections in surface system which includes mixing inside batch tank, into centrifugal pump, into triplex pump and through manifold and inside the wellhead (Modified after Teodoriu et al., 2015)

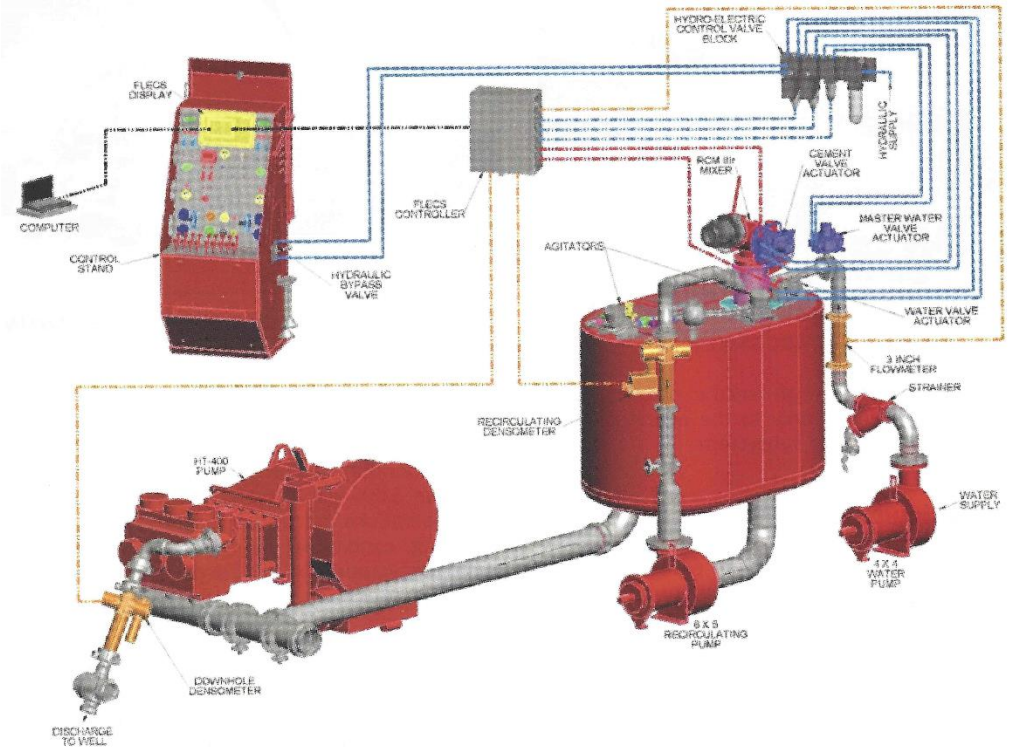

Figure 2.22 Schematic of Recirculating Cement Mixer (RCM). The RCM allows for more mixing energy than old style jet mixer (from Sweatman, 2015)

2.10 Summary

The literature study of mixing energy effects on cement produced different competing theories about the importance of cement mixing energy and other mixing variables. One group recommends including mixing energy in every aspect of cement design. This group considers mixing energy as an important criterion for successful cement jobs, as it affects most of the cement properties such as thickening time, fluid loss, rheology and strength. The other group does not deny the importance of mixing energy; however, they do not completely agree that mixing energy has a strong impact on every cement property. Some highlighted (Padgett, 1996 and Vidick, 1990) the importance of shear rate, deflocculation, cement type, additives or cement wetting efficiency, as well as other parameters that need to be investigated in conjunction with the mixing energy. A summary of these observations is shown in Table 2.10. As the Table 2.10 shows, there is a gap in our understanding of the impact different mixing variables such as shear rate, mixing time and mixing energy on various cement properties. Mixing time is another variable often ignored in the literature. According to mixing energy theory, it is possible to increase mixing energy either by mixing time, shear rate or decreasing the volume. Many of the studies reviewed in the literature do not describe procedures in increasing mixing energy, therefore it is difficult to draw definite conclusions. Additionally, some of the results reported in the literature are related to cement with different additives such as dispersants, polymer, or latex. This will further complicate the interpretation of the results. Finally, our literature survey shows absence of any mixing theory for oilwell cements that considers non-Newtonian characteristics of cement. Similarly, no scale up procedure to use cement mixing results from laboratory to field can be found.

Table 2.9 Summary of prior state of the art on the importance of mixing energy and shear rate for oil and gas cement slurries

Author	Importance of Mixing Energy	Importance of Shear Rate	Application and Variables
Orban et al., 1986	Important	NA	Rheology, Free Water, Fluid Loss, Thickening Time, UCS
Vidick et al., 1990	Important	Important	Rheology and Thickening Time
Heathman et al., 1993	Important	Minimal	Coiled Tubing Applications, Thickening Time, Fluid Loss
Vorkin et al., 1993	Important	NA	Coiled Tubing Applications, Fluid Loss, Rheology, Thickening Time
Hibbert et al., 1995	Important	NA	Batch Mixing Applications, Thickening Time, Rheology
Padgett, 1996	-Slight impact on Thickening Time -Not Important for Other Variables	Important	Thickening Time, Free Water, Fluid Loss, Yield Point
Hodne et al., 2000	Important	Important	Rheology
Teodoriu et al., 2015	Important	Important	Laboratory and Batch Mixing, Rheology

Chapter 3: Design of Experiments and Statistical Analysis

Chapter 2 showed that different mixing variables can impact its properties. Therefore, a robust experimental plan is required to investigate effect of these variables. This chapter presents summary of literature related to Design of Experiments (DoE) and its application in oil and gas industry. Goals of this chapter are; first, to present some of the previous studies using DoE to formulate and study effect of different variables, and second, to present an experimental matrix formulated for this study. DoE method since its invention by Fisher in 1920s, in agricultural studies, has evolved to a set of powerful tools in diverse applications from optimizing concentration of mixtures in a compound to testing new drugs. The golden rule in design of experiment is to gain maximum information from fewer experiments. A well designed experimental plan is more crucial than the actual analysis because no statistical analysis can rescue a poorly designed experiment.

3.1 Introduction

Design of experiments is a very powerful tool with diverse applications in all science and engineering fields. Many of the application are reported in the literature of physical and chemical sciences. Some of the pioneering textbooks provide insights and applications of DoE in various disciplines (Box and Draper, 2007; Myers and Montgomery, 1995). Research often deals with a number of variables that affect the response of interest. One of the common techniques is response surface methodology that relates the response variable to predictors by modeling, experiments, analysis and optimization (Jaynes, 2013). When dealing with two or more factors, factorial design becomes very efficient. The effect of a factor can be defined as the change in response

produced by a change in the level of the factor. This is referred to as the main effect. Sometimes there is interactional effects between various factors when response level from one factor is not same at all levels of other factors. Wu and Hamada, 2011 calls both main effects and interaction effects, factorial effects.

In early stages for factor screening, factors are leveled based on their importance typically using a two-level factorial or fractional factorial design, possibly with some center points (Jaynes, 2013). Some of the experiments in many disciplines are very costly and time-consuming therefore, it is often efficient to use cost-effective factorial design to investigate the effects of two or more factors simultaneously to identify key factors from a large pool of factors. Most commonly used factorial designs are the two and three level ones to investigate the effect of one factor on another. It is possible through the designs to find out main and interaction effects in different experiments. However, as the number of level and factors increases, size of these designs increases as well, therefore, an optimum design needs to be selected before experiments conducted.

In petroleum engineering discipline it has been successfully applied in reservoir engineering, drilling engineering, performance prediction, sensitivity studies, upscaling and history matching (Chu, 1990; Damsleth et al., 1992; Bu and Damsleth, 1996 and White et al., 2001).

The first step in design of any experiment is to question objective of research, hypothesis, expected data, experimental factors and expected responses for each factor. Some fundamental questions must be answered before experimental design can be concluded. These questions can be summarized as the steps shown in the Figure 3.1 (Lazic, 2006).

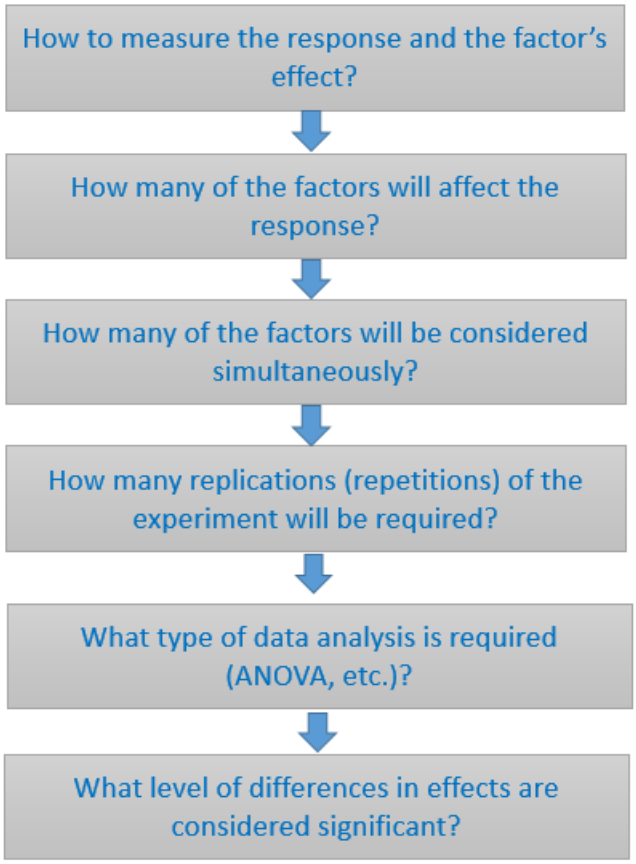

Figure 3.1 Fundamental research questions in DoE and statistical analysis (Figure prepared from Lazic, 2006)

A successful experiment can be designed by minimal time expenditure, and resources with the ability to collect maximum amount of data. Simplicity is the key for designing an experiment. Classical experiments design is based on investigating one factor at a time so that all other independent variables (factors) are held constant. This has been most favorable approach among engineers and scientists. For instance, if an experiment has five factors with five level of variations (different values), then the number of experiments are required will be 5^5 (3125). In some instances, due to time and budget constraints, the total number of experiments is reduced therefore selecting the combinations is key to increase confidence of conclusions. Another difficulty with

classical experimental design is interpretation of results due to a large number of tables and graphs. There are cases where classical design could not provide response in the expected time frame whereas by applying sophisticated design of experiments, solutions can be reached.

3.2 Design of Experiments

DOE is a planned approach for determining cause and effect relationships. Lazic, (2006) has mentioned several essential steps in the design of experiments, i) reducing or minimizing the number of experiments; ii) changes and varying factors simultaneously; iii) development of strategy to achieve solutions reliably in post experiments.

The first step in design of experiments is to identify all the impacting factors. These factors can be controllable and uncontrollable. Factor ranges should include all feasible factor values. Factors are usually scaled to span the range of -1, 1. Generally, it is desirable to have linear factor-response relationship which is difficult to obtain in some cases. Several statistical techniques are used to model factor-response relationships such as quadratic models. For a two-level factorial design, each factor is assigned to its maximum (1) or minimum value (-1) in all possible combinations with other factors (Figure 3.2). For three factors, we need 2^3 (8 total experiments). For n factors, 2^n experiments are required. As shown in Figure 2a represents two-level factorial design, 2b shows three-level factorial design and 2c is an example of Box-Behnken design which is a modified three-level factorial (White et al., 2001). There is no simple formula relating the number of required experiments to the number of factors for Box-Behnken designs; however, the number of required experiments will always be between 2^K and 3^K."

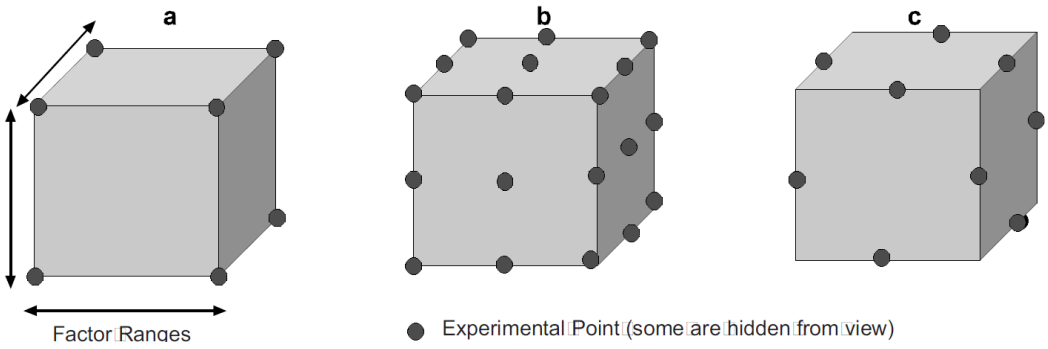

Figure 3.2 Examples of designs for three factors. (a) A two-level factorial, (b) a three-level factorial, and (c) a Box-Behnken design (from White et al., 2001)

A full factorial design of experiments is a design which includes all design points. Factorial design integrated with common statistical data analysis provide greater information on the system where conclusions can be more reliable. Depending on research problem, variables and other factors, a best technique in design of experiments can be chosen.

3.3 Analysis of Variance

ANOVA (analysis of variance) is a common technique in statistical analysis to determine whether or not significant differences exist among the means of several groups of observations. The ANOVA technique builds upon t-test which is used to determine if two means differ. This technique as first introduced by Fisher in 1920s. Fisher has said that the analysis of variance is merely “a convenient way of arranging the arithmetic." The statements can be interpreted to indicate that the principles underling ANOVA are quite simple; however, the calculations can be quite tricky. This technique is particularly useful when the difference between the groups cannot be stated quantitatively. One simple example on applicability of this technique can be for instance evaluating effects of four catalysts on setting time of a particular plastic. Several tests are run under identical

conditions for each catalysis, and then mean setting times of catalysts are compared by using one-way ANOVA technique; "to determine the effect of one independent variable (type of catalyst) on the dependent variable (setting time)." An example of two-way ANOVA application is the effect of temperature in catalysts example. Three different temperatures can be picked and the setting rate for each of the four catalysts can be determined. Two-way ANOVA technique can be used to determine significant differences among the setting times that we would obtain.

3.4 Applications of Design of Experiments (DoE)

3.4.1 Applications of DoE in Oil and Gas Industry

White et al., (2001) used experimental design analysis to identify and estimate significant geological parameters. In their work, they used a five factorial Box-Behnken design to evaluate variables in production predictions caused by geologic heterogeneity and uncertainty for a sandstone reservoir in north-central Wyoming. The five factors in their design were i) variogram range, ii) variogram nugget; iii) variogram anisotropy; iv) cement permeability and v) shale resistivity.

Chu, (1990) used factorial design method to predict steamflood performance in terms of project life, oil recovery and cumulative steam-oil ratio. His work discussed effect of various variables such as steamflood design, rock and fluid properties and operating conditions on steamflood performance. Methodology applied was based on first choosing primary variables impacting steamflood performance, second choosing the DoE, finally running simulations for each run and analyzing the results. Since there were 8 factors, a total of 2^8 (256 runs) will be needed for a complete two-level factorial design.

To minimize the number of runs without sacrifice of information obtainable from the design, a 1/4 replicate was used which calls for 2^6.

Greaves et al., (1989) used factorial design methods for in-situ combustion applications. Experiments were designed to evaluate the effect of investigate effect of different variables such as oxygen partial pressure, mole fraction, and flowrate. The study concluded that the oxygen partial pressure had no significant statistical impact. Flowrate was found to be the primary experimental variable dominating combustion time. Experiments were designed based on a three-factor, two-level. Partial pressure, flow and oxygen mole fraction were chosen as the three factors. Inspection of the results showed that the combustion time was dependent on the oxygen flux and mole fraction.

Ibeh, (2007) investigated changes in rheological properties of oil-based drilling fluids in HPHT conditions. A series of factorial experiments were used on typical oil-based drilling fluids to investigate change in rheological properties at extreme conditions of 200 to 600°F and 15,000 to 40,000 psig. Post statistical analysis was conducted on lab results using analysis of variance, linear and multiple regression and hypothesis testing. Primary factors were found to be pressure and temperature. The study concluded temperature has a dominant effect on viscosity of oil-based fluids at higher pressures (>20,000 psig) while the pressure effect is more dominant at lower temperatures (<350 ^{0}F). A model was developed relating plastic viscosity to pressure and temperature using statistical analysis.

Awoleke et al., (2012) conducted an experimental investigation of fracture conductivity using factorial design methods. Key parameters used in the design were flow back rate, proppant loading, polymer loading, closure stress and reservoir temperature.

Fracture conductivity tests were conducted using fracture cell by pumping fracturing fluids. They initially conducted few tests to determine the key variable in all of the five factors considered in the study. Analysis of experiments showed that closure stress has the most harmful effect on fracture conductivity. Design of experiments based on six factors and two levels (low and high) proved to be very useful in this investigations although study assumed liner relationship between fracture conductivity and selected factors.

Salehi et al., (2017) investigated effects of water ratio, alkaline/fly ash ratio, alkaline molarity plasticizer and retarder additives on compressive strength and thickening time cement slurries at various pressures and temperatures. Their statistical analysis indicated importance of alkaline/fly ash ratio on thickening time. Study concluded strong effect of temperature on thickening time although a reasonable thickening time can be achieved by optimizing mix design factors.

In a similar study by Okumo and Isehunwa, (2007) used a factorial design approach for developing a model to predict viscosity at different temperatures. A 2^3 design considering temperature, starch and potash as factor variables and viscosity as the response variable was used. Factorial design analysis on mud samples confirmed that viscosity of the mud samples is affected by additives (using starch and potash) and also downhole temperature.

3.5 Design of Experiments in this Research

As become evident from literature studies presented in Chapter 2, both shear rate while mixing and mixing energy impact cement properties; therefore, one objective of our experimental design is to formulate a robust set of experiments to investigate how

changing mixing energy and shear rate will impact cement properties. According to mixing energy theory (Equation 2.10 in Chapter 2), to change mixing energy, one can manipulate either shear rate, mixing time or volume. In this work we primarily relied on using API recommended Waring blender to prepare cement slurries. The API Waring blend has limitations in shear rate (between 3000 rpm to 18000 rpm) and mixing time (less than five minutes).

The methodology of mixing is composed of single step and two step (API) mixing procedure. In single step mixing, only one shear rate is considered and mixing time is calculated using mixing energy theory formula presented earlier in the literature chapter. In the two step API recommended procedure, mixing time was calculated based on 4000 rpm and 12000 rpm using the same formula. Calculated mixing time for all the experiments is reported in the Table 3.3. The original DoE for single step mixing has a two factor three level analysis (3^2). Two factors considered are mixing energy and shear rate. This design considered three shear rates at 6000 rpm, 12000 rpm and one mid-point of 9000 rpm. Mixing energy levels of 5.9 KJ/Kg, 8.9 KJ/Kg and 11.8 KJ/Kg were considered. API recommends 5.9 KJ/Kg mixing energy for all cement mixing work in the laboratory. 11.8 KJ/Kg was considered as twice mixing energy of API recommendation to evaluate cement properties. Lower than API mixing energy (5.9 KJ/Kg) was not considered in the experimental design due to equipment constraints. 8.9 KJ/Kg was considered as mid-point of upper and lower energy levels. API mixing procedure recommends mixing at 4000 rpm and 12,000 rpm. Therefore, upper limit of 12,000 rpm was considered in the experimental design, 6000 rpm (half of upper limit) was considered as lower limit for shear rates in the experimental design. Two testing matrixes were

considered as shown in Table 3.1 and Table 3.2. In Table 3.1, DoE is based on changing mixing energy and shear rate; API recommended mixing procedures are considered in Table 3.2. Since API mixing conditions consists of two steps, it cannot be combined in the DoE of Table 3.1. Each symbol in DoE tables represents different laboratory measurements at specified mixing energy and shear rate.

Table 3.1 DoE for single step mixing procedure

Mixing Energy Levels (KJ/Kg)	Mixing rpm		
	6000	9000	12000
5.9	●, ♦, ■,▲	●	●, ♦, ■,▲
8.9	●	●	●
11.8	●, ♦, ■,▲	●	●, ♦, ■,▲

●: UCS and UPV
♦: Thickening Time
■: Rheology
▲: NMR

Table 3.2 DoE for two step API recommended mixing procedure

Mixing Energy Level (KJ/Kg)	API Mixing Procedure
5.9	●, ♦, ■,▲
8.9	●
11.8	●, ♦, ■,▲

Final mixing time calculated based on mixing energy formula are reported in the Table 3.4. It must be noted again that for keeping mixing energy constant at different shear rates, mixing time will change. To increase mixing energy to the next level, mixing time will be increased further. For instance, to prepare a cement slurry at 11.8 E/M and 6000

rpm, 294 (sec) of mixing time is required. This drops to 73 (sec) for similar mixing energy and 12000 rpm.

Table 3.3 Calculated mixing time using mixing energy formula

Mixing Energy Level (KJ/Kg)	RPM	Mixing Time (seconds)
5.9	6000	147
5.9	9000	65
5.9	12000	37
8.9	6000	222
8.9	9000	99
8.9	12000	56
11.8	6000	294
11.8	9000	131
11.8	12000	73

Mixing time for two-step API mixing procedures were calculated based on 4000 rpm and 12000 rpm as summarized below:

1. 5.9 KJ/Kg, 15 seconds at 4000 rpm and 35 seconds at 12000 rpm
2. 8.9 KJ/Kg, 15 seconds at 4000 rpm and 54 seconds at 12000 rpm
3. 11.8 KJ/Kg, 15 seconds at 4000 rpm and 72 seconds at 12000 rpm

Chapter 4: Experimental Procedures

4.1 Overview

This section describes laboratory procedures employed in this study. Each section starts with a general synopsis of the test and its significance and then description of the equipment and apparatus that were used. Following experimental procedures were explained:

1) Thickening time
2) Rheology
3) Mixing and Sampling
4) Curing
5) Unconfined Compressive Strength (UCS)
6) Ultrasonic Pulse Velocity (UPV)
7) Nuclear Magnetic Resonance (NMR)

4.2 Determination of Slurry Thickening Time

The thickening time of a cement slurry is the measure of a time period for which the slurry stays liquid under downhole conditions and is fully capable of being pumped downhole efficiently. Thickening time is one of the key properties of cement slurry. It helps in determining whether the slurry will be fluid from the time it is mixed to when it is placed efficiently in the wellbore. It is, therefore, crucial to be able to interpret and validate the test results in order to make the necessary changes to the future design.

The test follows the guidelines as laid out in API spec 10B-2 (API 10B-2, 2013). The laboratory test conditions represent the time, temperature, and pressure to which a cement slurry will be exposed during pumping operation. Generally, cement slurries are designed

with thickening times greater than the actual pump time of the cement job. This safety factor is added in the thickening time for the contingencies, which allows for any changes in the job parameter that may be caused due to unforeseen well conditions and/or malfunction of equipment. Cement slurries exhibit various setting patterns during the thickening time test. The slurry's behavior during the test depends on many factors, such as density of the slurry, temperature, pressure, entrapped air, and solids distribution in the system. It is defined as the elapsed time from the initial application of the temperature and pressure to the time at which the slurry reaches a consistency deemed sufficient to make it unpumpable (e.g., 50 Bc to 100 Bc, Bc=Bearden units of consistency). This time shall be documented along with the final consistency at which the thickening time test is terminated.

4.2.1 Thickening Time Test Equipment and Experimental Procedure

In order to measure thickening time, a consistometer is required. Consistometer is an equipment to measure cement slurry consistency under different temperature and pressure conditions. Two major types of consistometer exist in the market. An atmospheric consistometer is used only in atmospheric conditions. HPHT (high pressure high temperature) consistometer is used to measure cement thickening time under different temperature and pressure conditions. Here, in this study a HPHT consistometer from Grace Instrument Company was used as following description:

- Grace Instrument HPHT Consistometer and Gel Strength Tester Model 7540 (Figure 4.1)

Figure 4.1 HPHT Consistometer and Gel Strength Tester Model 7540

Table 4.1 lists the operational range for the Model 7540 consistometer:

Table 4.1 Operational ranges for Model 7540 consistometer (courtesy of Grace Instrument, http://www.graceinstrument.com)

Dimensions	27" height x 18" width x 21" depth
Weight	85 lbs
Temperature Range	Up to 400°F
Pressure Range	Up to 20,000 psi
Slurry Cup Rotation	0 - 250 rpm
Compliance	API Spec 10A / ISO 10426-1

The slurry cup assembly, to be utilized in a pressurized consistometer, consists of a cylindrical outer cup, bottom cell cap with a hexagonal nut and a top locking ring, a paddle assembly, and a potentiometer (Figure 4.2).

The potentiometer should be kept as clean as possible. Consistometers must be calibrated regularly with weight loaded device to produce a series of torque equivalent values for consistency.

Figure 4.2 (Left to right). Slurry cup assembly, potentiometer, paddle assembly, bottom cell cap, top locking ring

The pressurized consistometer consists of a rotating cylindrical slurry cup equipped with a stationary paddle assembly, all enclosed in a pressure chamber. The design of the drive assembly determines the working pressure and temperature of the unit. Pressure is generated by an air-operated hydraulic pump and a complete hydraulic system with the normal reservoir, piping, valves, filters, and other required items. Heat is supplied by a 3000-watt internal tubular heater controlled by an automatic temperature program control system, or a manually controlled variable transformer, depending on the model. Thermocouples are provided for determining the temperature of the oil bath and the cement slurry. The slurry container is rotated at a constant speed of 150 ± 15 rpm by a synchronous motor and appropriate gear reduction. The consistency of the cement slurry is indicated and recorded as DC voltage obtained from a potentiometer mechanism within the pressure cylinder, which contains a standardized torsion spring to resist the rotating tendency of the paddle. Industry recommends well-simulation thickening time schedules provided by API-10B2. The schedules are based upon nominally vertical wells. The

choice of tables is based upon well depth. The choice of the column within a table is based upon thermal gradient.

4.3 Determination of Rheological Properties

Rheology is the study of deformation of fluids and their flow under stress. It describes the relationships between shear rate and shear stress needed to move a given fluid. Shear rate is defined as the difference in the velocity of two fluid particles divided by the distance between them, while shear stress is the frictional force created by the two particles rubbing against each other. The rheology tests conducted here follow the guidelines as laid out API spec 10B-2, (API 10B-2, 2013). Viscosity is the measure of a fluid's resistance to flow and is equal to shear stress divided by the shear rate. The behavior of cement slurries under varying temperatures and pressures is important in predicting its response under downhole conditions.

4.3.1 Test Equipment and Experimental Procedure

To determine rheological properties of cement slurry, a rotational direct reading viscometer is used. This viscometer is powered by a motor or without a gear reduction box. A viscometer utilized to determine the rheological properties of a fluid consist of concentric cylinders, a rotational sleeve, and a stationary bob. The sleeve rotates at a constant velocity for each RPM setting. The cement slurry creates a frictional drag between the sleeve and the bob. The readouts are proportional to the drag experienced by the bob. In this study, a Grace Instrument Automatic Rotational Viscometer Model M3600 was utilized (Figure 4.3). Operational ranges of the viscometer are reported in the Table 4.2.

Figure 4.3 Grace Instrument Automatic Rotational Viscometer Model M3600

A viscometer heat cup or equivalent shall be utilized to maintain the temperature of the slurry within ±5°F (±2°C) of the test temperature up to the temperature of 212°F (100°C).

Table 4.2 Operational ranges for a Grace Instrument Automatic Rotational Viscometer Model M3600 (courtesy of Grace Instrument, http://www.graceinstrument.com)

Dimensions	16" height x 5" width x 8" depth
Weight	12.5 lbs
Temperature Range	Ambient (20°F with chiller) to 212°F
Pressure Range	Atmospheric Pressure
Slurry Cup Rotation	0.01 to 600 rpm continuous
Compliance	API Spec 10A / ISO 10426-1

4.4 Mixing

For purpose of laboratory measurements, API recommends one-quart size container for mixing slurries. The mixing container and the mixing blade should be constructed of corrosion-resistant material. The mixing assembly should be constructed so that the blade

can be separated from the drive mechanism. Slurries were prepared using two Waring type blenders labeled here mixer 1 and 2 as shown in the Figure 4.4. They contain a torque monitoring module for adjusting the number of revolutions, a mixing cup, and a substructure which contains the blending motor. The two blenders can be operated constantly at the desired speed levels between 4000 ± 250 rpm and 12000 ± 250 rpm.

4.4.1 API Mixing Procedure

API recommended mixing procedure calls for weighing the dry materials properly before being added to the mixing fluid. The mixing container with the required weight of mix water and any liquid additives should be placed on the mixer base. The motor should be turned on and maintained at around 4,000 rpm, the cement and dry additive blend should be added at a uniform rate, in not more than 15 seconds if possible. When all the dry materials have been added to the mix water, the cover should be placed on the mixing container and mixing should be continued at around 12,000 rpm for 35 seconds.

Mixer 1 Mixer 2

Figure 4.4 Waring type blenders used for cement mixing

4.4.2 Sample Preparation and Molds

We used two-inch cube molds to form cement samples. According to API RP 10B-2 - Recommended Practice for Testing Well Cements, the molds must be watertight and it is important to coat the contact surfaces with a release agent – e.g. grease – before using them. All the cube molds must be tight fitted and each mold should not have more than three cube compartments. All molds were separable into not more than two parts. After mixing, cement slurry was poured into each compartment and filled to the top edge of compartment without spilling over the mold. After filling all the compartments, each mold was placed in the curing bath filled with deionized water. According to API, "if field mix water composition is unknown, deionized, distilled, or tap water may be used". All cement specimens were carefully removed from the mold after 1 day and allowed to cure in the same bath until testing time (1, 3, 7 and 21 days). Figure 4.5 shows the molds after pouring cement slurry. Figure 4.6 shows samples after removing from mold and curing in water bath.

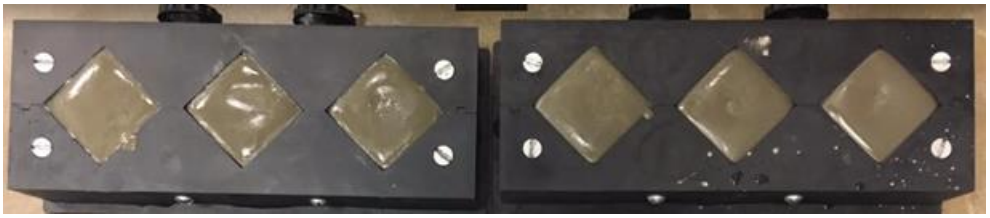

Figure 4.5 Curing cement slurry in 2 by 2 inch molds

Figure 4.6 Curing cement samples in deionized water

Figure 4.7 shows the impeller apparatus for Waring blender. For experiments conducted in this study, we used neat class H API cement. Recommended water to cement (W/C) ratio for class H cement is 38%. This ratio requires addition of 860 grams of dry cement and 327 grams of water to get 600 ml slurry volume. The density measurements in our experiments varied between 16.42-16.50 lb/gal (1.97-1.98 S.G).

Figure 4.7 Impeller apparatus for Waring blender

4.4 Curing

API recommends a curing bath or tank having dimensions suitable for the complete immersion of compressive strength molds in water. Both atmospheric and pressurized vessels can be used for curing. After the molds have been filled, they need to be placed in a water curing bath immediately. At approximately, 45 minutes prior to the age at which samples are to be tested, samples need to be removed from the water bath.

4.5 Specimen Dimensions

API RP 10B-2 recommends testing cubes with an edge length of 50,8 mm (2 inch). After removing the cured cement cubes from the molds, the specimen dimensions were measured by using a digital calibrated caliper. The length and width of the cube was measured at the points shown in Figure 4.8 to guarantee a strict observance of the recommended dimensions and to be able to calculate the area, needed to calculate the compressive strength. The edge length of the tested cubes should not deviate more than 5 % from the API recommended value.

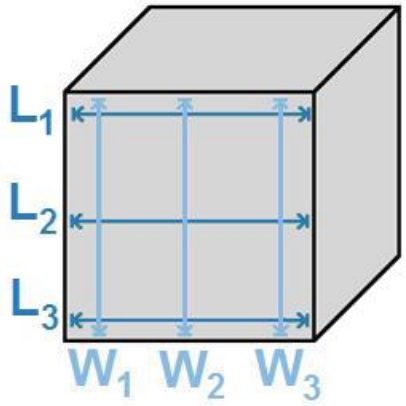

Figure 4.8 Cement cube and measurements (L: length, W: Width)

4.7 Determination of Compressive Strength (Destructive Method)

Compressive strength plays an important role in the cement and concrete industry. When cementing a wellbore, data about the compressive strength is used to predict the wait-on-cement time. This time designation indicates how long after pumping the cement slurry one must wait before implementing further activities, e.g. subsequent drilling activities or other well completion operations. The wait-on-cement time focuses on the early compressive strength development. Over a long period of time, the compressive strength is used as an indicator of the cement´s stability. The integrity of the cement and consequently the integrity of the well is partly based on the uniaxial compressive strength. The cement slurries are designed with compressive strength values specific to the job applications, such as, to provide structural support to the cemented casing/liner, and/or to ensure zonal isolation during critical well applications.

UCS test follow the guidelines as laid out in API spec. This test method requires prepared cement cubes to be cured at temperature and pressure for a predetermined time before crushing using an API approved compressive strength testing machine. Commonly used curing times of a cement specimen is 1, 3, 7 and 21 days; however, based on specific job applications, other curing times can be used to determine compressive strengths at those time periods. The compressive strength of cement cubes is calculated by dividing the force (lbf) required to crush the hardened sample by the smallest measured cross-sectional area (in^2) of the cement cube and is reported in pounds per square inch (psi). Multiple cement specimens (minimum of three) is recommended to be used for the compressive strength test at any given curing time and the compressive strength value be the average value at which the cement cubes fail.

4.8 UCS Test Equipment and Experimental Procedure

In these experiments, the compressive strength was determined using compression testing machine (CM-2500 series, Figure 4.9) with a testing range 2,500 to 250,000 lbs. (11 – 1,112 kN) with an accuracy of 0.5% of indicated load. It is certified unit by both ASTM and API. The device applies a uniaxial load to the cement cube at a rate of 72 kN ± 7 kN per minute.

The compressive strength tests were all carried out at room temperature. Accurate measurements of their dimensions (length and width) were conducted before used in a crush test. Average and maximum force are also documented for each test.

All the specimen for a given test are broken within the permissible time tolerance according to available standards as reported in the following table:

Table 4.3 Test age and permissible tolerance

Test Age	Permissible Tolerance
1 day	± 1/2 hr
3 day(s)	± 1 hr
7 day(s)	± 3 hr

Each specimen was wiped to a surface-dry condition and all the loose parts and grains are removed from cube faces. All the faces were checked for any unusual bumps or curvatures. Each specimen was placed in the testing machine below the center of upper block. The loading rate is set before crush test begins. The loading cannot change during test or at or before failure of the cube samples.

The compressive strength of each sample is calculated according to the following formula:

$S=F/A$……..…..(4.1)

where:

S= compressive strength in psi or MPa

F= the maximum load in lbf or (N)

A= area of loaded surface in 2 $inch^2$ (50.8 mm)

The compressive strength of all the specimen relevant to same curing condition are averaged and reported to the nearest 10 psi (0.1 MPa).

Figure 4.9 Certified UCS test machine used for destructive testing of cement samples.

4.9 UPV Testing Procedure (Non-destructive Strength Test)

Ultrasonic Pulse Velocity (UPV) of cement is a non-destructive test method to check the quality of cement (concrete). Using velocity measurements of ultrasonic pulses, it is possible to assess the strength and quality of specimen. The UPV equipment has a transducer, a receiver and an indicator for showing the time of travel from transducer to the receiver. The transducer is attached firmly to cement surface. The pulses go through

the specimen and travel to the receiver. The pulse velocity can be determined from the following equation:

V=L/T……...……...…(4.3)

where; L= length ; V=pulse velocity; T=transit time

All the UPV tests were conducted using The Pundit Lab instrument. It is a flexible UPV test instrument designed primarily for operation in laboratories (Figure 4.10). It supports all traditional UPV test modes. The features of test equipment are explained in Table 4.4:

Table 4.4 Pundit Lab UPV machine information

Bandwidth	20 to 500 kHz
Pulse voltage	125 to 500 V
Nominal transducer frequency	24 – 500 kHz
Measuring range	Up to 15 m depending on concrete quality

Figure 4.10 Ultrasonic Measurement Device

4.10 Nuclear Magnetic Resonance (NMR) Equipment and Testing Procedure

A 2 MHz Oxford Geo Spec 2TM instrument (Figure 4.11) was used to determine the NMR T_2 spectra for cement specimens in this study. This machine operates at a frequency of 2 MHz, similarly to NMR logging tools, and is paired with the Green Imaging Technology (GIT) software, enabling hardware control.

Cement specimens prepared at different mixing conditions and cured at different times (1 day, 3 days ,7 days and 21 days). Then cores were prepared and fitted into vial glass. Core dimensions roughly were one inch in diameter and two in length. Samples prepared using the core bit. These smaller samples were cored from 2 by 2-inch cube samples. The system is calibrated with a pre-configured calibration sample (water with 2% NaCl in a

sealed glass vial). Porosity of each specimen was quantified using the T_2 NMR spectra. T_2 *relaxation time*s are commonly acquired through a spin-echo sequence, such as the Carr-Purcell-Meiboom-Gill (CPMG) method (90°- τ -180°- τ). Accurate T_2 values depend on the static magnetic field strength and the length of the echo spacings. In this study, the NMR T_2 response was measured using eco spacing of 150 μs.

Figure 4.11 MHz Oxford Geo Spec 2™ for NMR Tests

Chapter 5: UCS and UPV Test Results

5.1 Overview

Wellbore cement is susceptible to many mechanical loads during the life of a well. Cement strength is a key property for the cement and overall wellbore integrity. As discussed in Chapter 2, many cement properties such as strength are developed during hydration of silicate phases. One of the key questions left unanswered in the cement literature is whether cement mixing condition can impact cement strength or not. Studies by Padgett, (1996) implied that 1-day cement strength is not function of mixing energy. Additionally, according to mixing energy theory, matching cement strength is achievable by equal mixing energy. Therefore, changing shear rate, scale and mixing equipment should not change cement strength. In order to evaluate the impact of cement mixing condition on cement strength, we have conducted both destructive unconfined compressive strength (UCS) and non-destructive ultrasonic pulse velocity (UPV). It is important to show results of both methods (UCS and UPV) since many of the cement labs rely only on UPV tests. Some of literature shows quite significant differences between UCS and UPV (Ichim, 2017).

In the first phase of experiments we kept the mixing energy constant by changing shear rate and mixing time according to the mixing energy formula. Cube samples were prepared from each mix design for UCS and UPV tests. In the second phase of experiments we increased the mixing energy and conducted UCS and UPV tests. As discussed in Chapter 3, the original DoE for single step mixing has two factor three level analysis (3^2). Two factors considered are mixing energy and shear rate. This design considered three shear rates at 6000 rpm, at 12000 rpm and at one mid-point of 9000 rpm.

Mixing energy levels of 5.9 KJ/Kg, 8.9 KJ/Kg and 11.8 KJ/Kg were considered. In order to keep mixing energy constant at various shear rates, mixing time will change. To increase mixing energy to the next level, mixing time will be increased further. Finally, we performed analysis of variance (ANOVA) to investigate importance of each variable. In some cases, cell means plots are reported for some results when there is an interaction effect.

5.2 UCS Testing Results

UCS are first presented for each individual mixing energy and then compared for each specific curing time. We must note that for having constant mixing energy at different shear rates, mixing time will change as well. All results are presented by including standard error in the charts. Details of standard errors in all measurements are presented in the Appendix B of this dissertation.

5.2.1 UCS Results for 5.9 KJ/Kg

Results of UCS testing for 5.9 KJ/Kg mixing energy level samples are reported in Figure 5.1 for all mixing conditions and 1, 3, 7 and 21 curing days. We also have compared UCS results for specimens prepared according to API two step mixing procedure as a control sample. It is clear that even though all samples have been prepared at the same mixing energy of 5.9 E/M, their UCS are not the same. Therefore, results imply that matching strength development is not observed at same mixing energy. Results of 1-day curing indicates lowest UCS for the specimen prepared at 12000 rpm. Also, the shortest mixing time is for specimen prepared at 12000 rpm (37 seconds). At three days curing, it is evident that as the shear rate is increasing from 6000 rpm to 12,000 rpm, UCS declines by about 29%. At 3 days curing, highest (24.34 MPa) and lowest UCS (17.31

MPa) are observed for slurry mixed respectively at 6000 rpm and 12000 rpm. We must note that lower shear rate is accompanied with longer mixing time which will provide longer hydration time and more precipitation of C-S-H gel and silicates therefore leading to higher strength. At 3 days curing time, UCS for samples prepared based on API mixing conditions is 20.25 MPa. This value is by average 14% more than UCS of samples prepared at 12,000 rpm and 16% less than UCS of the samples prepared at 6000 rpm. This can be explained by having both low and high shear mixing conditions in preparation of API samples.

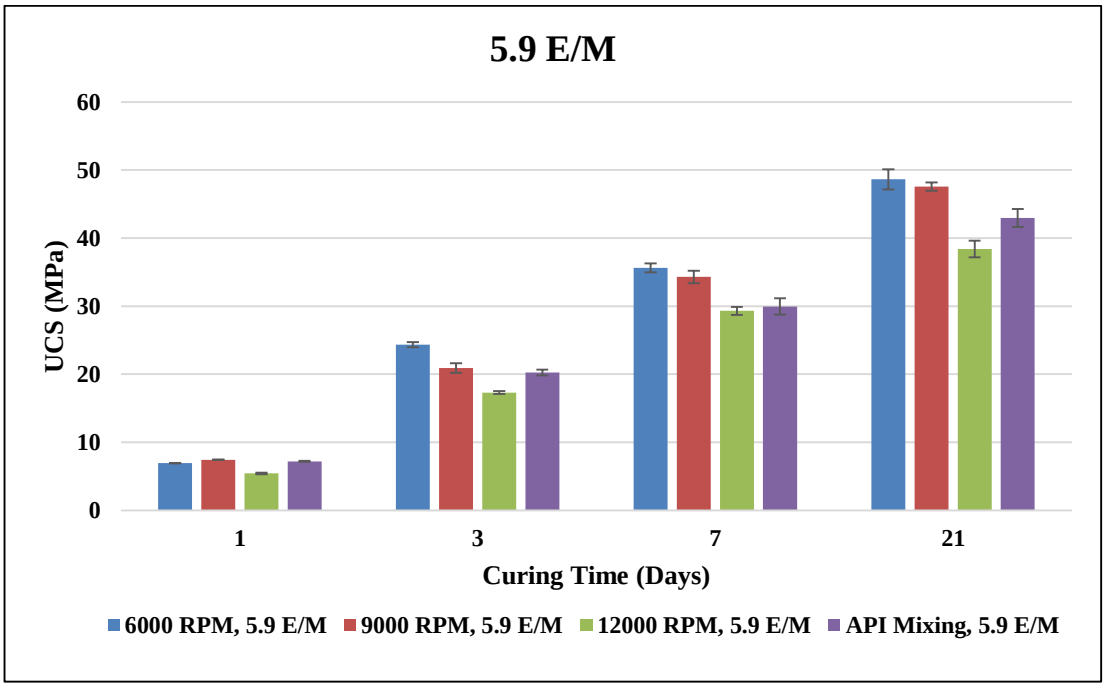

Figure 5.1 UCS test results for 5.9 KJ/Kg mixing energy levels at all mixing conditions. Mixing condition impacts UCS at 5.9 E/M. Samples with longer mixing time show higher strength

5.2.2 UCS Results for 8.9 KJ/Kg

Results of UCS testing at 8.9 KJ/Kg mixing energy are reported in Figure 5.2 for all mixing conditions and 1, 3, 7 and 21 curing days. In general, results of 8.9 E/M follow similar trend as 5.9 E/M. At one-day curing, UCS ranges from 7.37 MPa to 8 MPa. At 3

days curing, UCS is 24.71 MPa at 6000 rpm and 21.69 MPa at 12,000 rpm (12% difference). At 3 days curing time, UCS for samples prepared based on API mixing conditions is 20.34 MPa. At 7 days curing, a similar trend as 3 days is observed confirming higher UCS at lower shear rate (6000 rpm).

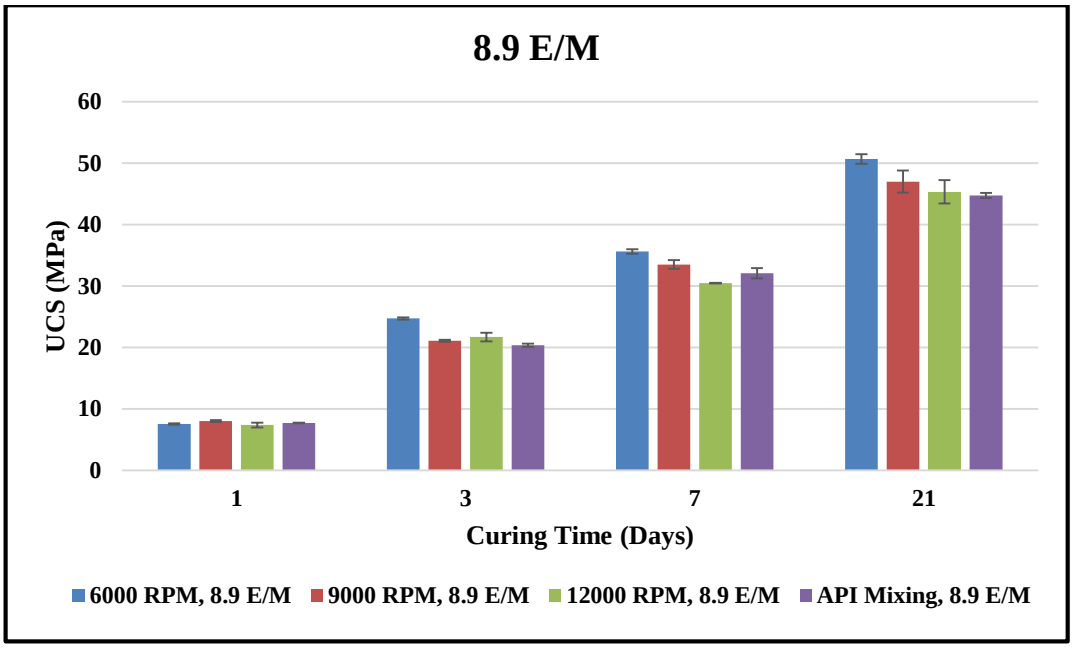

Figure 5.2 UCS testing results for 8.9 KJ/Kg mixing energy levels at all mixing conditions. Mixing condition impacts UCS at 8.9 E/M. Samples with longer mixing time show higher strength

5.2.3. UCS Results for 11.8 KJ/Kg

Results of UCS testing at 11.8 KJ/Kg mixing energy are reported in Figure 5.3 for all mixing conditions and in curing times of 1, 3, 7 and 21 days. We observe similar trend in UCS at 11.8 E/M as compared to 5.9 E/M and 8.9 E/M.

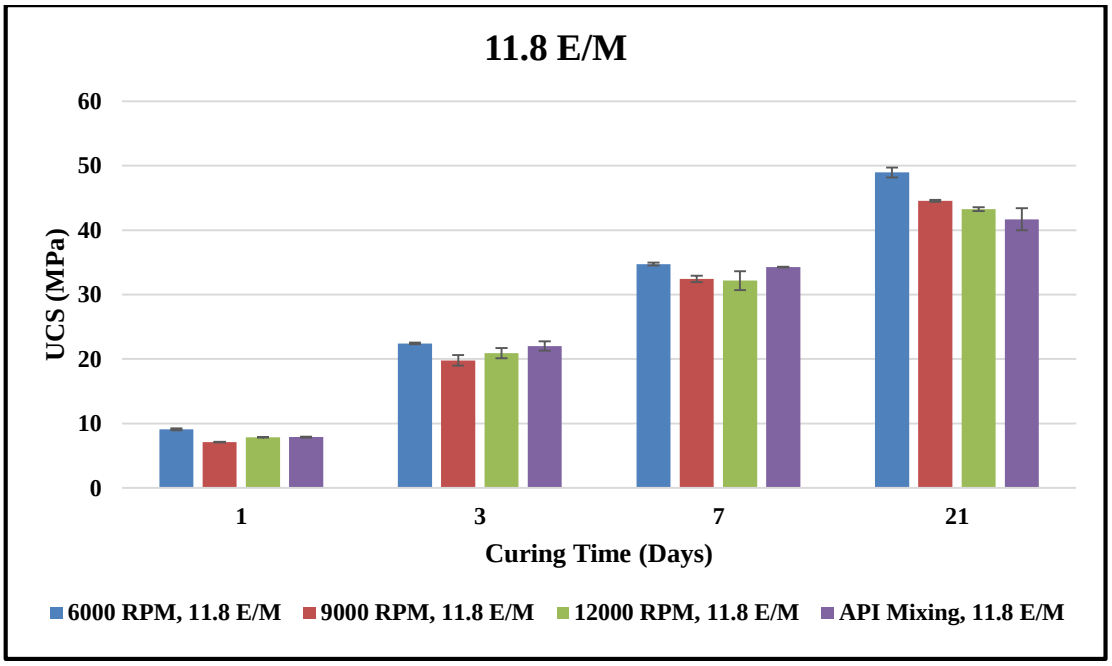

Figure 5.3 UCS testing results for 11.8 KJ/Kg mixing energy levels at all mixing conditions. Mixing condition impacts UCS at 11.8 E/M. Samples with longer mixing time show higher strength

5.2.4 One-day Curing

Here, we report and compare UCS based on each specific curing day for all the three energy levels. UCS for one-day curing time has lowest value of 5.42 MPa prepared at 12000 rpm and 5.9 E/M and maximum value of 9.08 MPa prepared at 6000 rpm and 11.8 E/M (40% difference). Note that highest and lowest UCS are tied respectively to 294 seconds mixing time (6000 rpm and 11.8 E/M) and 37 seconds mixing time (12000 rpm and 5.9 E/M). Mixing energy is tightly coupled with shear rate and mixing time. Hence, higher mixing time leads to higher mixing energy. This indeed shows that mixing energy, shear rate, and mixing time all impact UCS in first day of curing.

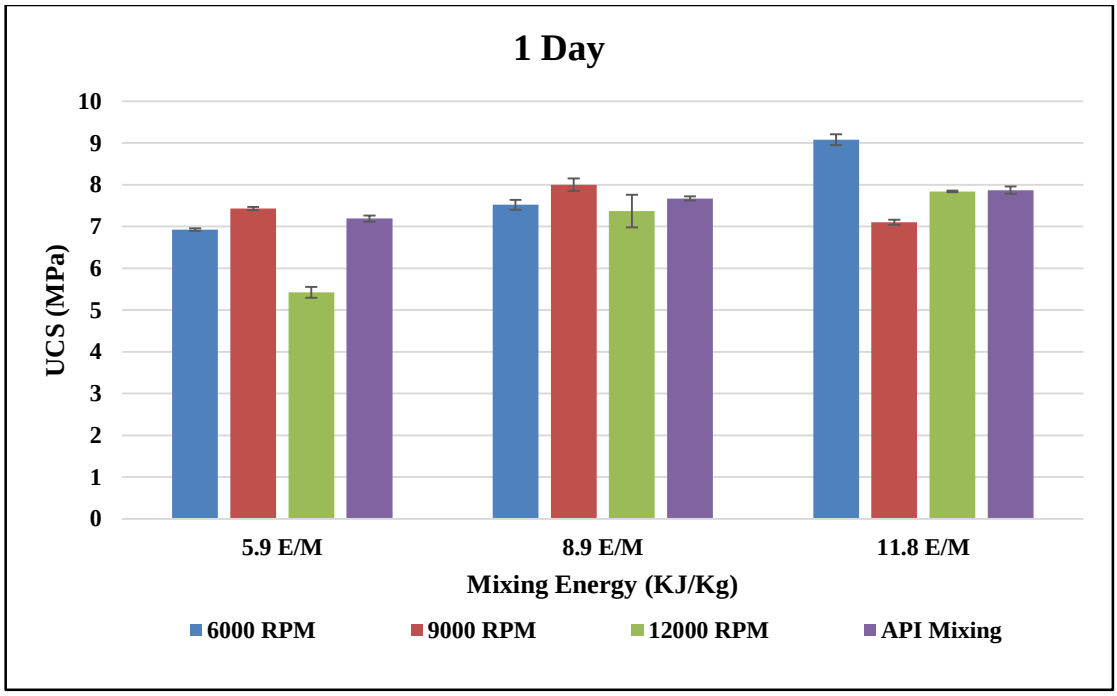

Figure 5.4 UCS testing results for one-day curing time at all mixing conditions. Highest and lowest UCS are tied respectively to 294 seconds mixing time (6000 rpm and 11.8 E/M) and 37 seconds mixing time (12000 rpm and 5.9 E/M)

To better understand the significance of differences, we performed an ANOVA (Analysis of Variance) for UCS obtained at each curing day.

5.2.4.1 One Day Curing ANOVA Results

Table 5.1 shows the ANOVA results for UCS at one-day curing. As shown in this table *SS* stands for sum squared, *df* stands for degree of freedom, *MS* stands for mean squared (ratio of *SS* column over *df*), F is ratio of variation between sample means and variation within the samples.

Among all these values, p-value is the most important cell of outcome and helps to determine significance of the results when you perform a hypothesis test. This value ranges from 0 to 1. A smaller p-value (usually less than 0.05) indicates that strong evidence exist against the null hypothesis. It simply indicates if we can accept the null

hypothesis or reject it. For conducting ANOVA, we set α (significance level) of 0.05, this is based on having 95% confidence level. After setting α, we want to test few different things:

- Is there any difference between shear rates (mixing times) or not?
- Is there any difference due to the mixing energy?
- Is there any difference due to interactions between shear rate (mixing time) and mixing energy?

There are a three sets of hypothesis tests which two-way ANOVA will handle. The following set of hypotheses have been considered for one-day UCS testing:

H_o: One-day cement UCS is not affected by mixing energy.

H_1: One-day cement UCS is affected by at least one level of mixing energy.

H_o: One-day cement UCS is not affected by shear rate (mixing time).

H_1: One-day cement UCS is affected by at least one level of shear rate (mixing time).

H_o: There is no interaction between shear rate and mixing energy.

H_1: There is interaction between shear rate and mixing energy.

Now, we can decide based on reported p-value results. Table 5.1 shows p-value for interaction is significantly smaller than α, therefore, H_o is rejected and strong evidence exists for interaction between mixing energy and shear rate (mixing time). In other words, the impact of one factor depends on the level of the other factor. In order to better understand interaction effects, a cell mean plot can be used. A cell mean plot or interaction plot is a line plot of UCS at different mixing condition for all the three mixing energy levels as shown in the Figure 5.5.

Table 5.1 ANOVA results for one day UCS tests

Source of Variation	SS	df	MS	F	P-value	F crit
Mixing Energy	9.67	2.0	4.83	41.79	1.7208E-07	3.55
Shear Rate	4.29	2.0	2.15	18.57	4.1967E-05	3.55
Interaction	8.90	4.0	2.22	19.23	2.6209E-06	2.92
Within	2.08	18.0	0.11			
Total	24.95	26.0				

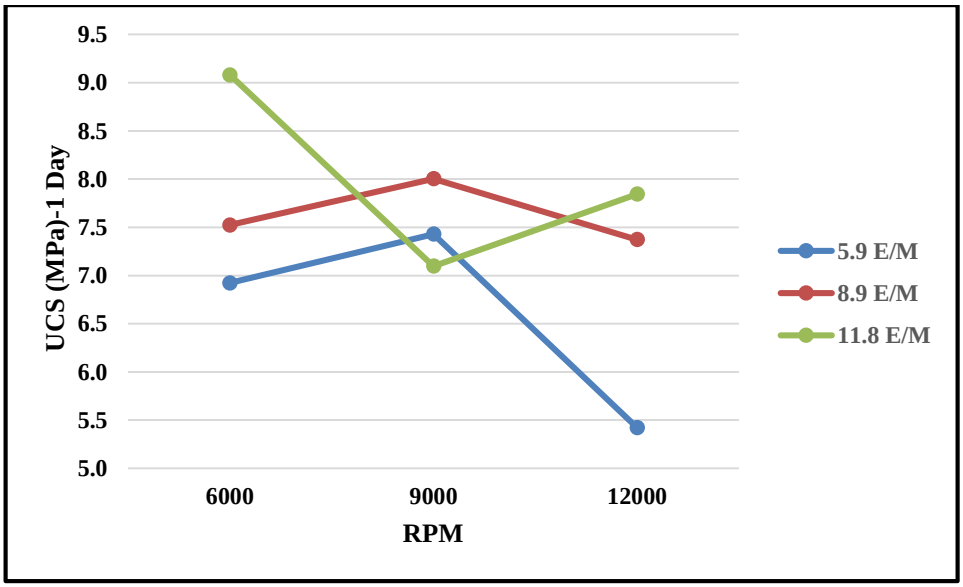

Figure 5.5 Cell mean plot for UCS at 1-day curing time

In this plot each line represents one of the mixing energy levels. Looking at 12000 rpm, UCS is weakest for 5.9 E/M and strongest for 11.8 E/M. At 6000 rpm, UCS has the same trend. But for 9000 rpm, UCS is highest for 8.9 E/M and lowest for 11.8 E/M. After explaining the interactions between shear rates and mixing energy, each individual hypothesis can be investigated. Based on p-values from ANOVA table (which are smaller than α), both shear rate and mixing energy are significant therefore, we reject the null hypothesizes. Also, it can be implied that both factors are individually significant when we analyze them independently and have interaction when we analyze them together.

5.2.5 Three-days Curing

Three days UCS for all mixing energies is shown in the Figure 5.6. Overall, a difference of 30% is observed between the highest and lowest UCS at 3 days curing respectively for 8.9 E/M, 6000 rpm and 5.9 E/M, 12000 rpm. This is a different trend than the UCS for one-day curing in which highest UCS was observed at 11.8 E/M, 6000 rpm where here highest UCS is seen for 8.9 E/M energy level mixed at 6000 rpm (222 seconds). In addition, we can observe that UCS of samples prepared at 9000 rpm and 12000 rpm are still high at 8.9 E/M compared to samples prepared under same shear rates in two other energy levels. As stated before, this may suggest an existence of a critical mixing time in which UCS reaches its peak and then slightly drops as mixing time increases. Comparing UCS for three energy levels at 12,000 rpm shows it is very similar at 8.9 E/M and 11.8 E/M but quite different than 5.9 E/M (20% difference). This again suggests existence of critical mixing time. In other words, 37 seconds mixing time used for preparation of samples at 5.9 E/M is not sufficient. For cement particles to react fully with water and formation of enough C-S-H gels and silicates useful for cement strength, a longer mixing time (more than 37 seconds) is required regardless of shear rate.

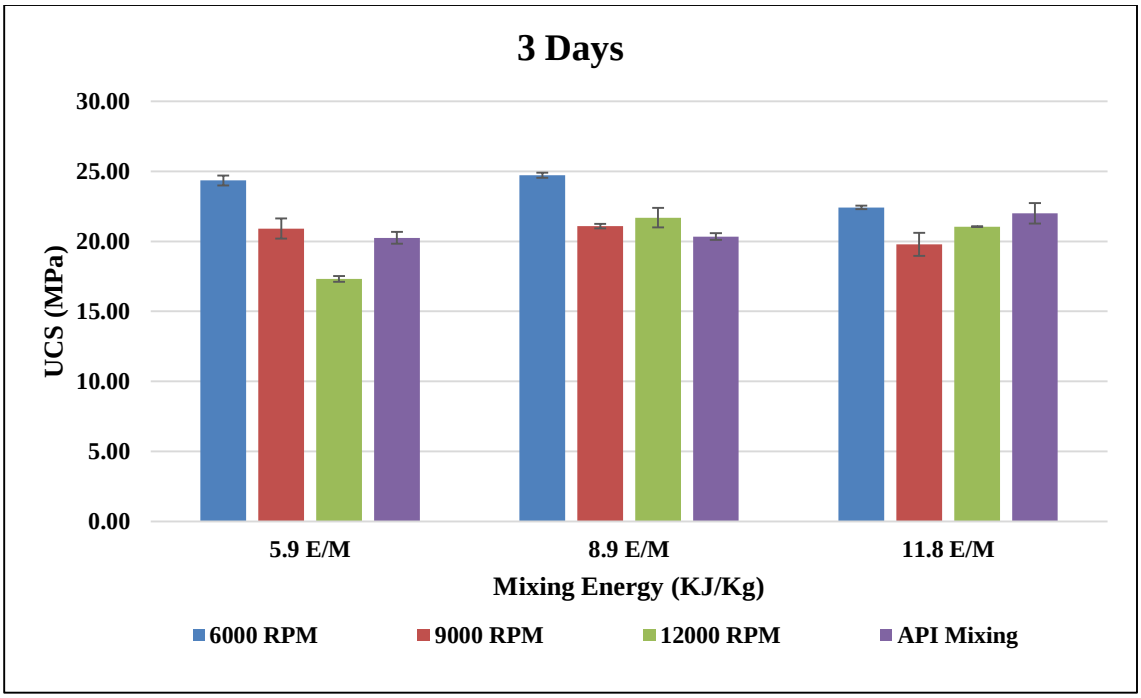

Figure 5.6 UCS testing results for three days curing time at all mixing conditions

5.2.5.1 Three-days Curing ANOVA Results

Similar set of hypotheses were considered for three days UCS testing. Table 5.2 shows ANOVA result of the data. Based on p-values, both mixing energy and shear rate (mixing time) are significant as well as interactions. Since there is an interaction effect, we show a cell mean plot.

Table 5.2 ANOVA results for 3 day UCS tests

Source of Variation	SS	df	MS	F	P-value	F crit
Mixing Energy	14.57	2	7.28	5.65	0.01245669	3.55
Shear Rate	76.93	2	38.46	29.83	1.9288E-06	3.55
Interaction	30.33	4	7.58	5.88	0.0032939	2.92
Within	23.20	18	1.28			
Total	145.04	26				

Figure 5.7 shows the cell mean plot for UCS in 3 days curing.

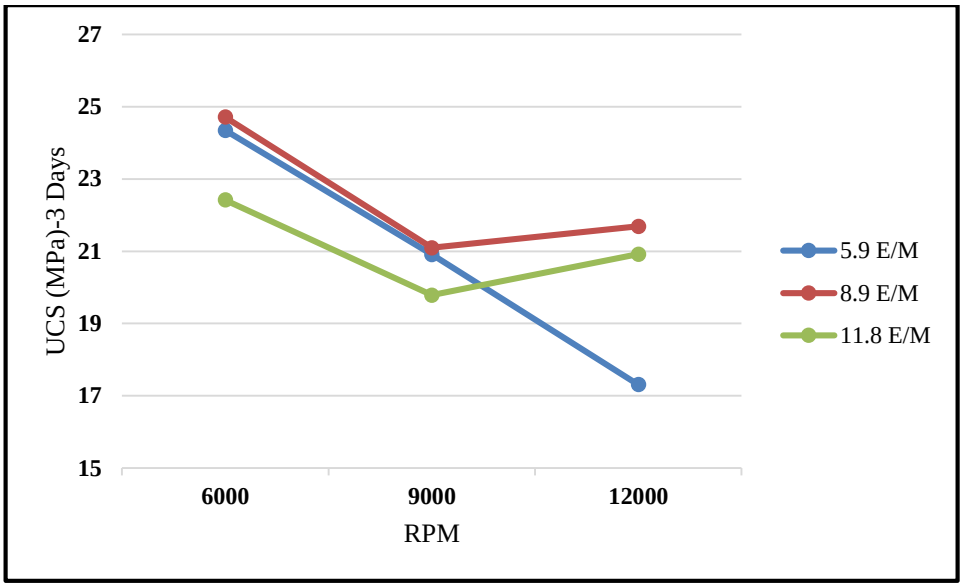

Figure 5.7 Cell mean plot for UCS at 3 days curing time

Based on this plot, at 6000 rpm and 9000 rpm, UCS of 5.9 E/M and 8.9 E/M samples are stronger than 11.8 E/M. Note that at 12000 rpm, 5.9 E/M samples have lowest UCS where 8.9 E/M samples have highest UCS. This indicates interaction where same trend is not observed at two different rpm. After explaining the interactions between shear rates and mixing energy, each individual hypothesis can be investigated. Based on p-values from Table 5.2 (which are smaller than α), both shear rate (mixing time) and mixing energy are significant. Therefore, we reject the null hypothesizes.

5.2.6 Seven-days Curing

UCS for 7 days is plotted in the Figure 5.8. Similar to UCS at 3 days, highest UCS at 7 days is for 8.9 E/M at 6000 rpm (35.64 MPa). However, it is slightly different than the maximum UCS at 6000 rpm for 5.9 E/M and 11.8 E/M (up to 3% difference). This indicates that as curing day increases, the difference between maximum UCS (at 6000 rpm) for three energy levels becomes smaller. Similar observations can be made for samples prepared at 9000 rpm in three energy levels where their UCS differ by less than

5%. In addition, UCS values for samples prepared at 12000 rpm is in close range for three energy levels. We can again infer that lowest UCS belongs to the samples prepared at 5.9 E/M and 12000 rpm (37 seconds mixing time). This implies that regardless of curing days, a very short mixing time can impact cement strength.

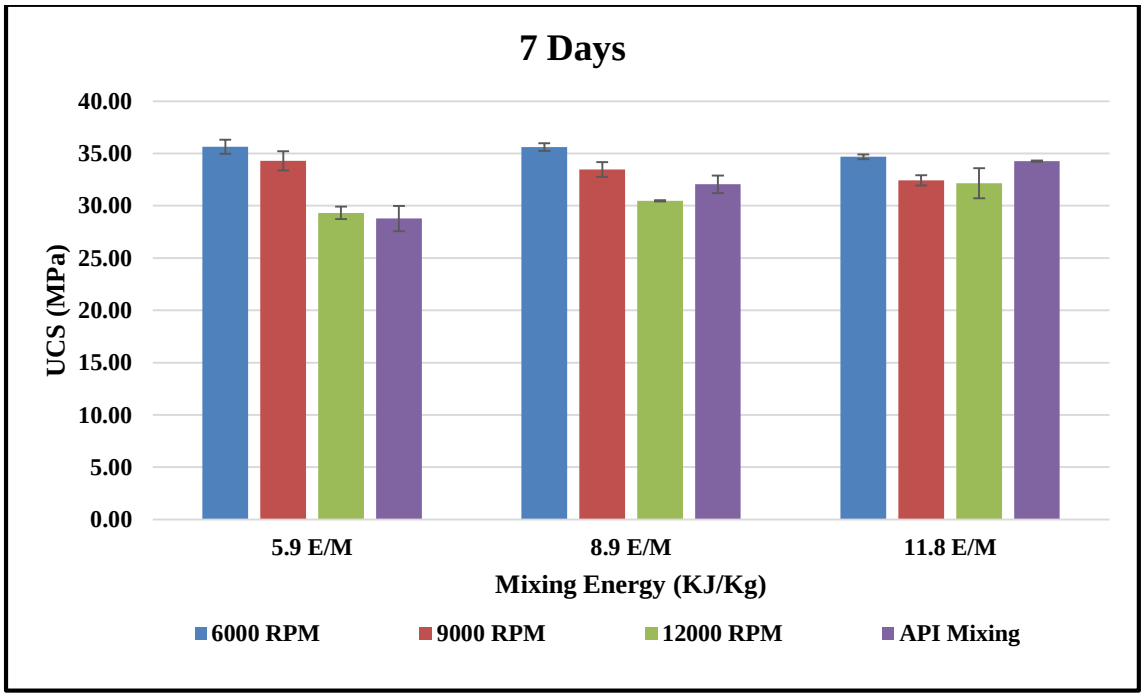

Figure 5.8 UCS testing results for seven days curing time at all mixing conditions

5.2.6.1 Seven-days Curing ANOVA Results

Similar set of hypotheses were considered for seven days UCS testing. Table 5.3 shows the ANOVA result of the data and it can be implied from p-values that unlike 1 and 3 days curing data, there is no interaction between mixing energy and shear rate. In addition, mixing energy p-value is significantly large so null hypothesis is accepted for mixing energy and the only significant factor is shear rate with a very small p-value. It demonstrates importance of shear rate for long term cement strength as compared to

mixing energy where its effect cannot be observed after one week. Furthermore, UCS is strongest at 6000 rpm and weakest at 12000 rpm.

Table 5.3 ANOVA results for 7 day UCS tests

Source of Variation	SS	df	MS	F	P-value	F crit
Mixing Energy	0.05	2	0.025	0.010	0.9896	3.55
Shear Rate	99.32	2	49.66	20.93	2.0044E-05	3.55
Interaction	19.01	4	4.75	2.004	0.1370	2.92
Within	42.69	18	2.37			
Total	161.07	26				

5.2.7 21 Days Curing

UCS for 21 days curing is plotted in the Figure 5.9. Similar to 3 and 7 days curing time data highest UCS in 21 days curing is for 8.9 E/M and 6000 rpm (50.66 MPa). Again, lowest UCS at 21 days curing belongs to samples prepared at 5.9 E/M and 12000 rpm (38.4 MPa). A difference of 24% is observed between the highest and lowest UCS.

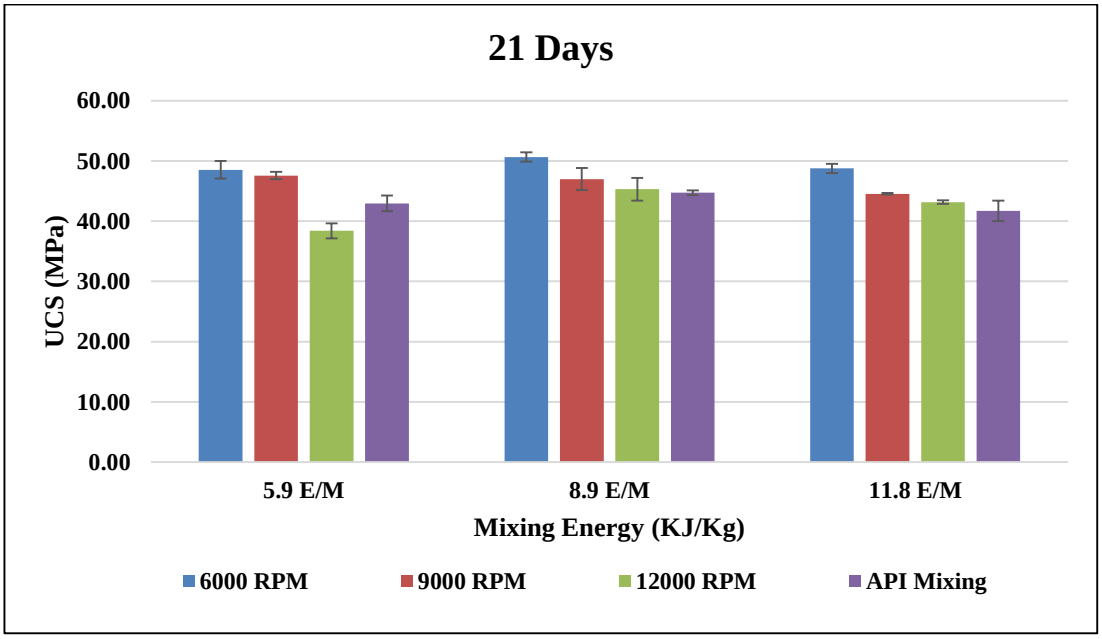

Figure 5.9 UCS testing results at 21 days curing time at all mixing conditions

5.2.7.1 21 Days Curing ANOVA Results

Similar set of hypotheses were considered for twenty-one days UCS testing. Table 5.4 shows the ANOVA result. Comparing p-values, it can be observed that mixing energy and interactions are not significant where shear rate impact is still significant. This trend proves the importance of shear rate to gain longer time (21 days) strength for cement slurry whereas mixing energy is only significant in one and three days cured samples.

Table 5.4 ANOVA results for 21 day UCS tests

Source of Variation	SS	df	MS	F	P-value	F crit
Mixing Energy	37.70	2.00	18.85	2.66	0.0972	3.55
Shear Rate	227.78	2.00	113.89	16.07	0.000099	3.55
Interaction	60.16	4.00	15.04	2.12	0.1200	2.93
Within	127.57	18.00	7.09			
Total	453.21	26.00				

5.2.8 API Mixing Results

For analyzing UCS based on API mixing procedure, we only considered one-way ANOVA since the only changing factor is mixing energy. ANOVA table is shown for one day UCS (Table 5.5). Based on the table, p-value is smaller than α, therefore, null hypothesis will be rejected and at least one inequality exists between different mixing energy levels.

Table 5.5 ANOVA results for UCS using API mixing procedures

Source of Variation	SS	df	MS	F	P-value	F crit
Between Groups	0.74	2.00	0.37	15.54	0.00423843	5.14
Within Groups	0.14	6.00	0.02			
Total	453.21	26.00				

Similar one-way ANOVA was conducted for 3, 7 and 21 days. All the p-values are found significantly larger than α , therefore, null hypothesis will be accepted which means there is no difference between levels of mixing energies.

5.3 Comparison of UCS Based on Mixing Time

Based on comparison of the UCS we can imply that a trend of increase in UCS can be seen as the mixing time increases. To better see this impact we have plotted all the UCS versus mixing time regardless of shear rate as shown in Figure 5.10. Some interesting observations can be made. First, there is a direct relationship between mixing time and UCS in which as mixing time increases, UCS increases as well. This is consistent with at least one other study in concrete literature as discussed in Chapter 2. Takahashi et al., 2011 showed that the hydrates are dispersed more uniformly when mixing time is longer. Additionally, more precipitation of silicates occurs when mixing time increases (Takahashi et al., 2011). Second, the slope of trend line is steeper at early mixing times (up to 65 seconds). This time may be an initial critical mixing time where beyond it only slight increase in UCS can be seen. Second, UCS has an increasing trend with mixing time up to 222 seconds. After this time, UCS slightly decreases (decreases by maximum 5% at 295 seconds measurements except at one-day curing). This may suggest a second critical mixing time where beyond that, increase in UCS is not achievable at 3,7, and 21 days.

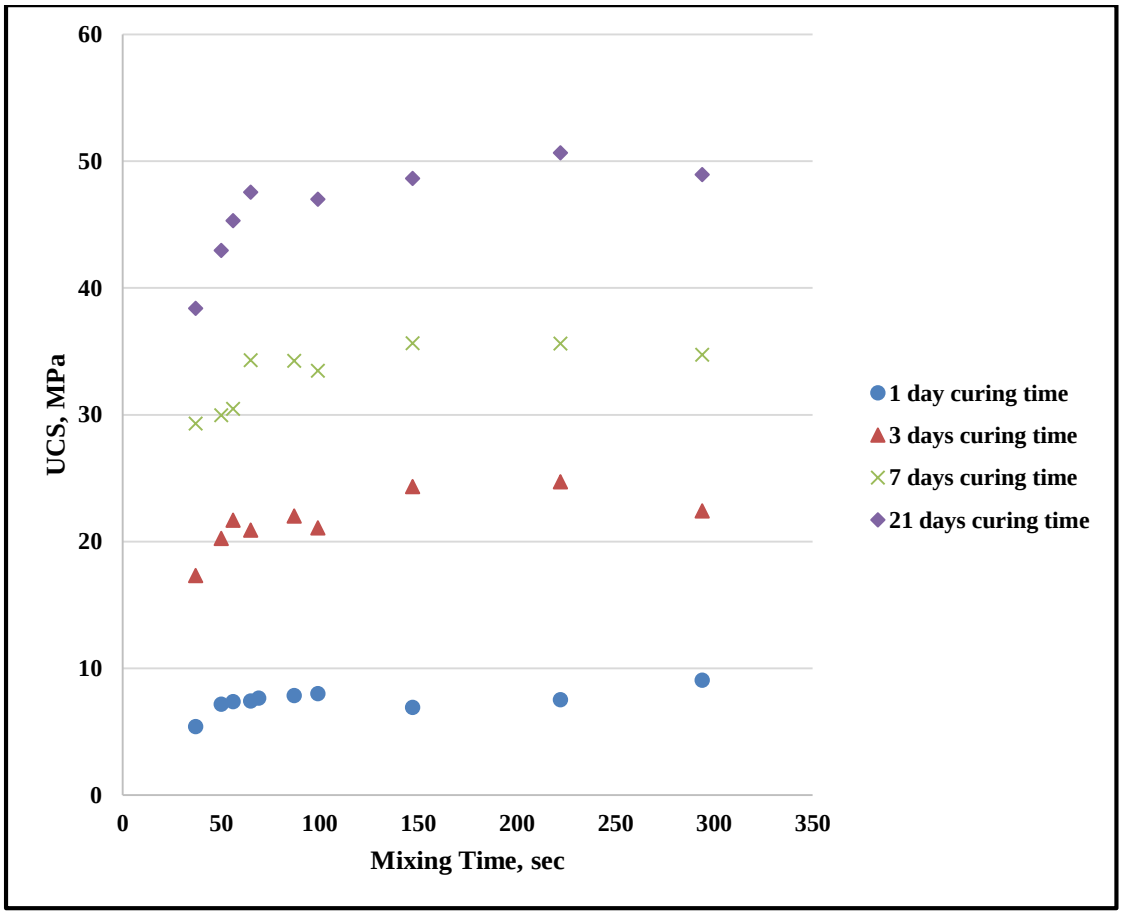

Figure 5.10 UCS versus mixing time for curing at 1, 3, 7 and 21 days. There is a direct relationship between mixing time and UCS in which as mixing time increases, UCS increases as well.

5.3.1 UCS Test Results at Low RPM

As discussed earlier API Warring blender used for cement mixing has ability mix at or above 3000 rpm. Therefore, to evaluate mixing at lower speeds we performed tests using another blender keeping the same API Waring container and blade. The new mixing equipment provided 2000 rpm. Conducting tests lower than 2000 rpm was not possible due to excessive vibration we observed in mixing process. Based on mixing energy theory, for 5.9 E/M, mixing time should be set to 1300 seconds. Results of UCS for 2000 rpm and 1,3,7 and 21 days are shown in Figure 5.11. Results imply that even though

mixing time significantly increased, the low shear rate used in the mixing yielded lower UCS at 3, 7 and 21 curing days compared to UCS of specimen prepared at 6000 rpm and 9000 rpm. Nearly 29% difference in UCS is observed at 3 days curing between UCS for specimen mixed at 6000 rpm (222 seconds) and the one mixed at 2000 rpm (1300 seconds). As outlined in Figure 5.10, there is a critical mixing time which beyond UCS gradually declines (more than 294 seconds). Some of the studies for concrete mixing show that very long prolonged mixing is detrimental to cement strength (Lerch et al., 2018). As noted by Lerch et al., (2018) "prolonged mixing can increase the performance, but too much mixing, does however reduce the performance."

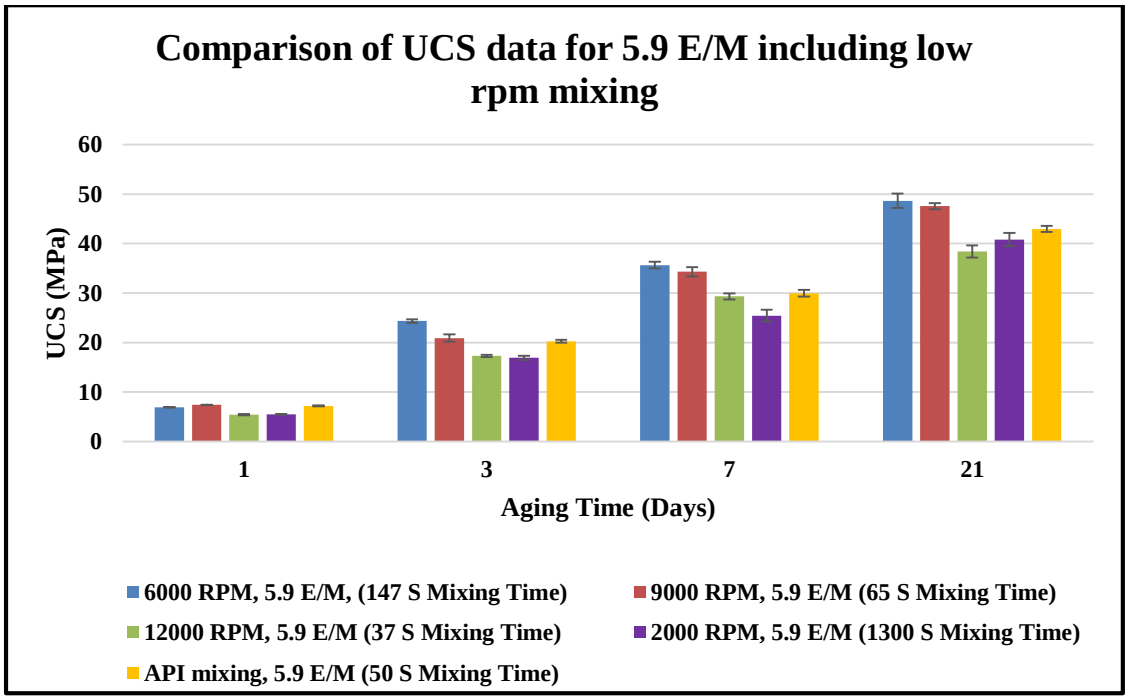

Figure 5.11 Comparison of 5.9 E/M UCS for high and low rpm mixing conditions

5.4 UPV results

In this section, we show results of ultrasonic pulse velocity (UPV) of cement samples prepared at different mixing conditions. Then, we compare UPV versus UCS to

understand their correlation for different mixing conditions. At first, we present UPV results at each individual mixing energy and then comparing for each specific curing time and finally showing ANOVA results.

5.4.1 UPV Results for 5.9 E/M

Results of UPV at 5.9 KJ/Kg mixing energy level are reported in Figure 5.12 for all mixing conditions and curing times of 1, 3, 7 and 21 days. Similar to UCS at one day, UPV for 9000 rpm is highest (2447 (m/s)). This drops to 2377 m/s and 2272 m/s respectively at 6000 and 12000 rpm (7 % difference). This difference is comparable to UCS in first day for 5.9 E/M (7% difference between highest and lowest UCS).

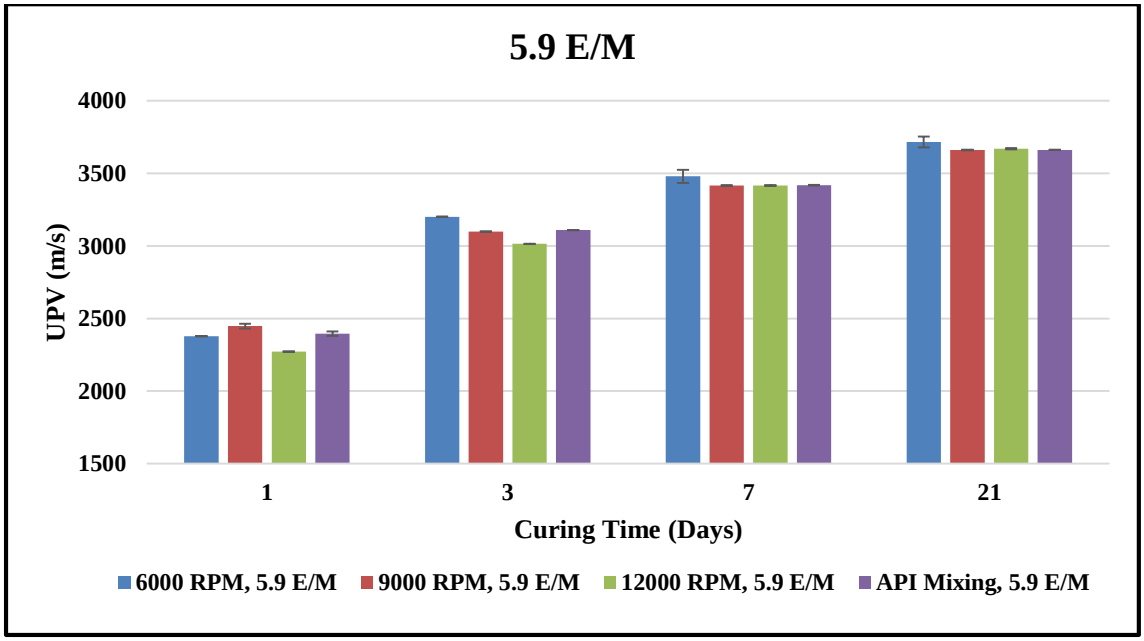

Figure 5.12 UPV results of 5.9 KJ/Kg mixing energy at all mixing conditions

5.4.2 UPV Results for 8.9 E/M

Results of UPV at 8.9 KJ/Kg mixing energy level are reported in Figure 5.13 for all mixing conditions and curing times of 1, 3, 7 and 21 days. Similar to 5.9 KJ/Kg results, at one-day, UPV for 9000 rpm is still highest at 2478 (m/s). This drops to 2460 m/s and

2457 m/s respectively at 6000 and 12000 rpm (less than 1% difference). This difference is much lower when compared to UCS in first day for 8.9 E/M (8% difference between highest and lowest UCS). Unlike UPV for 5.9 E/M at first day, UPV for 8.9 E/M does not show the difference between samples prepared at different shear rates.

In general, the difference in UPV is not as significant as UCS. Maximum difference of 4% observed between UPV for samples prepared based on using different shear rates.

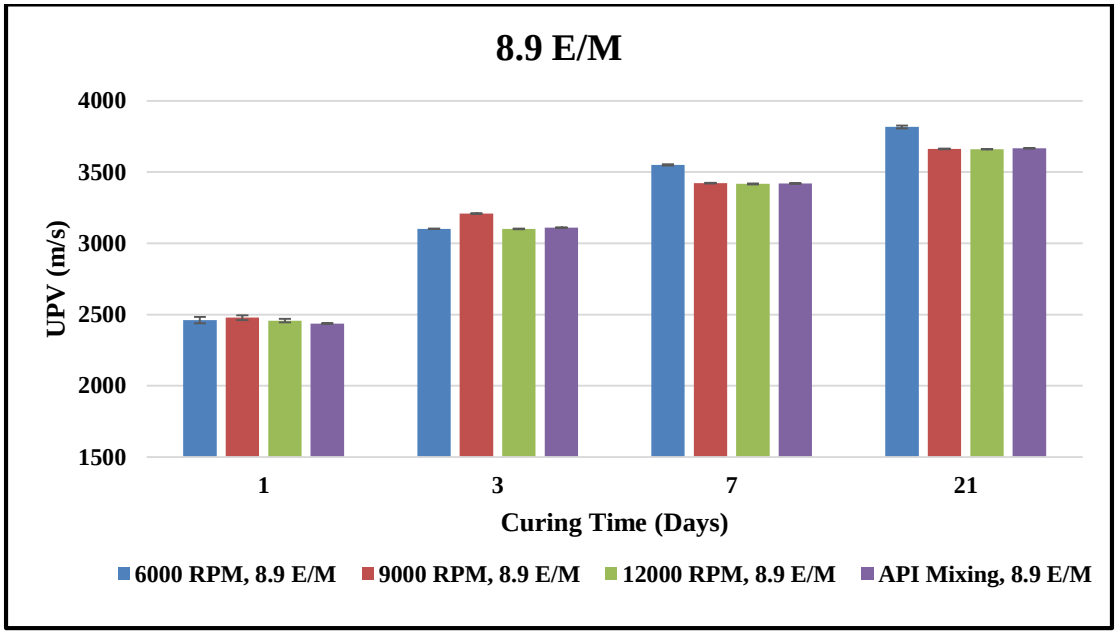

Figure 5.13 UPV results of 8.9 KJ/Kg mixing energy at all mixing conditions

5.4.3 UPV Results for 11.8 E/M

Results of UPV testing at 11.8 KJ/Kg mixing energy level are reported in Figure 5.14 for all mixing conditions and curing times of 1, 3, 7 and 21 days. We can observe similar trend, where the difference in UPV is not as significant as UCS.

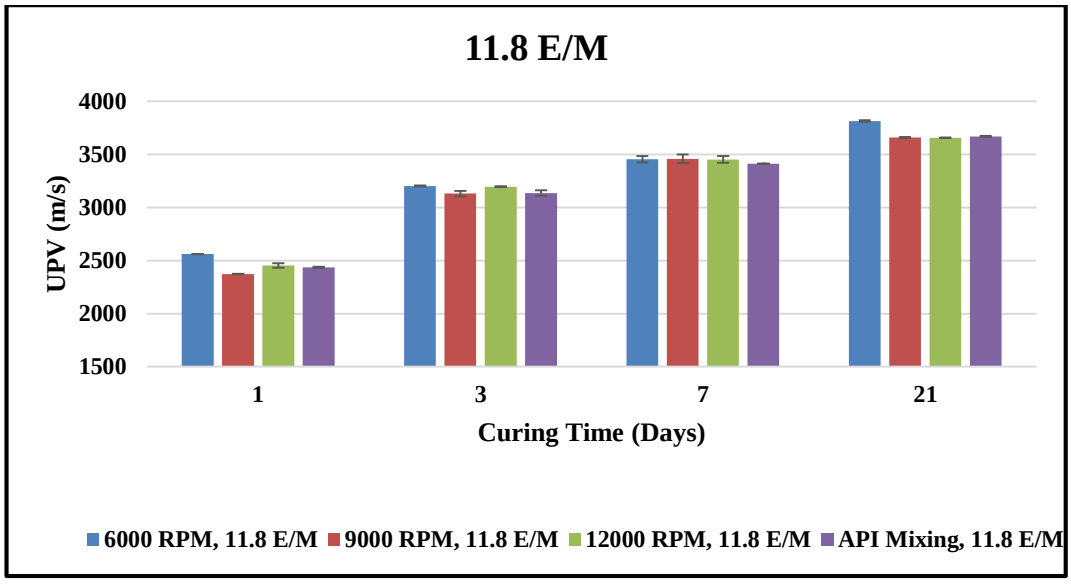

Figure 5.14 UPV results of 11.8 KJ/Kg mixing energy and all shear rate conditions

5.4.4 One Day Curing

We compared UPV for each specific curing time at different mixing energy levels. Figure 5.15 shows the UPV for samples prepared at one-day curing and different mixing energy levels. The highest UPV belongs to samples prepared at 11.8 E/M and 6000 rpm. The lowest UPV belongs to samples prepared at 5.9 E/M and 12000 rpm.

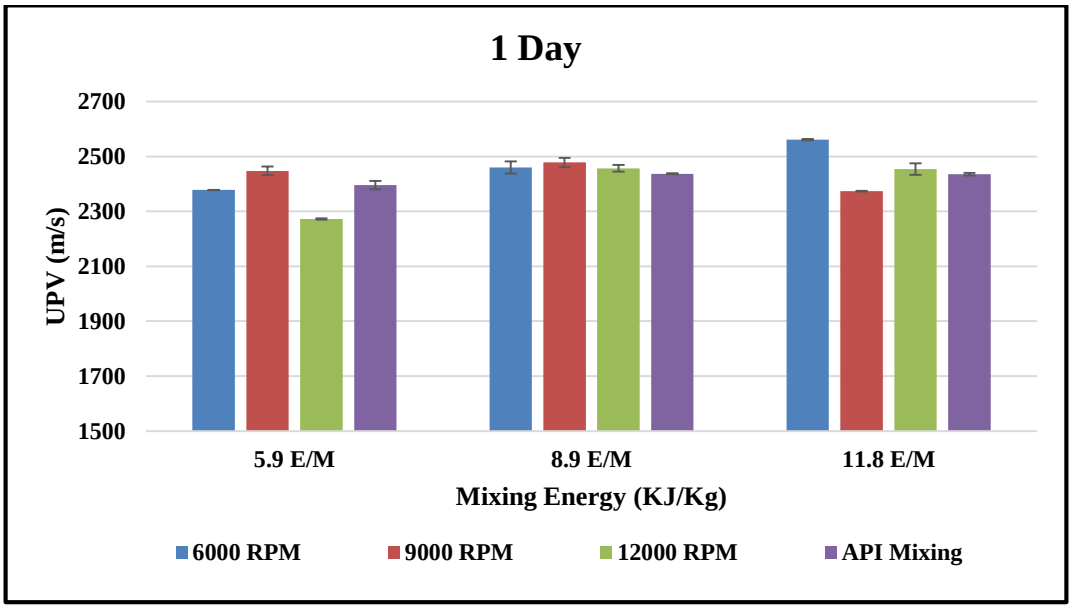

Figure 5.15 UPV testing results of 1-day curing for all mixing conditions

5.4.4.1 One Day Curing ANOVA Results

Based on ANOVA result of the data and p-values, we reject all the three null hypotheses. This indicates importance of mixing energy, shear rate and their interactions. Table 5.6 shows overall changes in UCS and UPV values for different curing days:

Table 5.6 Comparison of UCS and UPV test results for different curing days

1 Day	3 Days	7 Days	21 Days
$\Delta_{UCS} = 40\%$	$\Delta_{UCS} = 30\%$	$\Delta_{UCS} = 18\%$	$\Delta_{UCS} = 24\%$
$\Delta_{UPV} = 11\%$	$\Delta_{UPV} = 6\%$	$\Delta_{UPV} = 4\%$	$\Delta_{UPV} = 4\%$

5.4.5 Comparison of UPV for Low RPM Mixing

After mixing cement at 2000 rpm, UPV test results are shown in the Figure 5.16. Results indicate that even though mixing time significantly increased, the low rpm used in the mixing yielded lower UPV at 3, 7 and 21 curing days. This observation is consistent when comparing UCS at all conditions as shown by Figure 5.12.

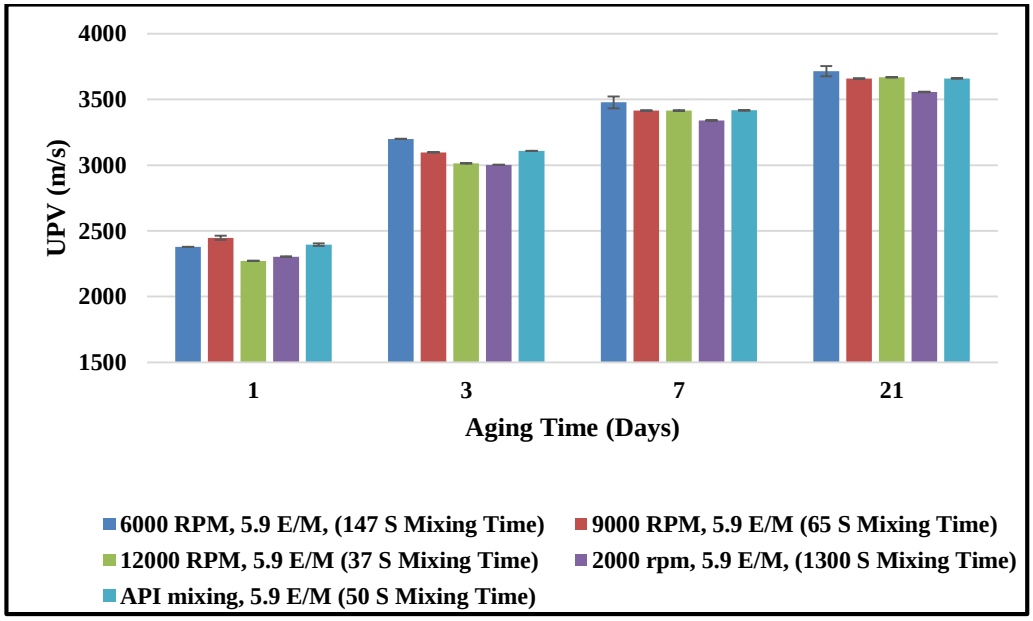

Figure 5.16 UPV testing results for 5.9 E/M at all mixing conditions

5.5 Relationship between UPV and UCS for Different Mixing Conditions

We evaluate empirical relationships between the ultrasonic pulse velocity values and the compressive strength measurements. Figures 5.17 to 5.19 show the data points graphically. In addition, exponential trend lines were added to obtain UPV vs. UCS correlations for each cement mixing condition. These correlations can be useful for future applications as base trend lines for impact of mixing energy on cement strength and to correlate with UPV measurements. Overall, results show a very good fit for all the trend lines.

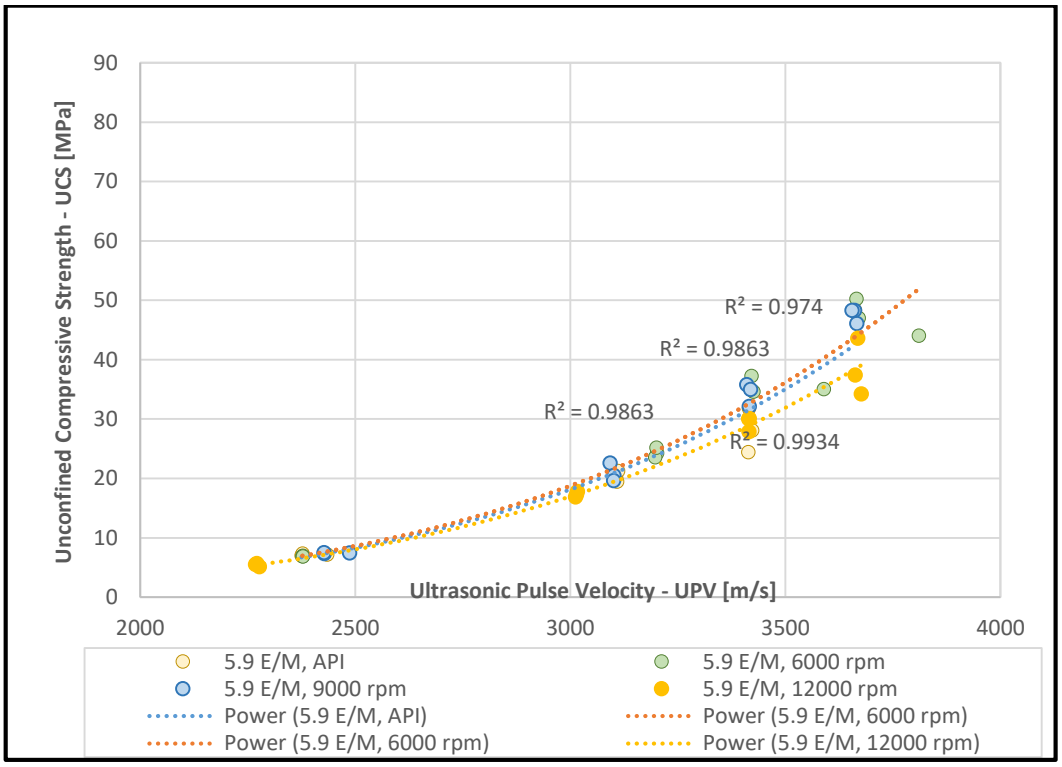

Figure 5.17 UPV versus UCS for 5.9 E/M samples

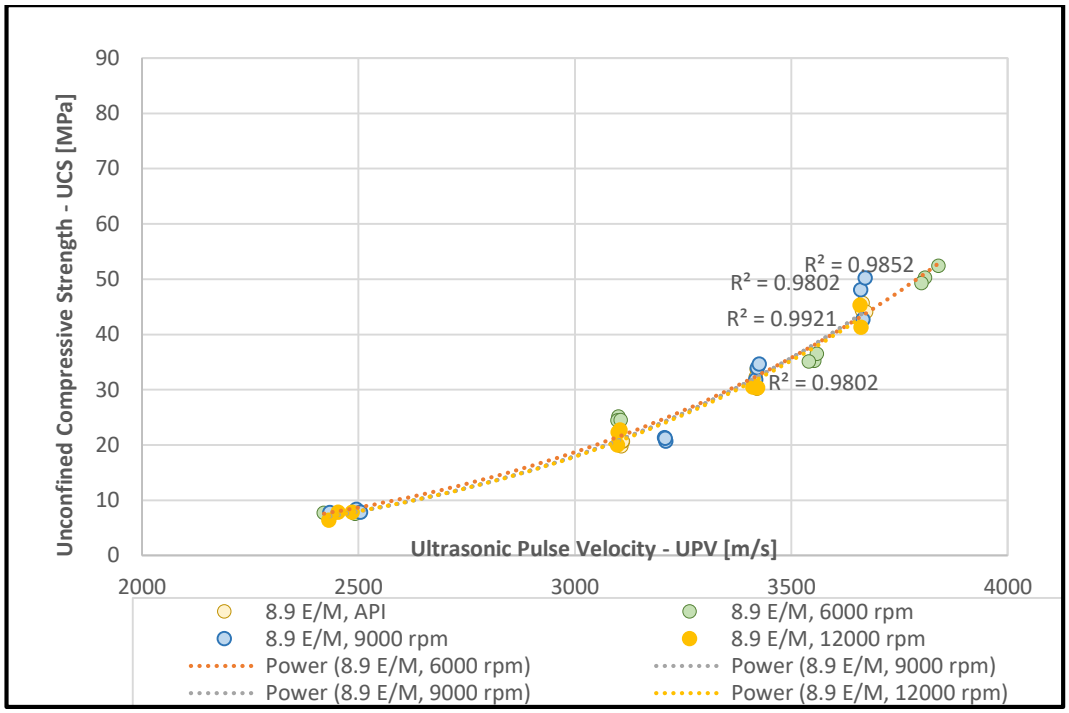

Figure 5.18 UPV versus UCS for 8.9 E/M samples

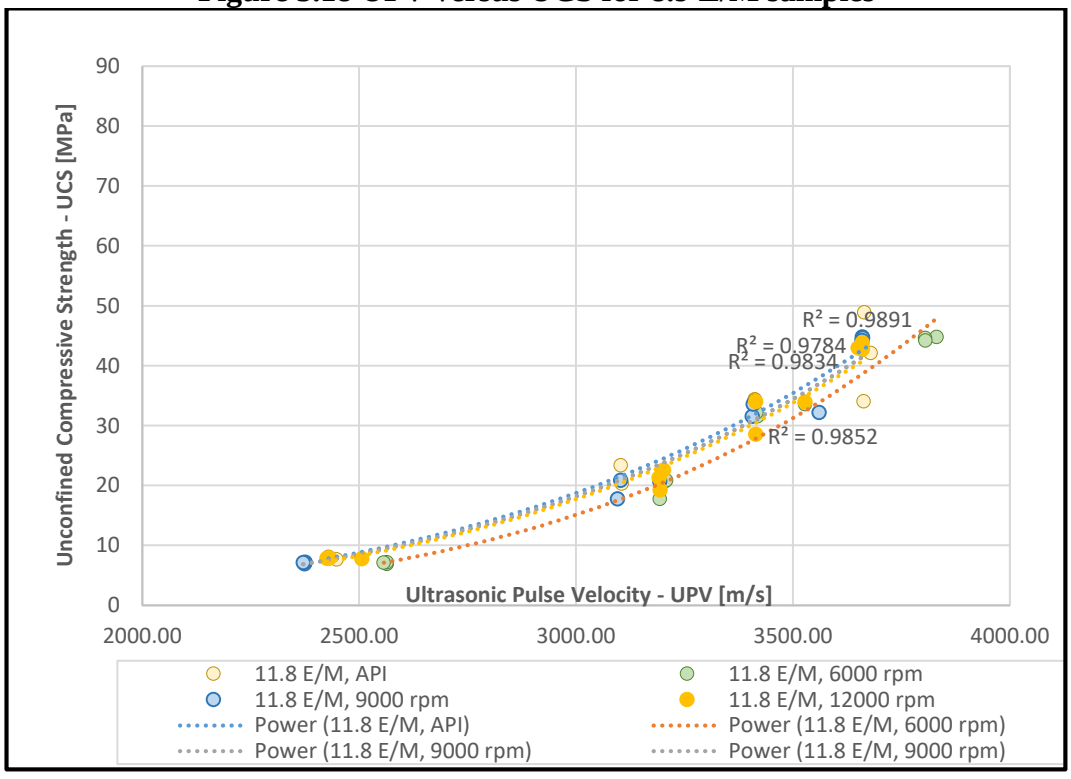

Figure 5.19 UPV versus UCS for 11.8 E/M samples

Chapter 6: Rheology and Thickening Time Tests

6.1 Overview

In the cementing operation, zonal isolation is dependent on a successful cement job. For a successful cement job, the slurry must have good rheological properties and be pumpable to the desired interval. In some cases, the slurry achieves a good strength in the desired time while it is not pumpable due to very short thickening time. It is crucial to understand cement rheological properties because of its impact for pumpability inside well and wellbore hydraulics. Changes in equivalent circulating density (ECD) of cement slurry is closely tied to wellbore hydraulic. Thick cement slurry may cause larger frictional pressure in wellbore annulus and leading to well fracturing and subsequent down time. Additionally, thickening time design is more critical in some cement job operations such as deepwater since a very narrow safety margin exists. Cement slurries are usually tested for their rheology profile by measuring shear stress at different shear rates. These parameters are pivotal in determining their flow properties. The testing procedure obtains yield stress, viscosity, and how the slurry reacts to shear stress.

The fundamental question we want to answer in this Chapter is whether cement mixing conditions can change its rheology and thickening time or not. Therefore, the primary objective of this chapter is first to show results of rheological measurements and thickening time tests for the DoE discussed in Chapter 3. Second, to gauge API mixing energy theory and whether slurries with same mixing energy will have equivalent rheology and thickening time. Thickening time and rheology tests were performed at two energy levels of 5.9 E/M and 11.8 E/M, mixed at 6000 rpm and 12000 rpm. In addition, tests were conducted using the API two step mixing procedure.

6.2 Rheology Tests

All rheological experiments were conducted according to API 10B2 standards for cement slurries and using commercially available rotational rheometer described in detail in Chapter 4. For all the testing results, measurements were conducted at six different shear rates as per API recommendations. All the rheological measurements were conducted at 102 ^{o}F temperature to be consistent with test conditions for thickening time. This temperature was selected from API recommended tables. After conducting measurements for each mixing described in the DoE table, a comparison of plastic viscosity (PV) and yield point (YP) based on Bingham plastic model is presented. The measurements were performed at least twice in order to check the repeatability and experimental error.

6.2.1 Rheology Test Results for Single Step Mixing

Test results for shear stress and shear rate of the slurry prepared at 5.9 KJ/Kg are shown in the Figure 6.1. It indicates that at higher shear rate mixing (12000 rpm), shear stress is higher compared to similar data at lower shear rate mixing (6000 rpm). Although it is mixed at higher shear rate, slurry becomes thicker when mixing time is short. When mixing time is short, larger particles are left inside the mix causing higher shear stress and viscosity. This can be explained by a cement slurry deflocculating process as discussed in Chapter 2. As discussed, deflocculation is a key physical process responsible in mixing. For instance, for cementing applications a proper deflocculation occurs when cement powders are properly mixed, and they are small enough to be fully wetted with water molecules.

Furthermore, these results are consistent with observation from UCS in which at higher shear rate and short mixing time, resulted in smaller UCS values.

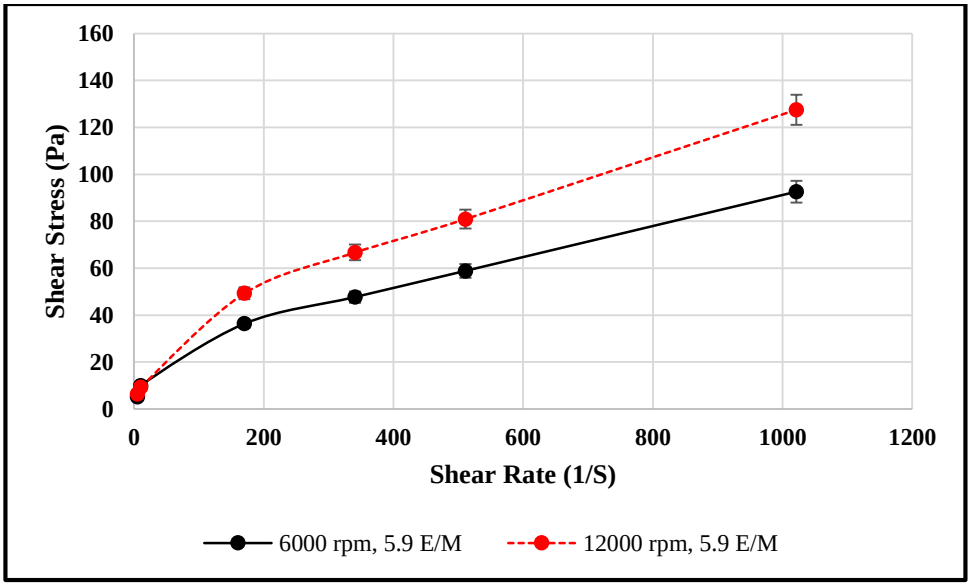

Figure 6.1 Rheology test results for 5.9 E/M and for slurries mixed at 6000 and 12000 rpm

Rheology test results of the slurry prepared at 11.8 KJ/Kg are shown in the Figure 6.2. We see similar trend for shear rate and shear stress as discussed for slurry prepared at 5.9 KJ/Kg mixing energy level. It indicates that at the higher shear rate of 12000 rpm and same mixing energy, shear stress increases. So far our results show that regardless of mixing energy, increase in shear rate at shorter mixing time thickens the sample. We note that although higher shear rate is desirable for mixing, this is only effective when enough mixing time is allowed. In order to compare results for 5.9 E/M and 11.8 E/M rheology, we show all the data in Figure 6.3. In general, the slurry prepared at 5.9 E/M and 12000 rpm is much thicker compared to the rest. This implies that 37 seconds mixing time is very short causing a thicker slurry as also causing lowest UCS. In addition, slurries prepared at higher mixing energy levels have lower shear stress compared to ones

prepared at lower energy levels. This can be explained by the fact that at higher mixing energy, the slurry is deflocculated better.

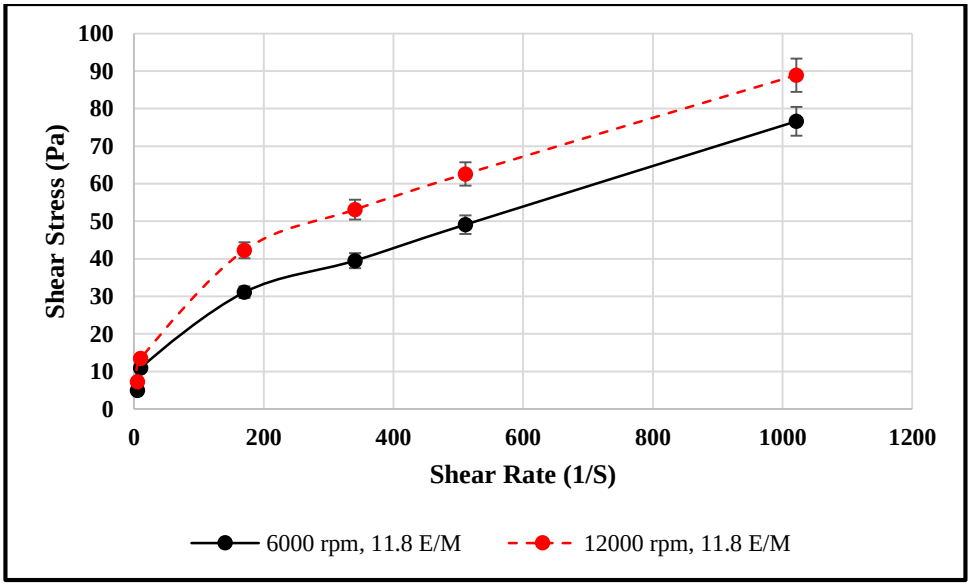

Figure 6.2 Rheology test results for 11.8 E/M and for slurries mixed at 6000 and 9000 rpm

We will show that these results are consistent with longer thickening time observed for 11.8 E/M slurries. Overall, we can see that the slurry prepared at 6000 rpm and 11.8 E/M mixing energy is thinner than the rest. Results from UCS tests showed very high strength for the specimen mixed at these condition. So we can infer that mixing procedure impacts not only cement strength but also its flow and thickening time.

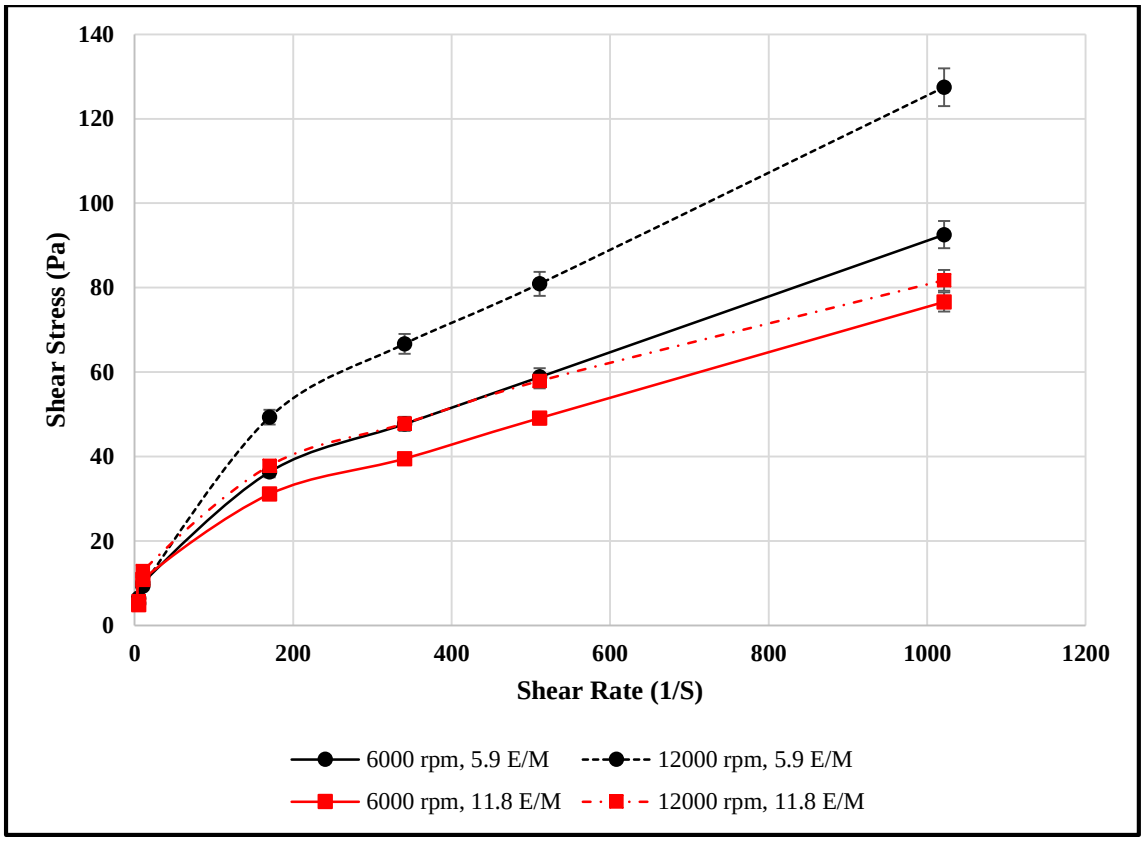

Figure 6.3 Rheology test results for 5.9 E/M and 11.8 E/M and for slurries mixed at 6000 rpm and 12000 rpm

6.2.2 Rheology Tests Based on API Mixing Procedure (Two Step Mixing)

Results of rheology tests for slurries prepared based on two-step API mixing procedure is shown in the Figure 6.4. Results infer similar trend as observed for one step mixing slurries. As energy level increases, slurries become thinner. The difference in shear stress is most notable at higher rheometer shear rates (1021 s^{-1} and 511 s^{-1}).

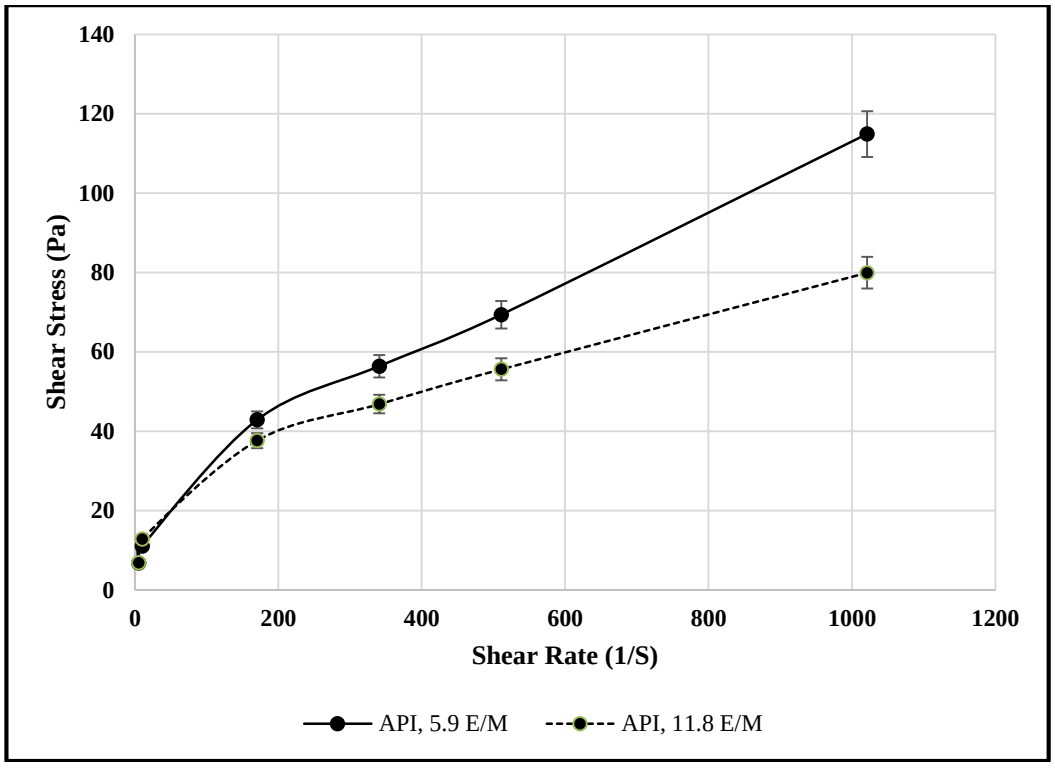

Figure 6.4 Rheology test results for 5.9 E/M and 11.8 E/M and for slurries mixed according to API mixing conditions

6.3 Plastic Viscosity (PV) and Yield Point (YP)

We have used the Bingham plastic model for comparing PV and YP for different mixing conditions. Before discussing results, we provide a short summary of this model and how PV and YP can be affected by mixing conditions.

Bingham plastic model is one of the most commonly used non-Newtonian models to describe rheological properties of cement slurries. In Bingham plastic model, flow starts at a minimum shear stress called yield stress. After yield stress is attained, behavior is similar to that of Newtonian fluid, i.e. viscosity is constant and does not vary with shear rate. Hence, plastic viscosity (PV) is the slope of the linear line for shear stress and shear rate. Cement slurries are usually composed of a continuous fluid phase in which solids

are dispersed. Plastic viscosity is that part of the resistance to flow caused by mechanical friction. The friction is caused by:

- Solids concentration.
- Size and shape of solids.
- Viscosity of the fluid phase.

The yield point is the initial resistance to flow caused by electrochemical forces between the particles. This electrochemical force is due to charges on the surface of the particles dispersed in the fluid phase. Yield point is a measure of these forces under flow conditions and is dependent upon:

- The surface properties of the solids
- The volume concentration of the solids and
- Ionic environment of the liquid surrounding the solids

Figure 6.5 shows PV calculated from rheology measurements (PV is reported in milli-Pa.S). It can be seen that when mixing energy increases, PV decreases. As explained previously, deflocculation process improves at higher mixing energy, therefore causing smaller particles to be left in the cement mixture and subsequently smaller plastic viscosity. Similar justification can be used for higher shear rate at short mixing time, which causes less deflocculation. This will leave much larger particles in the mixture and causing higher PV. The effect of shear rate is consistent to the results obtained from the thickening time tests. Considering effects of energy and shear rate, as mixing time increases, this will reduce PV. Figure 6.6 shows the yield point for the different mixing conditions. YP follow a similar trend as the PV, increasing with shear rate. Also when mixing energy increases, YP increases. As discussed earlier, YP is a function of hydrate

formation and chemical reactions rather than physical changes. In longer mixing time more C-S-H hydrates precipitate in the mixture, therefore, the YP increases by mixing energy level. Similar phenomena were observed by Vidick, (1990), in which after longer mixing time, a large number of hydrates were formed. The growth of these hydrates creates larger surface area and subsequently higher YP. At lower mixing energy, the YP will be lower due to smaller surface area.

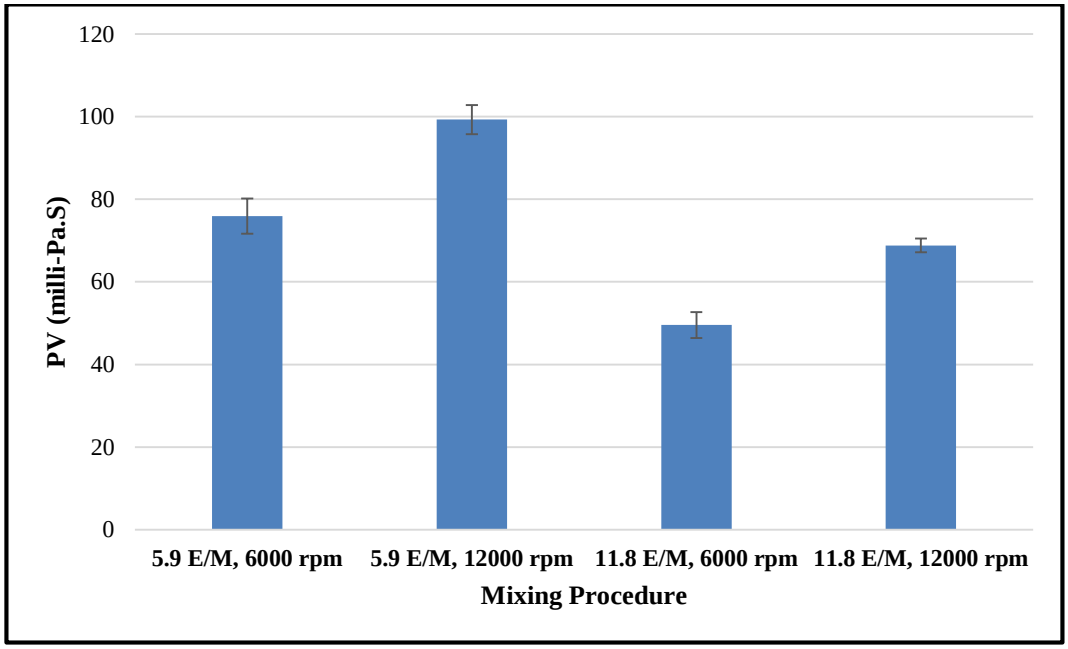

Figure 6.5 Plastic viscosity (PV) for slurries prepared using one step mixing procedure

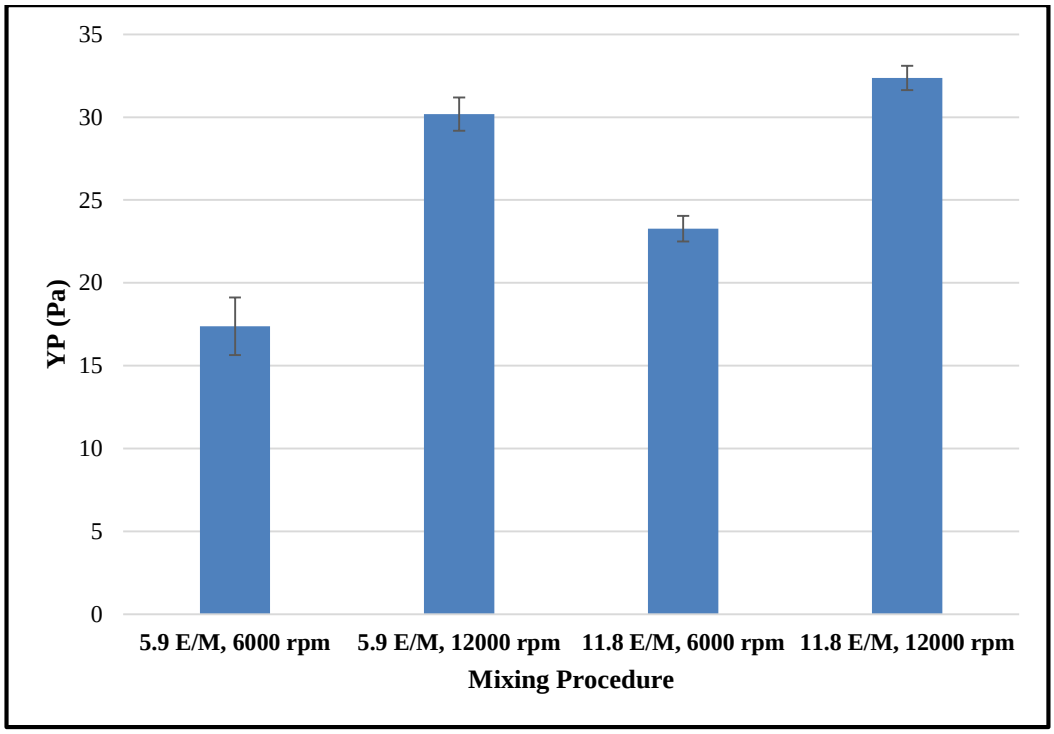

Figure 6.6 Yield point (YP) for slurries prepared using one step mixing procedure

Figures 6.7 and 6.8 show PV and YP for slurries mixed by API mixing procedures. It can be observed that similar trend exists between higher mixing energy and PV. This shows that regardless of mixing procedure, PV solely depends on deflocculation process. If proper deflocculation occurs, it yields to lower PV. As the mixing energy increases, this provides a longer mixing time and subsequently better deflocculation process. We can see similar trend for YP, increasing with mixing energy as observed in previous tests.

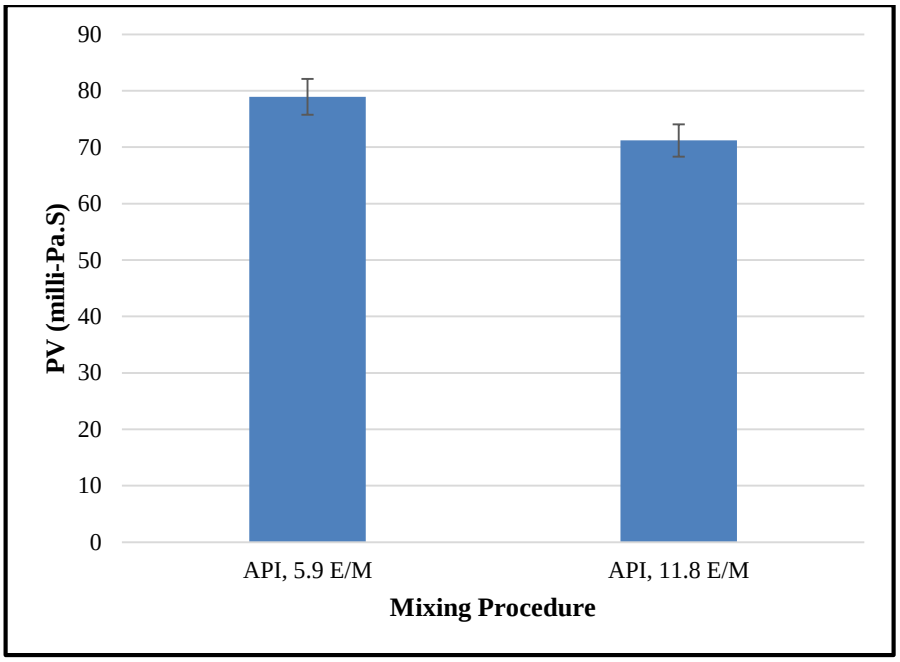

Figure 6.7 Plastic viscosity (PV) for slurries prepared using two step mixing procedure according to API recommended mixing procedure

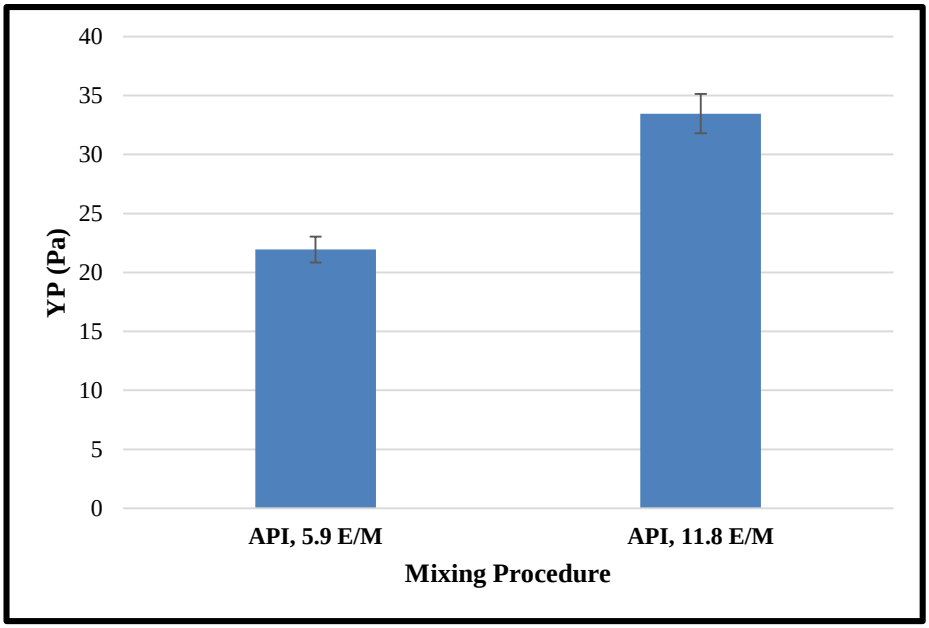

Figure 6.8 Yield point (YP) for slurries prepared using two step mixing procedure according to API recommended mixing procedure

6.4 Comparison with Previous Research

Studies investigating the effect of mixing process on rheological properties are limited. Hibbert et al., (1994), showed rheological tests results under different mixing conditions; these are presented in the Table 6.1. Comparison of results from this work with Table 6.1 implies similar trends. PV and YP, respectively, decrease and increase with increasing in mixing energy.

Table 6.1 Effect of mixing energy on cement rheological properties (Data after Hibbert et al., 1994)

Mixing Energy (KJ/Kg)	PV (mPa.S)	YP (Pa)
2.4	126	27
5.6	97	29
9.7	85	38

Similar results were observed by Vidick (1990) in which the effect of mixing conditions on viscosity was studied. Tests conducted on class G API cement showed a decrease in plastic viscosity as mixing energy increased. In addition, parallel experiments on particle size confirmed larger particles in cement mixing with the lower mixing energy (Figure 2.16 in Chapter 2).

6.5 Thickening Time

Thickening time is an important property of cementing operations. API 10B2 defines thickening time as the time for a cement slurry to develop a selected Bc, a Bearden unit of consistency. According to industry practices, a cement with thickening time of 70 Bc is not pumpable (Nelson and Guillot, 2006). However, safe industry practices consider Bc values of 50 or less as cut off value for thickening time depending on type of operation (Sweatman, 2000). Therefore, we considered Bc of 50 as a cut of value for thickening time.

6.5.1 Thickening Time Test Results for One Step Mixing

Results of thickening time tests are often plotted with consistency (Bc) units onvertical axis and time in minutes or hours on the horizontal axis. Consistometer unit's pressure, temperature and speed of the paddle are also often plotted on the same chart. A typical machine output for thickening time test is presented in the Figure 6.9 for 6000 rpm and 5.9 KJ/Kg mixing energy level. The blue line represents change in the consistency of the sample. The red line represents the temperature and dark blue line represents pressure. Vertical axis shows all variables and horizontal axis shows the time. Machine output presents all the data in one axis, it is difficult to see differences in consistency results; we replotted the consistency.

API-10B2 for cement testing describes guidelines for selection appropriate pressure and temperature for testing. These conditions are selected based on job requirements. For temperature, it should be increased from the slurry surface temperature to expected bottom hole circulating temperature. For pressure, it should be increased to the bottom-hole pressure expected in the downhole. Since, this research is not planned

for any specific cement job, we first considered atmospheric conditions to run the thickening time tests. However, in the atmospheric conditions, neat class H cement does not set. Our test run showed almost no changes in the consistency even after 10 hours of test duration which made it very challenging to continue experiments. Therefore, we decided to conduct experiments at a specific temperature and pressure using API tables. Therefore, we decided to conduct tests at a reasonable wellbore situation (6000 ft depth well). According to API 10B, at this depth and geothermal gradient of 1.3 ^{o}F /100 ft, 2300 psi and 102 ^{o}F is expected (Table 6.2).

Table 6.2 Well-simulation thickening time provided by API

Casing Well-Simulation Tests (Continued)

1	2		3		4		5		6		7		8	
			Temperature Gradient, °F/100 ft depth (°C/100 m depth) Temperature, °F (°C)											
Time, Min	Pressure psi	(kPa)	0.9 °F	(1.6) (°C)	1.1 °F	(2.0) (°C)	1.3 °F	(2.4) (°C)	1.5 °F	(2.7) (°C)	1.7 °F	(3.1) (°C)	1.9 °F	(3.5) (°C)
			Schedule 9.5											
	Depth	6,000 ft	(1830 m)								Mud density: 9.9 lb/gal (1.19 kg/L)			
0	450	(3100)	80	(27)	80	(27)	80	(27)	80	(27)	80	(27)	80	(27)
2	600	(4100)	82	(28)	82	(28)	82	(28)	82	(28)	82	(28)	83	(28)
4	800	(5500)	84	(29)	84	(29)	84	(29)	85	(29)	85	(29)	86	(30)
6	1000	(6900)	86	(30)	86	(30)	87	(31)	87	(31)	87	(31)	88	(31)
8	1200	(8300)	88	(31)	88	(31)	89	(32)	89	(32)	90	(32)	91	(33)
10	1400	(9700)	90	(32)	90	(32)	91	(33)	92	(33)	92	(33)	94	(34)
12	1600	(11000)	92	(33)	92	(33)	93	(34)	94	(34)	95	(35)	97	(36)
14	1700	(11700)	94	(34)	94	(34)	95	(35)	96	(36)	97	(36)	100	(38)
16	1900	(13100)	96	(36)	96	(36)	97	(36)	98	(37)	99	(37)	102	(39)
18	2100	(14500)	97	(36)	99	(37)	100	(38)	101	(38)	102	(39)	105	(41)
20	2300	(15900)	99	(37)	101	(38)	102	(39)	103	(39)	104	(40)	108	(42)
22	2500	(17200)	101	(38)	103	(39)	104	(40)	105	(41)	107	(42)	111	(44)
24	2700	(18600)	103	(39)	105	(41)	106	(41)	108	(42)	109	(43)	113	(45)
26	2900	(20000)	105	(41)	107	(42)	108	(42)	110	(43)	112	(44)	116	(47)
28	3000	(20700)	107	(42)	109	(43)	111	(44)	112	(44)	114	(46)	119	(48)
30	3200	(22100)	109	(43)	111	(44)	113	(45)	115	(46)	116	(47)	122	(50)
32	3400	(23400)	111	(44)	113	(45)	115	(46)	117	(47)	119	(48)	125	(52)
33	3500	(24100)	112	(44)	114	(46)	116	(47)	118	(48)	120	(49)	126	(52)
Heating Rate - Deg/min			0.97	(0.54)	1.03	(0.57)	1.09	(0.61)	1.15	(0.64)	1.21	(0.67)	1.39	(0.77)
Pressure Rate (per min)			92 psi (636 kPa)											
Time to Final Conditions			33 Minutes											

In most cases, consistency of cement will ramp up when cements start to set. After the thickening time, the condition of slurry needs to be visually inspected. Figure 6.10 shows the consistometer paddle and cement slurry for one of our tests conducted for this study. After concluding tests, we plotted consistency data in respect of time based on cut of value of 50 Bc to determine the thickening time. Each test was repeated at least

once to check the reproducibility of the data. First, we show the results of slurries using a one-step mixing procedure and then test results for the two-step API mixing procedure.

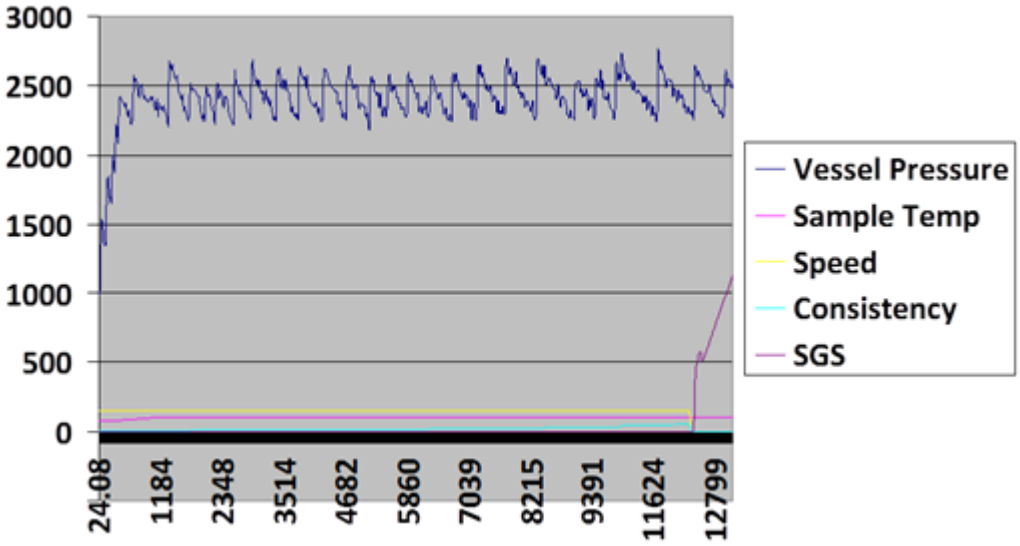

Figure 6.9 Thickening time test results FOR 5.9 E/M at 6000 rpm obtained from consistometer unit interface software.

Figure 6.10 Cement slurry after thickening time tests. Slurry should be pumpable in downhole pressure and temperature conditions

Because of number of data points for consistency measurement, it was difficult to show error bars. Therefore, for each test, we compared results with its repeat test for reproducibility and potential experimental error. Figure 6.11 shows thickening time test results for 6000 rpm at 5.9 KJ/KG energy level for the two tests. No significant difference was observed between original test and its repeat. Figure 6.12 shows results of thickening time tests at 5.9 KJ/Kg at low and high shear rate conditions. Results imply that at lower shear rate (6000 rpm) thickening time is longer than higher shear rate (12,000 rpm). Shorter thickening time in higher shear rate can be explained by the fact that higher shear rate is associated with shorter mixing time as observed in rheology tests. Shorter mixing time does not enable a complete deflocculation process. Previous literature (Nelson and Gulliot, 2006) show that thickening time is strongly correlated with the deflocculation

process. As seen in the results when shear rate is increased, we observed a shorter thickening time. Result also imply higher initial Bc for mixing at 12000 rpm compared to 6000 rpm. We attribute this change because of higher plastic viscosity in high shear rate condition and short mixing time. This correlated well with rheology measurements where higher shear stress was seen for slurries mixed at 12000 rpm.

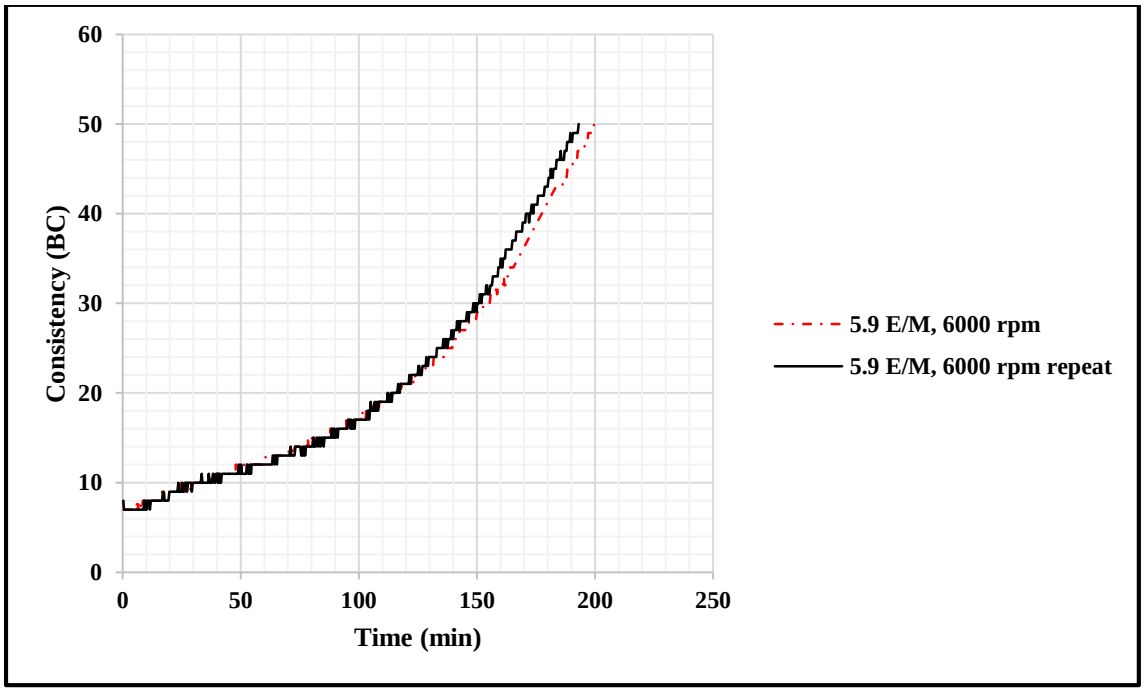

Figure 6.11 Consistency results of 5.9 E/M at 6000 rpm, and second repeat test. No significant difference was observed between original test and its repeat.

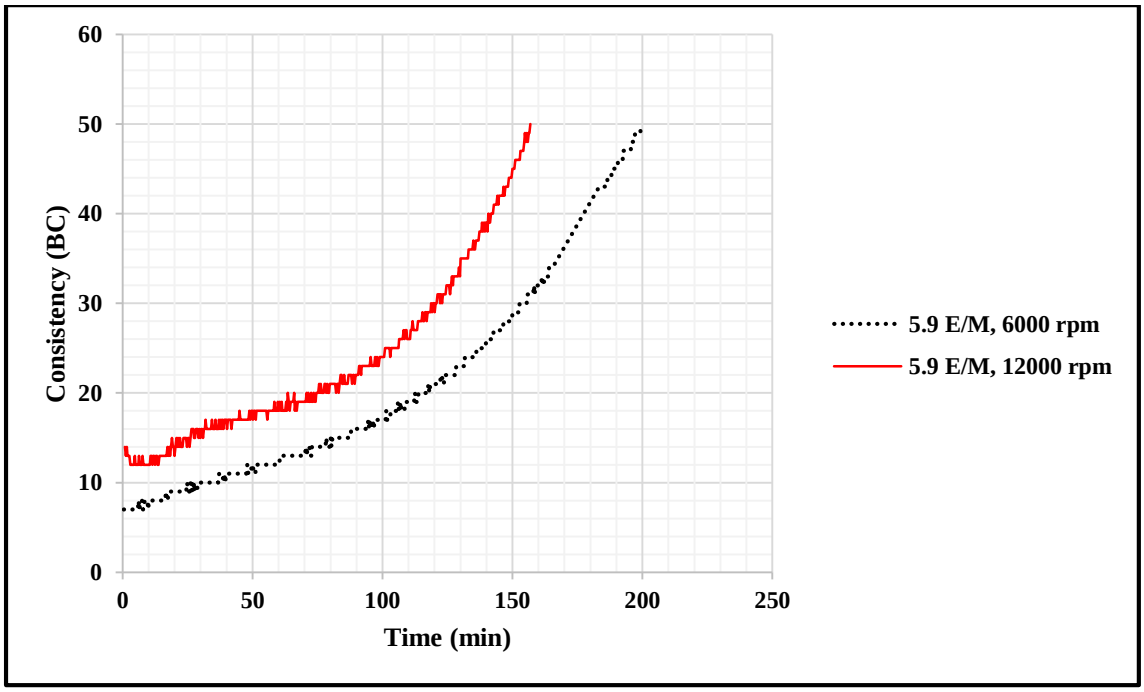

Figure 6.12 Consistency results of 5.9 E/M at 6000 rpm, 12000 rpm and API conditions. At lower shear rate (6000 rpm) thickening time is longer than higher shear rate (12,000 rpm)

Figure 6.13 compares the consistency data for mixing conditions at 11.8 KJ/Kg. As seen in the results when mixing energy increased, similar trend was observed with having a shorter thickening time at higher shear rate, albeit the difference was very small compared to 5.9 KJ/Kg mixing energy. We attribute smaller difference to higher mixing time at a higher energy level. In other words, when mixing time increases, we see less difference in thickening time regardless of shear rate.

Figure 6.14 shows thickening time test results for 6000 rpm at 11.8 KJ/KG mixing energy and one repeat test for the similar mixing condition. No significant difference was observed between the two tests.

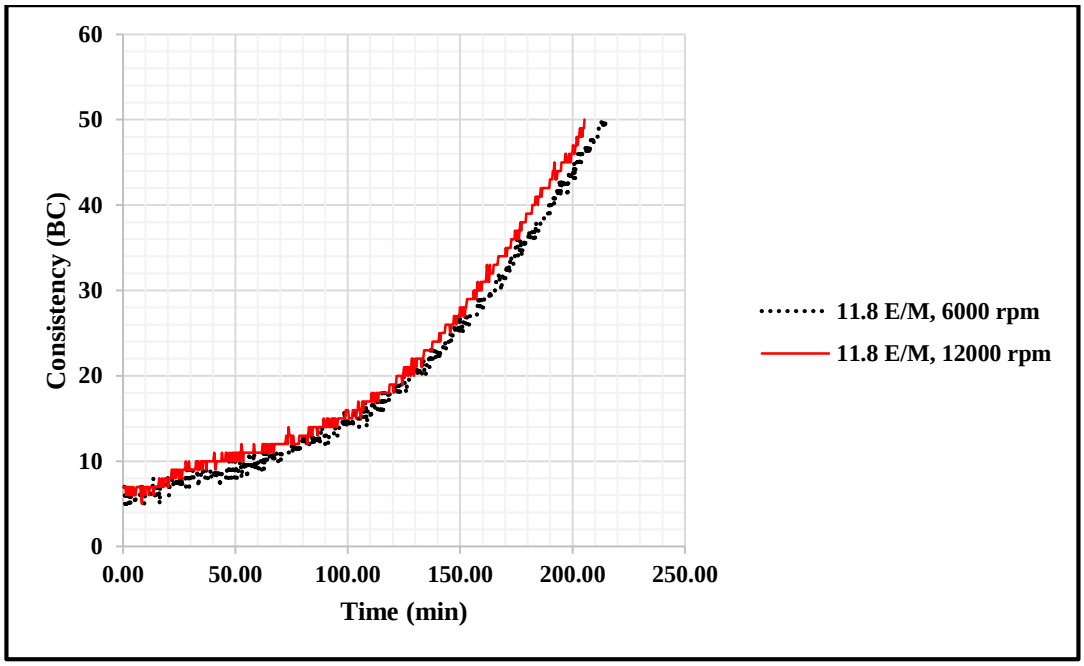

Figure 6.13 Consistency results of 11.8 E/M at 6000 rpm, 12000 rpm mixing conditions

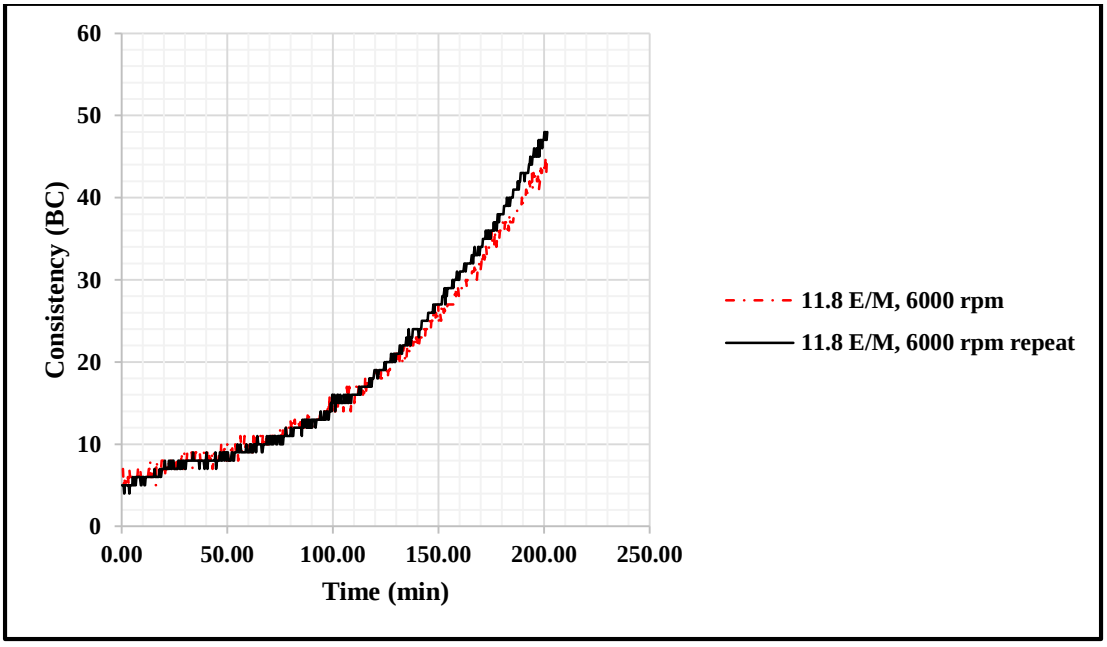

Figure 6.14 Consistency results of 11.8 E/M at 6000 rpm, and second repeat test

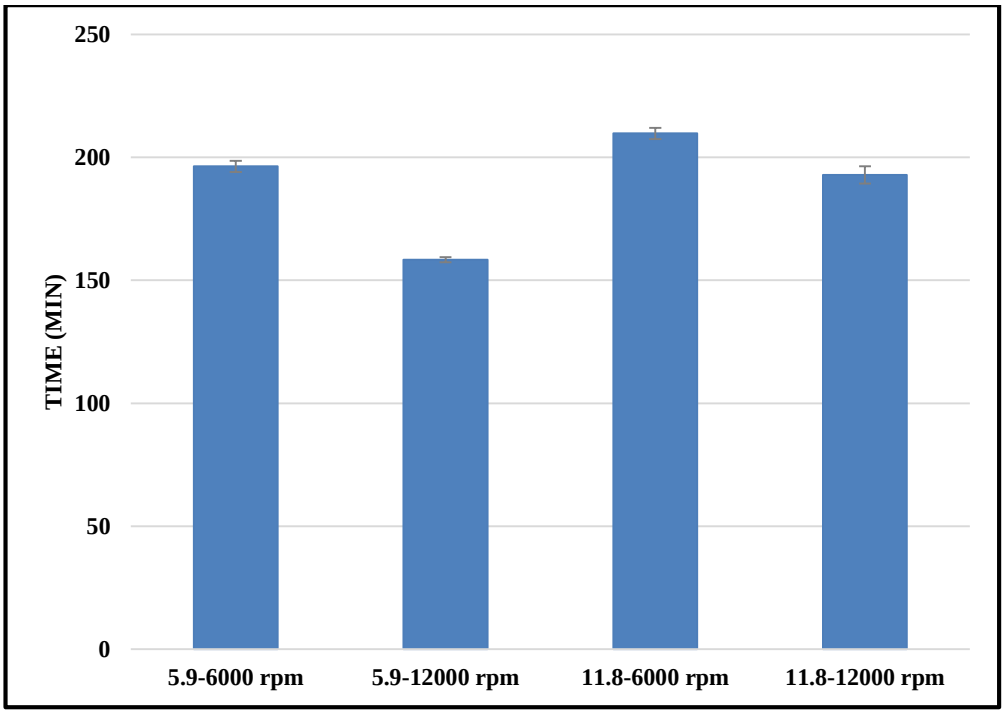

Figure 6.15 Summary of thickening time test results for slurries prepared using one step mixing procedure

Overall results of thickening time test for the four mixing conditions are reported in the Figure 6.15. Results show that as the shear rate increases in each mixing energy level, thickening time shortens. As explained previously, as higher shear rate (shorter mixing time), efficient deflocculation does not occur and leading to larger particles in the cement slurry. As for 5.9 KJ/Kg energy level, slurry mix at 12,000 rpm set nearly 36 minutes faster than the slurry at 6000 rpm. The difference was less when moving to the next energy level at 11.8 KJ/Kg, slurry mix at 12,000 rpm set nearly 18 minutes faster than the slurry at 6000 rpm. In general, comparing average of thickening time at similar shear rates for lower energy level at 5.9 KJ/Kg was slightly shorter than thickening time for 11.8 KJ/kg energy level. Longer thickening time in higher mixing energy level can be explained due to longer mixing time associated with higher mixing energy level. This

allows a better deflocculation process leading to smaller particles in the slurry and longer thickening time.

Previous studies only have compared thickening time results in yard mixing. As discussed in the Chapter 2, Hibbert et al., (1994) compared thickening time from samples captured through yard mixing. Results presented by Hibbert et al., (1994) imply that by increasing mixing energy level in yard mixing, thickening time decreases which opposite from the trend is observed in this study. However, one must note that Hibbert compared slurries having different additives (retarder, fluid loss, and dispersant) in yard mixing tests. They also reported inconsistency in results obtained from laboratory small scale mixing and yard mixing concluding that the difference in mixing procedure, they cannot be compared. In another study by Padgett (1996) (see Chapter 2), thickening time results were slightly affected by mixing energy which is in agreement to the results concluded from this study. Finally, a study conducted by Vidick (1990) showed that thickening time is function of deflocculation process in which after complete deflocculation, thickening time is only slightly impacted by the mixing energy.

6.5.2 Thickening time results for API recommended mixing (two step mixing)

Results of consistency profile for slurries prepared based on the two-step API mixing procedure is shown in the Figure 6.16. We can see some differences at the beginning of the test which become negligible at the end of the test. Consistency values get very close as time increases. At the beginning of the test, slurry prepared at 11.8 E/M is thinner which is consistent with observation from rheology test results (lower plastic viscosity). Two API tests show 3 minutes difference in final thickening time values as shown in the Figure 6.17.

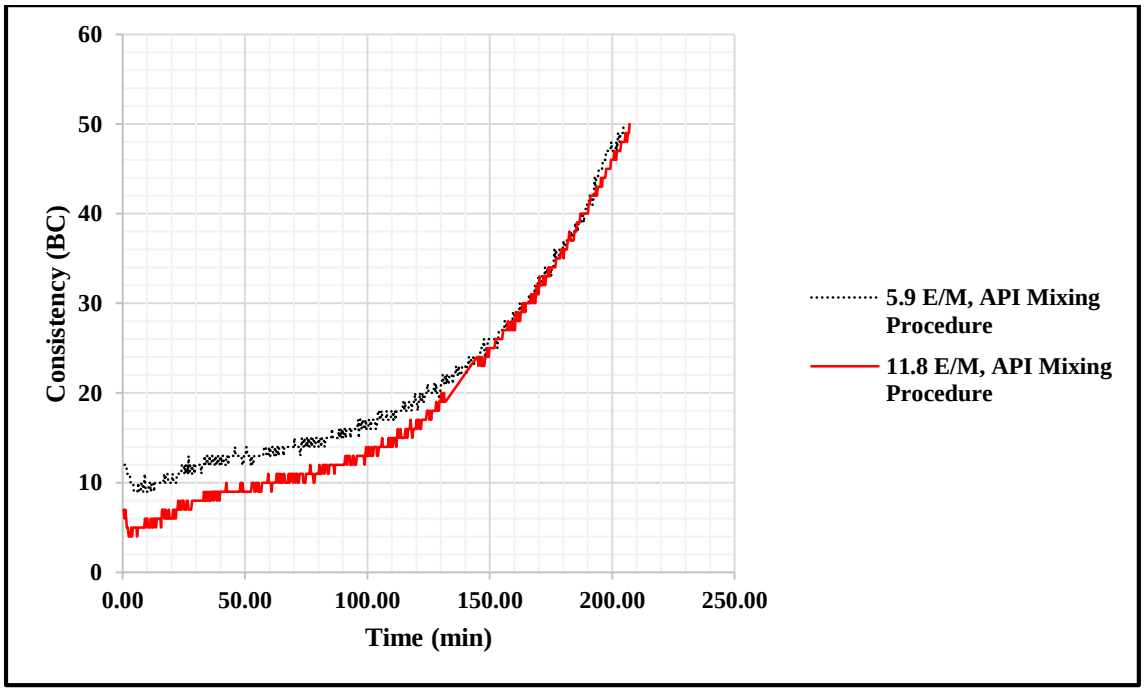

Figure 6.16 Consistency results of slurries prepared using two-step API mixing procedures at 5.9 and 11.8 E/M energy levels.

The two step mixing results show negligible difference in thickening times compared to one step mixing results. This can be explained because of using similar shear rates in API mixing. Figure 6.18 and 6.19 compare one step mixing results with API at both energy levels. At 5.9 E/M, consistency for mixing at 6000 rpm is close to API measurements. Also, at 11.8 E/M, consistency for all three mixing conditions are similiar. This again implies that as mixing time increases, we observe less difference in thickening time regardless of mixing procedure or shear rate.

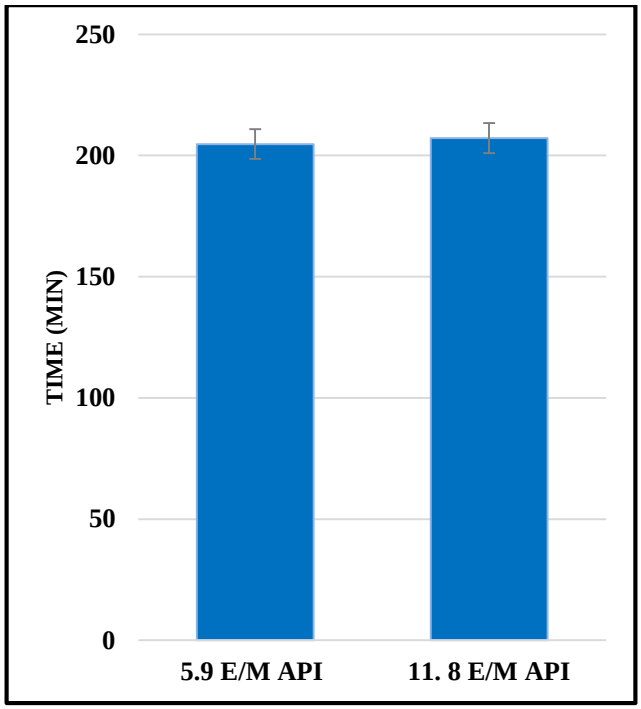

Figure 6.17 Thickening time test results for slurries prepared using two step mixing procedure according to API recommendations.

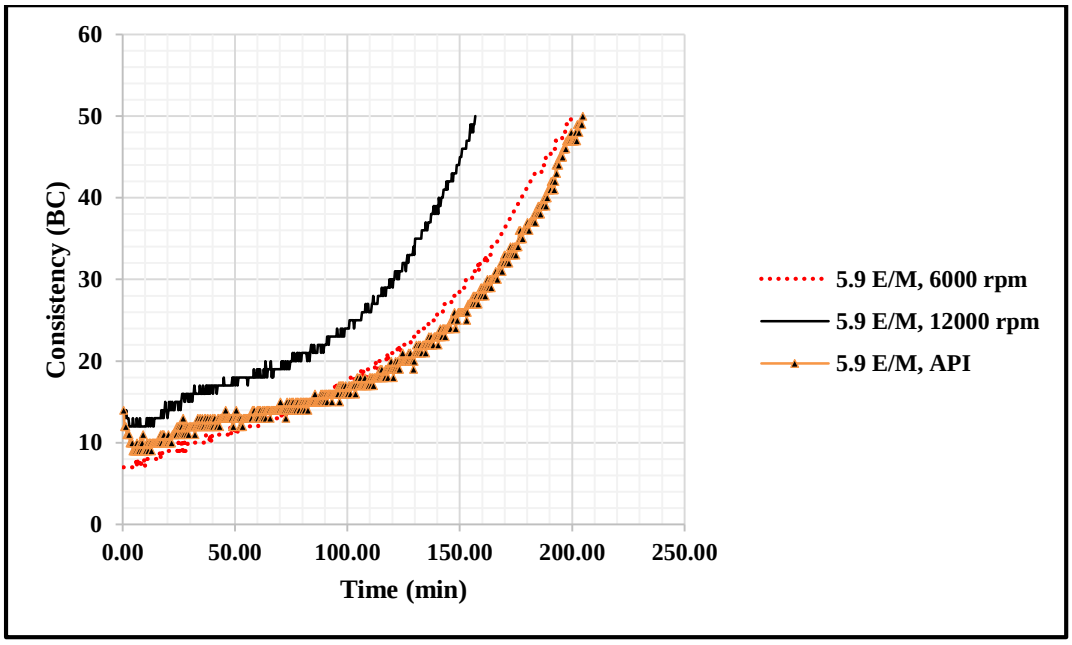

Figure 6.18 Consistency results for slurries prepared one step and two step mixing at 5.9 E/M

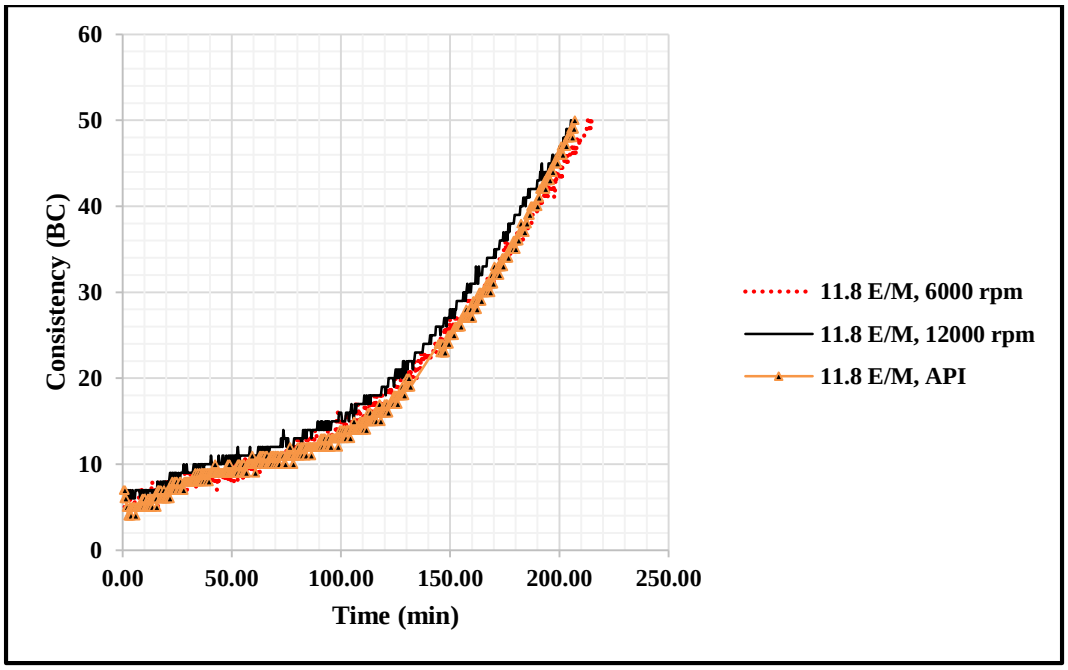

Figure 6.19 Consistency results for slurries prepared one step and two step mixing at 11.8 E/M

6.6 Effect of Mixing Conditions on Density

Density measurements were conducted on all the slurries using an atmospheric mud balance. Our results show that the change in density due to mixing condition was less than 1% for all measurements (16.42-16.50 lb/gal); this implies that density is not impacted by change in mixing energy or shear rate.

Chapter 7: Nuclear Magnetic Resonance

7.1 Overview

In this chapter, first an overview of NMR is provided followed by experimental results conducted to measure porosities in specimen from different mixing conditions. Similar to thickening time and rheology tests, the experimental design for NMR included two energy levels of 5.9 and 11.8 E/M and two shear rates at 6000 rpm and 12000 rpm. We measured NMR T_2 spectra on cement specimen cured at 1, 3, 7, and 21 days. Porosity data from NMR are paired with UCS at similar conditions. Finally, a correlation is developed between cement porosity and hydration time.

7.2 Introduction to NMR

The amplitude of NMR relaxation measurements is proportional to the amount of hydrogen sensed and can be used to determine specimen porosity (Kleinberg, 1993; Dunn et al, 2002).

Transverse relaxation time is known as T_2 or as the characteristic time constant; by measuring T_2 it is possible to determine total porosity, pore size distribution and permeability (Timur, 1969 and Kenyon, 1992). In the past two decades, one dimensional T_2 measurements have been the foundation of NMR evaluation (Anand, 2015).

The following equation captures the factors affecting the T_2 response:

$$\frac{1}{T_2} = \frac{1}{T_{2bulk}} + \rho_2 \frac{S}{V} + D\frac{(\gamma \times G \times TE)^2}{12} \quad \text{.....(7.1)}$$

Parameters in this equation defined as:

$\frac{1}{T_{2bulk}}$ is the bulk relaxation, ρ_2 is the surface relativity, $\frac{S}{V}$ is pore surface to volume ratio, D is the diffusion coefficient of the fluid, γ is the gyromagnetic ratio, G, is the magnetic

field gradient and TE is the spacing between the CPMG (Carr Purcell Meiboom Gill) spin echoes.

Random motion of hydrogen atoms causes relaxation in the bulk fluid (the first term in the equation) which is related to the fluid viscosity by following formula (Coates et al, 1999):

$$\frac{1}{T_{2bulk}} = \frac{1}{3}\left(\frac{298\eta}{T_K}\right) \quad \text{.....(7.2)}$$

where η is the viscosity (cP) and T_K is the temperature in ^{o}K.

Second term in the equation 7.1 above ($\rho_2 \frac{S}{V}$) is related to surface relaxation. This relaxation occurs at fluid-solid interface. The ratio ($\frac{S}{V}$) is often applied for converting incremental porosity to pore body distribution. The third term is diffusion relaxation which is caused by the presence of a gradient in the applied magnetic field (Bendel, 1990). Interoperation of transverse relaxation data (T_2) is complicated by diffusion effects. These effects can be minimized by applying uniform magnetic field. Therefore, transverse relaxation time is dominated by the first two terms in equation 7.1. According to Hirasaki et al. (2003), bulk relaxation in unconfined fluids is impacted by several factors such as intramolecular, intramolecular dipole-dipole interactions and spin rotation. For water, the bulk relaxation time is close to 3000 μs and therefore can be neglected in the Equation 7.1, hence T_2 in water saturated pores is controlled by surface relaxation (Cowan, 2005).

7.2.1 Porosity Determination Using NMR

Porosity is defined as the ratio of the pore volume to square bulk total volume. For specimen saturated with water, the total porosity is proportional to the number of the

hydrogen atoms in the fluid. The total area under T_2 distribution curve is related to sample porosity using a calibrated scaling factor given by the following formula:

$$\text{Porosity} = \frac{\text{Total Area}}{\text{Scaling Factor*Bulk Volume (ml)*No. of scans}} \quad \text{…..……..….(7.3)}$$

Scaling factor is dependent on NMR measuring instrument. This factor can be estimated from calibrating the NMR responses with known volumes of brine at room temperature. This work will focus mainly on the NMR data acquired on cement samples through low field T_2 (2 MHz) NMR measurements.

7.2.2 Application of NMR for Analysis of Cementitious Materials

NMR relaxation analysis and similar techniques have been previously used to study the micro characteristics of cementitious materials such as Portland cement. Although these materials are used for more than a century some basic questions remain regarding their microstructure and in particular, understanding formation of calcium silicate hydrate gel (C-S-H) while cement hardens. When cement and water is mixed this C-S-H forms and precipitates. The complex behavior of cementitious materials is somehow related to formation of this gel and its viscoelastic response to mechanical loading and hydration process (Allen et al., 2007).

Specific applications of NMR for these materials include determination of porosity, water interactions, identification of hydration stages and C-S-H gel changes by curing time. Since water is present in all cement recipes, NMR can potentially help to understand microstructural changes in cement during curing. In addition, since NMR is non-destructive, it is possible to follow porosity evolution during cement hydration process.

Another advantage associated for being non-destructive is that repeat measurement can be made on one sample or it is possible to monitor NMR signals over time. The first pioneer in applying NMR technique for studying cement pastes was Blinc et al., (1978). In their study, they investigated T_1 and T_2 relaxation times of water in cement specimen prepared by distilled and D_2O water. The hydration process was monitored from 10 minutes to 28 days. Using this technique, authors studied hydration process in each specific time and investigated effect of water type on hydration process. In similar study by Schreiner et al., (1985), they applied NMR techniques to investigate hydration process of Portland cement pastes. Authors characterized hydration mechanisms of cement pastes from one week to a year. They studied cement specimen with varying water to cement ratio (w/c) and discovered that the hydration behavior is very similar. They observed that T_1 decreases with time of hydration in all the specimen as shown in the Figure 7.1. This behavior explained since T_1 is inversely proportional to the specific surface of new grown hydration products. Figure 7.1 also indicates that T_1 decreases as the porosity develops and is generally greater in specimen with higher w/c (water/cement) ratios.

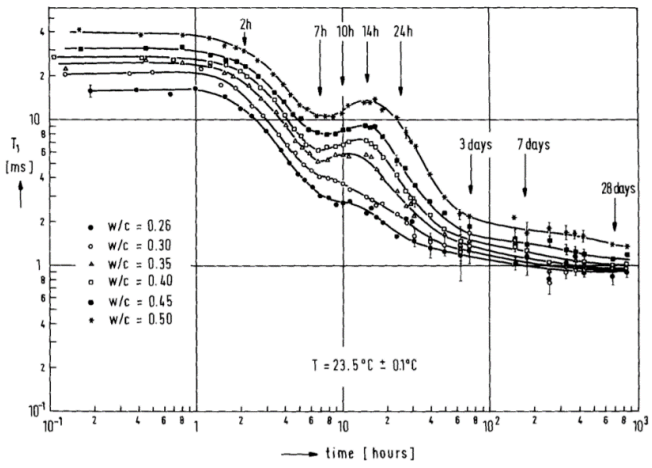

Figure 7.1 Investigation of hydration process of cement with changing water/cement ratio (w/c) ratios using T_1 (from Schreiner et al., 1985). They discovered that the hydration behavior is very similar regardless of water to cement ratio.

Valori et al. (2013) and Muller et al. (2013) used NMR to study C-S-H gel structure by quantifying water mass in different environments over time. Using mass balance and oxides conservation equations, the C-S-H chemical composition was investigated. In particular, they found that C-S-H gel is formed mainly during the first 2 days of hydration and then plateaus. They also found that C-S-H gel density increases with hydration time. Figure 7.2 shows mass and volume composition versus degree of hydration for a cement specimen with w/c of 0.4. Figure 7.2 shows different regions corresponding to free water, gel pore water, C-S-H, ettringite, $Ca(OH)_2$ and unreacted cement. Figure 7.2 also indicate continuous consumption of cement and water and the formation of hydration products.

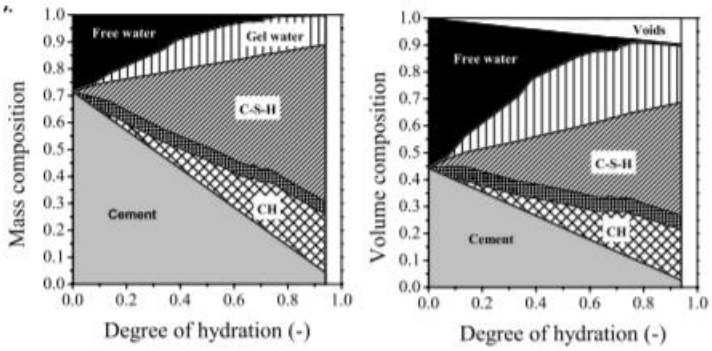

Figure 7.2 Degree of hydration for Portland cement versus mass (left) and volume (right). Figure shows different regions corresponding to free water, gel pore water, C-S-H, ettringite, $Ca(OH)_2$ and unreacted cement (Muller et al., 2013).

Furthermore, Valori et al., (2013) showed that NMR measurements can be diagnostic in the early stages of cement hydration. In different stages of hydration, T_2 relaxation rates change. After the induction period (as explained in Chapter 2), there is a rapid evolution in gel's porosity, and it stops increasing after 2-3 days of hydration. This is identified as

the critical time for change in density of C-S-H gel (formation of lower density to higher density C-S-H).

One other phenomenon that can be studied through NMR for cement is its shrinkage. Shrinkage is generally referred to as the overall decrease in volume occurring when cement reacts with water and hydrates are formed. NMR can be used to quantify this shrinkage by measuring the increase in total signal amplitude during hydration (Valori et al., 2013).

Analysis of NMR can be used for measuring pore sizes of cementitious materials. Previous researchers have shown excellent consistency between NMR measured pore sizes with other non-NMR techniques such as small angle neutron scattering (Allen et al., 2007). Wang et al., (2017) showed application of NMR technique for measuring pore structure of cement asphalt mortars. These materials are described as polymer modified cement or porous and organic-inorganic composite with wide application in railways. By using NMR, researchers measured pore size distribution of different samples and documented maximum pore radius.

7.3 NMR Test Results

NMR specimens were prepared according to previous DoE discussed in Chapter 3. All the NMR tests were repeated once for reproducibility. Figure 7.3 shows overall porosity measurements for various mixing procedures based on different curing days. Results imply that as the curing time increases, porosity of the cement decreases which is in consistent with findings (Ichim, 2017). With increasing hydration, the fluid filled pore sizes decreases as water is consumed. Highest porosity in 1 day curing is for the specimen prepared at 11.8 E/M and 12000 rpm (44.6 p.u.). In 3 days curing, highest and lowest

porosities are 37.4 p.u. and 33.4 p.u. reported, respectively, for specimen prepared at 5.9 E/M and 12000 rpm and 11.8 E/M, 6000 rpm. Very similar observation to 3 days is seen for porosity measurements at 7 and 21 days curing. In 7 day cured specimens, highest and lowest porosities of 29.3 p.u. and 27.4 p.u. are reported respectively for specimen prepared at 5.9 E/M and 12000 rpm and 11.8 E/M, 6000 rpm. These observations are consistent with differences in mixing time (see Chapter 5). Specimen prepared at 11.8 E/M and 6000 rpm has the longest mixing time of 294 seconds, whereas specimen prepared at 5.9 E/M and 12000 rpm has the shortest mixing time of 37 seconds. Longest mixing time causes uniform distribution of hydrates and C-S-H gel precipitation which will reduce cement porosity as observed with NMR measurements. This is consistent with UCS measurements where highest UCS values have observed when the mixing time increased.

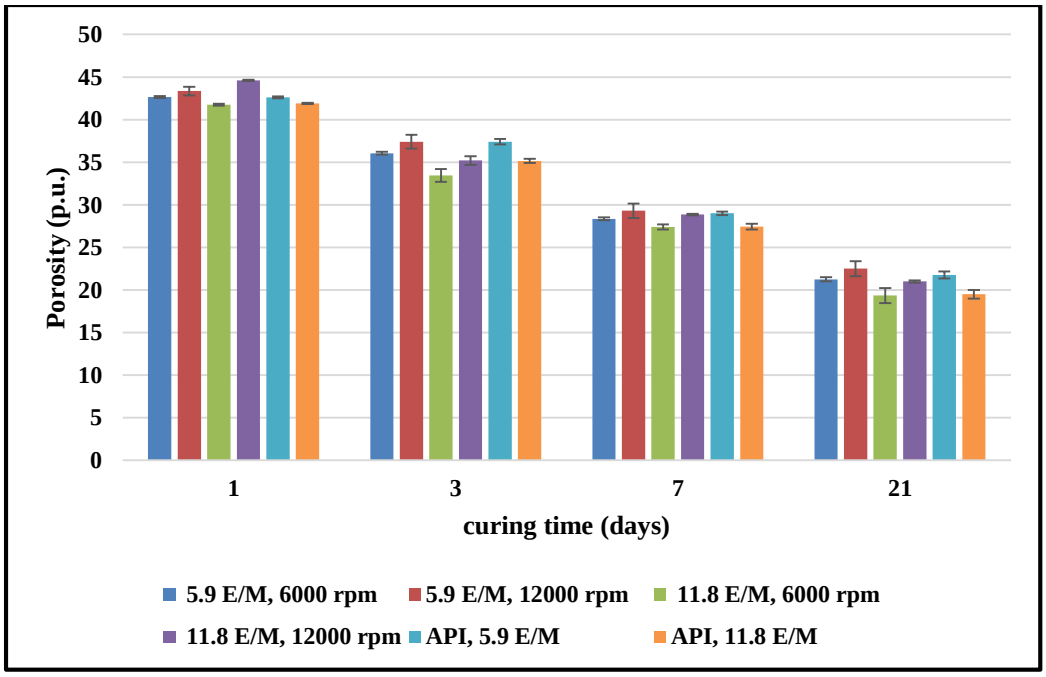

Figure 7.3 NMR porosity measurements for different mixing procedures versus curing days. Results imply that as the curing time increases, porosity of the cement decreases. Specimen prepared at 11.8 E/M and 6000 rpm show lowest porosity.

7.3.1 Porosity-hydration time plot

NMR measurements in this work is limited to the study of 21 days cured samples. Figure 7.4 shows the porosity versus hydration time for all the mixing procedures. The general trend from our data shows a decrease in porosity as hydration time increases which is consistent with similar study (Ichim, 2017) (Figure 7.5 for, τ_2=150 μs). The following correlation was obtained for samples prepared according to API recommendations in our study:

$$\phi = \frac{44.698}{T^{(0.227)}} \quad \text{.....(7.4)}$$

where ϕ is porosity and T is hydration (curing time) in days. This correlation will predict cement porosity after 230 days to be 12%. The NMR measurements presented by Ichim (2017) reports 9-10% porosity at the end of 230 days for neat class G cement. Therefore, correlation from this study is quite consistent. Note that, the difference could be because of different class of API cement (class G) used in experiments by Ichim (2017).

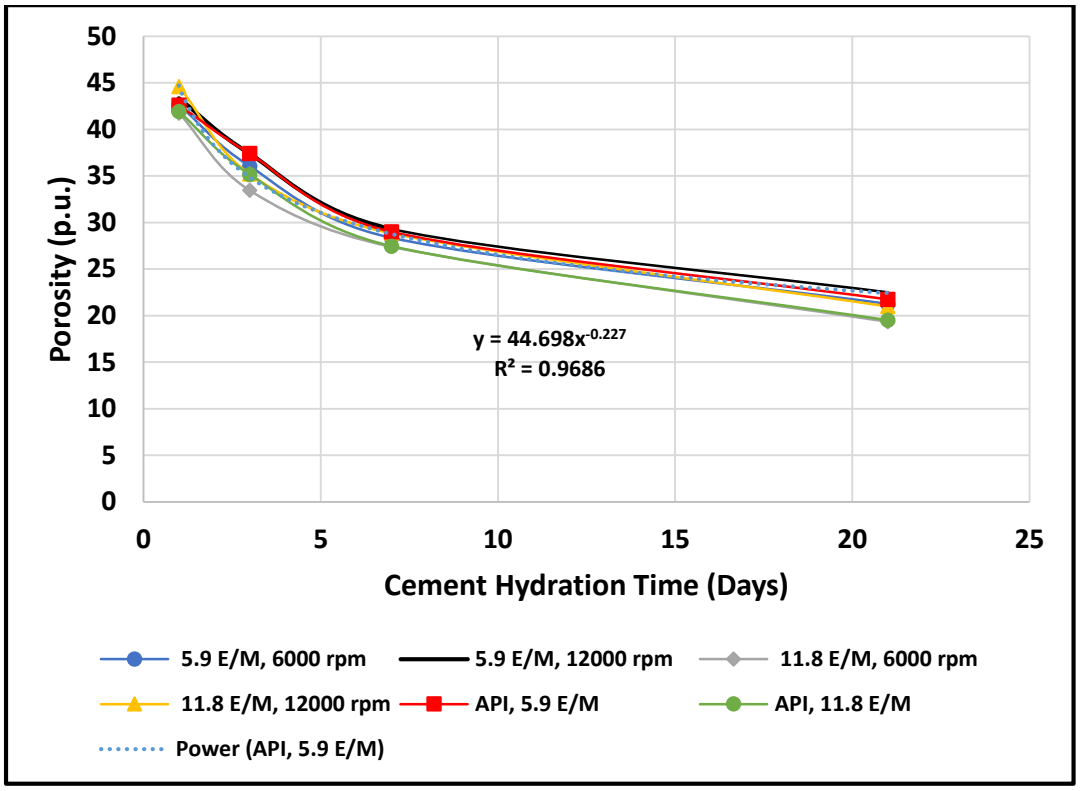

Figure 7.4 Porosity versus cement hydration time plot for slurries mixed under different conditions

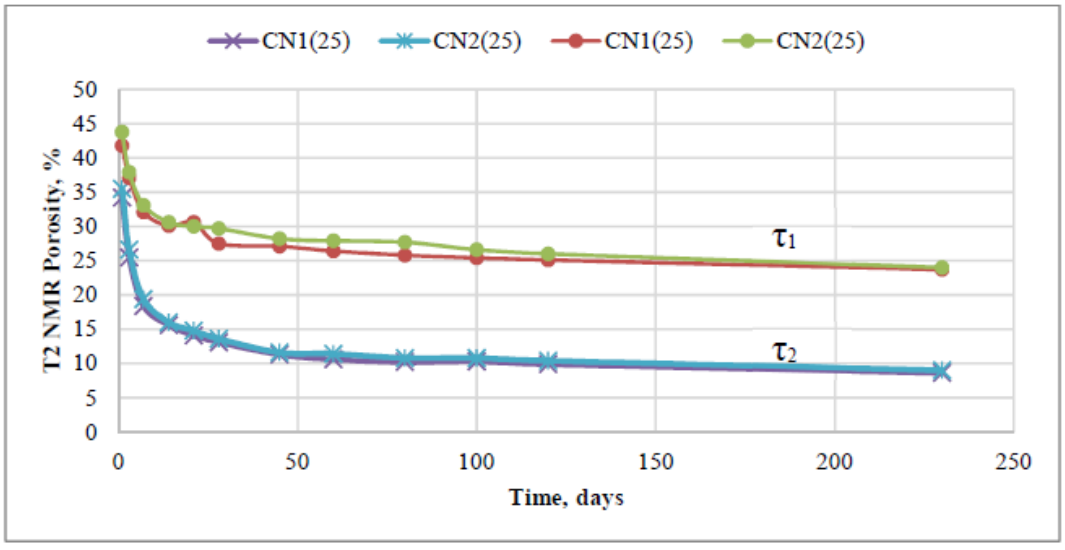

Figure 7.5 T2 NMR porosity from Ichim (2017) (Neat Cement Class G– 25°C – τ_1=57 µs, τ_2=150 µs)

7.3.2 NMR T_2 Response Plots

We can also review T_2 response for different mixing conditions at different curing times. First, T_2 relaxation times for one step mixing procedure specimens is presented and then results of two-step mixing based on API mixing procedures are presented.

Measured T_2 relaxation spectra reflects the distribution of pore body sizes within the specimen. The larger the relaxation time, the larger the pore body. Measured porosity based on 150 μs echo time (TE) for 1 day is within 41-44 p.u. Relaxation times for the specimen prepared at different mixing conditions range from 0.1 to 10 μs are shown in the Figures 7.6; the maximum T_2 peak shifts from 2.5 to 2.8 μs for all the specimen prepared at different mixing conditions. Figure 7.7 shows expanded version of T_2 distributions for all mixing procedures. Figure 7.6 and 7.7 show that changing mixing procedure has an effect on T_2 distributions. Specifically, it can be seen that there is quite a measurable difference in maximum T_2 peaks between 6000 rpm and 12000 rpm data at same mixing energy (11.8 E/M).

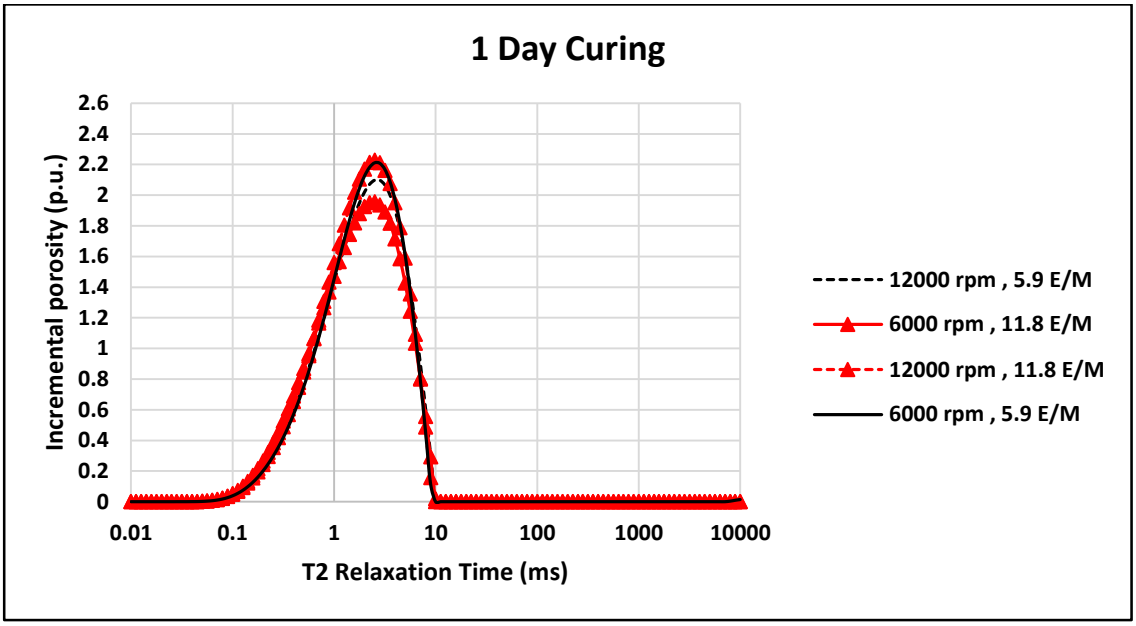

Figure 7.6 T_2 relaxation times for 1-day curing at all mixing conditions

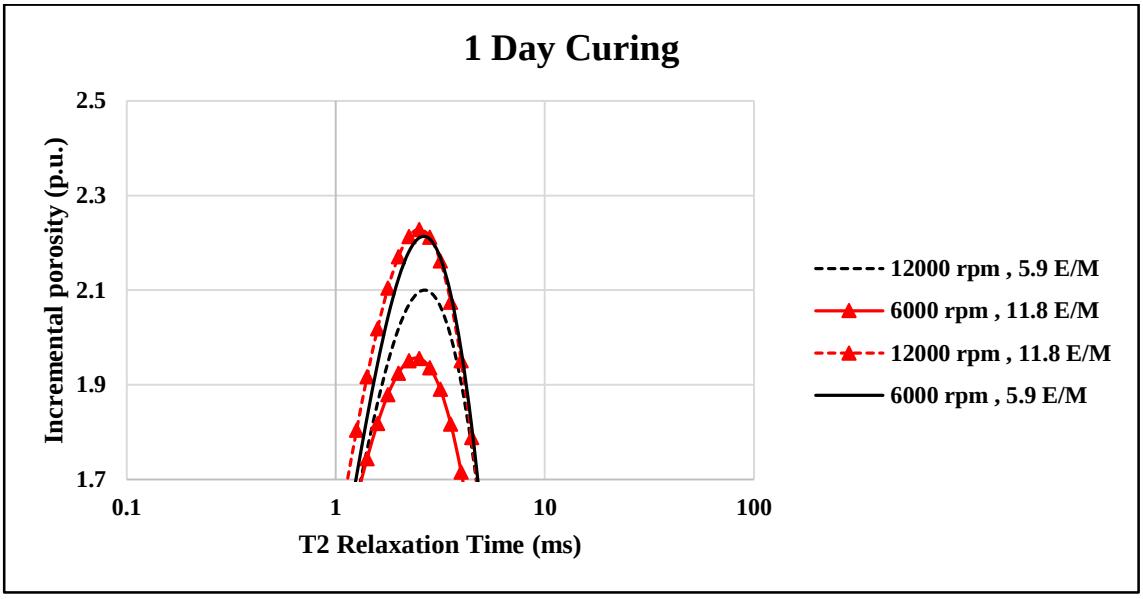

Figure 7.7 T_2 relaxation times for 1-day curing at all mixing conditions (expanded view)

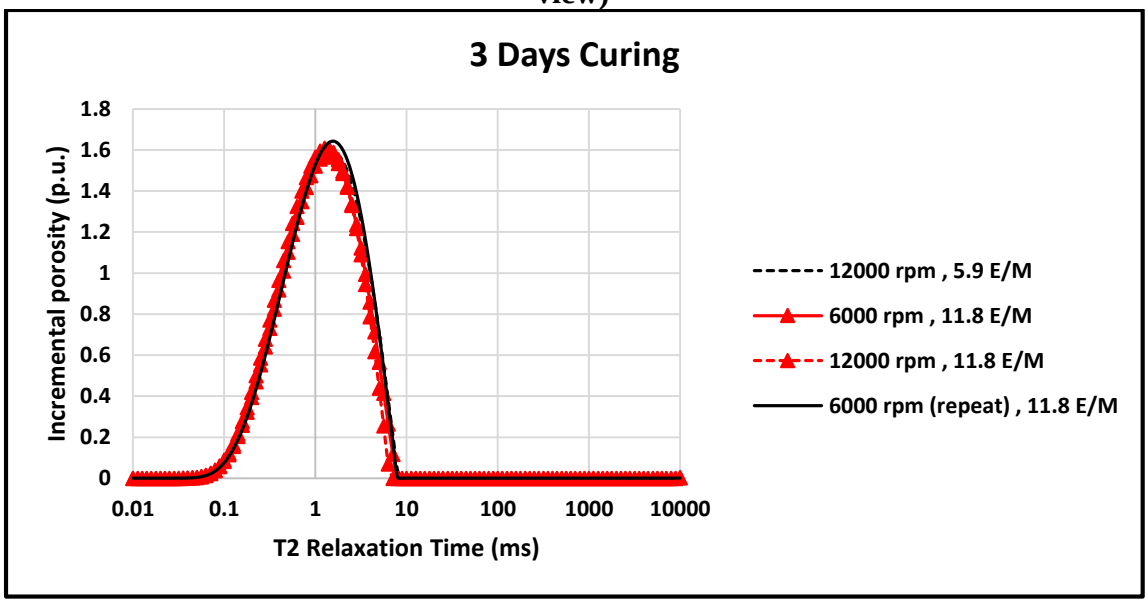

Figure 7.8 T_2 relaxation time for 3 days curing at all mixing conditions

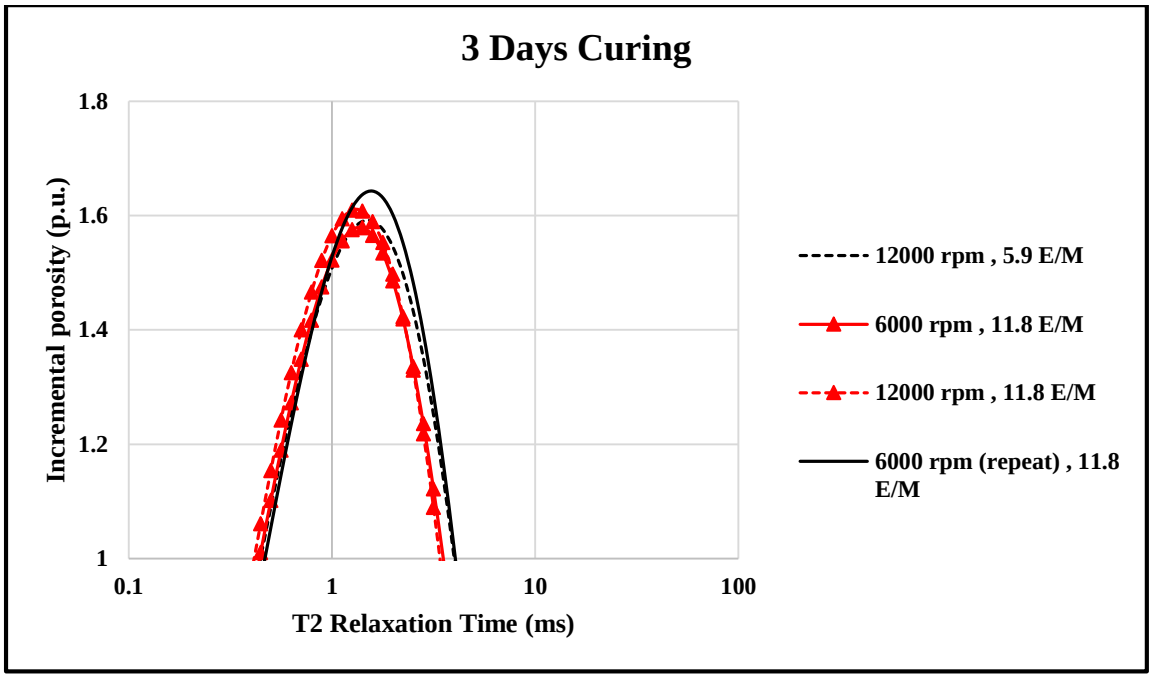

Figure 7.9 T_2 relaxation time for 3 days curing at all mixing conditions (expanded view)

Similar T_2 distribution curves are plotted for 3 days curing. Measured porosity for 3 days is within 34-38 p.u. It shows a decrease in porosity as cement hardens. Because of hydration and precipitation of C-S-H gel, overall porosity decreases (Nelson, and Guillot, 2006). Similar curve for relaxation time (0.07 to 8 μs) is shown in the Figure 7.8 and 7.9. Maximum T_2 peak shifts from 1.26-1.58 μs which is less than 1-day mean relaxation peaks. Overall, T_2 distribution for 3 days curing follows a similar trend to the first day. We can observe a systematic shift to smaller T_2 time which indicates smaller pores. This can be observed better in the Figures 7.14-7.17. T_2 distribution curves for 7 and 21 days curing are shown in the Figure 7.10-7.13.

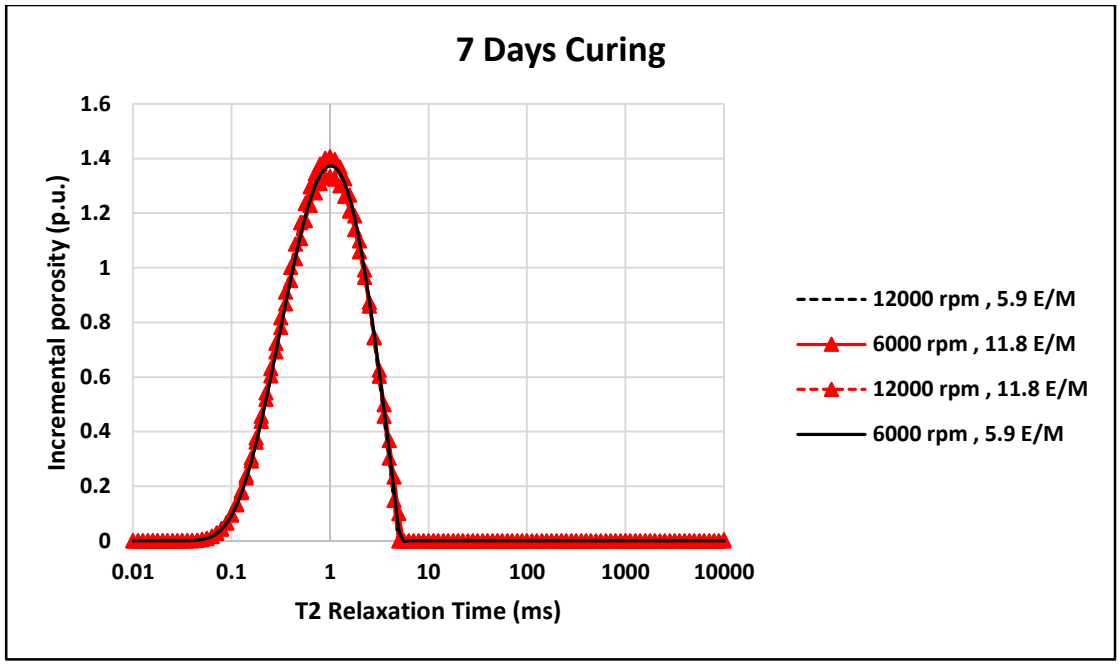

Figure 7.10 T_2 relaxation time for 7 days curing at all mixing conditions

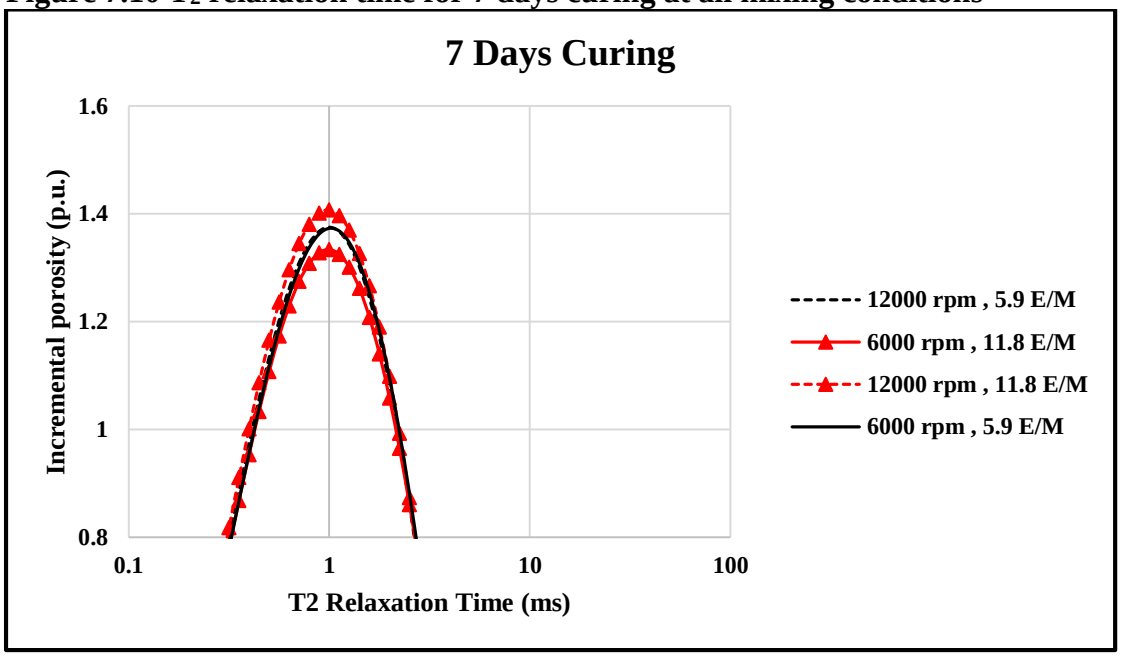

Figure 7.11 T_2 relaxation time for 7 days curing at all mixing conditions (expanded view)

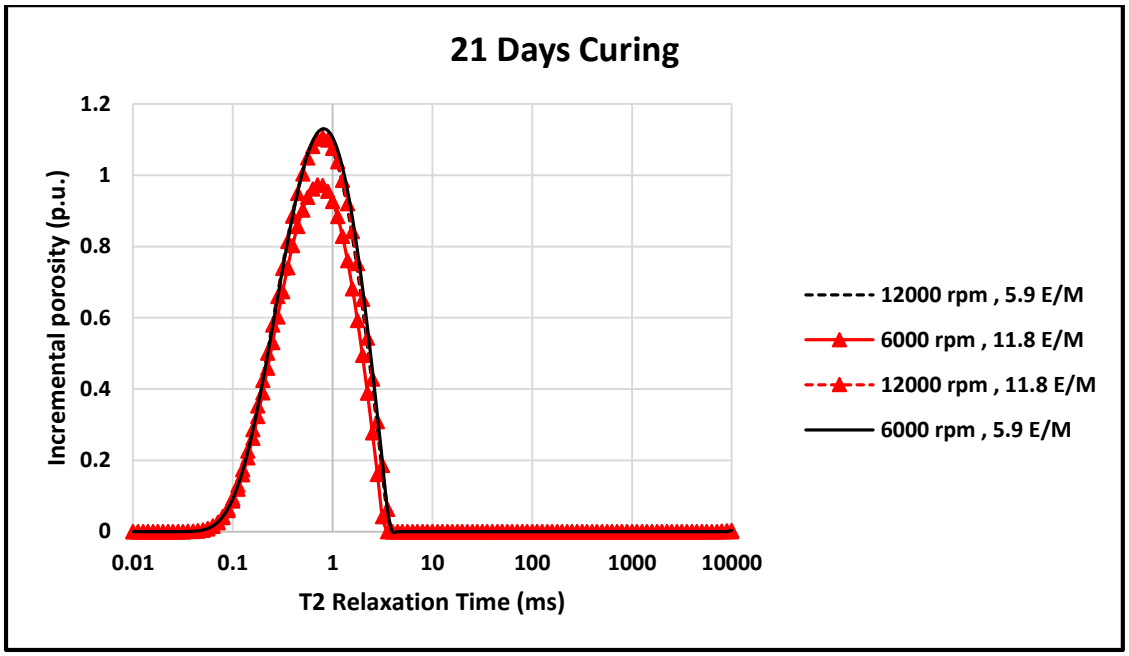

Figure 7.12 T_2 relaxation time for 21 days curing at all mixing conditions

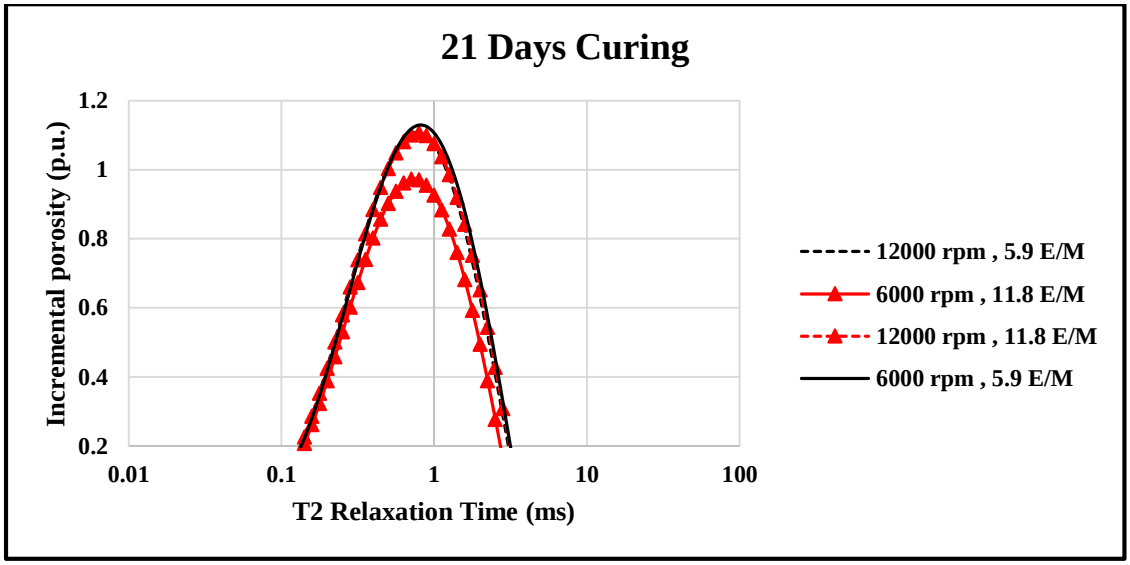

Figure 7.13 T_2 relaxation time for 21 days curing at all mixing conditions (expanded review)

Relation times for 7 days curing samples shift slightly to the left (0.07 to 7 μs). Maximum T_2 peak shifts from 1 to 1.12 μs. Measured porosity for 7 days decreased but are in the range of 27-30 p.u. For 21 days curing, porosity further dropped within 18-22 p.u. Relaxation times for 21 days curing samples shift slightly more to the left (0.06 to 4 μs).

The maximum T_2 peak shifts from 0.7 to 0.9 μs. The shift in relaxation time to the left indicates reduction in pore sizes as the cement hydration continues. Figures 7.14-7.17 also show relaxation times for each mixing energy for different days of curing for various mixing procedures. Results imply that specimen at 21 days curing time show the smallest pore size regardless of mixing conditions. Additionally, at 1 day curing, we observe the largest pore size regardless of mixing condition. These results are in agreement with similar tests conducted by Ichim (2017) on class G cement.

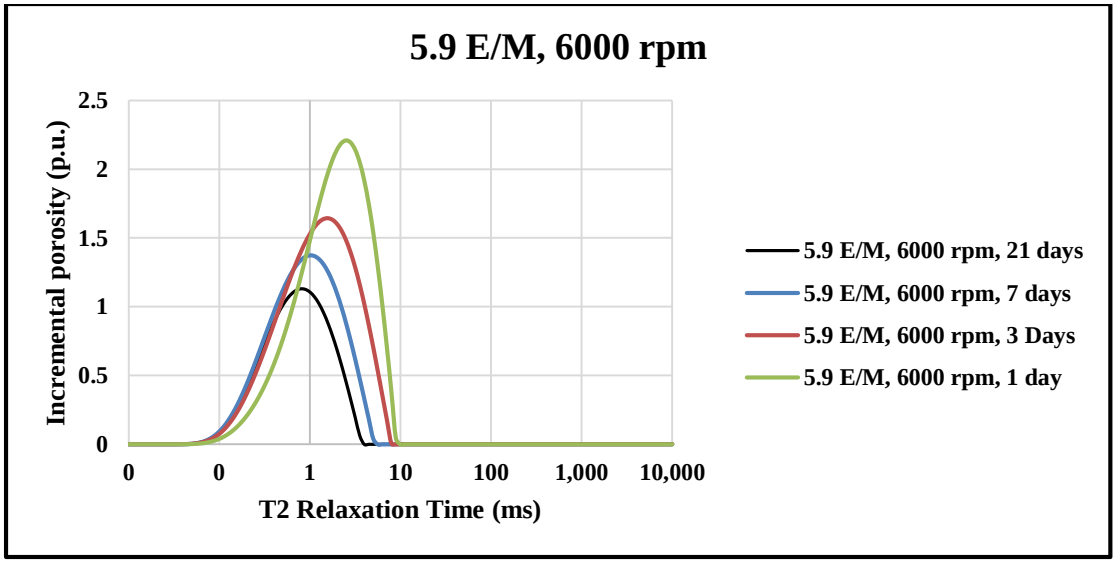

Figure 7.14 T_2 relaxation time for 5.9 E/M specimen prepared at 6000 rpm and different curing days

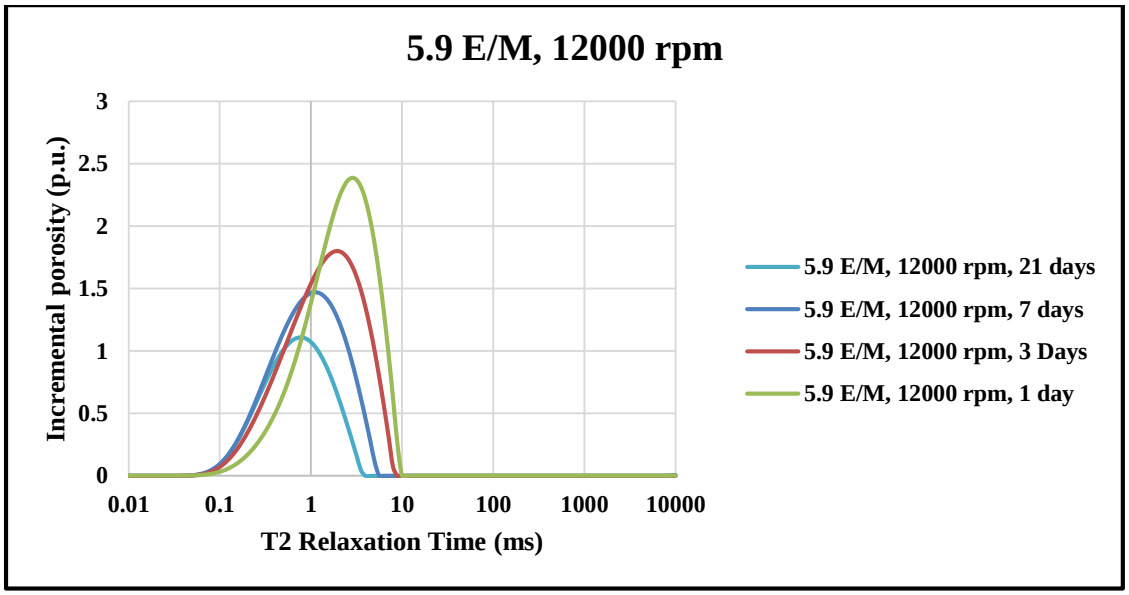

Figure 7.15 T_2 relaxation time for 5.9 E/M specimen prepared at 12000 rpm and different curing days

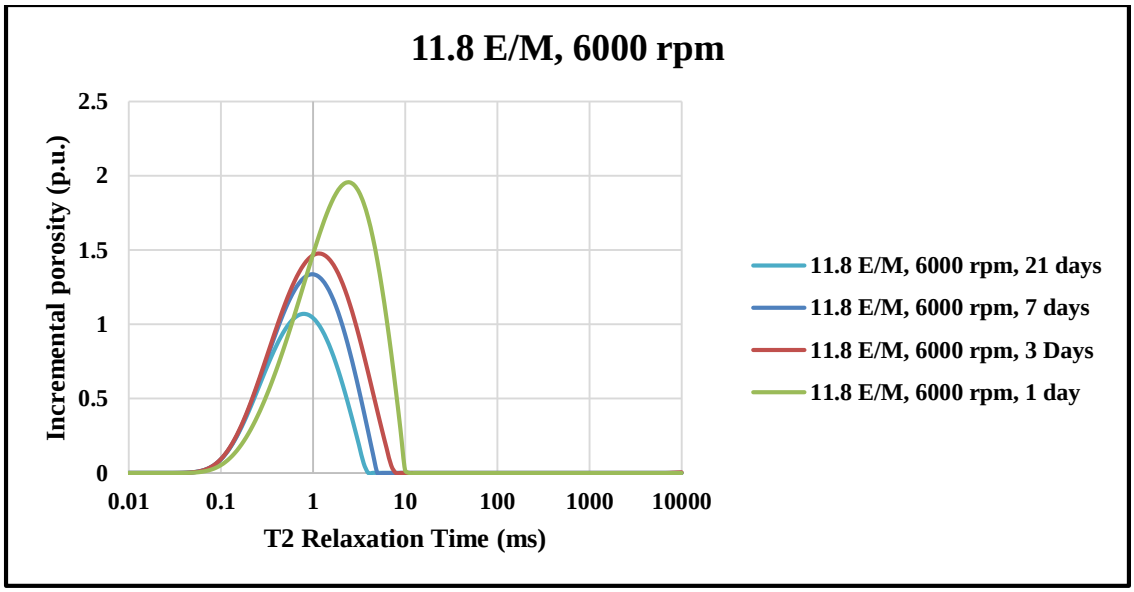

Figure 7.16 T_2 relaxation time for 11.8 E/M specimen prepared at 6000 rpm and different curing days

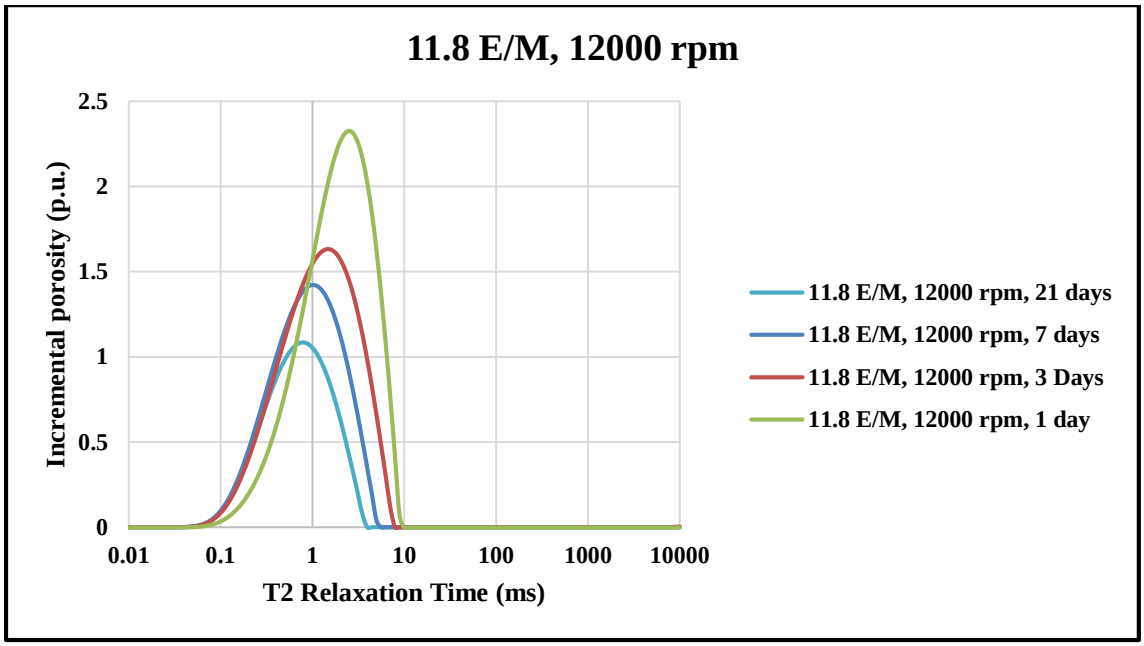

Figure 7.17 T_2 relaxation time for 11.8 E/M specimen prepared at 12000 rpm and different curing days

7.3.3 NMR Plots of Slurries Prepared by API Recommendations

Now, we present T_2 distribution curves for specimen prepared based on two step API mixing procedure. As shown in the Figures 7.18 and 7.19, relaxation time in range of 0.1 to 10 μs is observed for 1 and 3 days cured samples at 5.9 and 11.8 E/M energy levels. A shift to the left in relaxation time is observed when mixing energy is increased. Maximum T_2 peak shifts from 2.30 to 2.80 μs for one-day curing and 1.25 to 1.58 μs for 3 days curing. Porosity ranges from 41 to 42.7 p.u. repectively for 5.9 and 11.8 E/M (at one day cure). Porosity ranges from 34 to 37 p.u. repectively for 5.9 and 11.8 E/M (at 3 days).

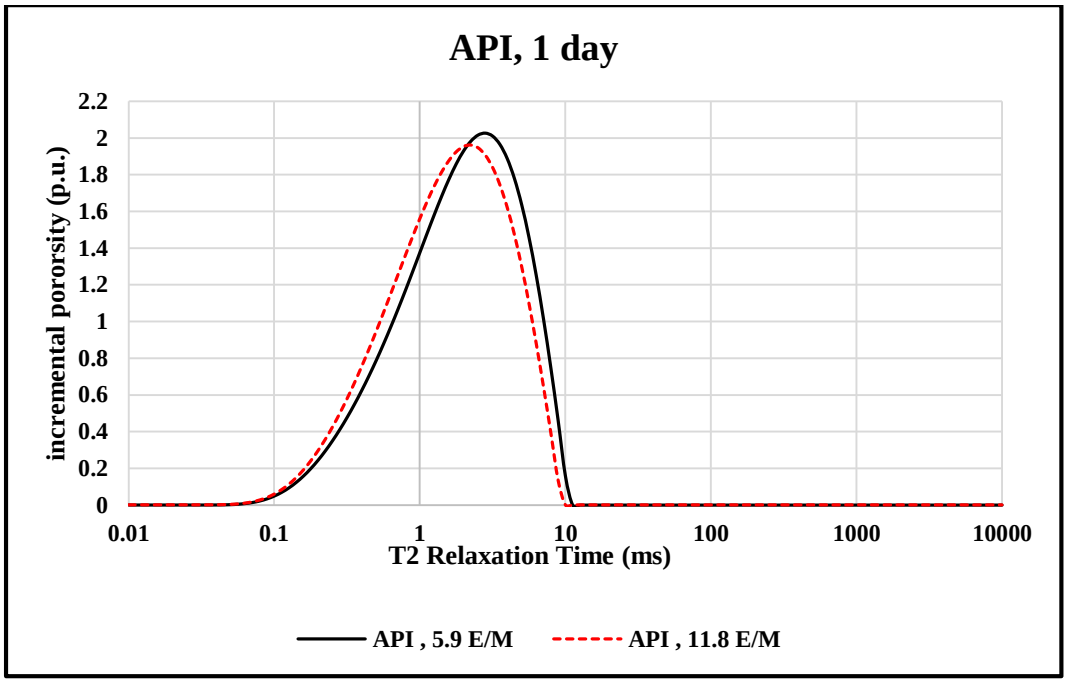

Figure 7.18 T_2 relaxation time for 1-day curing times using API mixing procedures for 5.9 E/M and 11.8 E/M

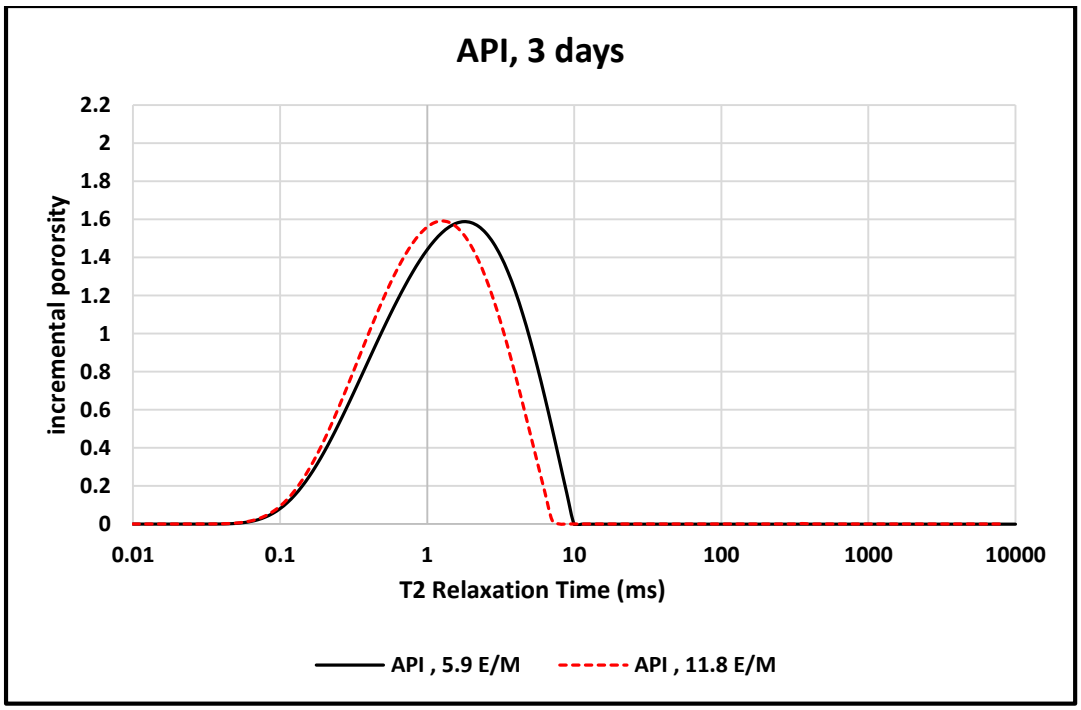

Figure 7.19 T_2 relaxation time for 3 days curing times using API mixing procedures for 5.9 E/M and 11.8 E/M

T_2 distribution curves for 7 and 21 days curing using API mixing procedure are shown in the Figures 7.20 and 7.21. Similar behavior as one step mixing procedure is observed where T_2 relaxation times shift to left indicating smaller pore size distribution with longer curing. Relaxation time in range of 0.06 to 7 μs is observed. The maximum T_2 peak changes from 1.0 to 1.12 μs for 7 days curing and 0.78 to 0.8 μs for 21 days curing. Porosity ranged from 27 to 29 p.u. for 7 days curing and 18 to 20 p.u. for 21 days curing. Similarly, to one-step mixing data, it is apparent that mixing energy, shear rate and mixing time all impact porosity and pore size distribution of cement. Different porosity results were observed when mixing energy kept is constant but other mixing variables changed.

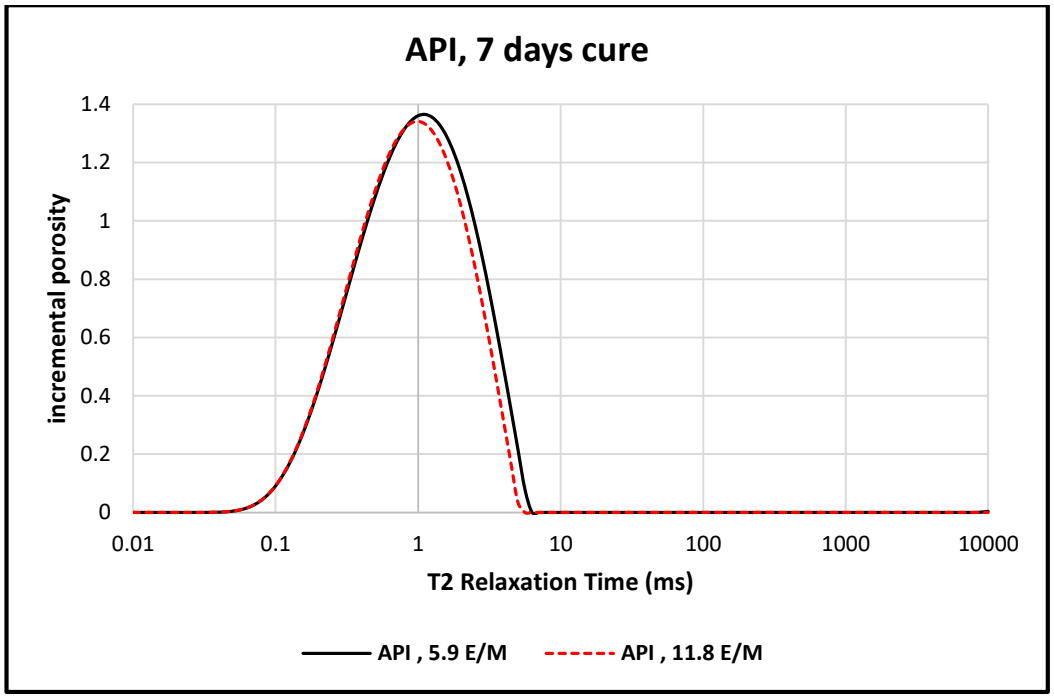

Figure 7.20 T_2 relaxation time for 7 days curing times using API mixing procedures for 5.9 E/M and 11.8 E/M

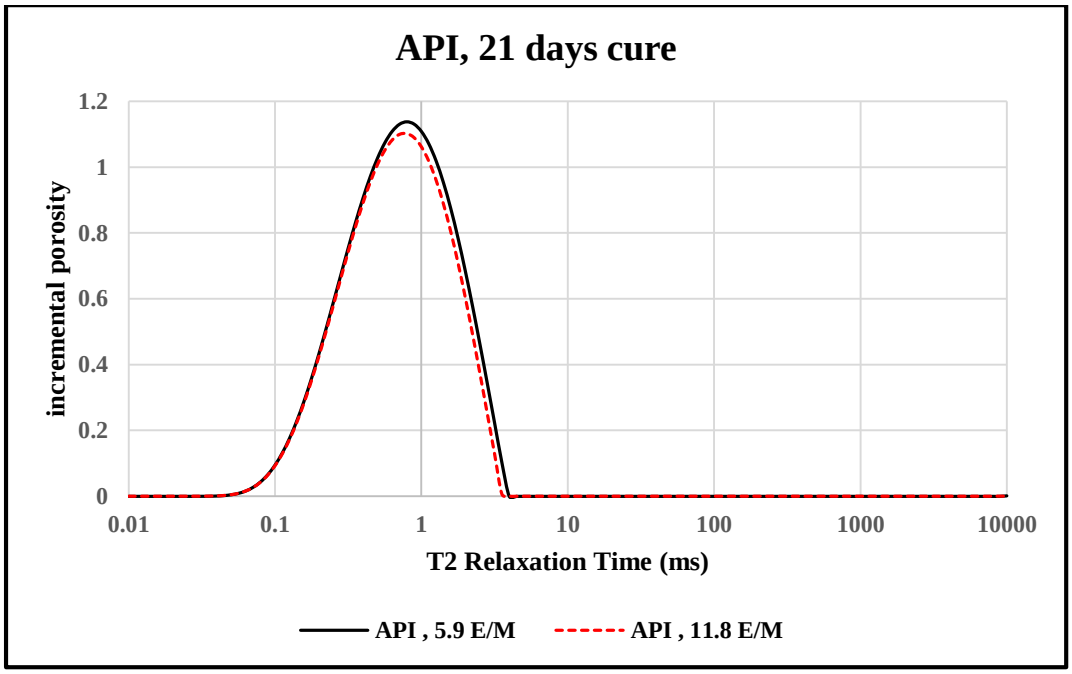

Figure 7.21 T2 relaxation time for 21 days curing times using API mixing procedures for 5.9 E/M and 11.8 E/M

Chapter 8: Yard Mixing

8.1 Overview

We used a yard mixer to compare results of mixing from API Warring blender in the lab to larger field scale. The primary objective for this comparison was to investigate whether or not cement properties will change if slurry a is mixed in larger scale with a yard type mixer (keeping same mixing energy in the two systems). In earlier chapters, we showed that slurries of equal mixing energies did not show similar properties for specimen prepared using API Warring blender. We investigate whether mixing at same energy using different scale mixing equipment will result in matching properties or not. For consistency with API recommended mixing energy, we used 5.9 E/M for mixing slurry using the yard mixer.

Figure 8.1 Drum baffled container and propeller used for mixing cement slurry

The propeller mixer, drum and mixing baffle are illustrated in the Figure 8.1. Mixing baffles are usually embedded for increased turbulence and mixing quality. Due to geometry of drum, minimum volume required for proper mixing was 36,000 ml (to ensure blender is inside in the slurry while mixing). In order to keep the energy level same as 5.9 E/M using the yard mixer, we used the horse power from the yard mixer (0.5 HP) and

calculated the required mixing time to reach the 5.9 E/M energy using the mixing energy formula as discussed in the Chapter 2 (Eq. 2.12). The required mixing time to reach 5.9 E/M was about 20 minutes. The rotational speed for the yard mixer was 1800 rpm which is considered a low shear type mixing compared to the mixing condition using API Warring blender. Deionized water was used for consistency with previous laboratory tests. After mixing, samples were collected immediately for purpose of UCS/UPV, rheology and thickening time tests. It was a challenge to conduct more than one test using the yard mixer because of time consuming process and larger volume of supplies required.

8.2 Results

8.2.1 UCS and UPV Results

Results of testing at 5.9 KJ/Kg mixing energy are reported in Figure 8.2. UCS and UPV are compared for API mixing, 6000 rpm and yard mixing conditions and in curing times of 1, 3, 7 and 21 days. Results of first day curing indicates very small difference between the measured values in the yard compared to the lab (less than 4%). UCS from yard mixer was higher than API but less than samples prepared at 6000 rpm. 12% difference was observed for UCS at 3 days between yard and 6000 rpm conditions (higher for 6000 rpm). When comparing UCS between API and yard, the difference was 5% (higher for yard). At 7 days, 6% difference is observed for UCS between yard and 6000 rpm conditions (higher for 6000 rpm). The difference was 10% for UCS between API and yard (higher for yard). 21 days UCS followed similar trend to 3 days. The difference can be also attributed to different mixing equipment. These results imply that even though mixing energy was kept constant, matching UCS was not observed. These differences may also attribute to the mixing equipment. Figure 8.3 shows results of UPV for samples mixed

under three mixing conditions. We can see that UPV follows similar trend observed in UCS tests, albeit the differences are smaller.

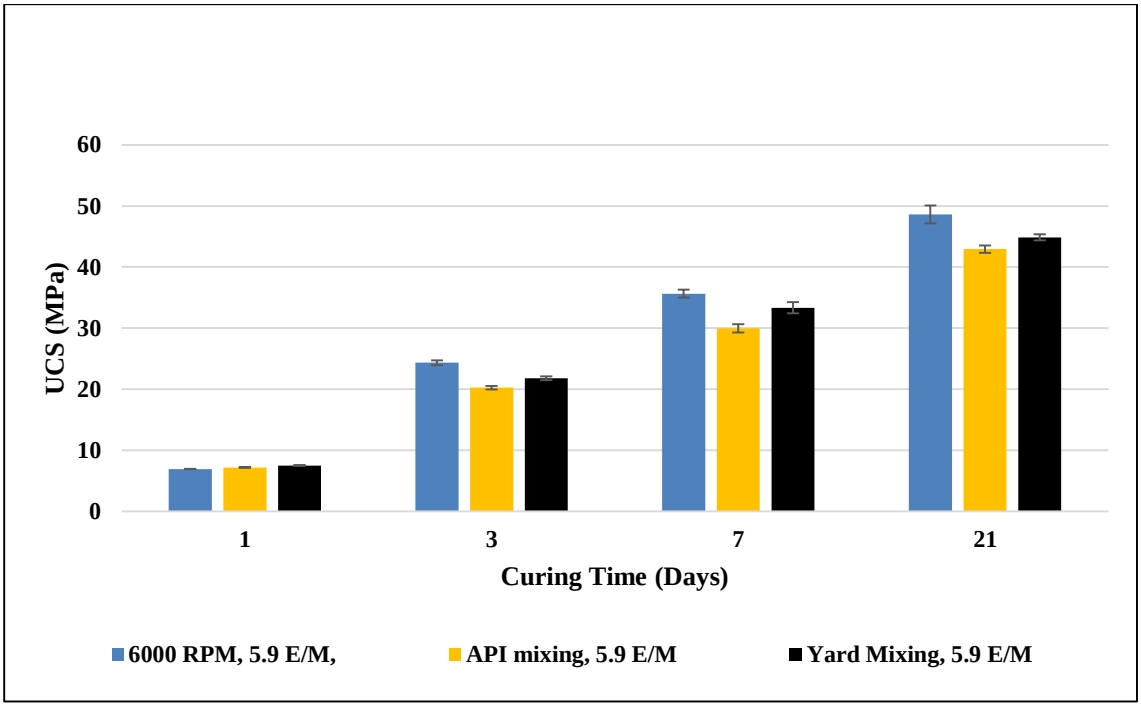

Figure 8.2 UCS test results for 5.9 KJ/Kg mixing energy for samples prepared by API Warring blender and yard mixer

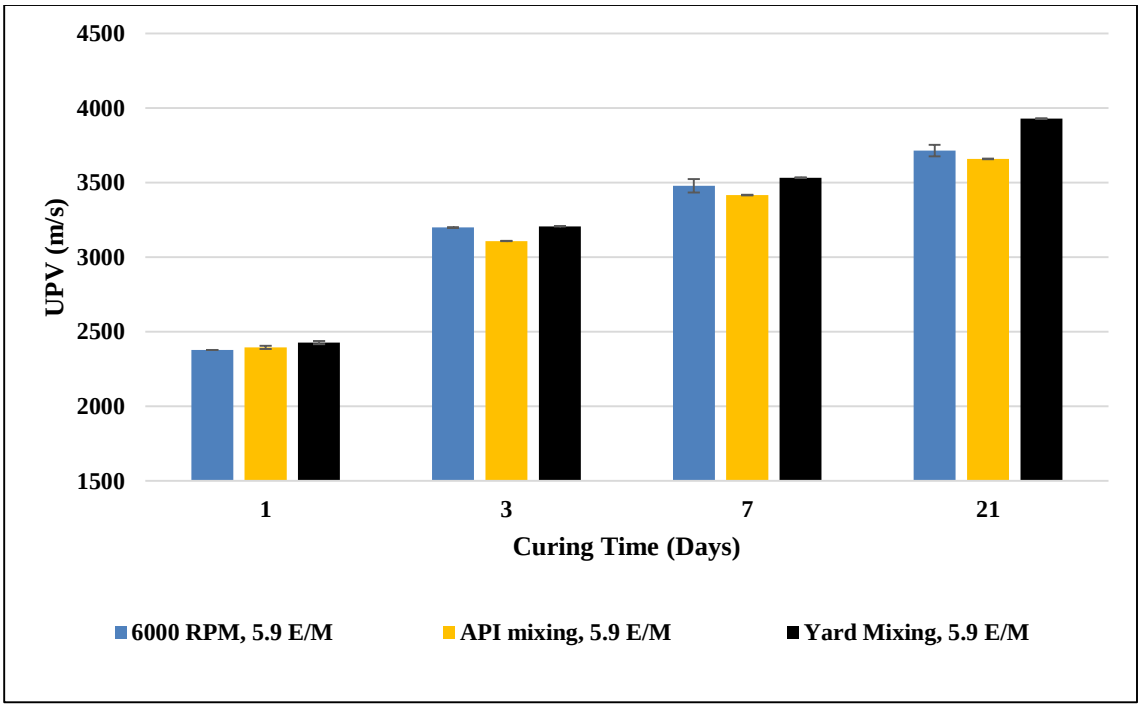

Figure 8.3 UPV test results for 5.9 KJ/Kg mixing energy for samples prepared by API Warring blender and yard mixer

8.2.2 Rheology and Thickening Time Results

Rheology test results at 5.9 KJ/Kg using laboratory and a yard mixer are shown in the Figure 8.4. Test results indicate higher shear stress in yard mix slurries compared to laboratory prepared slurries. In another word, sample appears thicker using yard mixer even though both samples were prepared at 5.9 E/M mixing energy. This observation is consistent with some of the rheology measurements in the literature (Teodoriu et al., 2015, see Chapter 2).

Furthermore, results of plastic viscosity (PV) and yield point (YP) are shown in the Figures 8.5 and 8.6. As expected, we see higher PV and YP for slurries prepared by yard mixer. These measurements are consistent with visual observations of slurries mixed using yard mixer. As shown in the Figure 8.7, larger cement particles were observed in

the slurry mixed with yard mixer. As explained in the Chapter 6, PV strongly correlate with size and shape of solids in addition to solids concentration. We can see that in yard mixing method, large solids remain therefore increasing PV. This is consistent with the deflocculation theory as well, where in yard mixing, due to poor deflocculation, larger particles were left inside the drum. Similarly, YP is strongly correlates with mixing time and growth of hydrates, therefore, having longer mixing time increased YP.

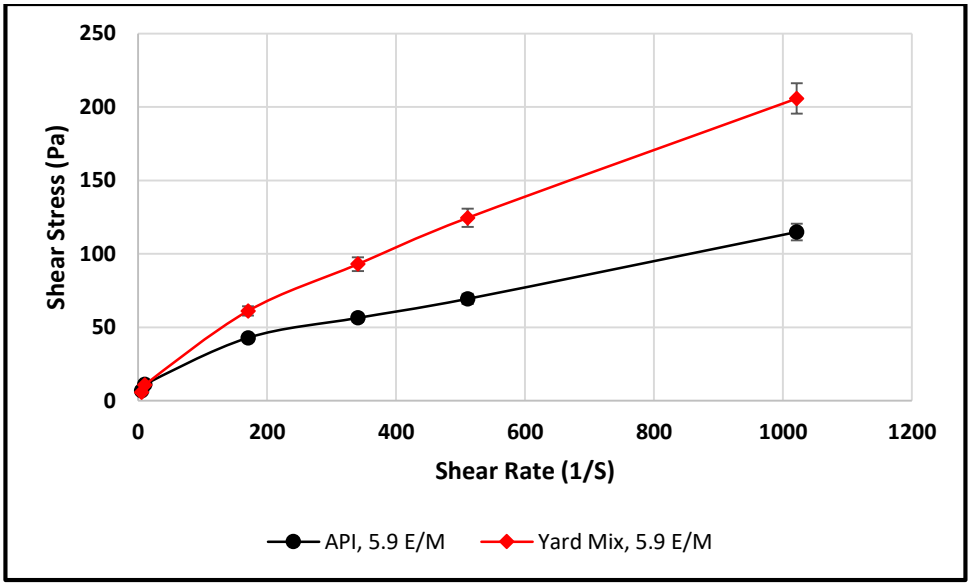

Figure 8.4 Rheology test results for 5.9 E/M and for slurries prepared by API Warring blender and yard mixer

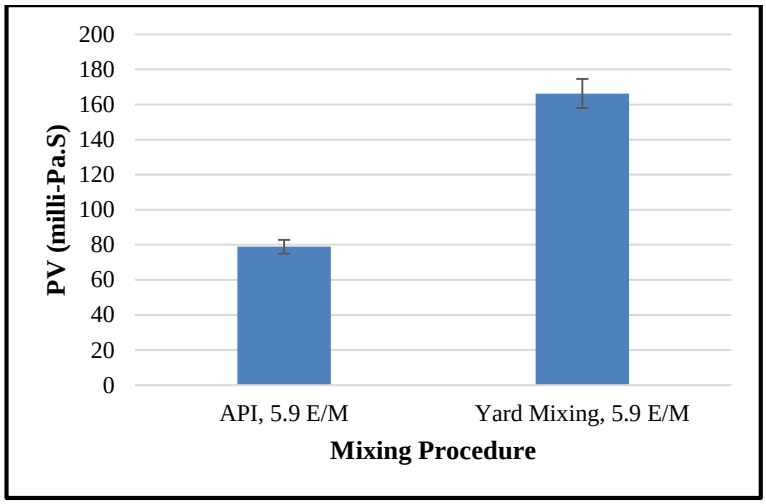

Figure 8.5 Plastic viscosity (PV) for slurries prepared by API Warring blender and yard mixer

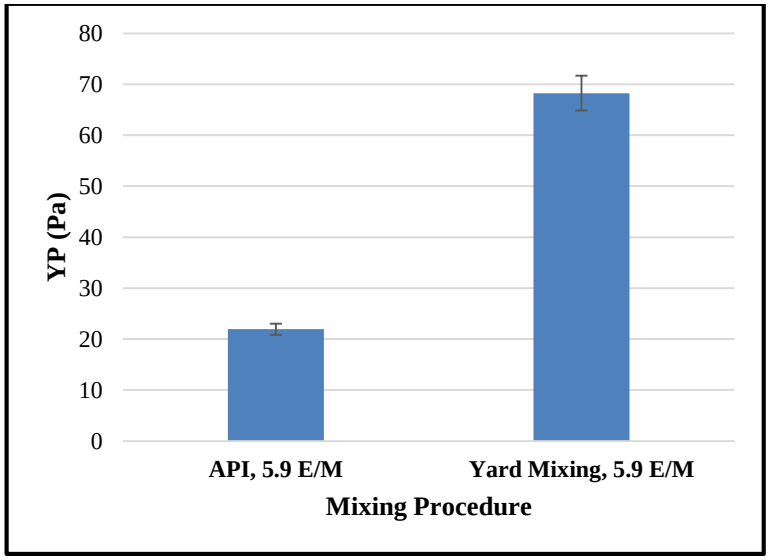

Figure 8.6 Yield point (YP) for slurries prepared by API Warring blender and yard mixer

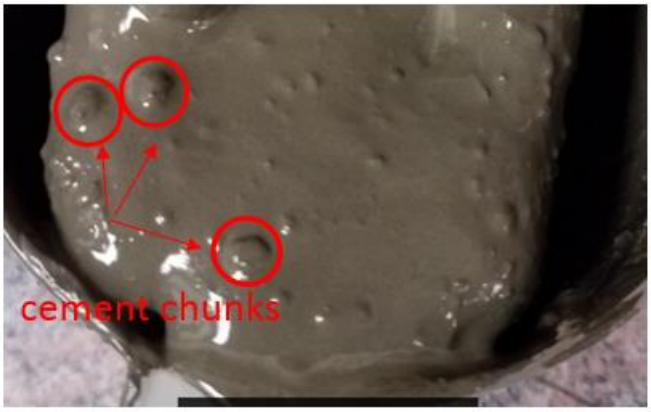

Figure 8.7 Large cement chunks can be seen inside the slurry prepared using yard mixer

8.2.3 Thickening Time

Attempts were made to measure thickening time of slurry from yard mixing, however, due to large cement chunks, consistometer machine could not operate. Significant increase in consistency was observed within few minutes of a test run. Therefore, no thickening time tests were concluded. We believe it is very likely to have a shorter thickening time for yard mixing slurry because of strong correlation between thickening time and PV.

Chapter 9: Mixing Power Consumption and Scale Up

9.1 Overview

One of the key parameters in the design of mixing process in the chemical processing industries is power consumption. Because of different flow patterns and mixing mechanisms, it is very convenient to consider power consumption to optimize a mixing process. A majority of the prior studies in these industries have conducted rheological studies, and mixing power consumption analysis to evaluate the mixing performance (Coulson et al., 1999; Skelland, 1967). Then, a procedure for scale up process is provided for using results from small mixers to larger mixer. As per studies for mixing power consumption and scale up in oilwell cement slurries, previous literature is scarce. Hence this study will be a pioneering in investigation of power consumption in mixing oilwell cement slurries considering non-Newtonian behavior of cement slurry. Therefore, major goals for this chapter are:

1. To present a theoretical literature of power consumption in mixing of Newtonian and Non-Newtonian fluids.
2. To develop empirical models based on power consumption for mixing neat class H cement in the laboratory using API recommended Waring blender and considering non-Newtonian characteristics.
3. To provide a scale up procedure for using results from laboratory mixing to field operations.

9.2 Power Requirements for Newtonian and Non-Newtonian Fluids

Power requirement is of critical importance in study of mixing systems. The study of power requirements and consumption of various liquids dates back to many decades ago. Pioneers such as Metzner and Otto (1957) presented quantitative relationships between power consumption and kinematic and fluid properties of non-Newtonian systems.

Considering a Newtonian fluid and other characteristics of mixing vessel, the power input and its relationship to other variables can be defined as function of i) geometric properties; ii) fluid physical properties; and iii) kinetic and dynamic properties (Skelland, 1967).:

$$P = f(\mu, \rho, N, g, D, D_T, other) \quad \text{.....(9.1)}$$

In this relationship, P is the impeller power which is defined as "energy per unit time dissipated within liquid", μ is the viscosity, ρ is the density, N is the speed of rotation, D is the impeller diameter, D_T is mixing tank diameter, and g is acceleration constant for gravity. The gravity can be of importance when power is used to "produce waves" on surface or to create vortex flow.

In Equation (9.1), the number of variables can be reduced by dimensional analysis and the power equation becomes:

$$\frac{P}{\rho N^3 D^5} = f\left(\frac{\rho N D^2}{\mu}, \frac{N^2 D}{g}, \frac{D_T}{D}, \frac{W}{D}, \frac{H}{D}, ...\right) \quad \text{.....(9.2)}$$

W is the blade width and H is depth of liquid in the tank.

The Reynolds Number for Mixing is:

$$\rho D^2 N / \mu \quad \text{.....(9.3)}$$

The Froude number is:

DN^2 / g ……..……..…….…….……(9.4)

Defining left hand side of equation as power number we will get:

$N_P = f(\text{Re}, F_r)$ ……..……..…..……..(9.5)

The simplest definition of function in above equation, we will get:

$N_P = K' \text{Re}^b F_r^c$ ……...……(9.6)

The constants K', b and c can be found from laboratory experiments. These factors will be dependent on flow regimes (laminar, turbulent, transition) and mixing vessel configurations. Previous studies also indicate that some impellers are more efficient than the others due to power consumption. This may change depending on liquid viscosity (Skelland, 1967). In the case of two immiscible fluid mixing, the interfacial tension between two liquids will be a contributing factor for power consumption.

Generally, a power curve is required to better understand the power requirements. Power curves for different impeller types can be found in the literature. An example of power curve is shown in the Figure 9.1. Top figure illustrates three distinctive regions:

i. Laminar Region: The laminar region corresponds to a very small Reynolds number. In laminar region, the power number has inverse relationships with Reynolds number

ii. Turbulent region: Power number is independent of Reynolds number in turbulent flow. In addition, power required for turbulent flow is not dependent on viscosity but proportional to fluid density.

iii. Transition region: There is a transition from laminar to turbulent flow in this region. Both density and viscosity affect power requirements in this region.

These power curves can be obtained by conducting laboratory experiments where impeller is rotated at different speeds changing fluid density and viscosity. These curves are usually prepared on a semi-log scale. These power curves can be used to calculate impeller power requirement as long as vessel/impeller geometry, impeller speed and fluid properties are known (Nienow et al., 1997). If new impellers are used or if no curve exists, then new experiments are needed to generate this curve.

Figure 9.1 (bottom) shows power curves for some particular impellers. These power curves can only applicable if fluid properties, geometry and speed are known. As seem in the Figure 9.1, the type of impeller has significant impact on power number as shown for various impellers such as helical ribbon, pitch bladed paddle and bladed disc turbine. In addition, the flow type will be different using different impellers. Figure 9.1 shows that for some of the impellers, increasing viscosity leads to increasing power consumption until the laminar region is reached. Other impellers can be designed in such a way that viscosity has no effect on power consumption over wide range of Reynolds number.

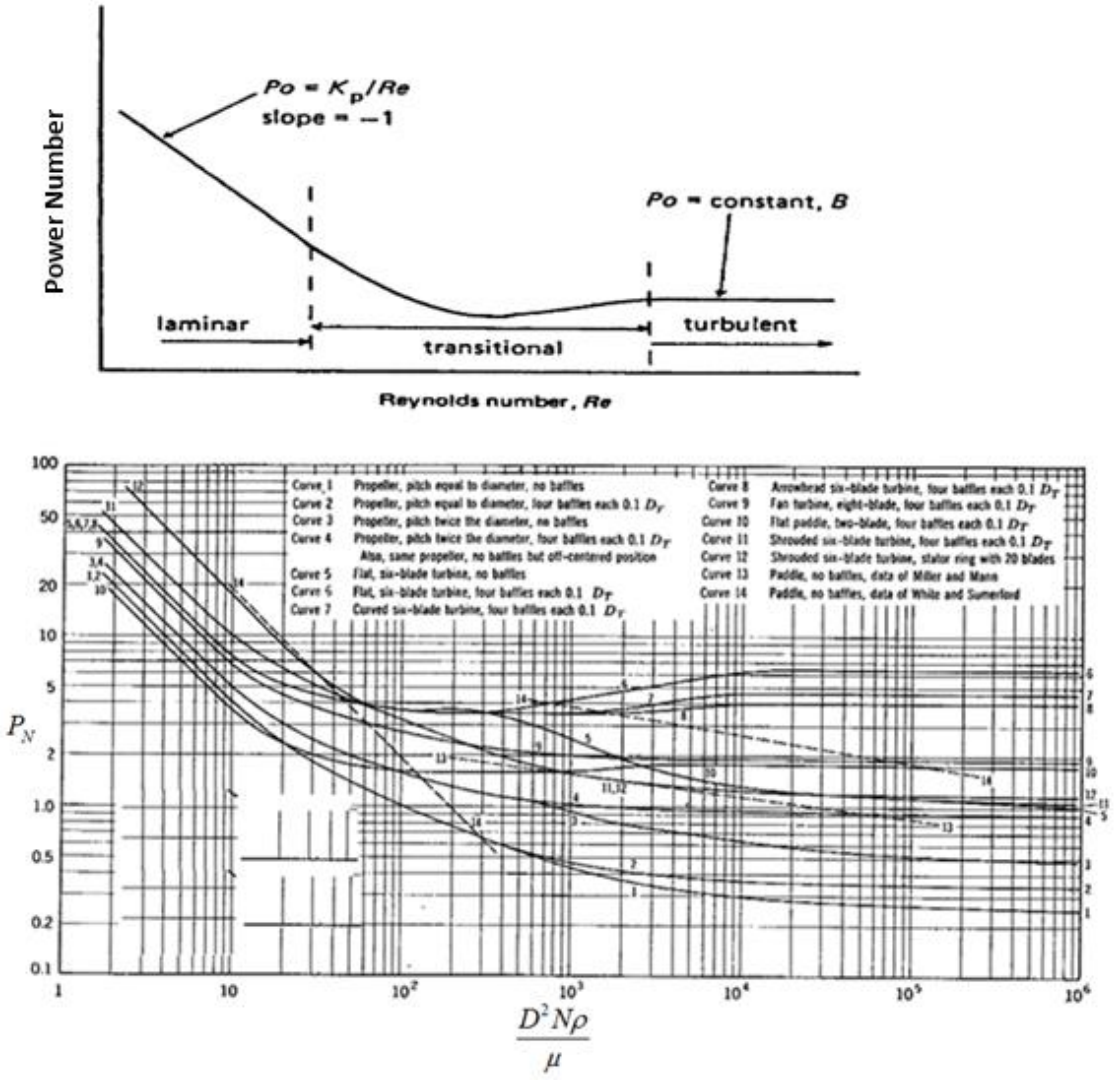

Figure 9.1 A typical power curve (top) (from Coulson et al., 1999); Correlation of power number for various impellors (bottom) (from Skelland, 1967)

9.2.1 Non-Newtonian Agitation

As described earlier for the power curve of Newtonian fluids, power number has a reverse relationship with Reynolds number; however, it becomes almost constant when in turbulent region. For this turbulent region, rheological properties become unimportant for prediction of power. This phenomenon is significantly different when dealing with Non-

Newtonian fluids due to difficulties for defining constant viscosity. In these type of fluids, it will be necessary to define an apparent viscosity for power number prediction.

Overall, three methods are presented in the literature for power requirements of non-Newtonian mixtures. Foresti and Liu (1959) developed a method for Newtonian and pseudo-plastic fluids. Various power–law systems such as silicone fluid, CMC solution, and Catalpo clay were used in conjunction with various mixers such as anchor, six blades turbine and different size cone impellors. The method lacked application for fully non-Newtonian systems where this correlation could not be used.

Metzner and Otto (1957) defined an alternative method for predicting power consumption of Non-Newtonian mixtures. The method is based on calculating apparent viscosities for various mixers. Reynolds number in the non-Newtonian case is found by substituting apparent viscosity in the Reynolds equation. This Reynolds can then be used for finding power number. A typical power curve for non-Newtonian fluids (Figure 9.2, various CMC solutions) was given by the Metzner and Otto (1957). The curve showed that the laminar region may extend to higher Reynolds number in pseudo-plastic fluids compared to Newtonian fluids. This behavior may not correlate with all types of non-Newtonian fluids since it was observed with pseudo-plastic solutions in laboratory experiments.

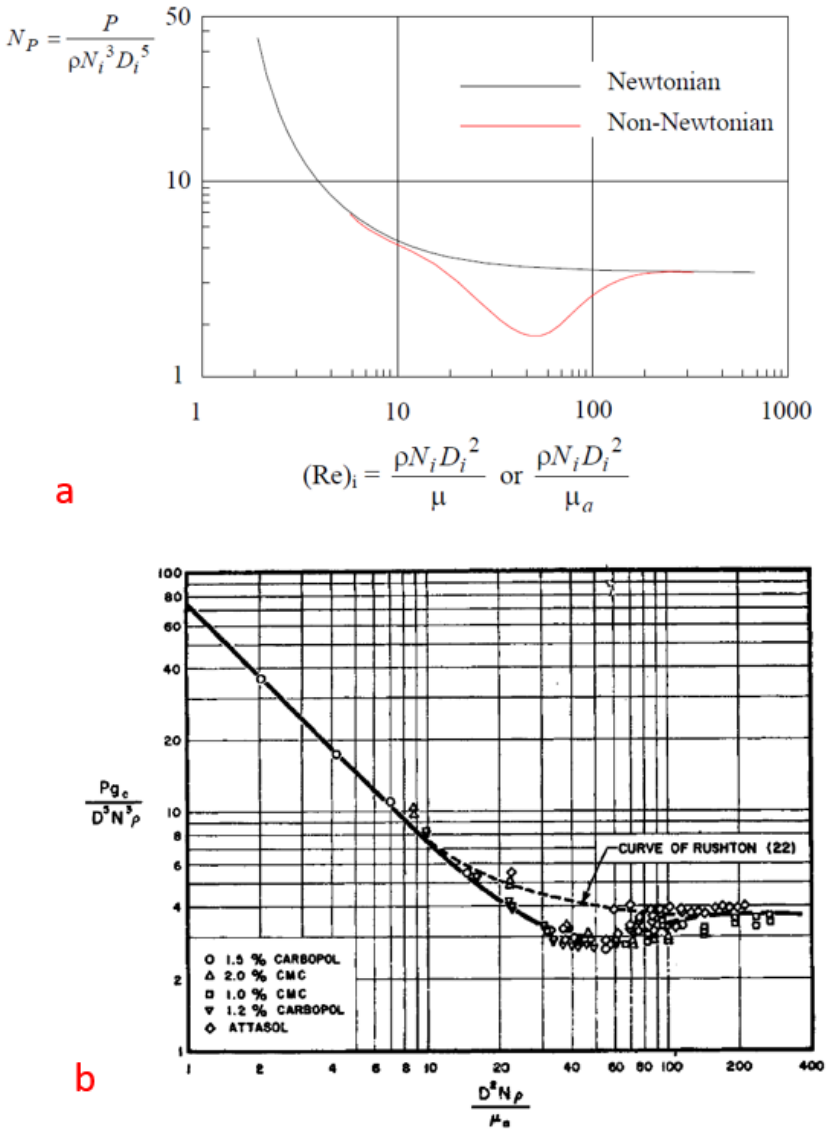

Figure 9.2 A typical power curve for non-Newtonian (a), recorded data for pseudo-plastic fluids (b) from Metzner and Otto (1957)

The third method for predicting power consumption of non-Newtonian systems was developed by Calderbank and Moo-Young (1959). The method was based on correlation for modified Power law and a generalized Reynolds number. Generalized Reynolds number is numerically proportional to mixing Reynolds number. Metzner and Otto suggested the use of generalized Reynolds number as an alternative to Reynolds number.

The main advantage of this method is its applicability over a wide range of agitation systems and it extends beyond laminar region.

Lee et al., (1957) pointed out that, the major reason for slow evolvement of study for non-Newtonian fluids compared to Newtonian was due to their complexity. Lee et al., (1957) showed that in polymeric non-Newtonian fluids, gradients in viscosity will lead to poor mass and heat transfers.

In non-Newtonian fluids, the mixing blender can affect total energy consumption due to dependence of viscosity upon the shear stress. Accordingly, non-turbulent conditions and poor mixing are likely to occur for non-Newtonian fluids. For instance, since non-Newtonian fluids have relatively low apparent viscosity in the high shear zone and high apparent viscosity in other places, a stagnant zone as shown in the Figure 9.3 can occur.

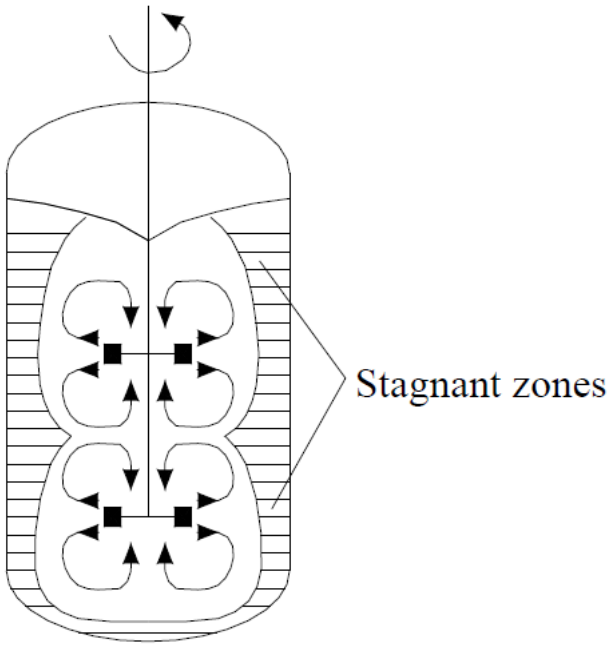

Figure 9.3 Stagnant zones in mixing of non-Newtonian substances. Non-Newtonian fluids have relatively low apparent viscosity in the high shear zone and high apparent viscosity in other places (Coulson et al., 1999)

9.2.2 Masiuk and Lacki Power Consumption Model

Similar to previous models, Masiuk and Lacki, (1992) presented a model for mixing non-Newtonian fluids. The basic concept behind development of their model was to relate power consumption (P) or mixing energy (P.t) to Reynolds number as:

$$P.t = C.R_e^A \quad \text{.....(9.11)}$$

The primary objective from work conducted by Masiuk and Lacki, (1992) was to select the lowest energy-consuming configuration of the agitator. The study used a 1.1 KW D.C. electrical motor and electrical instrumentation to measure power input for liquid mixing. The substance used for mixing was CMC-water solution which is a typical non-Newtonian power law fluid. The Power-law rheological properties were measured for each mixture used in the experiments. From the power consumption and mixing time, mixing energy was calculated and the value of P.t was plotted against Reynolds number. By plotting power consumption versus Reynolds number, constants C and A were found. For the five different agitators used in the study, all showed straight line relationship between mixing energy and Reynolds number. One of the agitators showed the lowest mixing energy value. In the next stage of experiments, the effect of agitator width on power consumption was investigated.

The study produced an empirical equation for calculating mixing energy:

$$Pt = R_{eg}^{0.5}[22\frac{w}{d} + 0.125(\frac{w}{d})^{-1}] \quad \text{.....(9.12)}$$

Where w/d defines the geometrical ratio for different mixer. The study results revealed that the shape of agitator has a significant influence on the mixing energy.

9.3 Scale Up

Design and construction of a large-scale system using experimental data from small scale equipment requires scaling up procedures. In the mixing process, it is necessary to deduce satisfactory arrangement when conducting experiments in small mixing vessel to larger unit (Coulson et al., 1999). Maintaining similar flow pattern requires following characteristics for consideration:

- Geometrical condition
- Kinematic conditions
- Dynamic similarity
- Boundary conditions

Many studies show that relating power used by the mixer (agitator) to mechanical and geometrical details can be used to understand requirements for scaling. More specifically, for having similar mixing systems; one has to achieve geometric and dynamic similarities between the two systems. Details of mathematical relationships to achieve scale up in two systems are given in Appendix C. The majority of papers published discuss scale up relationships for Newtonian fluids (Nienow et al., 1988; Chhabra et al., 2011 and Wilkens et al., 2003). Whereas, it is often challenging to develop scale up relationship for non-Newtonian fluids due to shear-rate dependent behavior of these fluids. Literature for mixing and agitation in chemical processes proposes several methods for scale up relationships as summarized in the Table 9.1 (Wilkens et al., 2003). Two of the recommended methods for scale up are bolded in the Table 9.1. These methods are:

1. Equal power per volume (P/V)
2. Equal torque per volume (T/V)

Therefore, in order to scale up any results from laboratory mixing to larger scale mixing measuring power and torque are necessary. Wilkens et al. (2003) explain that because of complexities involved for non-Newtonian flow behavior, using other scale up procedures are either too costly, inconsistent or not practically feasible.

Table 9.1 Summary of scale up relationships in the literature

Scale Up Method	Process Details	Advantage/Disadvantages
Equal Reynolds Number	Holding Reynolds fixed in two systems.	Inconsistent results. Not usually recommended.
Equal Tip Speed	The impeller tip speed (S_t) is a common scale up criterion for industrial mixers. $S_t = \pi ND$	Worked only in small scale studies. Good predictor of desirable product turbidity.
Equal Torque per Volume (T/V)	Torque/volume is measure of torque used by mixer. $V = \pi T^2 Z / 4$	**Relates directly to the size and torque of the mixer. A practical and common scale up criteria.**
Equal Bulk Fluid Velocity	$v_{bf} = 4q / \pi T^2$	Usually applied in low-viscosity applications.
Equal Blend Time	Blend time increases with tank volume (expensive).	Difficult and expensive for scale up criterion
Equal Froude Number	$F_r = N^2 D / g$, will decrease with volume increase.	Rarely used since only can be applied in large mixers.
Equal Power per Volume (P/V)	$P = N_p \rho N^3 D^5$	**Most commonly used criteria, very practical and easy. Correlates well with mass transfer characteristics in the mixer.**

S_t represents impeller tip speed, D is diameter of impeller, T is the torque, υ_{bf} is the bulk fluid velocity, Z here is the depth of liquid in the mixer, q is the impeller pumping rate, ρ is density, N is rotational speed and Np is dimensionless power number.

9.4 Development of non-Newtonian Power Consumption Model for Mixing Class H Cements

One major challenge with the API mixing energy formula is relying on characteristic of Newtonian substances. Even though the concept of mixing energy was developed to correlate similar properties with matching energy, our experimental data showed a significant difference in many of the measured properties. Here, in this section, our objective is to develop a relationship between cement mixing power consumption and non-Newtonian flow characteristics predicted through experiments. We follow similar experimental approaches available in the literature of chemical processes for non-Newtonian substances. In order to develop a robust correlation, one needs to conduct rheology experiments, calculate corresponding Reynolds number and correlate with other cement properties. As discussed earlier, as an alternative to mixing Reynolds number, we use generalized Reynolds number developed based on considering apparent viscosity for non-Newtonian fluids. The concept of generalized Reynolds number for non-Newtonian fluids can be shown by following relationships:

$$\frac{D^2 N \rho}{\mu_a} \quad \text{.....(9.13)}$$

N is the shear rate, d is diameter of agitator, and μ_a is apparent viscosity (Skelland, 1967). By conducting rheological measurements, one can calculate apparent viscosity for predicting generalized Reynolds number. Generalized Reynolds number is numerically proportional to mixing Reynolds number. (Crespi-Liorens et al., 2015; Skelland, 1967). Other parameters such as rheological properties will be obtained by mixing cement using API Warring blender. In order to measure mixing power, the blender was connected to

the power measurement unit (Figure 9.4). During each mixing, the power consumption numbers were read after they were stabilized near to end of mixing process.

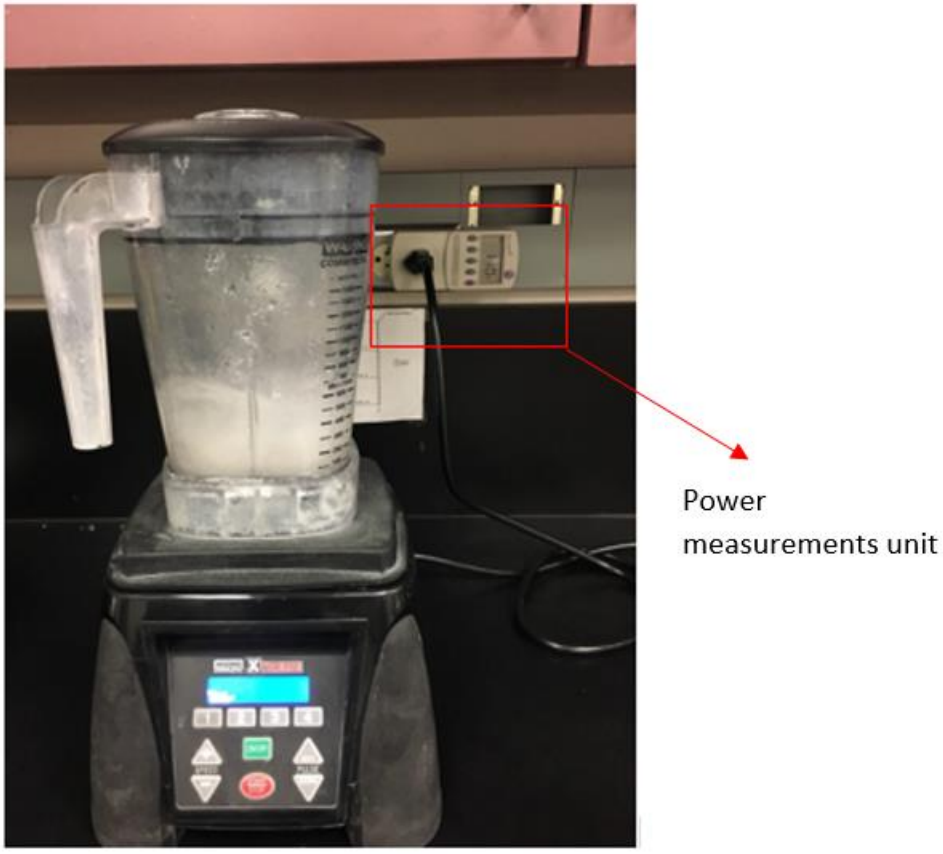

Figure 9.4 API Warring blended connected to power measurement unit

9.4.1 Design of Experiments

An experimental procedure was designed by changing shear rate from 3000 rpm to 12,000 rpm; these limits are equipment constraints for API Waring blender. The following procedures were used:

1. Cement slurries were mixed at specific rpm (each individually) in the mixer and power consumption for each experiment was recorded. Fifty seconds mixing time was used in the experiments.

2. Rheological properties of each slurry was carefully measured and documented.
3. Step 1 above was repeated to prepare same mixture for pouring in the cubes for 3 days UCS tests. Three cubical samples were collected.
4. Steps 1-2 was repeated for reproducibility of the data.
5. After experimental measurements, rheological data were used to calculate apparent viscosities and generalized Reynolds number for each mixing condition.
6. Power consumption and UCS versus generalized Reynolds number were plotted to find empirical correlation of Power-Reynolds.
7. Power number were calculated and plotted versus generalized Reynolds number

9.4.2 Results

Here we present results of experiments. First, we show results of rheology tests. As shown in the Figure 9.5, shear stress versus shear rate for range of 3000 rpm to 12000 rpm is provided. It can be observed that at lower shear rates range (3000 rpm to 6000 rpm, shown by solid lines), there is progressive increase in shear stress by increase in the rheometer shear rate. When comparing rheological data for slurries prepared at higher shear rate (7000 rpm to 12000 rpm, shown by dashed lines), we observe an abrupt decrease in shear stress values.

As shown in the Figure 9.5, a critical shear rate can be inferred where a sharp decline in shear stress is observed. The critical range based on our data is between 6000 to 7000 rpm. It is no surprise that cement as non-Newtonian fluid shows such a shear rate dependent behavior but to our knowledge observing a critical mixing shear rate has not been in the literature. When comparing flow behavior, we can infer that cement is

becoming more thin (smaller n) by increase in shear rates. These results may imply that a critical shear rate for mixing exists where a complete deflocculation occurs. We have shown apparent viscosity versus shear rate in the Figure 9.6. We can infer similar from comparing apparent viscosities. In the next step, we have used apparent viscosities to calculate generalized Reynolds number.

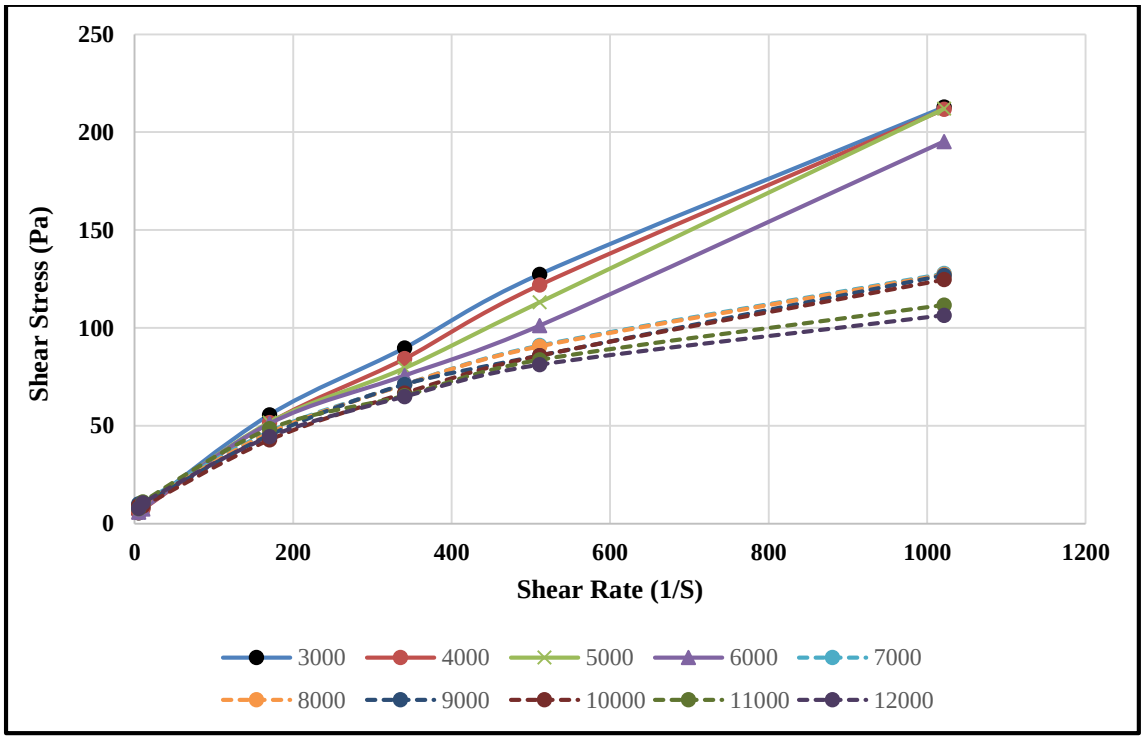

Figure 9.5 Rheological measurements for slurries mixed at different rpms. A critical mixing shear rate at 6000 rpm can be observed where shear stress declines afterwards

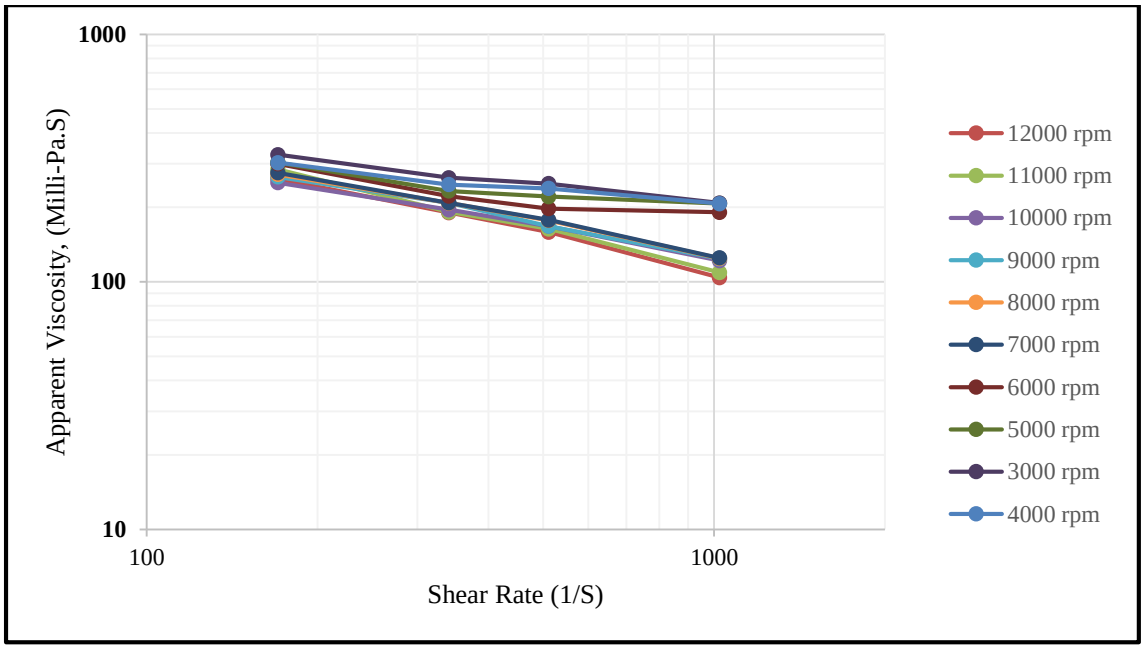

Figure 9.6 Apparent viscosity versus shear rate for different mix conditions. A critical mixing shear rate at 6000 rpm can be observed where shear stress declines afterwards

Important note here is that we have fixed mixing time to 50 seconds and observed changes in rheological profile (changing shear rate only). This time was selected according to the API referenced mixing time.

Figure 9.7 shows generalized Reynolds number versus measured power in the experiments. Generalized Reynolds number is illustrated in semi-log chart as customarily done in the literature. As seen from the Figure 9.7, there is gap in calculated generalized Reynolds number. This is observed for data points related to Re_g at 6000 rpm and 7000 rpm. This can be explained by the changes in rheological profile as explained earlier and Figure 9.4 and 9.5.

In order to find coefficients of power equation, we fitted two separate curves in the P-Re_g plot as shown in Figure 9.8. Data imply transitional zone in flow pattern in mixing shear rates range from 6000 rpm to 7000 rpm. At 7000 rpm, we can see a sharp change

in Reynolds number which can be representative of more turbulent regime. According to the literature, the turbulent regime is fully developed at Reynolds number > 10^3 or 10^4 for small impellers (Coulson et al., 1999). Additionally, we can imply that difference in power consumption at these two points (6000 rpm and 7000 rpm) is less. This may be explained because of completion of deflocculation process at this range where less power for mixing is required. However, more experiments are required to draw a firm conclusion. Furthermore, we can see how well data correlate in Figure 9.8. This figure is same as Figure 9.7 by including specific rpm related to each measurement for better understanding.

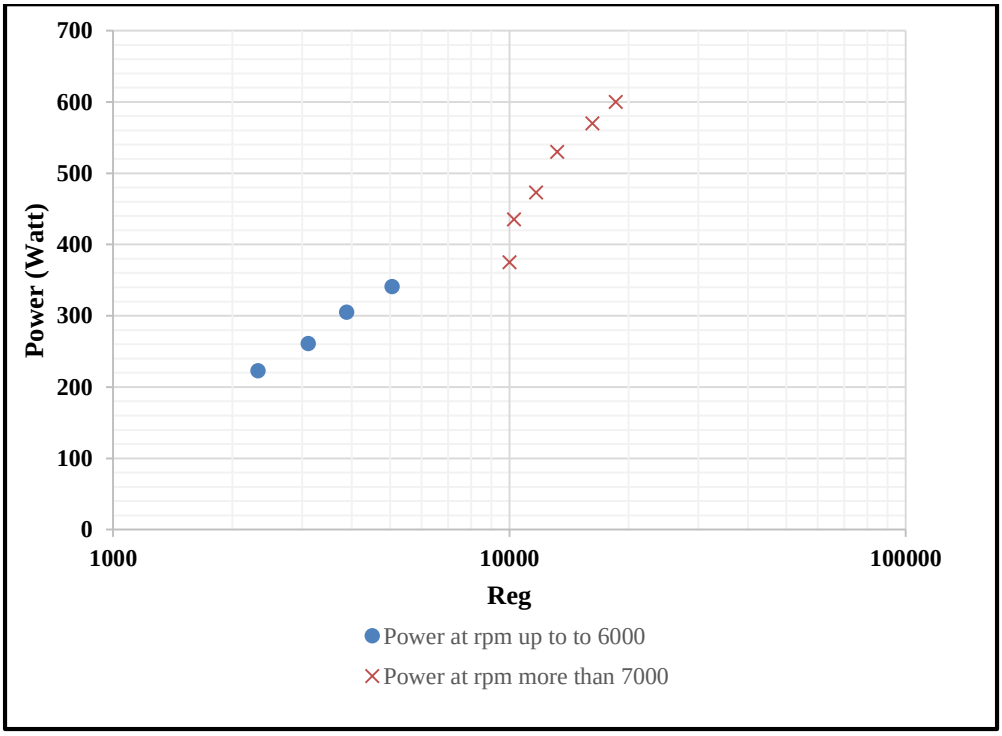

Figure 9.7 Mixing power consumption and generalized Reynolds number. Abrupt change in generalized Reynolds number can be observed in range of 6000 to 7000 rpm.

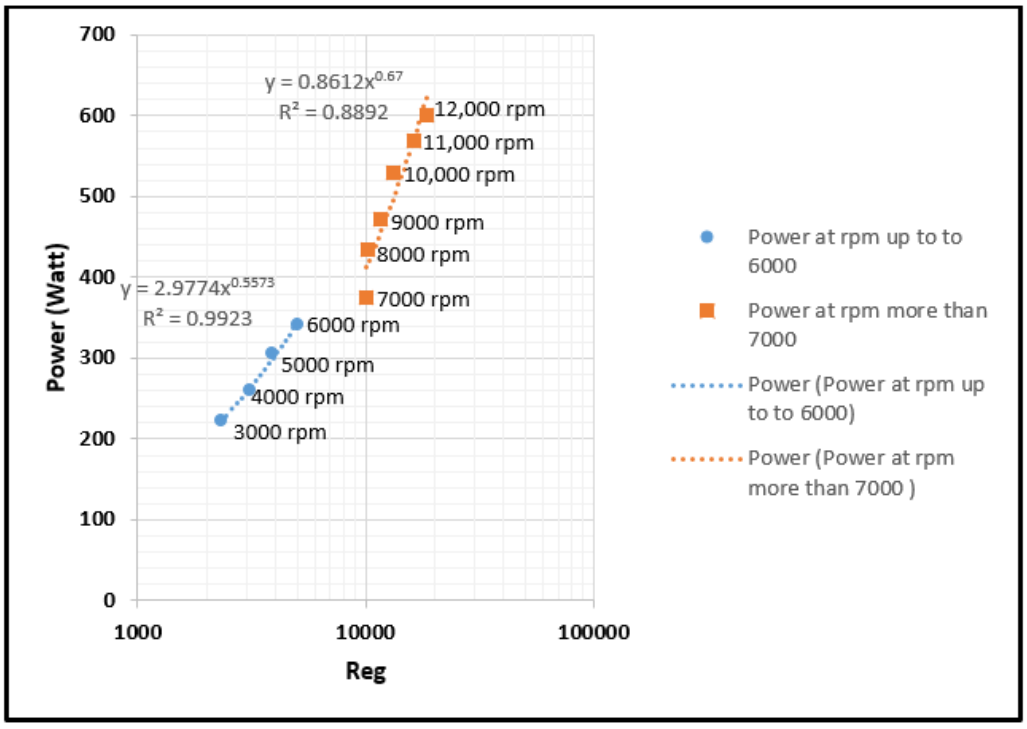

Figure 9.8 Mixing power consumption and generalized Reynolds number at each rpm

Results from our study show a strong impact of rheology on generalized Reynolds number. Mixing energy theory for cement mixing does not take into account any effect from changes in non-Newtonian flow behavior which is big drawback. To our knowledge, all the models published in the chemical processing literature for mixing non-Newtonian substances relate mixing power and energy to flow patterns developed while mixing (Wilkens et al., 2003; Skelland, 1967).

The following empirical power consumption models were obtained for neat class H cement:

for shear rates at or less than 6000 rpm:

$$P = 2.97\,\mathrm{Re}_g^{0.5573} \qquad (9.14)$$

for shear rates at or higher than 6000 rpm:

$$P = 0.86\,\mathrm{Re}_g^{0.67} \quad (9.15)$$

We report measured UCS values for various mixing in Figure 9.9. We only have conducted tests on 3 days curing. Seven and 21 days UCS usually followed 3 days trend in most instances as discussed in the previous UCS tests in this study (Chapter 5). Therefore, any pattern observed at 3 days, most likely will occur in longer curing time.

Although, we expected UCS to increase with shear rate, a sharp change in UCS can be observed in 5000 rpm to 6000 rpm. More than 20% increase in UCS is evident. This change in UCS can be explained by results from rheological measurements. When slurries mixed at critical shear rate, because of better deflocculation, an increase in strength can be achieved. For slurries mixed at shear rate more than 6000 rpm, a gradual increase in UCS can be observed. Specifically, we can see very slight increase in UCS measurements at 6000 rpm to 7000 rpm. Turbulent conditions while mixing provides good mixing conditions for a slurry to achieve full deflocculation and therefore higher strength. Data for UCS measurements versus generalized Reynolds number are plotted in the Figures 9.10. Table 9.2 reports the data points used for calculations.

Similar to previous plots, we fitted two curve lines, one for UCS for slurries mixed at or less than 6000 rpm and one for UCS for slurries mixed at more than 6000 rpm (Figure 9.10). Because of abrupt change in UCS at 6000 rpm, the correlation for blue curve is not as robust as the correlation for red curve.

Our results imply that critical changes in rheology starts to develop between 6000 rpm to 7000 rpm. However, critical changes in UCS start to develop between 5000 to 6000 rpm range. We believe, mixing at 5000 rpm is accompanied by the start of deflocculation process that can be seen by strength measurements while full deflocculation occurs at

7000 rpm. The latter can be implied from rheological measurements. That being said, more experiments are required to confirm these findings.

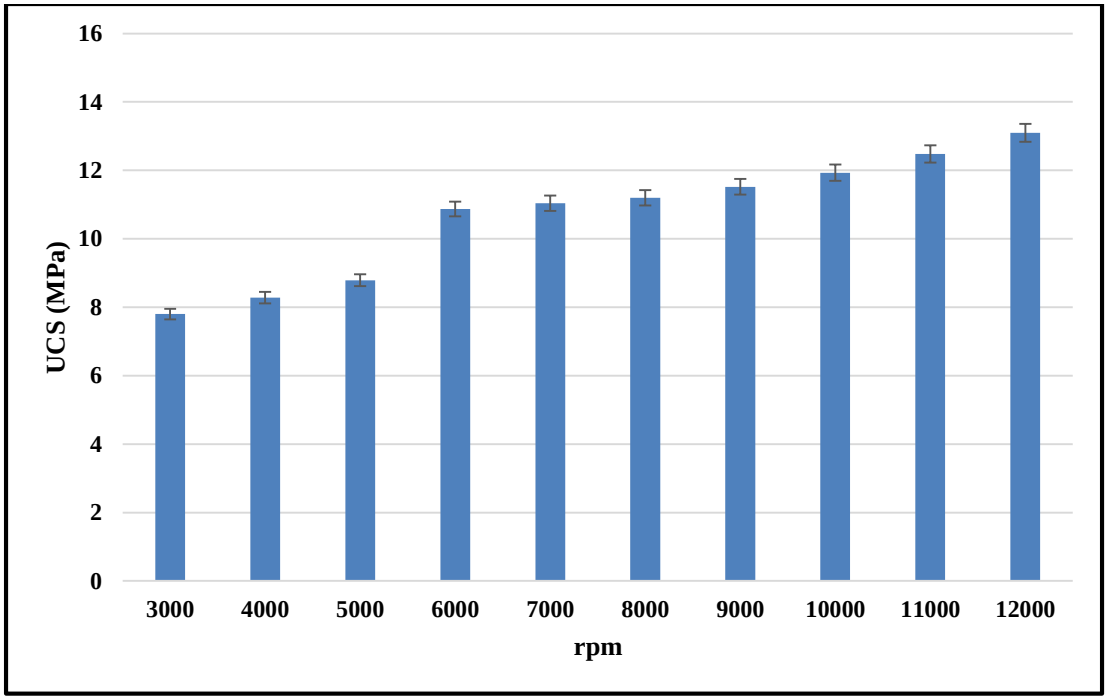

Figure 9.9 UCS (3 days curing) for various slurries prepared at different shear rates. A sharp change in UCS can be observed for shear rates at 5000 rpm to 6000 rpm. Mixing time was set 50 seconds for all mixing conditions.

Based on these results, we conclude that measured UCS and flow patterns while mixing are dependent. The power characteristics are suitable for design purposes especially if it can be used for scaling up from laboratory to field operations.

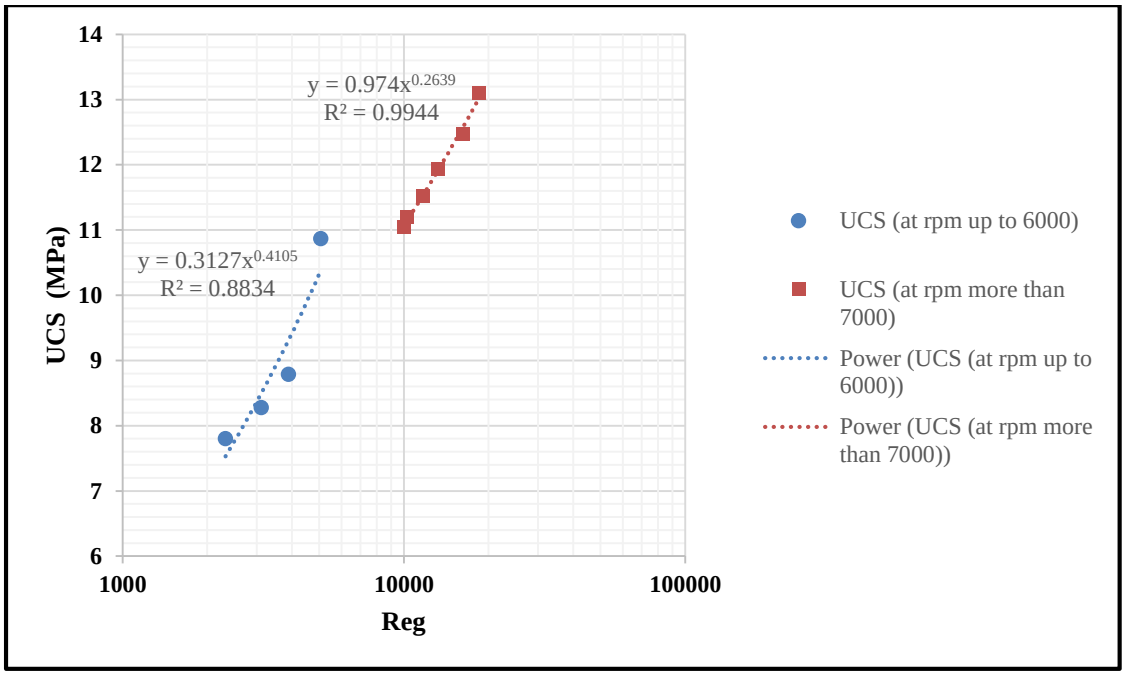

Figure 9.10 UCS and generalized Reynolds number. Data show a sharp change in generalized Reynolds number for shear rates at 6000 rpm to 7000 rpm

Table 9.2 Data points used for calculations

Rpm (used in mixing)	**Apparent Viscosity, Pa. S. (at 1021 S^{-1})**	**Reynolds number (Generalized)**	**Power (Watt)**	**UCS (MPa)**
3000	0.2082	2320	223	7.81
4000	0.2071	3110	261	8.28
5000	0.2074	3882	305	8.79
6000	0.1910	5058	341	10.87
7000	0.1215	10016	375	11.04
8000	0.1255	10263	435	11.21
9000	0.1241	11676	473	11.52
10000	0.1220	13198	530	11.93
11000	0.1092	16212	570	12.48
12000	0.1041	18555	600	13.11

Figure 9.11 shows both UCS and power consumption versus Re_g which can be useful to compare cement strength development based on flow pattern. We can see a very similar pattern for data in the two trends (UCS and power consumption).

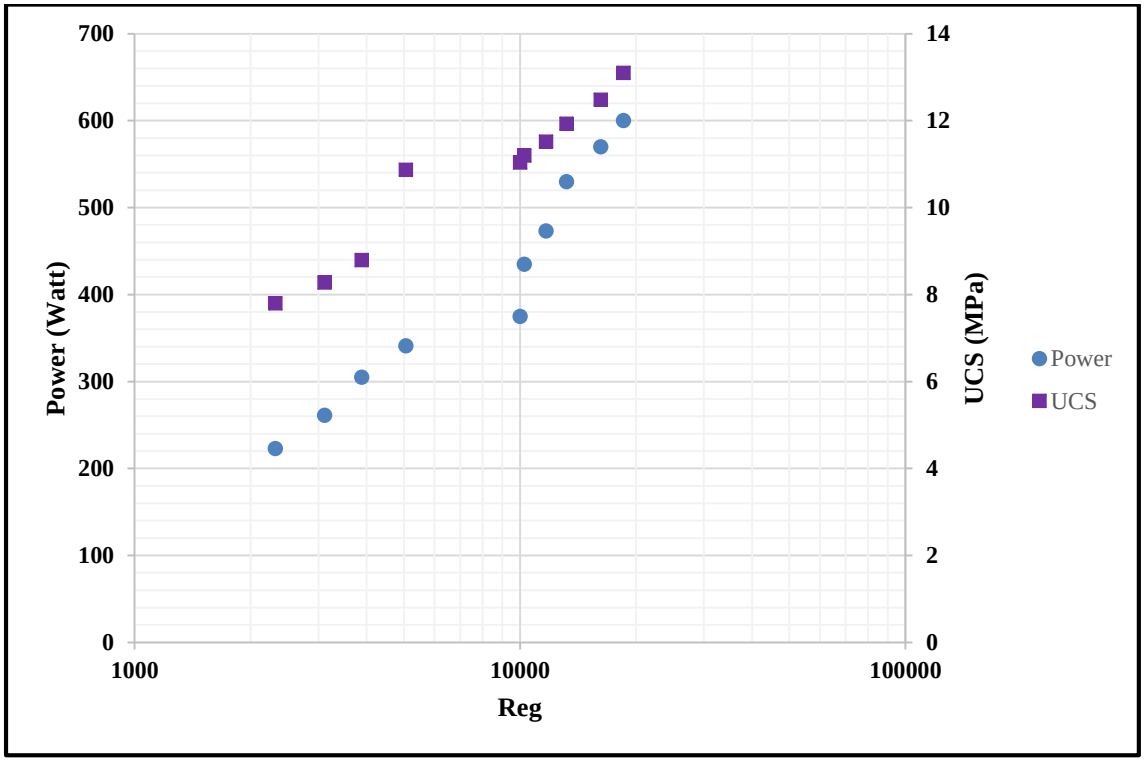

Figure 9.11 UCS and power measurements versus generalized Reynolds number

Figure 9.12 represents dimensionless power number ($\frac{P}{\rho N^3 D^5}$) developed for neat class H cement. Power number is reversely proportional to the shear rate; therefore, it will decrease by increase in shear rate as discussed earlier in the literature (Figure 9.1). As mentioned earlier, power curve can be very useful in finding power requirement from one system to another. Dimensionless power numbers allow for comparisons between very different systems. Another advantage from this curve is to extrapolate data points for very small or large Reynolds number. For instance, if mixing occurs in shear rate at less than 3000 rpm and more than 12000 rpm, data can be extrapolated to predict power numbers.

Following correlations are obtained for power number for laminar and turbulent flow patterns as illustrated in Figure 9.13 and Figure 9.14:

Correlations for laminar region (Re_g less than 10,000):

$$UCS = 0.3127\ \mathrm{Re}_g^{0.4105} \tag{9.16}$$

$$Np = 8\times10^{6}\ \mathrm{Re}_g^{-2.142} \tag{9.17}$$

Correlations for turbulent region (Re_g more than 10,000):

$$UCS = 0.974\ \mathrm{Re}_g^{0.2639} \tag{9.18}$$

$$Np = 2.8\times10^{5}\ \mathrm{Re}_g^{-1.66} \tag{9.19}$$

Combining above correlations, one can develop new relationship between power number and UCS for each region. Figure 9.15 shows the calculated power number and UCS for low (less than 1000) and high (more than 10,000) generalized Reynolds number. Whether these predictions are accurate or not only can be confirmed by more laboratory experiments. For instance, we may expect a different trend in UCS when flow behavior becomes heavily turbulent or heavily laminar. As it stands, this curve can provide a good benchmark for mixing requirements to achieve optimized cement properties. Additionally, more experiments for other cement properties such as cement porosity and thickening time can be included in this chart.

Furthermore, these curves are only generated for neat class H cement. Hence, design in field operations often has different additives in the cement mix such as bentonite, barite, retarders and other additives. Therefore, we expect these correlations change due to changes in kinematic of reactions.

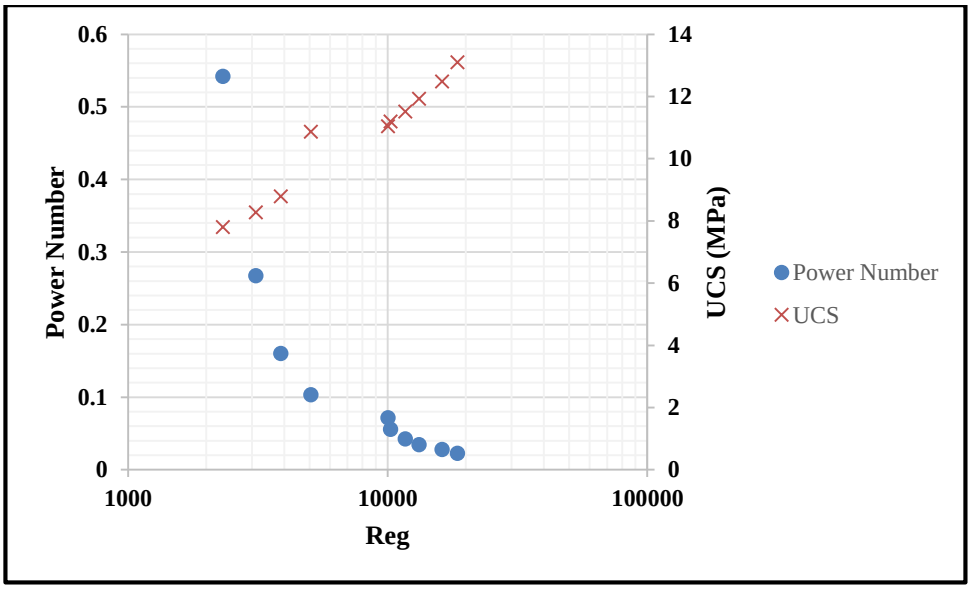

Figure 9.12 Dimensionless power number and UCS for neat class H cement

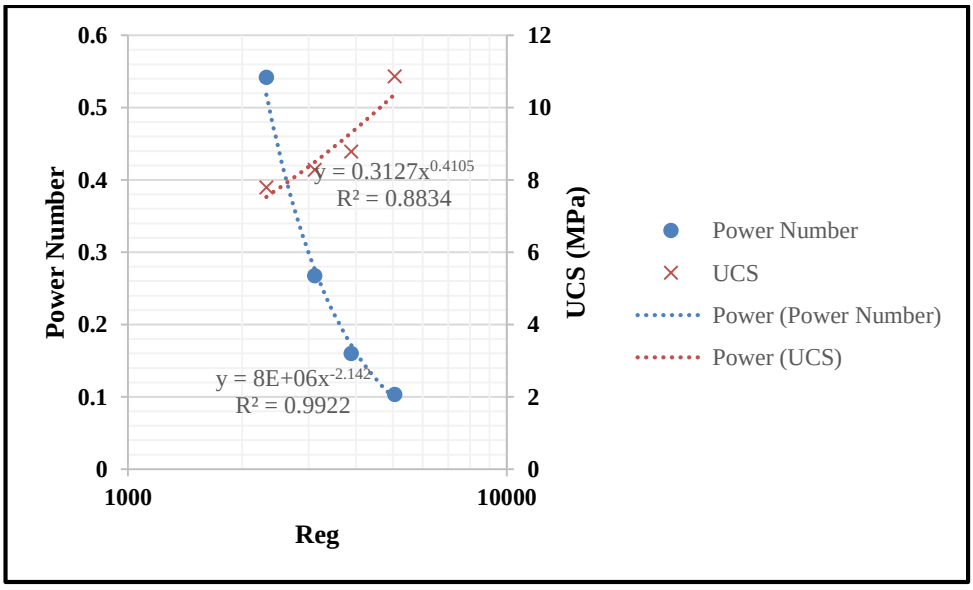

Figure 9.13 Power curve and UCS in the low range of generalized Reynolds number (between 1000 to 10000)

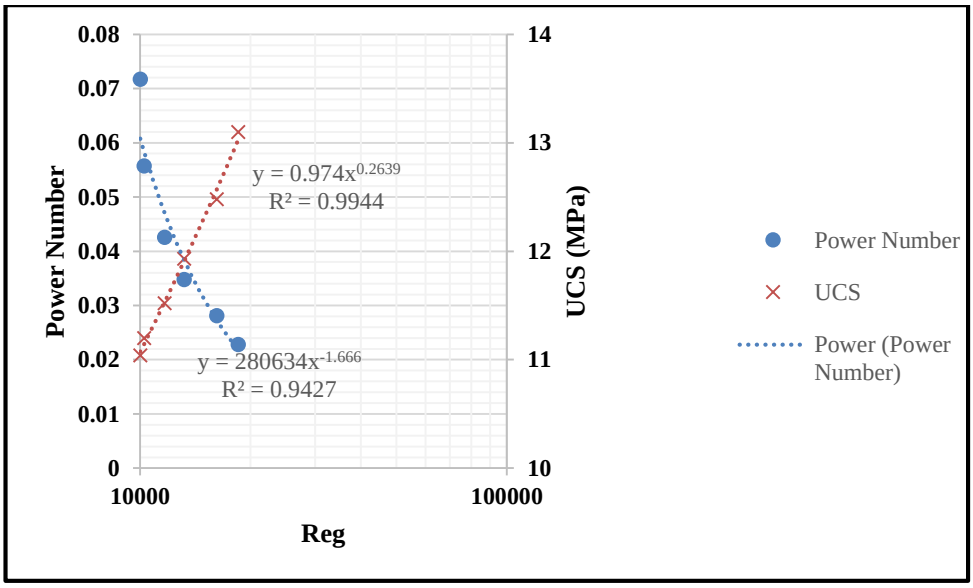

Figure 9.14 Power curve and UCS in the high range of generalized Reynolds number (more than 10,000)

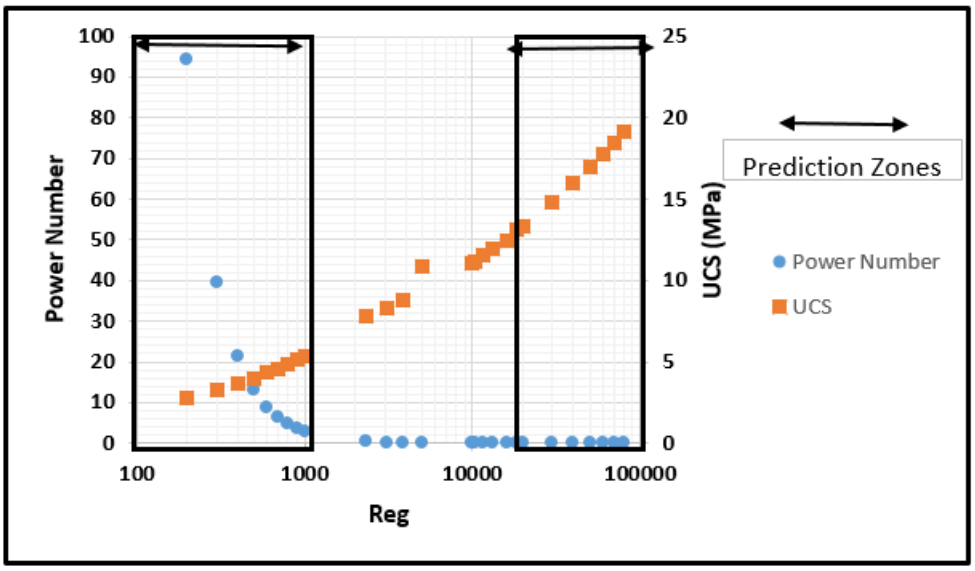

Figure 9.15 Power curve and UCS by including predictions for low and high generalized Reynolds number

9.5 Scale up Procedure

It would be ideal to develop a scale up design procedure that would work reliably for non-Newtonian cement slurries. The prospect of such logic is only likely if one has developed robust relationships for power requirements in laboratory mixing by considering non-Newtonian characteristics. Scale up of mixing in non-Newtonian fluids can be complex because of changes in apparent viscosity by shear rate. This can shift flow regimes into transitional or turbulent from laminar (Wilkens et al., 2003).

The current industry practice for oilwell cements considers conducting laboratory experiments for the same cement recipe that will be applied in field operations. To our knowledge, no scale up procedure is provided in the oil and gas cementing literature. Therefore, we intend to provide a procedure based on the findings from this study. According to the literature summarized for several scale up procedures (Table 9.1), the recommended methods for scale up are power over mixing volume (P/V) and torque over mixing volume (T/V). Since the method outlined in this dissertation is based on power of mixing, the scale up procedure can be power base.

Following steps can be recommended for two scales:

Scale 1-Laboratory:

1. Identify the required volume for mixing.
2. Prepare and mix slurry based on different mixing conditions at given shear rate and mixing time.
3. Measure and record powers while mixing.
4. Measure rheological properties (x, y and z) for each mixing condition.
5. Calculate apparent viscosities and generalized Reynolds number based on Step 4.

6. Repeat Step 2 and prepare samples for UCS (this step can be repeated for measuring other cement properties such as porosity, thickening time, etc.).
7. Calculate ratio of power over mixed volume based on Step 1 and 3.
8. Plot power and UCS versus generalized Reynolds number obtained in Step 5.
9. Find an acceptable mixing condition based on desirable UCS, and other cement properties.

Scale 2-Field:

Power for field scale mixing will be obtained from power curve available from laboratory measurements. Then by knowing the P/V ratio, desirable volume can be calculated for field mixing. The scale up procedure presented here requires verification before it can be applied practically. Furthermore, scale up can be done more conveniently if power curves for desired cement systems are available. For instance, the curve presented in the Figure 9.17 can be used for scaling up in field conditions (only for class H cement).

Chapter 10: Summary, Conclusions and Recommendations

10.1 Summary

10.1.1 UCS Comparison at 5.9 E/M for All Mixing Conditions

Here, we summarize major results from the experiments conducted in this study. For UCS, we can combine all the strength measurements for 5.9 E/M in the Figure 10.1:

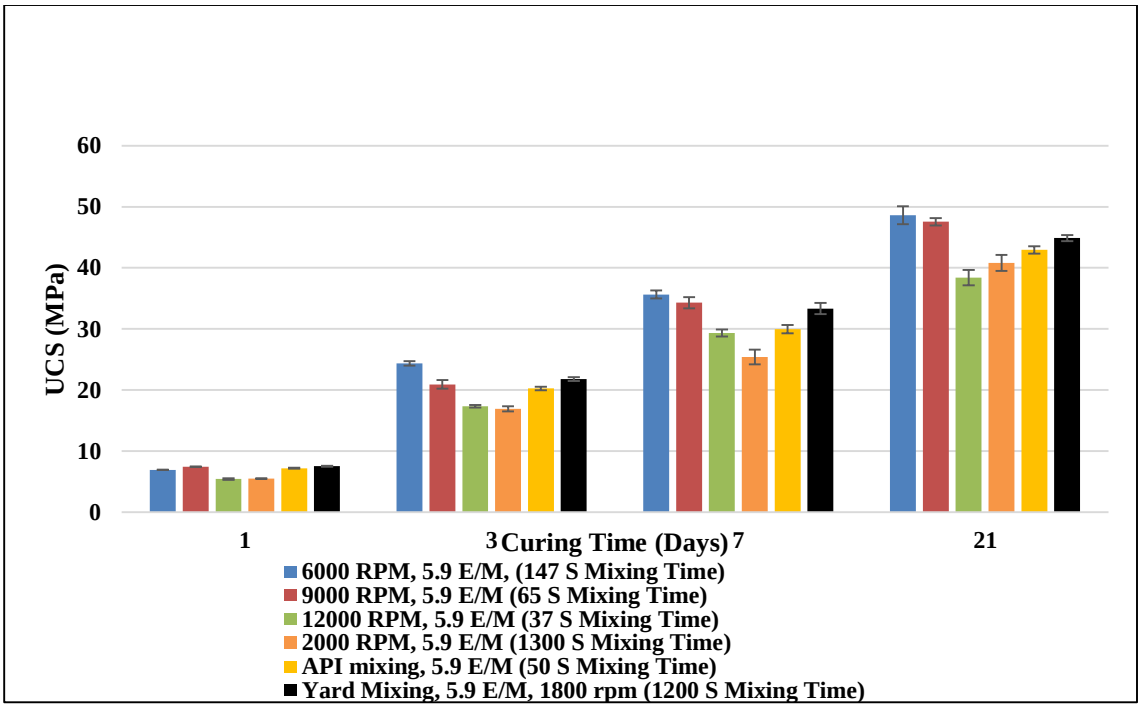

Figure 10.1 UCS for all strength measurements in 5.9 E/M. UCS is highest for specimen prepared at 6000 rpm in the lab condition. Lowest UCS belongs to specimen prepared at 12000 rpm (37 sec mixing time). UCS for yard mixing at 1800 rpm and lab mixing at 2000 rpm are comparable.

Results imply that matching UCS is not observed when mixing energy is kept constant. In addition, results show dual impact of shear rate and mixing time, longer mixing time do not necessarily result in higher strength (i.e. mixing at 2000 rpm and 1300 seconds mixing time). Additionally, higher shear rate does not necessarily result in higher strength (i.e. mixing at 12000 rpm and 37 seconds). An optimum condition for mixing can improve

its strength (i.e. mixing at 6000 rpm and 147 seconds mixing time). UCS for specimen prepared at 6000 rpm and 9000 rpm are very similar. Furthermore, UCS for yard mixing at 1800 rpm and lab mixing at 2000 rpm are very similiar. This can be explained because of similar shear rate and mixing time in both systems.

Earlier in Chapter 5, we also compared UCS versus mixing time in Figure 5.10. We showed that UCS and mixing time have a linear relationship up to a critical mixing time.

10.1.2 UCS-Porosity Correlation

We observed that as cement curing day increases, its porosity decreases. In a different trend, cement UCS increases with curing days as shown in the Figure 10.2. All the UCS are shown by the dashed lines. As discussed earlier, lowest porosity is related to the slurry that is mixed at 11.8 E/M and 6000 rpm. Here we show a correlation for UCS and hydration time (T) for specimen prepared based on API procedure as:

$$UCS = 8.63T^{0.5781} \quad \text{.....(10.1)}$$

Similar correlations can be obtained for other mixing procedures. In addition, by combining these correlations, one can find a correlation between porosity and UCS for neat class H cement.

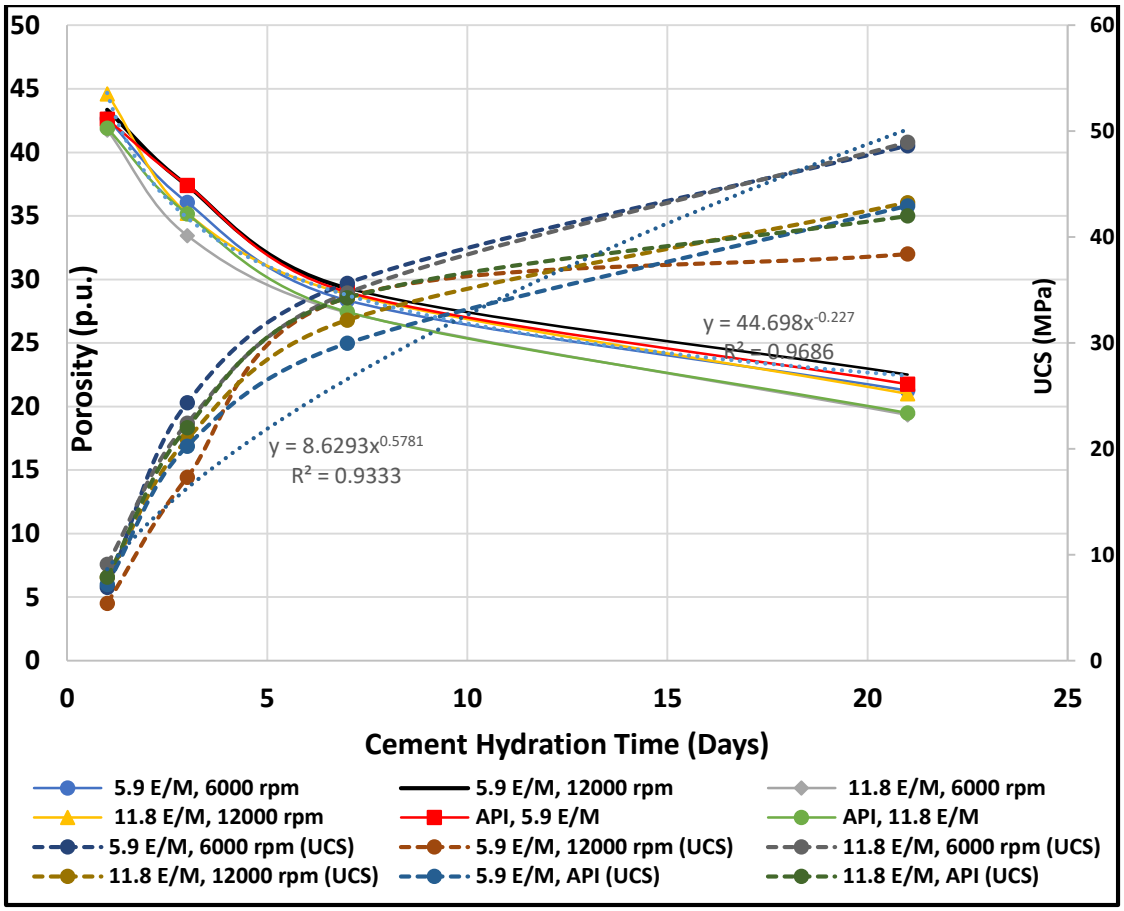

Figure 10.2 UCS-Porosity versus cement hydration time

10.1.3 Plastic viscosity, UCS and Thickening Time Correlation with Mixing Time

Plastic viscosity (PV) and thickening time correlate very well. When PV increases, thickening time decreases. We have summarized comparison between PV, UCS and thickening time for all the laboratory tests conditions versus mixing time in Figure 10.3. Numbers shown on the plot give additional mixing information such as shear rate and mixing energy.

In general PV has decreasing trend with mixing time. Additionally, UCS correlates well with PV, and thickening time. When PV decreases, UCS increases. Good mixing conditions yields smaller particles (better deflocculation) causing more strength development.

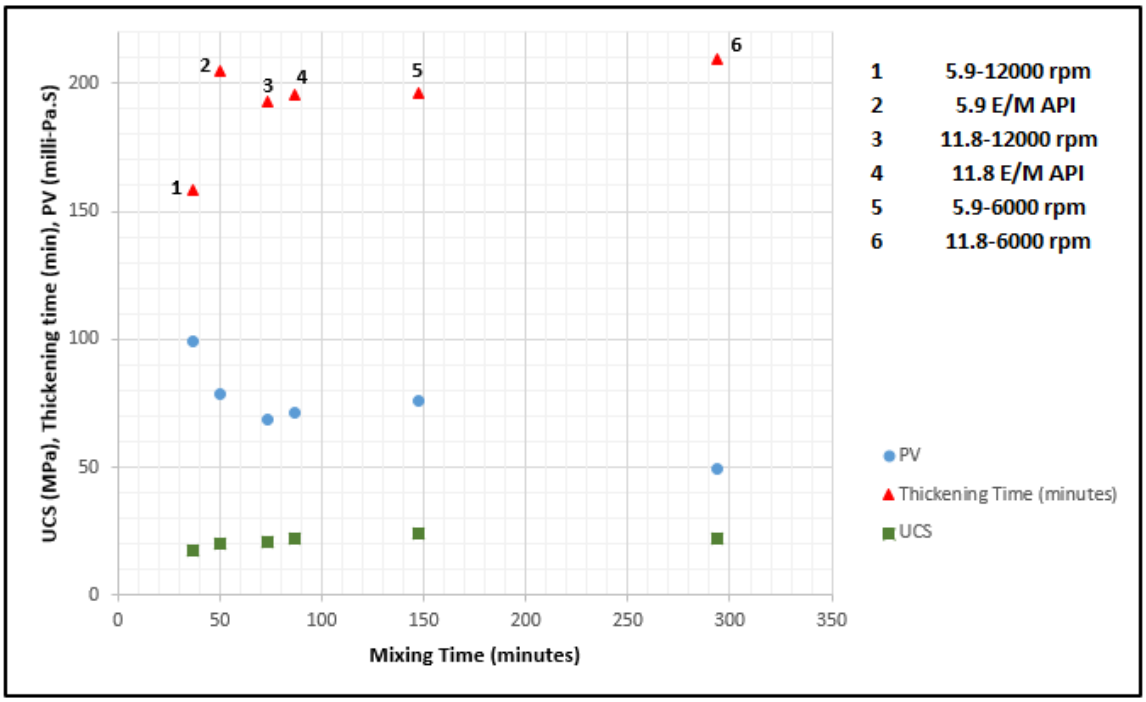

Figure 10.3 PV, UCS and thickening time versus mixing time. PV has decreasing trend with mixing time. Additionally, UCS correlates well with PV, and thickening time

10.2 Conclusions

The following are the major findings in this research:

1. Slurries of equal mixing energies do not show similar properties. Our results imply that the theory of mixing energy proposed by API is a poor concept to be used for achieving identical cement properties. Cement properties are impacted by other mixing variables in addition to mixing energy such as shear rate and mixing time. Our findings indicate that consideration of both shear rate and mixing time are important and these variables may have different impacts on mechanical (deflocculation) and chemical (hydration) processes.
2. Mixing energy is tightly coupled with shear rate and mixing time. Our data analysis based on ANOVA shows interaction effects between mixing energy and shear rate in some instances (1 and 3 days curing time).
3. Change in mixing procedure such as two steps API mixing procedure may result in different cement properties.
4. Our result shows that UCS has increasing trend with lab mixing time (up to 65 seconds). This can be considered as an initial critical mixing time. Beyond this time, there is only slight improvement in UCS. Furthermore, a very long mixing time (beyond 222 seconds) does not improve UCS.
5. In general, UPV followed similar pattern as UCS. However, it showed less sensitivity compared to UCS. Maximum difference in UPV for different mixing conditions was 11% in first day of curing.
6. When comparing UCS and rheology from laboratory to yard mixing, similar properties were not observed by keeping same mixing energy. Quantifying the

mixing energy alone does not provide a robust basis to measure cement performance in the laboratory and the yard. In addition, UCS from yard mixing is in good agreement with UCS from mixing at low shear rate (2000 rpm) in the lab.

7. Increase in shear rate, when mixing time is kept constant; causes shear thinning behavior in rheology and an increase in UCS.
8. Cement porosity measurements through NMR correlate very well with UCS measurements. Slurries prepared with longer mixing time show higher UCS and lower porosity.
9. Rheology tests show an increase in both plastic viscosity (PV) and yield point (YP) with increase in shear rate. When comparing rheology results from lower mixing energy (5.9 KJ/Kg) to higher mixing energy (11.8 KJ/Kg), plastic viscosity decreases; however, yield point increases. This implies dual an opposite effect mixing time on PV and YP.
10. Results from rheology measurements correlate well with thickening time. Slurries prepared at lower shear rate show longer thickening time. When comparing thickening time from lower mixing energy (5.9 KJ/Kg) to higher mixing energy (11.8 KJ/Kg) at each specific shear rate, thickening time increases.
11. A correlation between porosity and hydration time based on the NMR measurements was developed which is in good agreement with available experimental work in the literature.

12. Specimen prepared under the shortest mixing time (37 seconds) in the lab have lowest UCS, highest porosity, highest plastic viscosity, and shortest thickening time.
13. For the first time in oilwell cement literature, a mixing power consumption model based on non-Newtonian characteristics was developed. This model takes into account effects of shear rate and non-Newtonian rheological properties. Furthermore, comparison of power consumption data and UCS implies a range of critical shear rate between 5000 rpm and 7000 rpm.
14. A power curve was developed for neat class H cement. UCS measurements were added to the power curve which may provide a benchmark for comparing power consumption with cement strength.
15. A scale up procedure to compare results from laboratory to field mixing was presented based on ratio of mixing power consumption to slurry volume. This new procedure may be applied to get matching properties in different systems.

10.3 Recommendations

1. As previously noted, when cement mixed with water, both physical process (deflocculation) and chemical process (hydration) impact cement properties. Thus, future studies need to investigate these two processes in more detail. For instance, we recommend study of hydration kinetics using calorimeter and other tests such as SEM (Scan Electron Microscopy) and EDS (Energy Dispersive Spectroscopy).
2. Results presented in this study are based on experiments that were conducted over 21 days curing time. We recommend more experimental studies over long duration to understand effect of mixing condition for impacts on long term well integrity.
3. We only performed limited yard tests in this study, we recommended more yard tests under various conditions (very low rpm) and changing in mixing time. These tests will provide more insights for mixing conditions in the field operations. Additionally, we recommend thickening time tests for yard mixed slurries.
4. The mixing power correlation and power curve presented in this study are based on neat class H cement; however, in field operations often cement with a class of different additives are used. Therefore, we recommend development of similar models for cement with additives. Furthermore, we only reported UCS and rheology measurements for comparison with power consumption. We recommend addition of other tests such as thickening time, porosity and fluid loss.

5. The scale up procedure presented in his study needs further verification before it can be applied.
6. The majority of experiments in this study are based on mixing at 2000 rpm shear rate and higher. Therefore, we recommend experiments at low shear rate (less than 2000 rpm) and different mixing procedures.

Nomenclature

API	–	American Petroleum Institute
ASTM	–	American Society for Testing and Materials
ANOVA	–	Analysis of Variance
Bc	–	Bearden units of consistency
BSEE	–	Bureau of Safety and Environmental Enforcement
BWOC	–	By weight of cement
BWOW	–	By weight of water
CPMG	–	Carr-Purcell-Meiboom-Gill
$CaCO_3$	–	Calcium carbonate
C_3A	–	Tricalcium aluminate
C_3S	–	Tricalcium silicate
C_2S	–	Dicalcium silicate
CSH	–	Calcium silicate hydrate, 3CaO.2SiO2.3H2O
DoE	–	Design of Experiments
°F	–	Degree Fahrenheit
hrs.	–	hours
HPHT	–	High pressure high temperature
in	–	inch
ITZ	–	Interfacial-transition zone
lbm	–	pound mass
lbf	–	pound force
min	–	minute
ml	–	millilitre
NMR	–	Nuclear Magnetic Resonance spectroscopy
ppg	–	pounds per gallon
psi	–	pounds per square inch
PV	–	Plastic Viscosity
rpm	–	Revolutions per minute
SEM	–	Scanning Electron Microscopy
UCS	–	Unconfined Compressive Strength
UPV	–	Unconfined Pulse Velocity
YP	–	Yield Point
WOC	–	Wait on cement
W/C	–	Water Cement Ratio
τ	–	Shear Stress
γ	–	Shear Rate
ω	–	Mixing Shear Rate
μ_a	–	Apparent Viscosity

ρ	–	Density
V	–	Volume
L	–	Length of small eddy
P	–	Mixing power
N	–	Speed of rotation
N_P	–	Power number
R_e	–	Reynolds number
Re_g	–	Generalized Reynolds number
t	–	Mixing time
T_2	–	NMR T_2 Relaxation Time
K	–	Power law consistency Index
n	–	Power low flow behaviour index
E/M	–	Mixing Energy per unit mass

References

1. Ahmed, R., Shah, S., Osisanya, S., Hassani, S., Omosebi, O., Elgaddafi, R., Maheshwari, H., Srivastava, A., Hwang, J., Sharma, M., Tale, S., Jeon, J. 2015. Effect of H_2S and CO_2 in HPHT wells on tubulars and cement. Final report to BSEE, June 2015.

2. Allen, J.J. Thomas, H.M. Jennings. 2007. Composition and density of nanoscale calcium–silicate–hydrate in cement, Nat. Mater. 6 (2007) 311–316

3. Anand, V., Ali, M.R., Al-Adani, N., Willis, D., Freedman, R., Hamichi, F., Abubakar, A., Grover, R., Neto, O., Aboud, M. and Iglesias, J.G. 2015. New generation NMR tool for robust, continuous T1 and T2 measurements. In SPWLA 56th Annual Logging Symposium. Society of Petrophysicists and Well-Log Analysts.

4. API. 10B2, 2013, Recommended practice for testing well cements, second edition.

5. Awoleke, O.O., Romero, J.D., Zhu, D. and HIll, D. 2012. Experimental investigation of propped fracture conductivity in tight gas reservoirs using factorial design. In SPE Hydraulic Fracturing Technology Conference. Society of Petroleum Engineers.

6. Baret, J.F. 1988. Why cement fluid loss additives are necessary. In International Meeting on Petroleum Engineering. Society of Petroleum Engineers.

7. Barret, P., Ménétrier, D., and Bertrandie, D. 1983. Mechanism of C3S dissolution and problem of the congruency in the very initial period and later on, Cem. Concr. Res. 13, 728 – 738.

8. Bendel, P., 1990, Spin-Echo attenuation by diffusion in non-uniform field gradients, Journal of Magnetic Resonance, vol. 86, p. 509-515.

9. Blinc, M. Burgar, G. Lahajnar, M. Rozmarin, V. Rutar, I. Kocuvan. 1978. NMR relaxation study of adsorbed water in cement and C_3S pastes, J. Am. Ceram. Soc 61 (1978) 35–37.

10. Box, G. E. P. and Draper, N. R. 2007. Response Surfaces, Mixtures, and Ridge Analyses, 2nd edition. Wiley, New York.

11. Bu, T. and Damsleth, E.1996. Errors and Uncertainties in Reservoir Performance Prediction, SPEFE (September 1996) 194.

12. Calderbank, P. H., and Moo-Young, M. 1959. The prediction of power consumption in the agitation of non-Newtonian fluids." Trans. Inst. Chem. Eng 37.3 (1959): 26-33.

13. Coulson, J.M., Richardson, J.F., Backhurst, J.R. and Harker, J.H., 1999. Fluid flow, heat transfer and mass transfer. Butterworth-Heinemann.

14. Cowan, M. 2007. Field Study Results Improve Squeeze Cementing Success. Society of Petroleum Engineers. doi:10.2118/106765-MS.

15. Chhabra, R.P. and Richardson, J.F., 2011. Non-Newtonian flow and applied rheology: engineering applications. Butterworth-Heinemann.

16. Crespí-Llorens, D., Vicente, P. and Viedma, A., 2015. Generalized Reynolds number and viscosity definitions for non-Newtonian fluid flow in ducts of non-uniform cross-section. Experimental Thermal and Fluid Science, 64, pp.125-133.

17. Coussot, P. 2012. Introduction to the Rheology of Complex Fluids. Understanding the Rheology of Concrete, edited by N. Roussel, 2012 Woodhead Publishing Limited.

18. Cowan, B., 2005. Nuclear magnetic resonance and relaxation. Cambridge University Press.

19. Coates, G., Xiao, L., and Prammer, M. 1999. NMR Logging: Principles and Applications. Houston: Gulf Publishing Company.

20. Chu, C.F. 1990. Prediction of Steamflood Performance in Heavy Oil Reservoirs Using Correlations Developed by Factorial Design Method, paper SPE 20020 presented at the 1990 California Regional Meeting, Ventura, California.

21. Celia, M. A., S. Bachu, J. M. Nordbotten, S. Gasda, H. K. Dahle, 2004. Quantitative estimation of CO2 leakage from geological storage: Analytical models, numerical models, and data needs, In, E.S.Rubin, D.W.Keith and C.F.Gilboy (Eds.), Proceedings of 7th International Conference on Greenhouse Gas Control Technologies. Volume 1: Peer-Reviewed Papers and Plenary. Presentations, IEA Greenhouse Gas Programme, Cheltenham, UK.

22. Damsleth, E., Hage, A. and Volden, R. 1992. Maximum Information at Minimum Cost: A North Sea Field Development Study with Experimental Design," JPT (December 1992) 1350.

23. De Larrard, F., Ferraris, C.F. and Sedran, T., 1998. Fresh concrete: a Herschel-Bulkley material. Materials and structures, 31(7), pp.494-498.

24. Duan, S., and Wojtanowicz, A. K. 2005. A method for evaluation of risk of continuous air emissions from sustained casinghead pressure. Society of Petroleum Engineers. doi:10.2118/94455-STU.

25. Dunn, K.J., Bergman, D.J. and LaTorraca, G.A. 2002. Nuclear magnetic resonance: Petrophysical and logging applications (Vol. 32). Elsevier.

26. Elgaddafi, R., Ahmed, R. and Shah, S., 2017. Modeling and experimental studies on CO_2-H_2S corrosion of API carbon steels under high-pressure. Journal of Petroleum Science and Engineering, 156, pp.682-696.

27. ExproSoft, 2017. Loss of well control occurrence and size estimators. Final Report to BSEE, report no. ES201471/1.

28. Fink, J. 2015. Petroleum Engineer's Guide to Oil Field Chemicals and Fluids. 2nd. Elsevier.

29. Fisher, R.A., 1937. The design of experiments. Oliver and Boyd; Edinburgh; London.

30. Foresti, R., and Liu, T. 1959. Ind. Eng. Chem., 51, 860-4.

31. Foucault, S., Ascanio, G. and Tanguy, P.A., 2005. Power characteristics in coaxial mixing: Newtonian and non-Newtonian fluids. Industrial & engineering chemistry research, 44(14), pp.5036-5043.

32. Gauffine-Garrault, S. 2012. The rheology of cement during setting, Woodhead Publishing Limited, 2012.

33. Glen, B., 2011. Expert Report. “Deepwater Horizon” in the Gulf of Mexico, on April 20, 2010. Evaluation of the cementing on the 9 7/8 x 7” production string on the Macondo well.

34. Greaves, M., Dudley, J.W.O. and Field, R.W. 1989. Factorial experiments in in situ combustion.

35. Graham, B., Reilly, W., Beinecke, F., and Boesch, D. 2011. Report to the President. Deep Water: The Gulf Oil Disaster and the Future of Offshore Drilling. National Commission on the BP Deepwater Horizon Oil Spill and Offshore Drilling.

36. Gutteridge, Walter A., and John A. Dalziel. 1990. Filler Cement: The Effect of Secondary Component on the Hydration of Portland Cement. Cement and Concrete Research (Pergamon Press plc.) 20: 778-772. doi:10.1016/0008-8846(90)90011-L.

37. Gibson, S., A. 2011. Novel solution to cement strength retrogression. SPE/IADC Drilling Conference and Exhibition. Society of Petroleum Engineers, 2011.

38. Han, D. and Ferron, R. 2015. Effect of mixing method on microstructure and rheology of cement paste, Construction and Building Materials (Impact Factor: 2.3). 09/2015; 93. DOI: 10.1016/j.conbuildmat.2015.05.124.

39. Heathman, J.F., Sands, F.L., Sas-Jaworsky, A. and Badalamenti, A.M. 1993. A study of the effects of mixing energy imparted on cement slurries by field equipment and coiled tubing. In SPE Annual Technical Conference and Exhibition. Society of Petroleum Engineers.

40. Hibbert, A. P., Kellingray, D. J., and Vidick, B. 1995. Effect of mixing energy levels during batch mixing of cement slurries. SPE Drilling & Completion, 10(01), 49-52.

41. Hirasaki, G.J., Lo, S.W. and Zhang, Y., 2003. NMR properties of petroleum reservoir fluids. Magnetic resonance imaging, 21(3), pp.269-277.

42. Hodne, H., Saasen, A., O'Hagan, A. B., and Wick, S. O. 2000. Effects of time and shear energy on the rheological behavior of oilwell cement slurries. Cement and concrete research, 30(11), 1759-1766.

43. Ibeh, C.S., 2007. Investigation on the effects of ultra-high pressure and temperature on the rheological properties of oil-based drilling fluids (Doctoral dissertation, Texas A&M University).

44. Ichim, A.C., 2017. Experimental determination of oilfield cement properties and their influence on well integrity.

45. Jaynes, J.L., 2013. Contributions in design of experiments: Methods and applications (Doctoral dissertation, University of California Los Angeles).

46. Kleinberg, R.L., Straley C., Kenyon W.E., Akkurt, R., and Farooqui, S.A. 1993. Nuclear magnetic resonance of rocks: T1 vs. T2. Presented at the 68th Annual Technical Conference and Exchibibtion of SPE, Houston, Texas, 3-6 October.

47. Kenyon, W.E. 1992. Nuclear magnetic resonance as a petrophysical measurement. Nuclear Geophys, pp. 153 - 171.

48. Lake, L.W. and Mitchell, R.F. 2006. Petroleum engineering handbook. Vol. 2. Drilling engineering. SPE.

49. Lazic, Z.R., 2006. Design of experiments in chemical engineering: a practical guide. John Wiley & Sons.

50. Lee, R. E., Finch, C. R., and Wooledge, J. D. 1957. Mixing of high viscosity Newtonian and non-Newtonian fluids. Industrial & Engineering Chemistry,49(11), 1849-1854.

51. Lerch, J.O., Bester, H.L., Van Rooyen, A.S., Combrinck, R., de Villiers, W.I. and Boshoff, W.P., 2018. The effect of mixing on the performance of macro synthetic fibre reinforced concrete. Cement and Concrete Research, 103, pp.130-139.

52. Masiuk, S., Rakoczy, R., and Kordas, M. 2008. Comparison density of maximal energy for mixing process using the same agitator in rotational and reciprocating movements. Chemical Engineering and Processing: Process Intensification, 47(8), 1252-1260.

53. Masiuk, S., and Łącki, H. 1993. Power consumption and mixing time for Newtonian and non-Newtonian liquids mixing in a ribbon mixer. The Chemical Engineering Journal, 52(1), 13-17.

54. Milestone, N. and Aldridge, L., 1990. Corrosion of cement grouts in aggressive geothermal fluids. Geothermal Resources Council Transactions, 14, pp.423-429.

55. Metzner, A.B. and Otto, R.E. 1957. Agitation of non-Newtonian fluids. AIChE Journal, 3(1), pp.3-10.

56. Metzner, A.B., Feehs, R.H., Ramos, H.L., Otto, R.E. and Tuthill, J.D., 1961. Agitation of viscous Newtonian and non-Newtonian fluids. AIChE Journal, 7(1), pp.3-9.

57. Muller, A.C., Scrivener, K.L., Gajewicz, A.M. and McDonald, P.J. 2012. Densification of C–S–H measured by 1H NMR relaxometry. The Journal of Physical Chemistry C, 117(1), pp.403-412.

58. Myers, R.H. and Montgomery, D.C. 1995. Response surface methodology: process and product optimization using designed experiments, Wiley, New York City (1995) 700.

59. Nelson, E., and Guillot, D. 2006. Oilwell Cementing, Second edition, Schlumberger publications.

60. Nehdi, M., and Rahman, M.A. 2004. Estimating rheological properties of cement pastes using various rheological models for different test geometry, gap and surface friction. Cement and Concrete Research 34 (11): 1993-2007. http://dx.doi.org/10.1016/j.cemconres.2004.02.020.

61. Nonat, A. and Mutin, J.-C. 1992. From hydration to setting. In Hydration and Setting of

62. Cements, proceedings of the international RILEM workshop.

63. Nienow, A. W., Edwards, M. F., and Harnby, N.1997. Mixing in the process industries. Butterworth-Heinemann, 1997.

64. Nienow, A.W., 1988. Aspects of mixing in rheologically complex fluids. Chem. Eng. Res. Des., pp.5-15.

65. Nygaard, R., Salehi, S., and Lavoie, R. 2011. Effect of dynamic loading on wellbore leakage for the Wabamun area CO2 sequestration project, SPE Annual Technical Conference and Exhibition, Canadian Unconventional Resources Conference (11CURC), 15 - 17 Nov 2011, 2011.

66. Omosebi, O., Maheshwari, H., Ahmed, R., Shah, S. and Osisanya, S., 2017. Experimental study of the effects of CO2 concentration and pressure at elevated temperature on the mechanical integrity of oil and gas well cement. Journal of Natural Gas Science and Engineering, 44, pp.299-313.

67. Okumo, I. and Isehunwa, S.O. 2007. January. Prediction of the viscosity of a water-base mud treated with cassava starch and potash at varying temperatures using factorial design. In Nigeria Annual International Conference and Exhibition. Society of Petroleum Engineers.

68. Orban, J. A., Parcevaux, P. A., and Guillot, D. J. 1986. Specific mixing energy: a key factor for cement slurry quality. In SPE Annual Technical Conference and Exhibition. Society of Petroleum Engineers.

69. Petroleum Services Association of Canada (PSAC), 2015. Well Cost Study. PSAC Canada.

70. Padgett, P. Shear rate has greater influence on cement slurry properties than total mixing energy. Oil Gas J 94(41):84–90.

71. Rocha-Valdez, T., Hasan, A.R and Mannan, S. 2014. Assessing Wellbore integrity in Sustained-casing-Pressure Annulus. SPE 169814. SPE Drilling and Completion Journal, V29, 131-138.

72. Ravi, K., Biezen, E. N., Lightford, S. C., Hibbert, A., and Greaves, C. 1999. Deepwater Cementing Challenges. Society of Petroleum Engineers. doi:10.2118/56534-MS.

73. Rusch, D. W., Sabins, F., and Aslakson, J. 2004. Microannulus Leaks Repaired with Pressure-Activated Sealant. Society of Petroleum Engineers. doi:10.2118/91399-MS.

74. Scrivener, K.L. and Nonat, A., 2011. Hydration of cementitious materials, present and future. Cement and concrete research, 41(7), pp.651-665.

75. Sabins, F. L. 1990. Problems in Cementing Horizontal Wells. Society of Petroleum Engineers. doi:10.2118/20005-PA.

76. Saleh, F.K. and Teodoriu, C., 2017. The mechanism of mixing and mixing energy for oil and gas wells cement slurries: A literature review and benchmarking of the findings. Journal of Natural Gas Science and Engineering, 38, pp.388-401.

77. Saleh, F., Rivera, R. Salehi, S. and Teodoriu, C. 2018. How does mixing water quality affect cement properties. SPE International Conference & Exhibition on Formation Damage Control. SPE-189505. Lafayette, Louisiana, February 7-9, 2018.

78. Salehi, S., Khattak, M.J., Rizvi, H., Karbalaei, S.F. and Kiran, R., 2017. Sensitivity analysis of fly ash geopolymer cement slurries: Implications for oil and gas wells cementing applications. Journal of Natural Gas Science and Engineering, 37, pp.116-125.

79. Sweatman, R. 2000. Overview: Cementing Technology (August 2000). Society of Petroleum Engineers. doi:10.2118/0800-0022-JPT.

80. Stiles, D., and Hollies, D. 2002. Implementation of Advanced Cementing Techniques to Improve Long Term Zonal Isolation in Steam Assisted Gravity Drainage Wells. Society of Petroleum Engineers. doi:10.2118/78950-MS.

81. Shahriar, A. 2011. Investigation on rheology of oil well cement slurries. Diss. 2011. The University of Western Ontario, 2011.

82. Shen, J. and Pye, D., 1989. Effects of CO2 attack on cement in high-temperature applications, SPE/IADC 18618. In SPE/IADC Drilling Conference, New Orleans, LA, February.

83. Shahriar, A., and Nehdi, M.L. 2012. Optimization of rheological properties of oil well cement slurries using experimental design. Materials and Structures 45 (9): 1403-1423. doi:10.1617/s11527-012-9841-2.

84. Skelland, A. H. P. (1967). Non-Newtonian flow and heat transfer. Wiley.

85. Sweatman, R. 2015. Well Cementing Operations, IADC Publications.

86. Schreiner, J.C., Mactavish, L., Miljkovic, M.M., Pintar, R., Blinc, G., Lahajnar. 1985. NMR line shape-spin-lattice relaxation correlation study of Portland cement hydration, J. Am. Ceram. Soc. 68 (1985) 10–16

87. Timur, A. 1969. Pulsed nuclear magnetic resonance studies of porosity, movable fluid, and permeability of sandstones. Journal of Petroleum Technology. 21, 775-786 (1969).

88. Takahashi, K., Bier, T. A., & Westphal, T. 2011. Effects of mixing energy on technological properties and hydration kinetics of grouting mortars. Cement and Concrete Research, 41(11), 1167-1176.

89. Teodoriu, C., Ugwu, I. O., and Schubert, J. J. 2010. Estimation of Casing-Cement-Formation Interaction using a new analythical model. In SPE EUROPEC/EAGE Annual Conference and Exhibition. Society of Petroleum Engineers.

90. Teodoriu, C., Okolieocha, P. A., and Falcone, G. 2015. A theoretical comparison of cement slurry mixing energy in field and laboratory conditions. Environmental Earth Sciences, 73(11), 7043-7051.

91. Teodoriu, C., Kosinowski, C., Amani, M., Schubert, J., and Shadravan, A. 2013. Wellbore integrity and cement failure at HPHT conditions. International Journal of Engineering, 2(2), 2305-8269.

92. Valori, A., McDonald, P.J. and Scrivener, K.L. 2013. The morphology of C–S–H: Lessons from 1 H nuclear magnetic resonance relaxometry. Cement and Concrete Research, 49, pp.65-81.

93. Vidick, B., Nash, F. D., and Hartley, I. 1990. Cementing through coiled tubing and its influence on slurry properties. In European Petroleum Conference. Society of Petroleum Engineers.

94. Vidick, B. 1989. Critical mixing parameters for good control of cement slurry quality. In SPE Production Operations Symposium. Society of Petroleum Engineers.

95. Vorkinn, P. B., and Sanders, G. S. 1993. Cement slurry qualification, field mixing, and quality assurance procedures for coiled-tubing squeeze operations in Prudhoe Bay, Alaska. In SPE Western Regional Meeting. Society of Petroleum Engineers.

96. USEPA (US Environmental Protection Agency). 2011. Plan to Study the Potential Impacts of Hydraulic Fracturing on Drinking Water Resources. Office of Research and Development, US Environmental Protection Agency, November 2011, Washington.

97. Watson, T.L. and Bachu, S. 2009. Evaluation of the Potential for Gas and CO_2 Leakage Along Wellbores. SPE Drill & Compl 24 (1): 115–126. SPE-106817-PA. http://dx.doi.org/10.2118/106817-PA.

98. Wilkens, R.J., Henry, C. and Gates, L.E., 2003. How to scale-up mixing processes in non-Newtonian fluids. Chem Eng Prog, 99(5), pp.44-52.

99. Wu, C.J. and Hamada, M.S., 2011. Experiments: planning, analysis, and optimization (Vol. 552). John Wiley & Sons.

100. Vicente, G., Coteron, A., Martinez, M. and Aracil, J. 1998. Application of the factorial design of experiments and response surface methodology to optimize biodiesel production. Industrial crops and products, 8(1), pp.29-35.

101. White, C.D., Willis, B.J., Narayanan, K. and Dutton, S.P., 2001. Identifying and estimating significant geologic parameters with experimental design. SPE Journal, 6(03), pp.311-324.

Appendix A: API Mixing Energy Formulas

Waring Blender

The Waring blender engine works at imposed rotational speed: the power is automatically adjusted to maintain the required speed. The mechanical power supplied by the engine of the blender to the fluid is (Orban et al., 1986):

$$P = \tau\omega \quad \text{.....(A.1)}$$

where P is mechanical power , τ is the torque (N.M) and ω is the rotational speed (rad/s). The torque is a function of both the imposed speed and the resistance of the fluid (together with the shape of the blades); because the motion is highly turbulent, the fluid resistance is entirely described by its density. Thus the torque can be expressed as:

$$\tau = k\rho\omega \quad \text{.....(A.2)}$$

where k is experimental constant measured experimentally, using normalized blades k is $\approx 6.1\times10^{-8} m^5/s$

After a given duration, the energy transferred to the fluid is:

$$E = k\rho\omega^2 t \quad \text{.....(A.3)}$$

Where E is energy in J, t is mixing time in s.

Expressing the energy per unit mass of fluid (specific energy), we obtain:

$$\frac{E}{M} = \frac{k\omega^2 t}{V} \quad \text{.....(A.4)}$$

where V is mixing bowl volume (m^3)

Appendix B: Reported Experimental Errors

B.1 Sample Size Effects and Errors in UCS and UPV Measurements

As mentioned earlier for each UCS and UPV test, three samples were prepared. All the three samples dimension were measured accurately by digital caliper before testing. Three different points on face of cubes were considered for measurements. API RP 10B-2 recommends the testing of cubes with a 2-inch edge (or 50.8 mm). For the cubes used in this work, most of the cube samples were always within 5% of the API recommendations.

A comparison of UCS for 5.9 E/M based on sample dimension for 1 day and 21 days are shown in the Figures B.1 and B.2. As shown for the reported data in 1 day, the difference in UCS of three samples has less than 2% error. Up to 6% difference in UCS was observed for 21 days. Analysis of data shows that UCS and UPV measurements were conducted consistently and results are credible.

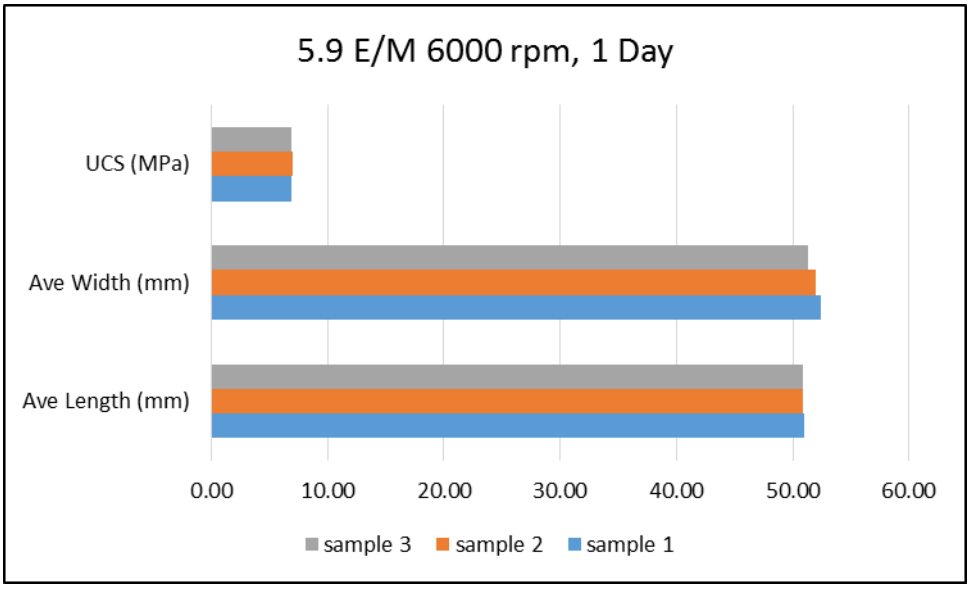

Figure B.1. Measured dimensions and UCS for three samples at 1 Day curing

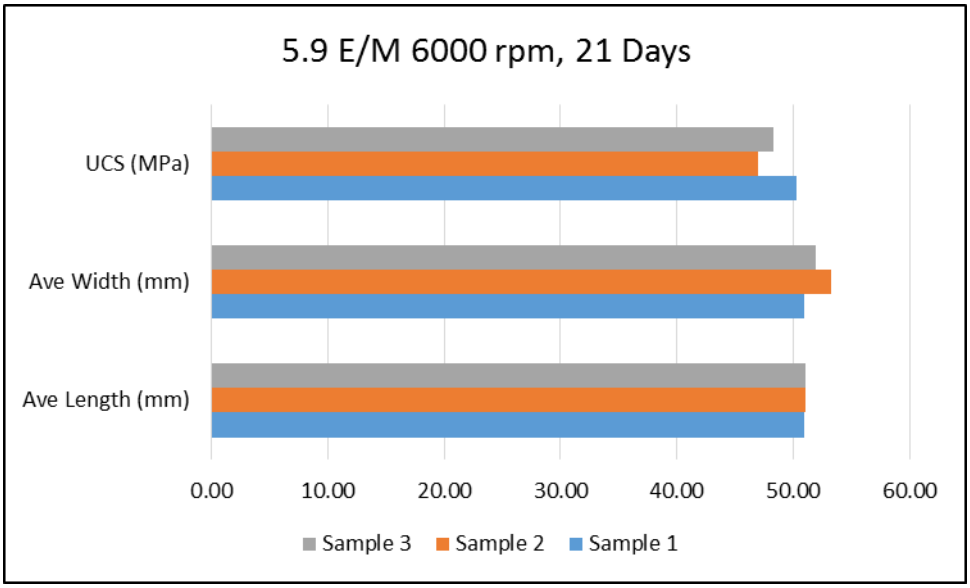

Figure B.2. Measured dimensions and UCS for three samples at 21 Days curing

In order to determine errors in the measurements we conducted 24 UCS tests at one of the mixing conditions (prepared according at 6000 rpm and 11.8 E/M). Table B.1 shows UCS standard error and deviation for 3 days curing.

Table B.1. UCS standard error and deviation

Curing and Mixing Condition	UCS Standard Error	Mean (MPa)	UCS Standard Deviation
3 days, API Mixing Condition	0.31	22	1.52

Here we report all the standard error for UCS and UPV measurements:

UCS

Table B.2. Standard errors for UCS measurements at 5.9 E/M

1 Day	3 Days	7 Days	21 Days	
0.03	0.38	0.66	1.47	Mixed according to 6000 RPM
0.04	0.72	0.91	0.61	Mixed according to 9000 RPM
0.13	0.21	0.59	1.24	Mixed according to 12000 RPM
0.07	0.43	1.20	1.31	Mixed according to API

Table B.3. Standard errors for UCS measurements at 8.9 E/M

1 Day	3 Days	7 Days	21 Days	
0.12	0.18	0.38	0.76	Mixed according to 6000 RPM
0.15	0.16	0.70	1.82	Mixed according to 9000 RPM
0.39	0.69	0.05	1.90	Mixed according to 12000 RPM
0.05	0.24	0.84	0.40	Mixed according to API

Table B.4. Standard errors for UCS measurements at 11.8 E/M

1 Day	3 Days	7 Days	21 Days	
0.13	0.12	0.23	0.78	Mixed according to 6000 RPM
0.06	0.83	0.49	0.13	Mixed according to 9000 RPM
0.02	0.80	1.45	0.28	Mixed according to 12000 RPM
0.09	0.73	0.06	1.70	Mixed according to API

UPV

Table B.5. Standard errors for UPV measurements at 5.9 E/M

1 Day	3 Days	7 Days	21 Days	
0.24	1.11	45.00	38.00	6000 RPM, 5.9(E/M)
16.00	2.40	2.17	2.50	9000 RPM, 5.9(E/M)
2.06	0.92	0.32	3.35	12000 RPM, 5.9(E/M)
15.00	1.00	2.19	0.98	API, 5.9(E/M)

Table B.6. Standard errors for UPV measurements at 8.9 E/M

1 Day	3 Days	7 Days	21 Days	
22.00	1.74	4.50	9.80	6000 RPM, 5.9(E/M)
17.00	0.74	1.96	2.20	9000 RPM, 5.9(E/M)
12.00	1.40	2.60	0.50	12000 RPM, 5.9(E/M)
2.08	0.86	0.81	2.50	API, 5.9(E/M)

Table B.7. Standard errors for UPV measurements at 11.8 E/M

1 Day	3 Days	7 Days	21 Days	
1.98	3.60	30.00	7.20	6000 RPM, 5.9(E/M)
1.00	25.00	41.00	0.40	9000 RPM, 5.9(E/M)
21.00	2.54	31.00	2.60	12000 RPM, 5.9(E/M)
5.00	25.21	0.35	4.20	API, 5.9(E/M)

Plastic Viscosity and Yield Point

Table B.8. Standard errors for Plastic Viscosity (PV) and Yield Point (YP)

	5.9 E/M, 6000rpm	5.9 E/M, 12000rpm	11.8 E/M, 6000rpm	11.8 E/M, 12000rpm
PV stn error	4.24	3.54	3.13	1.68
YP stn error	1.74	1.00	0.78	0.74

Thickening Time

Table B.9. Standard errors for thickening time measurements

5.9 E/M, 6000rpm	5.9 E/M, 12000rpm	11.8 E/M, 6000rpm	11.8 E/M, 12000rpm
2.30	1.01	2.32	3.53

NMR Porosity Measurement

Table B.10. Standard errors for porosity measurements

1 Day	3 Days	7 Days	21 Days	
0.11	0.18	0.18	0.25	6000 RPM, 5.9(E/M)
0.50	0.81	0.85	0.88	12000 RPM, 5.9(E/M)
0.11	0.74	0.28	0.88	6000 RPM, 5.9(E/M)
0.07	0.49	0.11	0.14	12000 RPM, 11.8 (E/M)
0.11	0.32	0.22	0.41	API, 5.9 E/M
0.09	0.25	0.34	0.51	API, 11.8 E/M

Appendix C: Scale Up Relationships in Two Systems

For a system shown as in Figure C.1:

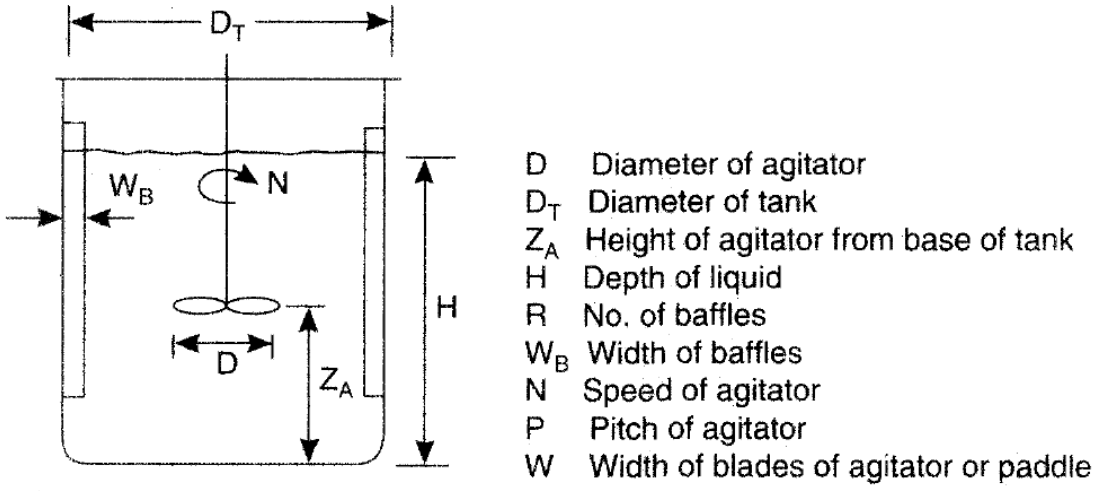

Figure C.1. Configuration and geometrical details of an agitated vessel (from Coulson et al., 1999)

For *geometric similarity;* following ratios must be same in two systems:

$$\frac{D_T}{D};\frac{Z_A}{D};\frac{W_B}{D};\frac{W}{D};\frac{H}{D} \quad \text{.....(C.1)}$$

For *kinematic similarity* in two geometrically similar systems, velocities at "corresponding points must have a constant ratio" in addition to similar flow patterns. It is important to note that flow types will change by impeller geometry. For instance, turbine blades generate more axial flow compared to flat paddles (Nienow et al., 1997).

For *dynamic similarity* in two geometrically similar units, it is required to have constant ratio for corresponding forces at various counterpart locations. For instance, in two systems of laboratory (1) and large scale (2), various force types exhibiting such as Fa, Fb, and Fc:

$$\frac{F_{a1}}{F_{a2}} = \frac{F_{b1}}{F_{b2}} = \frac{F_{c1}}{F_{c2}} = ...const. \quad \text{(C.2)}$$

Some of the important forces in the system include:

1) Inertial Forces (Forces that resist changes in object motion):

$$F_i = f(\rho D^4 N^2) \quad \text{(C.3)}$$

2) Viscous forces (forces that arise due to fluid flow)

$$F_v = f(\mu D^2 N) \quad \text{(D.4)}$$

3) Gravity forces (forces due to gravity)

$$F_g = f(\rho D^3 g) \quad \text{(C.5)}$$

4) Surface Tension Forces

$$F_s = f(\sigma D) \quad \text{(C.6)}$$

Substituting forces described in Equation as Fa, Fb with Fi, Fv, Fs, Fg we will get:

$$\left(\frac{F_i}{F_v}\right)_1 = \left(\frac{F_i}{F_v}\right)_2 \quad \text{(C.7)}$$

Using Fi and Fv relationships we will have following:

$$\left(\frac{\rho D^2 N}{\mu}\right)_1 = \left(\frac{\rho D^2 N}{\mu}\right)_2 \qquad \text{(Reynolds Number)} \qquad \text{(C.8)}$$

For other forces, we will get:

$$\left(\frac{F_i}{F_g}\right)_1 = \left(\frac{F_i}{F_g}\right)_2 \tag{C.9}$$

Which results:

$$\left(\frac{DN^2}{g}\right)_1 = \left(\frac{DN^2}{g}\right)_2 \quad \text{(Forude number)} \tag{C.10}$$

And,

$$\left(\frac{F_i}{F_s}\right)_1 = \left(\frac{F_i}{F_s}\right)_2 \tag{C.11}$$

Which results:

$$\left(\frac{D^3N^2\rho}{\sigma}\right)_1 = \left(\frac{D^3N^2\rho}{\sigma}\right)_2 \quad \text{(Weber number)} \tag{C.12}$$

Appendix D: List of Publications

Following papers were published as result of this study:

Peer Reviewed and Journals

1. Saleh, F.K. and Teodoriu, C., 2017. The mechanism of mixing and mixing energy for oil and gas wells cement slurries: A literature review and benchmarking of the findings. **Journal of Natural Gas Science and Engineering, 38, pp.388-401**.

2. Saleh, F., Ichim, A., Mbainayel, D. and Teodoriu, C., 2017, June. A Quantification of Mixing Energy During the Whole Cementing Cycle. In **ASME 2017 36th** International Conference on Ocean, Offshore and Arctic Engineering (pp. V008T11A042-V008T11A042). American Society of Mechanical Engineers.

Conference Proceedings

3. Saleh, K. F. and Teodoriu. 2018. Mixing energy of Well Cements: the gap between laboratory testing and field job, paper presented at 2018 AADE Fluids Technical Conference and Exhibition.

4. Saleh, F.K., Rivera, R., Salehi, S., Teodoriu, C. and Ghalambor, A., 2018, February. How Does Mixing Water Quality Affect Cement Properties. In SPE International Conference and Exhibition on Formation Damage Control. Society of Petroleum Engineers.